SOLID STATE ULTRASONIC IMAGING

A thesis submitted by

S.O. HARROLD, B.Sc.Eng., A.C.G.I.

for the degree of Doctor of Philosophy in

Engineering Science of the

University of Warwick.

August 1974.

PAGE NUMBERS CUT OFF IN THE ORIGINAL

Abstract

The development and performance of a transistor scanned solid state ultrasonic image converter are described and the results of investigations into various applicable signal processing techniques to produce visible pictures are presented. The general requirements of an ultrasonic imaging system are considered and this is followed by a critical survey of the more sensitive ultrasonic image conversion methods. The operation and basic performance of the transistor scanned converter are discussed and its resolution and sensitivity investigated, resulting in an apparent practical limit to the resolution in the image plane of $\frac{1}{3}$ mm, and an estimated limiting sensitivity of approximately 10^{-13} W cm^{-2}. Possible methods for the fabrication of a multielement converter are suggested and discussed. Three signal processing techniques are investigated and compared; that using an acoustic lens in a conventional camera arrangement, an on-line computer which effectively performs electrically the function of a lens, and a scanned array Doppler system on which only a feasibility study was carried out. It is argued that if flexibility is important then the computer "lens" is the most fitting method, and results for both near field focusing and far field beam deflection are presented, although at the moment in 1-dimension only. A relatively simple extension to the program will make 2-dimensional image reconstruction possible. The Doppler system described provides a simple electrical method of determining the range and bearing of far field targets and results adequately confirm the developed theory.

Acknowledgement

The author is indebted to Dr. D.I. Crecraft for his understanding and patient supervision, much of which has been carried out under difficult circumstances, and also to Dr. H.V. Shurmer without whose invaluable support in the final stages this thesis would not have been presented. Thanks are due to Dr. N.G. Meadows and Mr. F. Dellow for their encouragement and assistance, and to Dr. D.J. Harris whose helpful advice and interest in the last stages have provided the necessary impetus to complete the work.

The author wishes to acknowledge the assistance of the Science Research Council who financed the major part of the project, Lanchester College of Technology (now Lanchester Polytechnic), and Portsmouth Polytechnic, in particular the Department of Electrical and Electronic Engineering, who supplied all the necessary facilities.

Special thanks are due to Mr. R.C. West whose exceptional undergraduate project contributed greatly to the success of the work described in Chapter 7. Thanks are also due to Miss S.G. Westmore for typing this thesis, and to the photographic section for reproducing the many oscilloscope photographs, etc.

Above all the author wishes to thank his wife for her patience and encouragement throughout.

Table of Contents

List of Figures, Tables and Programs

1. Introduction

Imaging, as distinct from other forms of information display, may be defined as being the formation of a visible image of an object plane or space, the latter lying usually normal to the axis of wave propagation and parallel to the converter image plate. The image has height and breadth only, there being no time related dimension except in the special case of 3 dimensional imaging. Thus the photographic camera, television, radiography and the eye are all imaging systems. A basic ultrasonic imaging system is shown in figure 1.1 in which it is assumed, as is normally the case, that conversion to an electrical signal is performed as an intermediate step between the ultrasonic and optical images. Parts T,

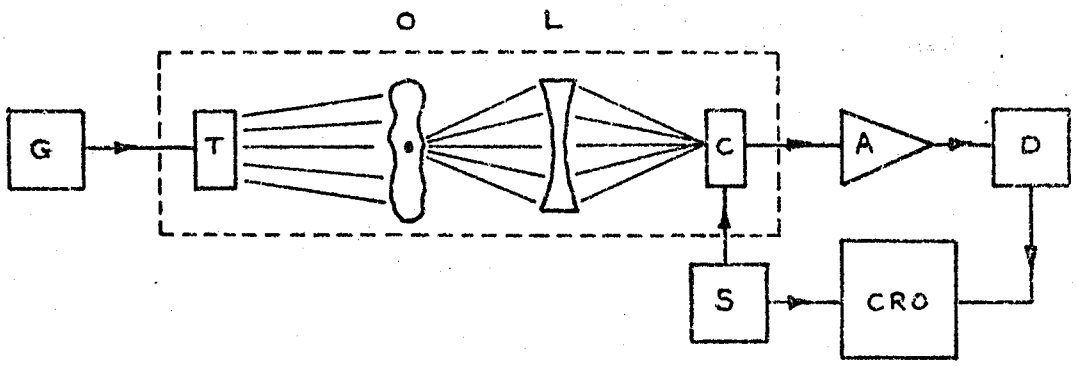

Figure 1.1 A typical ultrasonic imaging system using an acoustic lens.

O, L and C are all immersed in a liquid (usually water) so that they are acoustically coupled. A generator G produces an electrical sinusoidal drive signal at the appropriate ultrasonic frequency to the electro-acoustic transmitting transducer T which radiates towards the test object O. ~~Diffraction~~ Scattering occurs at discontinuities and irregularities in the test

object and the acoustic lens L focuses the diffracted rays to form a diffraction image on the image plate of the acousto-electric converter C. The output of C is normally in the form of a serial line-by-line scan of the image plate, being similar to a television video signal. After amplification by A and, if necessary, detection by D it is presented to a CRO as an intensity modulating signal. Scanning of both converter plate and CRO is controlled by unit S. This system uses through transmission, the transmitter being sited on the opposite side of the object to the receiving converter. Sometimes it is advantageous to have the transmitter placed on the same side as the converter so that the latter collects reflected signals from the test object.

The possibilities of ultrasonic imaging were first practically realised by Sokolov[1] in 1937. He successfully produced an electron scanned piezoelectric plate "camera" system which effectively became the prototype for development by other workers in Russia[2,3], Germany[4], Britain[5,6] and the U.S.A.[7] over many years. Although improvements are still being made, these converters possess some serious inherent shortcomings, as is evident when it is realised that they are still in the main used only as laboratory research instruments.

The requirements of a flexible ultrasonic image conversion system may be listed as follows:

(i) High sensitivity.

(ii) Image plate dimensions equivalent to at least 100 x 100 wavelengths in the transmission medium.

(iii) Linear resolution equal to or better than 1 wavelength in the transmission medium.

(iv) Retention in the output electrical signal of the ultrasonic pressure image phase information.

(v) Pulsed operation possible.

(vi) High reliability and minimal setting up procedure.

The objectives of this research programme may be divided into two clear sections:

(a) The production of an ultrasonic image converter to satisfy as many of the above requirements as possible, and,

(b) To investigate and compare various ways of processing the signals to produce a visible image using the converter developed in (a).

Chapter 4 deals in detail with (a) and chapters 5, 6 and 7 with (b). The objective of section (a) has been achieved by effectively forming the converter image plate into a matrix of piezoelectric elements which are then sequentially sampled by arrays of field effect transistors. The result is a highly sensitive and reliable system with potentially none of the inherent limitations of the Sokolov type tube converters. Three forms of signal processing have been considered for section (b), an acoustic lens, a form of holographic reconstruction using an on-line computer and a scanned array technique based on the change in Doppler frequency shift associated with target bearing. The techniques are compared and their limitations and those of the solid state image converter discussed, together with suggestions for further work, in chapter 8.

Ultrasonic imaging has important applications in two widely different areas, underwater visualisation for ranges of up to 10 m or so, and medical diagnosis and associated work. Television is preferable for underwater viewing in clear water, but most requirements are for coastal or inland waters where optical visibility is usually very poor. Under these

conditions ultrasonic wave propagation, although suffering increased attenuation, is still possible[30]. Medical uses would include amongst many others, observation of the foetus, where X-rays are damaging, and heart surgery where continuous visualisation is an advantage. Short pulsed operation is essential[31], however, if the image converter is ever to become a useful medical tool. Non-destructive flaw detection of solid materials, although a very desirable and much sort after application, is inherently a more difficult problem. The image converter requires virtually perfect homogeneous coupling between its whole frontal surface and the object to be viewed. In the unlikely situation where this has an appropriate and large enough flat surface, then coupling may be achieved directly using a thick oil or grease, but for most applications immersion in a coupling fluid (water or oil) is necessary. This introduces a reduction in the system sensitivity due to impedance mismatch, and loss of definition due to refraction caused by the irregular or non-coplanar face of the object through which the ultrasound passes.

It is evident that there is an as yet unsatisfied need, over a very wide field, for a suitable ultrasonic image converter. It is hoped that the FET scanned solid state converter may, after further development, prove to be an answer to this clear requirement.

2. Ultrasonic Imaging Techniques

2.1 Introductory Review

Although many forms of ultrasonic image converters have been devised, all but the electron tube and solid state types would appear to be either too slow or to possess insufficient sensitivity. Table 2.1 lists for comparison some of the more sensitive forms of converter that have been developed, giving their measured sensitivities, resolutions and image formation times. The list has been restricted to those with sensitivities greater than 10^{-3} W/cm^2. The first two provide direct conversion to a visual image whereas the rest are all acousto-electric and therefore require some form of electro-optical converter in order to complete the imaging process. There are other solid state converters whose sensitivities have not as yet been published and are therefore not included in table 2.1. Details of these are given in sections 2.3 and 2.4.

There have been several comprehensive reviews of ultrasonic imaging methods[12, 13, 14]. This review will be limited to electron tube and solid state converters since the former is the only type with a comparable performance to the latter.

Technique	Limiting sensitivity W/cm	Resolution	Image formation Time. Seconds.
Optical detection of liquid surface deformation[8].	$1{\cdot}5\times10^{-3}$	A few mm	< 1
Mechanical alignment of flakes in liquid - Pohlman Cell[9].	$2{\cdot}5\times10^{-3}$	several wavelengths	< 1 Depends upon intensity
Sokolov tube:- Quartz face plate[6]. Ba Ti O_3 face plate[3]	7×10^{-7} $1{\cdot}3\times10^{-8}$	1 → 2 times thickness of plate.	< ·02
Cathode stabilised tube:- Quartz face plate[5].	$1{\cdot}4\times10^{-7}$		
Mechanically scanned quartz plate[10].	3×10^{-12}		3 → 120
Solid state:- Bipolar transistor scanned PZT plate[11] (2·5 MHz)	7×10^{-11}	1·5 wavelengths	< ·02
FET scanned PZT plate (the product of this research programme)	$1{\cdot}3\times10^{-13}$		

Table 2.1 List showing the more sensitive ultrasonic image converters.

2.2 Electron Tube Converters

Sokolov in 1937 pioneered the ultrasound camera with his ultrasonic microscope[1,15], although he gave very few details at the time. He was the first to realise that a liquid damped piezoelectric plate, rather than vibrate as a whole, responds point by point to the incident local sound intensity. This fact was vital to the satisfactory operation of the image converter, which used a single homogeneous piezoelectric plate as the first stage in the conversion process. Cameras later developed in Russia[2,3], Germany[4], Britain[6] and America[7] are all based on the same principle of operation. A piezoelectric plate forms the end wall of a cathode ray electron tube so that its back face may be scanned by an electron beam, whilst its front face is subjected to the ultrasound pressure image. At equilibrium, the piezoelectric plate being a good insulator, the primary electron beam current will equal the secondary electron current passing back to what is termed the collector. However, the ultrasonic pressure variations on the front of the plate change the voltage on the back face, and the equilibrium voltage therefore requires reestablishing. This means that the secondary electron current will reduce as the piezo voltage tends to rise and increase as it tends to fall. The output from the collector, consequently, takes the form of an amplitude modulated wave at the ultrasonic frequency, the modulation representing the line-by-line spatial distribution of ultrasound intensity across the piezo plate. In order to produce a visible image this electrical signal may be fed to the grid of a conventional display cathode ray tube whose scanning is synchronised to that of the converter. This form of electron scanned tube is termed collector stabilised.

Smyth[5,16] and Sayers[17,18] between 1954 and the early 1960's developed a form of tube converter which was based on the very limited details

which Sokolov had published on his tube. Its operation differs in one major respect; the output is not coupled to the piezoelectric plate voltage via a secondary electron current. Instead a signal plate is included on the outer surface of the transducer and there is no collector ring within the tube. Acoustic to electric conversion is effectively completed in two separate electron scans. First, with the ultrasound off, a low velocity primary electron beam scans the target so that no secondary emission takes place. Consequently, in order to satisfy the equilibrium conditions, the target surface potential will be reduced to that of the cathode at which stage no further electrons will reach the target. The ultrasound is then switched on, a pressure image focused onto the front face of the transducer, and the target once more scanned. More electrons may now arrive at every point on the target surface where the ultrasound impinges, but only during the positive half cycles of the piezoelectric potential excursions. A charge distribution is thus built up over the surface of the target which will be directly proportional to the ultrasound intensity at any point. The build up of this charge will induce corresponding currents in the signal plate, which is earthed to the ultrasonic frequency, and these are used to provide an electrical output signal. With the ultrasound off the first electron scan is then repeated and now performs a discharging process in order to remove the negative charge distributed over the target face. The low velocity electron beam contains a sufficient number of positive ions to make this possible, and consequently the target potential is raised to that of the cathode in the time available. The target is then ready for the next charging or imaging scan. The output of this converter is a serial video signal corresponding to the line-by-line distribution of sound intensity over the image plate, and <u>not</u> an amplitude modulated carrier wave as with

the Sokolov tube. Because the target potential is maintained at that of the cathode, this type of tube converter is known as cathode stabilised.

2.3 Solid State Transistor Scanned Converters

Two bipolar transistor scanned ultrasonic image converters were developed quite independently between 1966 and 1968, one in America under the direction of Knollman[11], and the other[19] in Britain, forming the early part of this research programme (see Appendix A).

The former consisted of a 2·5 MHz half-wave thickness resonant piezoelectric plate having on its uninsonified face a 10 x 10 matrix of square silver electrodes, and with overall dimensions of approximately 0·7 x 0·7 inches. A 10 x 10 matrix of transducer gates controlled in rows and columns effectively scans the transducer elements and connect them sequentially to a common load. In order to overcome the capacitive signal feedthrough in the "off" gates at 2·5 MHz, frequency conversion is carried out within the "on" gates creating a relatively low (500 kHz) intermediate frequency. By selectively amplifying only this intermediate frequency, the feedthrough signals which will be at 2·5 MHz are rejected. Mixing is performed by interrupting the gating signals at the local oscillator frequency so that a time varying switch conductance results. The sensitivity of this converter based on initial tests was approximately 5×10^{-12} W/cm^2, but later publications[20,21] claimed figures of around 10^{-11} and better than 10^{-10} W/cm^2.

The transistor scanned converter developed here at the start of this project, although basically very similar to the converter described above, did not employ mixing to reduce the cross-coupling problems. For this reason it was limited to operating frequencies of 1 MHz or less. A composite clamp-series switch arrangement was investigated in an attempt to overcome this and this gave excellent results for signal levels above

10 mV or so. Since the clamp transistor had an inherent offset voltage, signals of lesser amplitude than this were not affected and the circuit therefore offered little advantage over that using a single series transistor. Matrix drive signals were derived from two shift registers rather than decade counters and decoders. Results were marred by unreliable connections to the transducer elements and by the high level of cross-talk or breakthrough signal (typically 50% of the total output signal). No meaningful sensitivity tests were therefore made, and further work on this converter was quickly abandoned in favour of one using FET gates. These gates showed great promise, with an "on" to "off" signal output ratio of greater than 50 dB's at 6 MHz compared with less than 30 dB's at 1 MHz using the bipolar transistor gate. This lead to the development of the FET scanned piezoelectric plate image converter which has formed the basis of most of the experimental work carried out under this research programme.

A detailed description of the FET scanned converter is given in chapter 4. Operating at an ultrasonic frequency of 1 MHz it uses a PZT5A ceramic disc transducer, the rear face of which is formed into a 10 x 10 matrix of separate square silvered areas. Each of these areas is connected to a common output line via two FET linear gates, one to locate the row and the other the column. Two shift registers control the gates so that the transducer elements are scanned sequentially line by line. The output thus takes the form of an amplitude modulated wave at the ultrasonic frequency, the modulation representing the ultrasound intensity distribution across the front face of the transducer. For unity signal to noise ratio at the electrical output, an ultrasound intensity of approximately 10^{-13} W/cm^2 is required.

The principle has been further developed by Maginness[22] at the University of Stanford in 1973. A transmit-receive mode of operation at an ultrasonic frequency of 3·5 MHz is used in conjunction with an acoustic lens. The scanning both for transmitting and receiving employs special FET integrated MOS arrays. These are bonded directly to a thin interconnecting layer which carries the necessary address and signal conductors and which is built up on the back face of the transducer matrix. The result is an extremely compact and reliable arrangement, and although at the time only a 10 x 10 matrix had been produced, extension to a 32 x 32 was considered quite feasible. The production of such a device using modern solid state technology has been the long term aim of this project (see Appendix A). Realisation of this objective has been prevented by the problem associated with reliably bonding the many required electrical connections on the underside of a silicon chip to the appropriate signal and addressing conductors on the back face of the transducer. With this overcome the solid state ultrasonic image converter should at last become the viable tool which to date no other ultrasonic image converter may claim to be.

2.4 Surface Acoustic Wave Scanned Transducer

A new type of ultrasonic imaging device[23] which uses acoustic surface wave delay lines in conjunction with FET mixers to scan a transducer matrix in two dimensions was proposed by Havlice et al.[23] at the University of Stanford in 1973. A one dimensional version had at that stage been constructed, and, in conjunction with mechanical scanning in the other dimension, produced acceptable visual images on a CRO. The single delay line has taps evenly distributed along its length, each tap feeding a mixer (diode or FET) the other input of which is the electrical

signal, at the ultrasonic frequency ω_s, from the appropriate transducer element. The mixer outputs are commoned so that as a short pulse of frequency ω_1 is sent up the delay line and successively passes the taps, transducer elements are effectively scanned to produce a serial output at an intermediate frequency of $\omega_s + \omega_1$. In addition to linear scanning it is relatively easy by using a suitable frequency modulated linear chirp as the input to the delay line to create a focusing action and hence remove the necessity for an acoustic lens. Two dimensional scanning was to be achieved by using two acoustic delay lines, one to scan the x direction and the other the y, forming a rastor scan of the transducer elements which lies at 45° to the x and y axies.

2.5 Discussion

The primary requirement of the ultrasonic image converter, in order that the signal processing detailed in chapter 6 might be carried out, was that it should retain in its electrical output the phase of the ultrasonic signals. The Smyth cathode stabilised tube did not fulfil this, and at the beginning of the research programme the Sokolov collector stabilised tubes improved by Jacobs[7] and Kennedy[24] were not yet commercially available. In any case these tubes which included an electron multiplier, although more reliable, did not have a significantly improved general performance. The inherent limitations which are brought about by the necessity for a vacuum and the fact that the signal path includes a low conductivity secondary electron current section were still present. The former limits the maximum safe image plate diameter, although there have been numerous attempts to overcome this[24-29], and the latter limits the sensitivity due to both its noise content and the attenuation it introduces.

A new form of image converter, therefore, was required and with the concept of the solid state transistor scanned transducer it became a worthwhile aim in itself. This converter, later developed to an FET scanned version (see chapter 4), does not have an inherent limitation on image plate diameter, although in a non-integrated form the cost becomes a prohibitive factor. Sensitivity measurements indicate this to be possibly 5 orders higher than that claimed experimentally by Sokolov. This comparison, however, takes no account of the "noise" introduced by the transducer element to element output variations, which in the present converter for even image plate insonification may be as high as 20%. Image resolution across the piezoelectric image plate could be somewhat better, since the transducer's rear face may be acoustically damped to further reduce the mechanical Q. The solid state converter developed by Maginness[22] has greatly improved the prospects of this form of converter, since its unique transmit-receive capability may be used with both lenses and electrical signal processing techniques. The surface acoustic wave delay line scanned converter by Havlice, a completely new method, although up to the present only briefly described[23], could prove to be an extremely flexible and efficient arrangement, providing the proposed 2 dimensional scanning is practically feasible. Capacitive cross-coupling between the effective x and y strip electrodes placed on each side of the transducer may prove to be a serious problem.

3. Signal Processing Methods Applied to Ultrasonic Imaging

3.1 Acoustic Lenses and Mirrors

Acoustic waves in almost all respects behave in the same manner as light waves; they are refracted, diffracted, reflected and absorbed, but show little dispersion. There is an important difference however; acoustic waves are subject to mode changes, particularly at liquid solid interfaces, where a proportion of the longitudinal wave energy (if that is the original mode of transmission) is converted into shear waves (there is also some conversion to surface waves). These increase as the angle of incidence of the longitudinal waves to the interface increases.

On the basis of refraction and reflection it is clearly possible to focus acoustic waves using both acoustic lenses or mirrors, and to thereby form acoustic images. The resolvable detail of these will, in the main, be limited by the same criteria as those applicable to optical images. Image aberrations will occur, particularly if a simple spherical design is used, and the best achievable resolution in the image plane will be the Airy disc of diameter $1{\cdot}22\ \lambda \frac{f}{d}$, where λ is the wavelength in water (the transmission medium), f is the focal length and d the diameter of the lens or mirror.

The material of an acoustic lens should have an acoustic impedance as near as possible to that of the surrounding medium in order to minimise reflections, and should have a significantly different acoustic longitudinal wave velocity. The reflected energy increases with the angle of incidence, and therefore it is advantageous for the lens material to have a high refractive index, since this results in a larger radius of curvature for a given focal length. The processing action performed by a convergent lens may be considered as being a spatial spherical phase advance function operating in the plane of the lens, such that non-paraxial rays suffer a

greater phase advance than those on the axis. This is achieved by forming the lens into a spherical shape such that, in the case of a lens material where the acoustic velocity is higher than the surrounding medium, it is concave, and for the reverse situation it is convex.

Acoustic mirrors have the advantage that complete reflection is ideal and in practice is more easily achieved than the perfect impedance match required by a lens. Where very large apertures are acceptable, for example underwater imaging[32], mirrors are very successful, but for the visualisation of small objects at short range a short focal length is needed, resulting in an aperture limitation. In the latter case, the converter may seriously obscure the mirror, since the mirror is necessarily on the same side as the incident waves to the converter. The problem becomes clearly impossible if unity magnification is required; the object and image planes are physically in the same place. The signal processing action of the spherical mirror is almost identical to that of the spherical lens; non-paraxial rays are reflected before paraxial and a spatial spherical phase advance function thus operates on the reflected rays so that they are brought to a focus in the image plane.

3.2 Acoustic Holography

3.2.1 Principles[33,35]

In order to establish a simple physical picture of the principles involved in the formation of acoustic holograms and their image reconstruction, a 2-dimensional system will be considered using geometric ray theory. No loss of generality results from the consideration of only two dimensions.

Consider a ray, defined as a narrow beam which nevertheless is a sufficient number of wavelengths in cross section, to behave as an infinite plane wave over moderate propagation distances, radiating from the object

at $z = z_o$ and meeting the Z-axis at z , as shown in figure 3.1.

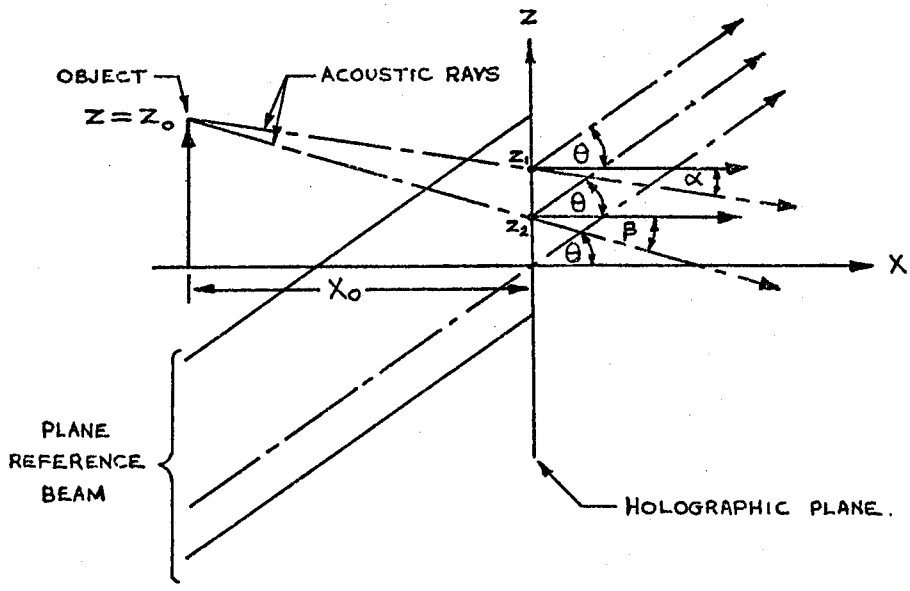

Figure 3.1 Formation of a hologram.

In the region of z_1 this wave may be represented by the expression:

$$A(z_o) \cos \left[\omega t + \phi(z_o) + \frac{2\pi}{\lambda} \sin \alpha \, z \right] \quad \ldots\ldots \quad 3.1$$

where ω and λ are the acoustic angular frequency and wavelength respectively, t the time, α the angle the ray makes with the X-axis, $A(z_o)$ the amplitude of the ray, z a point on the Z-axis near z_1, and $\phi(z_o)$ the phase of the ray. Similarly the reference beam may be represented at the Z-axis, assuming unity amplitude, by the expression:

$$\cos \left[\omega t - \frac{2\pi}{\lambda} \sin \Theta \, z \right] \quad \ldots\ldots \quad 3.2$$

where Θ is the angle of the reference beam to the X-axis. Now consider the effect of these two waves being ~~multiplied~~ summed together on the Z-axis ~~or on the Z-plane.~~ and subsequently squared. The relevant term of the result would be:

$$\tfrac{1}{2} A(z_o) \cos \left[\frac{2\pi}{\lambda} (\sin \Theta + \sin \alpha) \, z + \phi(z_o) \right] \quad \ldots\ldots \quad 3.3$$

Note that this expression is independent of time and may thus be recorded for various values of z to form an intensity pattern or hologram.

Assuming that the hologram has been recorded on an optical transparency, image reconstruction is carried out by means of a beam of coherent light, and if this is considered to be plane, then, in the plane of the hologram may be represented by the expression:

$$\cos \left[\omega_1 t - \left(\frac{2\pi}{\lambda_1}\right)\left(\frac{\lambda_1}{\lambda}\right) \sin \theta . z \right] \qquad \ldots\ldots \quad 3.4$$

where ω_1 and λ_1 are respectively the angular frequency and wavelength of the light. The inclination of the light beam to the X-axis is a function of the ratio of the optical to acoustical wavelengths, and is given by:

$$\sin^{-1} \left[\left(\frac{\lambda_1}{\lambda}\right) \sin \theta \right] \qquad \ldots\ldots \quad 3.5$$

It is therefore approximately the angle θ reduced by the ratio of the wavelengths.

The rays passing through the hologram will have their amplitudes multiplied by the intensity patterns recorded by the original object rays. For the light rays passing through the region around z_1 of the hologram the wavefront emerging is obtained by multiplying together expressions 3.3 and 3.4, resulting in:

$$\tfrac{1}{4} A(z_o) \cos \left[\omega_1 t + \phi(z_o) + \left(\frac{2\pi}{\lambda_1}\right)\left(\frac{\lambda_1}{\lambda}\right) \sin \alpha . z \right]$$

$$+ \tfrac{1}{4} A(z_o) \cos \left[\omega_1 t - \phi(z_o) - \left(\frac{2\pi}{\lambda_1}\right)\left(\frac{\lambda_1}{\lambda}\right)(2 \sin \theta + \sin \alpha) z \right] \ldots. \quad 3.6$$

Comparing the first term of expression 3.6 with expression 3.1 it will be seen that they are identical except that the former is inclined to the X-axis, or hologram normal, at an angle of:

$$\sin^{-1} \left[\left(\frac{\lambda_1}{\lambda}\right) \sin \alpha \right] \simeq \frac{\lambda_1}{\lambda} . \alpha \qquad \ldots\ldots \quad 3.7$$

for small values of α. Thus a distorted virtual image of the object lies

at an approximate distance of $(\frac{\lambda}{\lambda_1})x_o$ from the hologram, where x_o, as will be seen in figure 3.1, is the original object Z-axis distance. Similarly the second term of expression 3.6 represents a real image of the object at the same distance from the hologram as the virtual image, but angularly separated.

3.2.2 Practical Considerations

Most successful experimental systems[33, 34, 36] use an electrical square law detector or multiplier to perform the essential reference signal multiplication. If a multiplier is used then it is possible to introduce the reference as an electrical signal whose phase is automatically controlled by the mechanical scanning of the Z-plane by the acoustic probe. At present almost all Z-plane sensing is carried out by using a mechanically controlled probe which scans the required area at a suitable pitch. The application of an electrical/electronic acousto-electric image converter to this problem would offer a tremendous advantage, but the resolution required, and in particular the aperture, is too great for any device available at the moment. In order to correct for the vast difference in the wavelengths of the acoustical and optical waves the hologram is reduced by a certain factor (around 10), and whilst this reduces the image size by the same factor, the distance that the image lies from the hologram is reduced by the square of this factor. This effect may be corrected in practice by optically magnifying the image before viewing.

Aldridge[33] used in his system 1 μS pulses and an ultrasonic frequency of 10 MHz, and this gave him a limiting resolution of about $\frac{1}{6}$ mm in water and, with range gating, provided a resolution in depth of around 1·5 mm. A facsimile recorder synchronised to the probe scanner produced the original intensity plot, and this was then photographed and reduced in size to create the optical transparency. Crossed linear arrays[37] have been

used in conjunction with a computer to perform simulated holographic functions and it is claimed that the process is superior to the normal area holograms. The application of a scanned linear array[38] has been considered, where a transistor scanned linear array of transducers is moved mechanically to create the second dimension.

The striking 3-dimensional visualisation afforded with optical holograms is not in practice possible with acoustic holograms. Because of the effectively very large apertures readily attainable with light, the viewer may look at the image through only a small part of the aperture and in so doing may view the image from different directions. In principle the same is possible in the acoustic case, but in practice the apertures are small (a relatively small number of wavelengths across) and the loss of resolution resulting from using only a small portion of the aperture is usually unacceptable.

3.3 Image Reconstruction by Computer

3.3.1 General Principles

Figure 3.2 shows the basis of an imaging system comprised of an electro-acoustic image converter and an insonified object situated in the object plane. The arrangement is lensless, the computer providing the necessary signal processing to image the object.

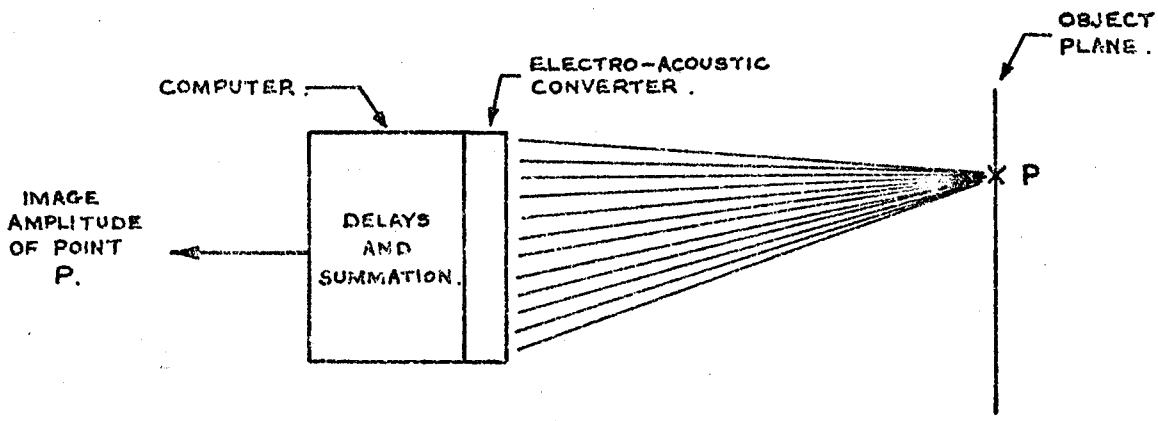

Figure 3.2 Image reconstruction by computer.

The action of a lens, as described previously, would be to focus the divergent "rays" eminating from the object so that only at one point in the image plane was the energy from this source concentrated. It may be considered to do this by imposing a spherical phase or time delay function on the incident "rays" so that, as they leave, their phases are such that the resulting signals are only in phase at one point, the focus. There are thus three regions where spatial time variations occur; between object and lens, within the lens itself, and between lens and image. The computer must provide the last two in order to perform the analogous function. It must arrange that the phases of all the received signals radiating from the object point are equalised before a summation is made to produce the image magnitude of the point. The computer delay function for a given situation, although ~~approximately~~ spherical, is therefore not identical to that of the lens.

3.3.2 Experimental Systems

A system using very short pulses and in consequence possessing a wide bandwidth was developed by Maginness[39,41,42], and this resulted in providing the additional facility of being able to image over a range of harmonically related frequencies. Transmitted signals consisted of pulses of approximately 2 cycles duration of a 5 MHz wave, and recordings were made of the signals reaching the receiving aperture by means of a mechanically scanned transducer matrix. The signals were sampled at an effective rate of 24 MHz before quantisation and conversion into a paper tape format. After completing the recording of all 144 matrix element signals, the tapes were fed into a large computer, programmed to perform the necessary processing. The latter took the form of a fast Fourier transform. The output, in the form of a 2-dimensional graded intensity print out, displayed the acoustic images, over a limited range of frequencies, of

slices through the material being viewed (an aluminium block) by calling up the various object planes and frequencies as desired. The result was a very satisfactory and flexible processing system, the weak link being the long time involved in both the mechanical scanning of the transducer matrix and the production of and inputting to the computer of the paper tape records.

Shondhi[40] developed an experimental system in air at an audio frequency of 6·7 kHz, again using mechanical scanning and off-line computer. Results, showing the images of simple objects, are impressive.

Both the systems described suffer from the one major disadvantage; the long delay between the acoustic image formation and the production of the final visual image. The wide-band system, if it was to use its wide-band properties, had a further problem; it required very large immediate access computer word storage. These two factors encouraged the investigation into an on-line narrow band single frequency system, described in detail in chapter 6, and which forms one of the main applications of the solid state ultrasonic image converter. For most anticipated practical applications of any imaging system, real time working is almost essential, a few seconds being at the most acceptable. Thus an essentially simple approach was considered in order to minimise computer time and storage requirements. Hence the processing performed by the computer is basically as outlined in section 3.3.1 and consists of the addition of appropriate phase increments to the digitised transducer element signals so that on summation they appear to eminate only from the point in the object plane being imaged. The elements of a 10 x 10 matrix are scanned electronically (see chapter 4) and the phase and amplitude of each measured, converted into a digital form, and transferred to the computer store within the minimum sampling time of 60 μS. After acquiring all the digitised data

the computer modifies the phases of the element signals to "focus" a particular point in the object plane. The modified signals are summed to complete the "focusing" action for the point, and a repetition of this process for all the other points in the object plane produces, after suitable digital to analogue conversion, a visual picture.

3.4 Scanned Array Doppler System

An echo returning from an insonified target situated in the far field of an array of ultrasonic transducers will strike this array at an angle dependent on the target bearing. If the array is linear and consists of equally spaced elements which are sampled sequentially at a known and fast enough rate, then the resultant electrical samples after demodulation will produce a sinusoidal signal whose frequency is a function of the angular bearing, Θ, of the target. This resultant frequency is given by the Doppler expression:

$$f_R = f_T \left[1 - \frac{C_s}{C_1} \sin \Theta \right] \qquad \ldots\ldots \quad 3.8$$

where $C_s = f_s d$ is the sampling velocity across the array,

f_T is the frequency of the incident wave,

d the distance between adjacent element centres,

C_1 the velocity of sound in the transmission medium,

and f_s the sampling frequency.

In order to satisfy the sampling theorem f_s must clearly always be greater than $2f_R$ thus giving a boundary to the range of Θ for a given f_s.

In practice with a finite array, and where sampling is continuous, only certain discrete characteristic frequencies corresponding to discrete bearings are reconstructable.

For a continuous resultant sine wave to be produced the phase of the signal from the last element should be $\Delta\phi$ behind the phase of the first, where $\Delta\phi$ is the phase difference between adjacent elements. The discrete bearings caused by this limitation are given by:

$$\theta = \sin^{-1}\left[\frac{q\lambda_1}{dn}\right] \qquad \ldots\ldots \quad 3.9$$

where q is an integer,

and n the total number of elements.

The limitation expressed by this equation is brought about only by the manner in which information is extracted from the resulting signal. A single set of n samples across the array contains all the required bearing information.

A practical system[43, 44] was developed to establish the validity of the theory and details of this will be found in chapter 7. It proved to be a successful preliminary investigation and showed that further more detailed work would be useful. Although not referred to at the time a similar scheme had been attempted in 1962 using a scanned line hydrophone[48]. The electronics used was not at the time good enough, it would seem, to encourage further work, and although some useful results were obtained particularly regarding noise performance, no publications since that date have, as far as is known, been produced.

3.5 Comparison of Processing Techniques

The use of the signal phase information forms a common thread which runs through all the techniques discussed above. In the case of lenses and mirrors and image reconstruction using a computer it is very evident that this is so. With holographic processing the phase is retained in the hologram by virtue of the interference pattern created by the reference

beam, and for the scanned array Doppler system the instantaneous amplitude of the incident wave is sampled and the samples analysed for a phase coherence at certain frequencies.

By far the simplest processing method is that using lenses or mirrors. If carefully designed these can produce results which are difficult to improve upon by other processing techniques using comparable aperture dimensions. They are, however, somewhat inflexible in that the field of view and magnification may not be rapidly changed when desired. They require an intermediate coupling medium between the converter and the object to be viewed, and whereas in an immersion system this presents no problems, where imaging within the human body or within relatively large solid objects is required, direct coupling of the converter to the body is advantageous. With the other three processing methods discussed this is possible, although it is not suggested that this could be usefully applied to the scanned array Doppler system where far field operation is required at present (although a focusing action should be possible).

The holographic technique provides excellent results, probably the best that have been produced by any method so far, but the apertures used are relatively large and these are essentially part of the image conversion section of the system, rather than part of the processing technique. If the same apertures were used with the other processing methods, then they would also be expected to produce comparable results. The imaging system is more flexible than that provided by a lens, since the field of view may be varied at will. This advantage is heavily outweighed by the long processing time required for the scanning and photographic copying.

The most inherently flexible technique is that provided by computer processing, and if a real time on-line system is considered, all imaging requirements could be provided for. There are problems, however, one of the most serious of these being that as the resolution is improved so the

computation time increases approximately as the square of the aperture dimensions. Another problem, which is shared with all systems where the aperture is scanned before processing takes place, is that operation with short pulses in conjunction with large apertures necessarily leads to a long data collection time. A lens, on the other hand, does not have this problem because processing of all the image points is effectively done in parallel, i.e. at the same time.

The scanned array Doppler system has the same correlation between resolution and aperture. Although an inherently very simple processing method, in its present form it suffers from lack of sensitivity since only one element of the array is acting as a receiver at any one time. It should be possible to overcome this, but at the expense of increased complexity. Much further work is required to be done investigating this technique before a proper assessment on its qualities, or otherwise, can be made.

To summarise, it would seem that lenses and mirrors offer the simplest and most effective method of image construction for applications where immersion is possible and where rapid changes of the field of view are not required. Where flexibility in conjunction with reasonable speed is required, computer processing offers distinct advantages, and where resolution is the overriding objective, a holographic method should be used.

4. The Solid-State Converter

4.1 Converter Development

By 1968 the highly reliable and relatively high frequency silicon planar transistor was fast becoming a readily available and inexpensive component. This fact and the expectation of a rapid advance in integrated circuit technology, particularly in fabrication techniques, decided consideration should be given to the feasibility of using transistor analogue gates as a means of sampling the electrical signals developed on the back face of a piezoelectric transducer. It had been shown by Smyth[5] and others that electron beam scanning of a piezoelectric plate transducer was currently the most sensitive method of conversion, so that the sensitivity of the proposed method was confidently expected to be at least equal to and probably better than this. A ten element bipolar transistor (2N706) scanned transducer array was constructed and results from underwater tests with this were very encouraging. As a consequence of this initial success a complete ten by ten transducer matrix, scanned by bipolar transistors with shift register control was built. Full details, including results, of this converter are given in Appendix A. This simple system proved to be highly reliable and within the limits of the inherent picture "grain" size (0·1 inch square on transducer plate), produced easily recognisable pictures of simple objects. However, it was clear that serious image degradation was being caused by the capacitive coupling of signals across cut-off transistors. This cross-talk problem has been virtually overcome in the present converter by the use of field effect transistors which possess a very low OFF capacitance (typically around 0·1 pf) between their input and output terminals. The following sections provide details of the design, construction, component characteristics and results of this FET scanned converter.

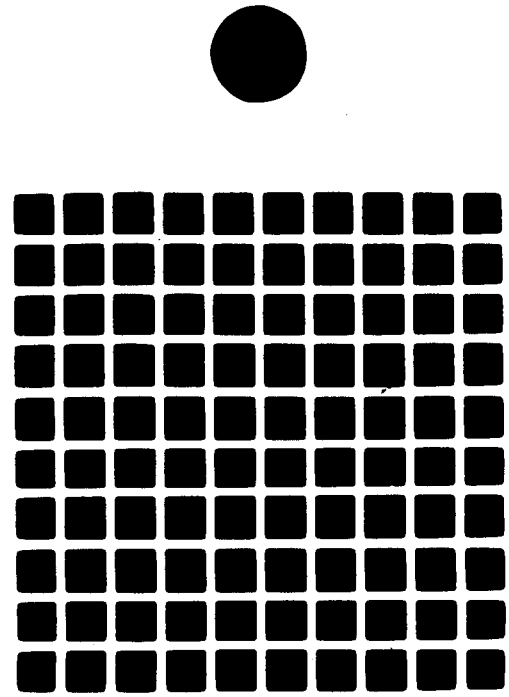

Figure 4.1 Converter transducer rear face electrode pattern.

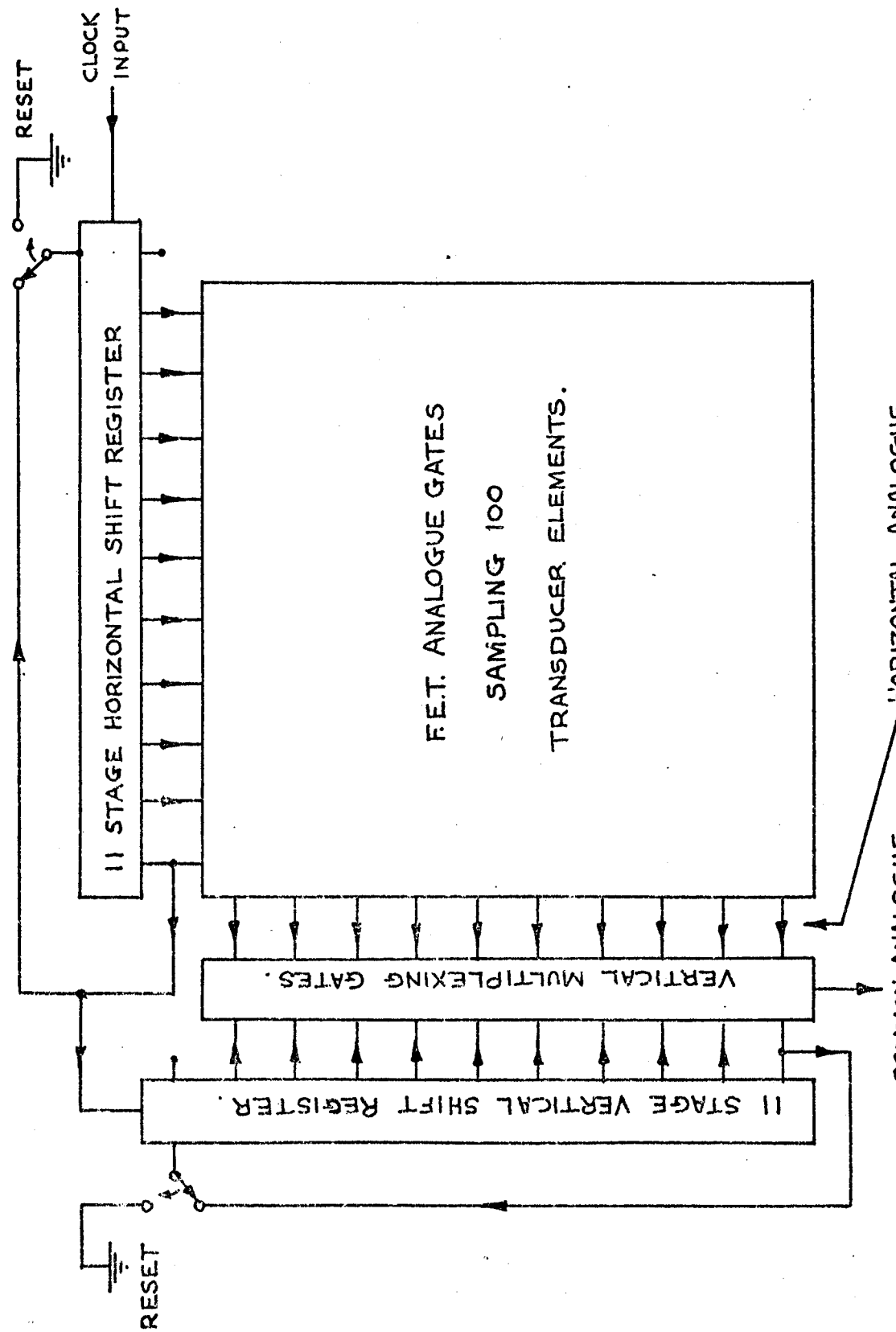

FIGURE 4-2. CONVERTER ELECTRICAL SYSTEM.

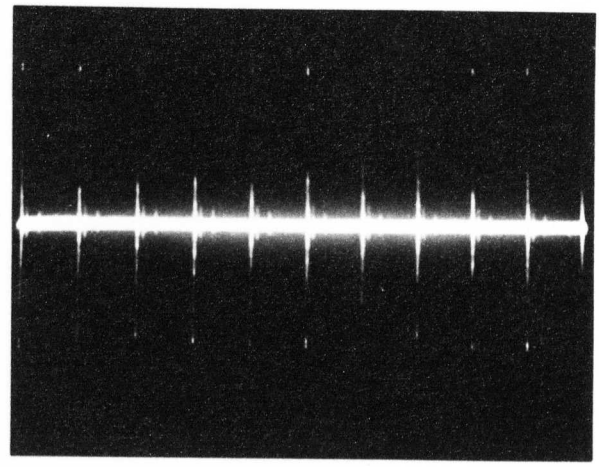

Figure 4.3(a) Typical converter output-transmitter off.

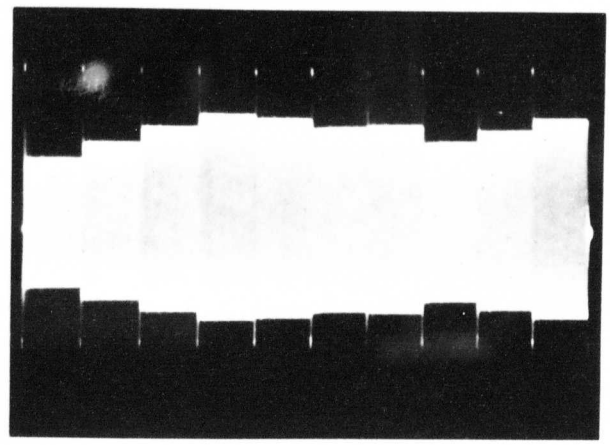

Figure 4.3(b) Typical converter output-transmitter on.

4.2 General Principles of the FET Scanned Converter

The transducer, a lead-zirconate-titanate disc, has its front face (i.e. that upon which the ultrasonic waves impinge) completely silvered and its rear face partially silvered to form a ten by ten matrix of one hundred equal area but electrically isolated squares (figure 4.1). The electrical signals from the one hundred effective transducer elements so formed are each passed through an FET analogue gate, their outputs being commoned in such a way as to form ten separate lines representing the ten horizontal lines of the matrix (figure 4.2). A ten stage shift register is connected to these gates so that a single "0" shifted through the stages causes vertical columns of gates to be successively opened. Thus a horizontal scan of the transducer matrix is performed, but the output appears on ten lines and vertical multiplexing has yet to be carried out. These ten lines are then vertically scanned by a further ten FET gates controlled in the same manner by a second ten stage shift register so that after each horizontal scan is completed, the vertical scan is shifted one line down. The resulting output becomes a single line on which the complete transducer matrix signals in a multiplexed serial form appear. Since the analogue gates do not perform any demodulation process, this output signal is an amplitude modulated carrier at the ultrasonic frequency, the peak amplitude of which at any instant is proportional to the ultrasonic intensity on the transducer element being sampled at that instant (see figure 4.3).

4.3 Constructional Details

The FET converter matrix was constructed in two parts, the transducer assembly and the FET scanning matrix, these being electrically connected before final encapsulation. A third part, the control circuitry, is remote from the converter matrix and twenty-three wires connect this to the first two parts.

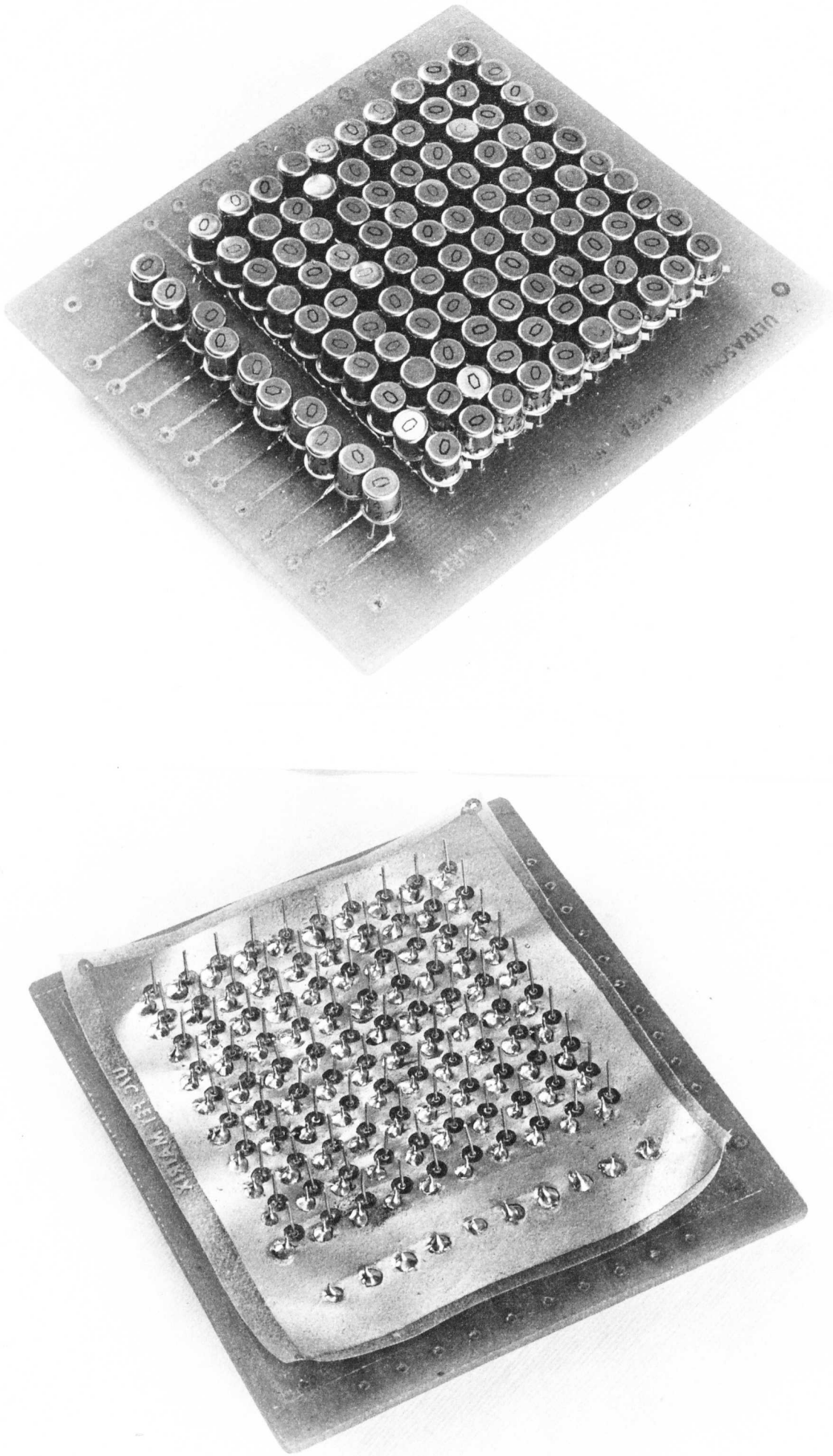

Figure 4.4 The FET scanning matrix before encapsulation.

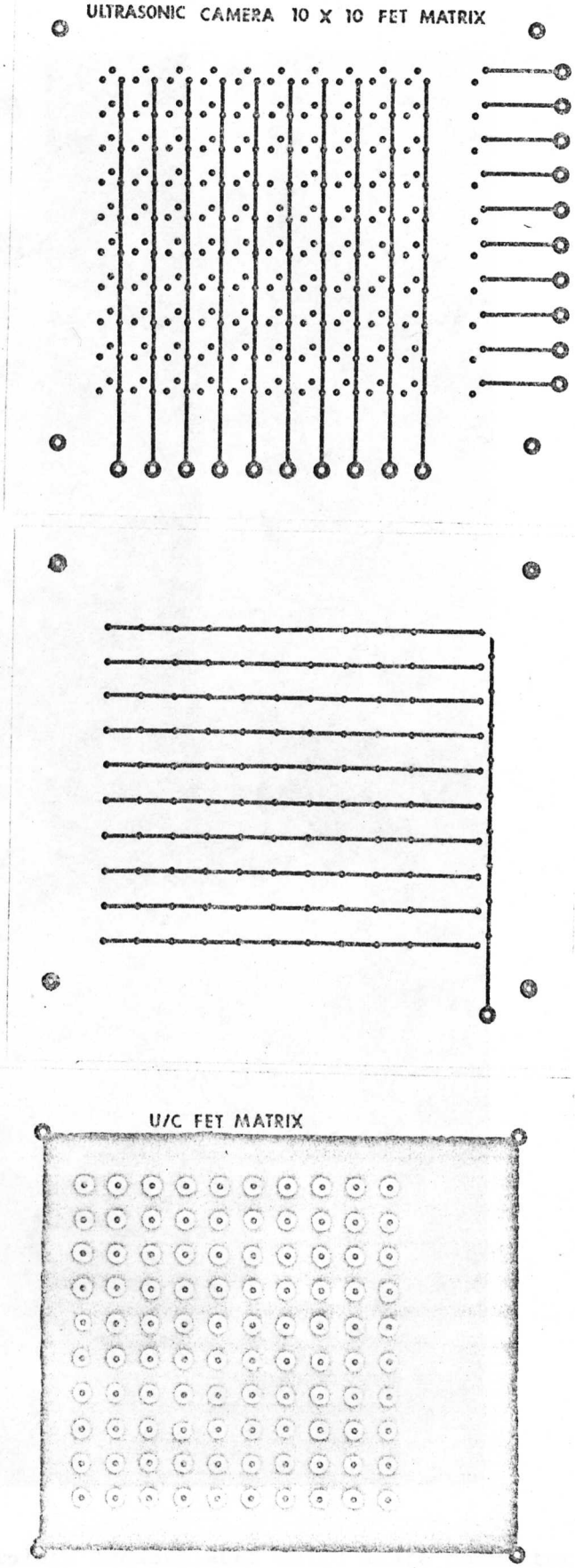

Figure 4.5 Printed circuits for the FET scanning matrix.

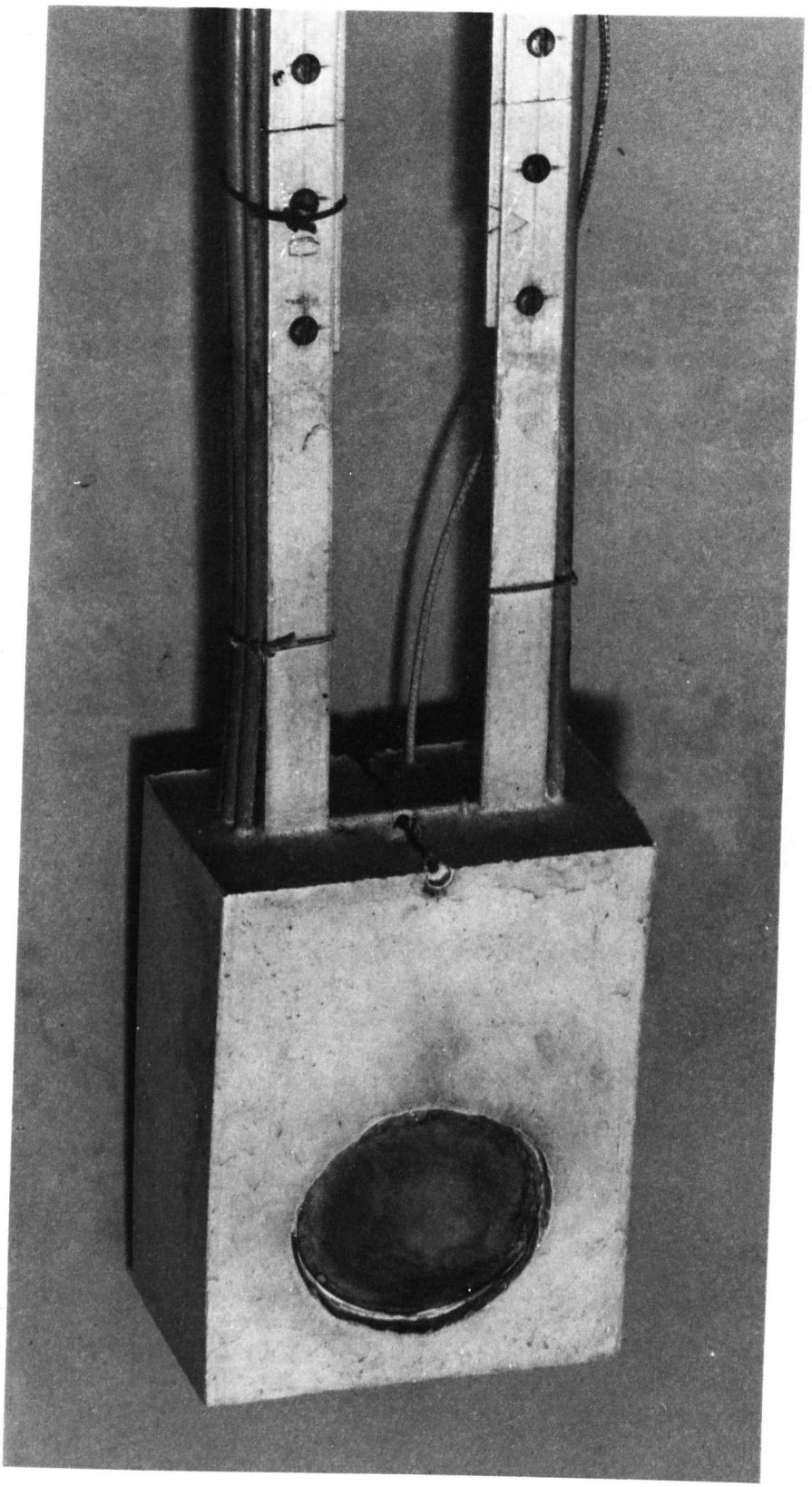

Figure 4.6 The complete encapsulated solid state converter.

The transducer assembly consists of a PZT5 (manufactured by Vernitron Ltd.) disc of 50 mm diameter, thickness resonant at 1 MHz. Both faces have a double layer of fired on silver, but, by request, the special priming layer between ceramic and silver had been omitted so that etching could be carried out. Using a photo-resist technique a pattern of electrodes (figure 4.1) was etched with a ferric nitrate etchant. The pattern includes a small circular electrode to be used as a transmitter for pulse-echo work. The main area consists of a square matrix of one hundred elements, each 80 mil by 80 mil with overall dimensions of one inch by one inch. Low temperature silver loaded solder and a temperature controlled iron enabled one inch long unscreened 32 SWG wires to be attached to each matrix electrode without fear of exceeding the Curie temperature. To insure adequate mechanical strength after soldering a potting epoxy resin was applied to a depth of approximately ½ inch around the wires.

The FET scanning matrix was constructed (figure 4.4) using a multilayer printed circuit (figure 4.5) to form the electrical interconnections between the 110 FET's. The 100 FET source leads to be connected to the transducer electrodes were arranged to project on the under surface so that by positioning the scanning matrix over the transducer assembly the appropriate wires on one could be soldered to those on the other.

Finally, when a supporting frame and all the necessary control and signal wires had been attached, the combined assembly was encapsulated in silicone rubber (Silastoner 70). The final unit measures approximately 90 x 115 x 50 mm (see figure 4.6).

4.4 The Transducer

4.4.1 Choice of Transducer Material

Its high price and the difficulty of obtaining a large enough plate diameter prohibited the use of quartz, but it is of interest to consider

whether the choice, if unrestricted, would have remained with the lead-zirconate-titanate ferro-electric ceramic PZT-5A used. Three properties of the material are important in relation to its application to the image converter. Namely:

(i) its Curie point temperature should preferably allow soldering direct to the transducer metal coating,

(ii) it should have a high receiving sensitivity coupled with a low output resistance in relation to the electrical load,

(iii) the lateral spreading of waves within the transducer should be as small as possible.

Table 4.1

	Quartz x cut.	PZT-4	PZT-5A	PZT-5H	PZT-7A	PZT-8
Curie point temp. ^{o}C	573	328	365	193	350	300
Receiving const. g_{33} 10^{-3} V m N^{-1}	57·8	26·1	24·8	19·7	39·9	24·8
Piezoelectric const. e_{33} C m^{-2}	0·17	15·1	15·8	23·3	9·5	13·8
Mechanical Q	> 25×10^{3}	500	75	65	600	> 10^{3}

Consideration of the various constants given in table 4.1 for quartz and the available PZT materials would immediately exclude PZT-5H owing to its low Curie point temperature. With the exception of PZT-8 it can be seen, as may be expected, that those materials with high mechanical Q's also

have high receiving constants and are therefore more sensitive. In this respect quartz is clearly the best, with PZT-7A next. However it has been suggested[40] that a greater lateral spreading of the waves occurs in materials which possess high mechanical Q's, and on this basis PZT-5A would be the choice, PZT-5H already having been excluded. Further investigation of the lateral spreading phenomenon is needed but it is understood to be closely connected with mode conversion to shear and surface waves within the transducer material (and possibly also within the backing material, if solid). The effective electrical source resistance of the transducer is also an important consideration, since some finite loading due to the amplifier input resistance must be present. The piezoelectric constant e_{33} determines the mechanical to electrical transformation ratio and calculations for both quartz and PZT-5A are given in section 4.4.2 following. They show quartz as having a source resistance more than 4 orders larger than that for PZT-5A.

4.4.2 Source Resistance of Tuned Receiver Element

The back face loading of the transducer elements is virtually incalculable since the depth of solder, araldite and silicone rubber is not accurately known, and in any case varies from element to element. It will therefore be assumed that the element is symmetrically loaded.

The mechanical resistance R_m is given by,

$$R_m = \rho C A \qquad \ldots\ldots \quad 4.1$$

where ρ is the density of the water in kg m^{-3}, C is the velocity of sound in water in m s^{-1}, and A is the transducer element cross-sectional area in m^2. The transformation factor α_T converts the mechanical resistance into the effective electrical source resistance, R ohms, so that,

$$R = \frac{R_m}{\alpha_T^2} \qquad \ldots\ldots \quad 4.2$$

where α_T, a constant for the transducer, is given by,

$$\alpha_T = \frac{A\, e_{33}}{t} \qquad \ldots\ldots \quad 4.3$$

where e_{33} is the piezoelectric stress constant in C m^{-2} and t is the transducer thickness in metres. Combining equations 4.1, 4.2 and 4.3 gives,

$$R = \frac{\rho\, C\, t}{A\, e^2_{33}}\ \Omega \qquad \ldots\ldots \quad 4.4$$

For the PZT-5A experimental transducer array used, A = $6{\cdot}45 \times 10^{-6}$ m^2, t = $2{\cdot}18 \times 10^{-3}$ m and e_{33} = 15·8 C m^{-2}.
For water $\rho\, C = 1{\cdot}5 \times 10^6$ kg m^{-2} s^{-1}. Hence, using equation 4.4, R = 4·4 kΩ. The corresponding source resistance of an element for an equivalent quartz array would be $6{\cdot}5 \times 10^4$ kΩ, this very large difference being caused almost entirely by its low piezoelectric stress constant.

The source resistance of a single tuned element was measured using a resistive load and the half open circuit voltage technique. This gave a value of 4 kΩ ± 10% which compares very favourably with the theoretically derived figure of 4·4 kΩ.

4.4.3 Acoustic Element to Element Cross-Coupling

In order to establish some quantitative information regarding the acoustic coupling between adjacent transducer elements a number of two element receivers were constructed having dimensions identical, as far as possible, to those of the converter transducer matrix. Some were slotted between each section to a depth of approximately half the total thickness in order to determine whether this would significantly reduce the cross-coupling. For reasons of electrical insulation the transducers were encapsulated in epoxy resin, leaving their front faces exposed. Figure 4.7

shows the construction of a slotted test transducer with one element "blanked" by a piece of expanded polystyrene.

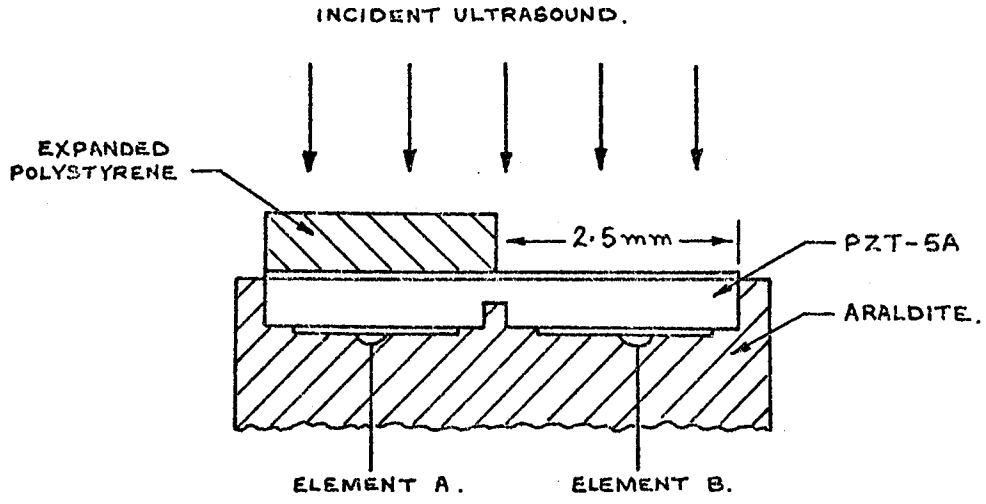

Figure 4.7 Transducer construction for 2nd stage of cross-coupling test.

For the first stage of the testing procedure the transducer front face was completely covered by a thin sheet of expanded polystyrene, immersed in the water bath, insonified and elements A and B output voltages noted. These figures, V_{1A} and V_{1B}, which should ideally be zero, gave an indication of the level of the ultrasonic signal reaching a "blanked" transducer. Next, the second stage, the polystyrene "blanking" was removed from one element (see figure 4.7) and the output voltages again measured, giving V_{2A} and V_{2B}. The cross-coupled signal V_c expressed as a ratio of the "unblanked" element signal V_s is then given approximately by:

$$\frac{V_c}{V_s} \simeq \frac{(V_{2A} - V_{1A})}{V_{2B}} \qquad \ldots\ldots \quad 4.5$$

Results from these tests showed that the completely "blanked" transducer output signals, V_{1A}, may be neglected, being around 0·5 mV, so that

equation 4.5 may be approximated further to:

$$\frac{V_c}{V_s} \simeq \frac{V_{2A}}{V_{2B}} \qquad \ldots\ldots \quad 4.6$$

Table 4.2 lists the results obtained from these measurements.

Table 4.2 Cross-coupling test results.

Test Transducer	V_{2A} mV	V_{2B} mV	Ratio	dB's
1 (slotted)	7·0	32·0	4·6	-13·2
2 (slotted)	7·0	31·0	4·4	-13·0
3 (unslotted)	8·5	36·0	4·2	-12·5
4 (unslotted)	8·4	36·4	4·3	-12·6

It will be noted that slotting between the two elements caused only a slight reduction (< 1 dB) in the cross-coupling. This was to be expected since near homogeneity was re-established by the resin encapsulation.

Since neither a point probe acoustic source nor a point receiver was used it is difficult to interpret the results in a way which enables them to be compared with those of Smyth et al.[5]. However, it would seem that if resolution is in this case defined as an element to element cross-coupling of 50%, then the transducer matrix used should be considerably better than this. Smyth stated the resolution limit for quartz to be approximately the transducer thickness, in this case half a wavelength, but that the use of lower Q materials such as PZT may possibly cause an improvement on this figure. The half wavelength in PZT5A at 1 MHz is 2·18 mm and the element pitch is 2·54 mm, so that a reduction of the latter to about 2 mm would certainly be acceptable if required.

4.5 The FET Sampling Gate

The Union Carbide UC734 (see Appendix B for manufacturer's data), an n-channel junction field effect transistor, is used as the transducer element sampling gate. A gate-source voltage of around 0 volts (V_{ce} sat of drive transistor) with this device provides a sufficiently low channel "on" resistance over the range of signal amplitudes to be sampled, whilst -5 volts adequately switches it "off" (see section 4.5.1). Figure 4.8 shows how these FET gates are interconnected to form the switching matrix or multiplexer. The load on the multiplexer output is tuned to the ultrasonic frequency using the inductance of L and the circuit stray capacitances, and in order to provide a reasonably narrow noise bandwidth this is followed by a common-collector stage. The resulting high impedance load also has the advantage of reducing the effect on the output signal level of channel "on" resistance variations from FET to FET.

4.5.1 Static "on" Characteristics

The static "on" performance is essentially provided by the forward and reverse low level drain characteristics of the device. Typically, for an n-channel junction FET, these will be of the form shown in figure 4.9 below. At small drain-source voltages these curves are well approximated by straight lines passing though the origin, whose slopes represent the "on" resistance for the various gate-source voltages.

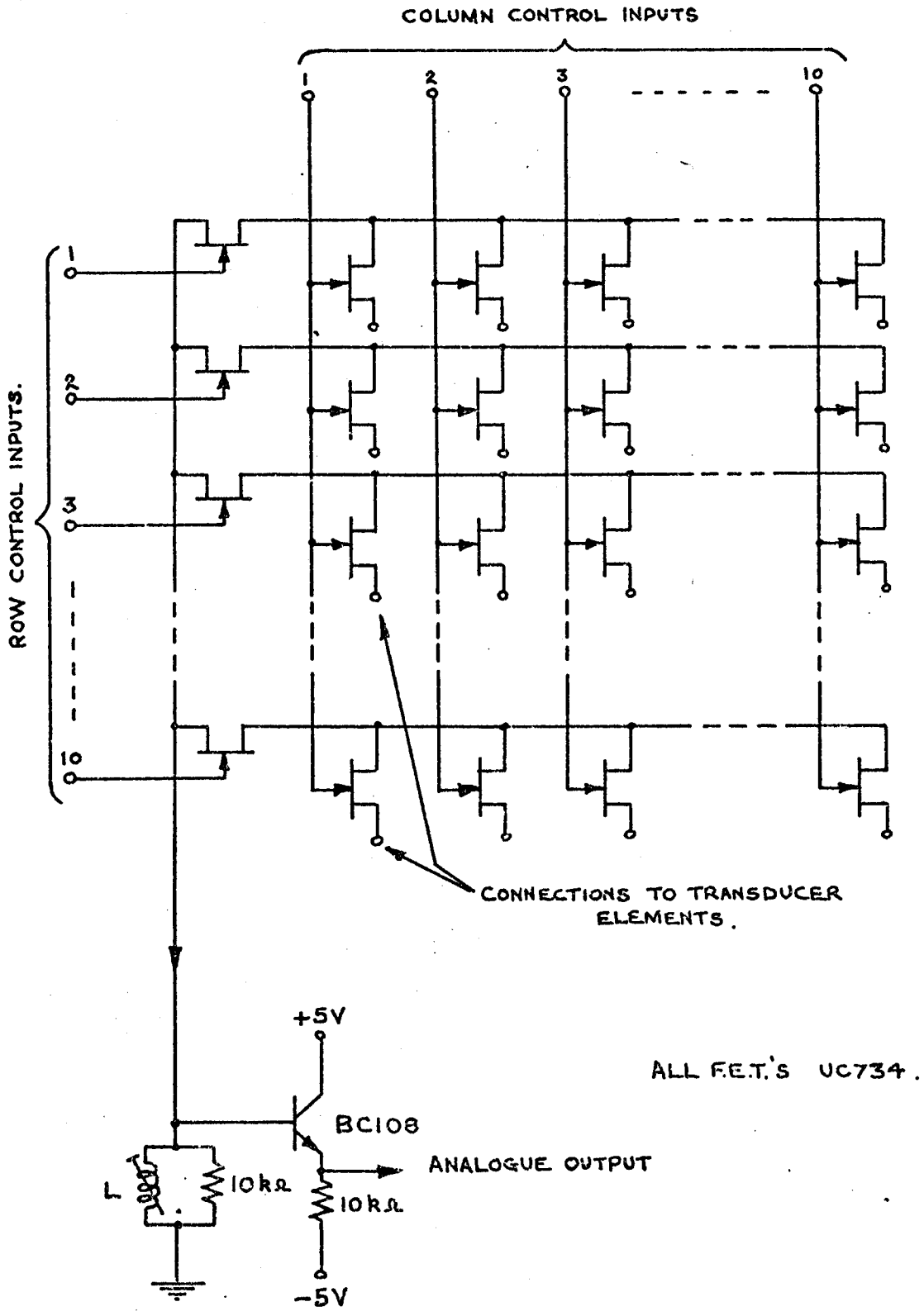

FIGURE 4·8. F.E.T. SCANNING MATRIX CIRCUIT.

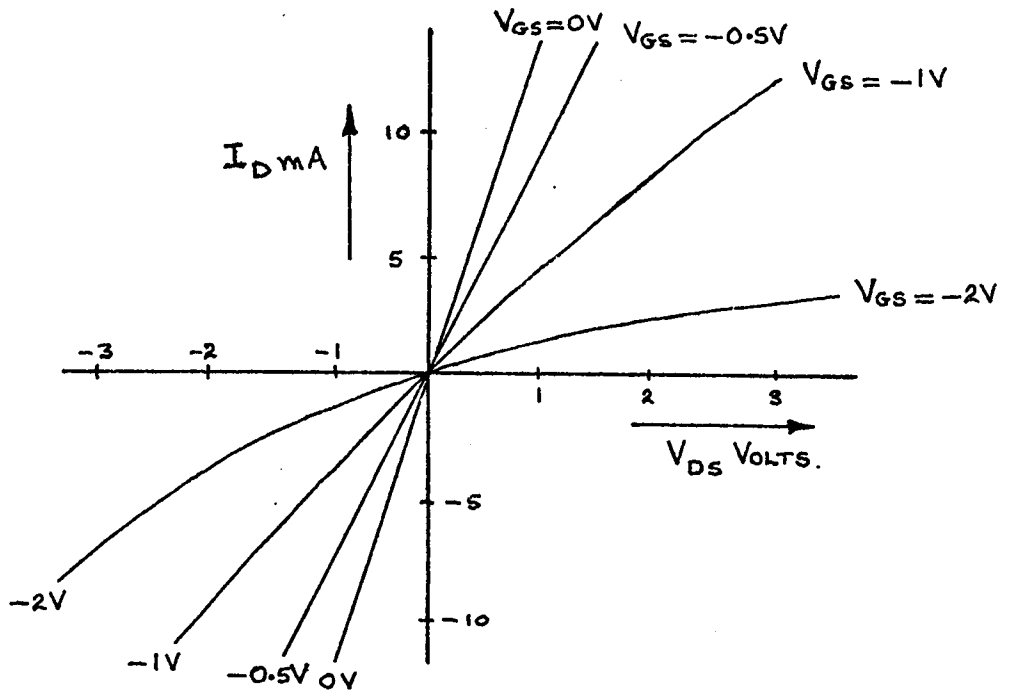

Figure 4.9 Typical low level drain characteristics for an n-channel junction FET.

The simple form of the sampling gate circuit used does not provide, under operating conditions, a constant gate-source "on" voltage. This means that the dynamic drain characteristic will not lie precisely along the V_{GS} = 0 line. Its slope will be slightly more inclined to the horizontal, representing a small increase in "on" resistance, when the sampled signal is positive. When the sampled signal is negative, however, the characteristic will be more inclined to the vertical, representing a small decrease in "on" resistance. This inherent non-linearity may be neglected since in practice the level of the sampled signals would rarely exceed a few mV, and in consequence the static V_{GS} = 0 characteristic is virtually identical to the dynamic characteristic.

The sampling gate is required to transmit, in this application, the transducer element voltage without loss to the common load, and it is therefore the voltage transfer characteristic which provides the information on which the static performance of the gate may be assessed. Using the test circuit arrangement shown below in figure 4.10 the voltage transfer characteristic was obtained and is given in figure 4.11. As far as

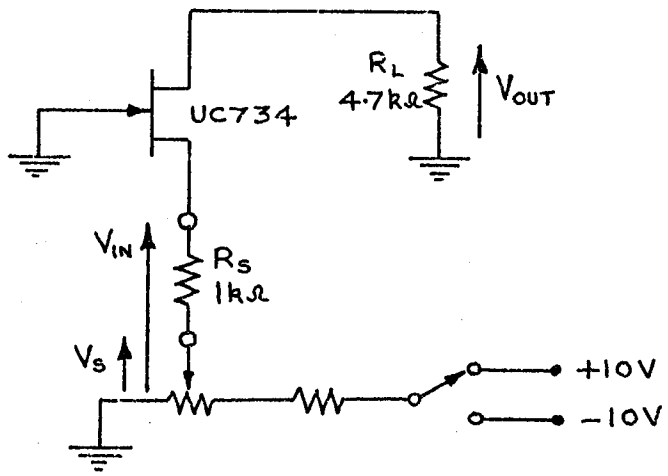

Figure 4.10 Test circuit for voltage transfer characteristic.

possible the test circuit modelled statically an individual converter sampling gate, R_s and V_s representing the source impedance and e.m.f. respectively of a transducer element at resonance, and R_L the total effective load. R_s was somewhat lower than that for a real transducer element, but this does not affect the significance of the results obtained. Reference to figure 4.11 will show that almost perfect bipolar linearity exists up to a source voltage of around 500 mV. At negative voltages greater than this the gate-channel junction becomes significantly forward biased and a large gate current is possible causing loss of signal voltage across R_s. V_{IN} versus V_{OUT}, however, is still linear, but this feature is only of relevance if a pure voltage signal source is available. An estimate of the

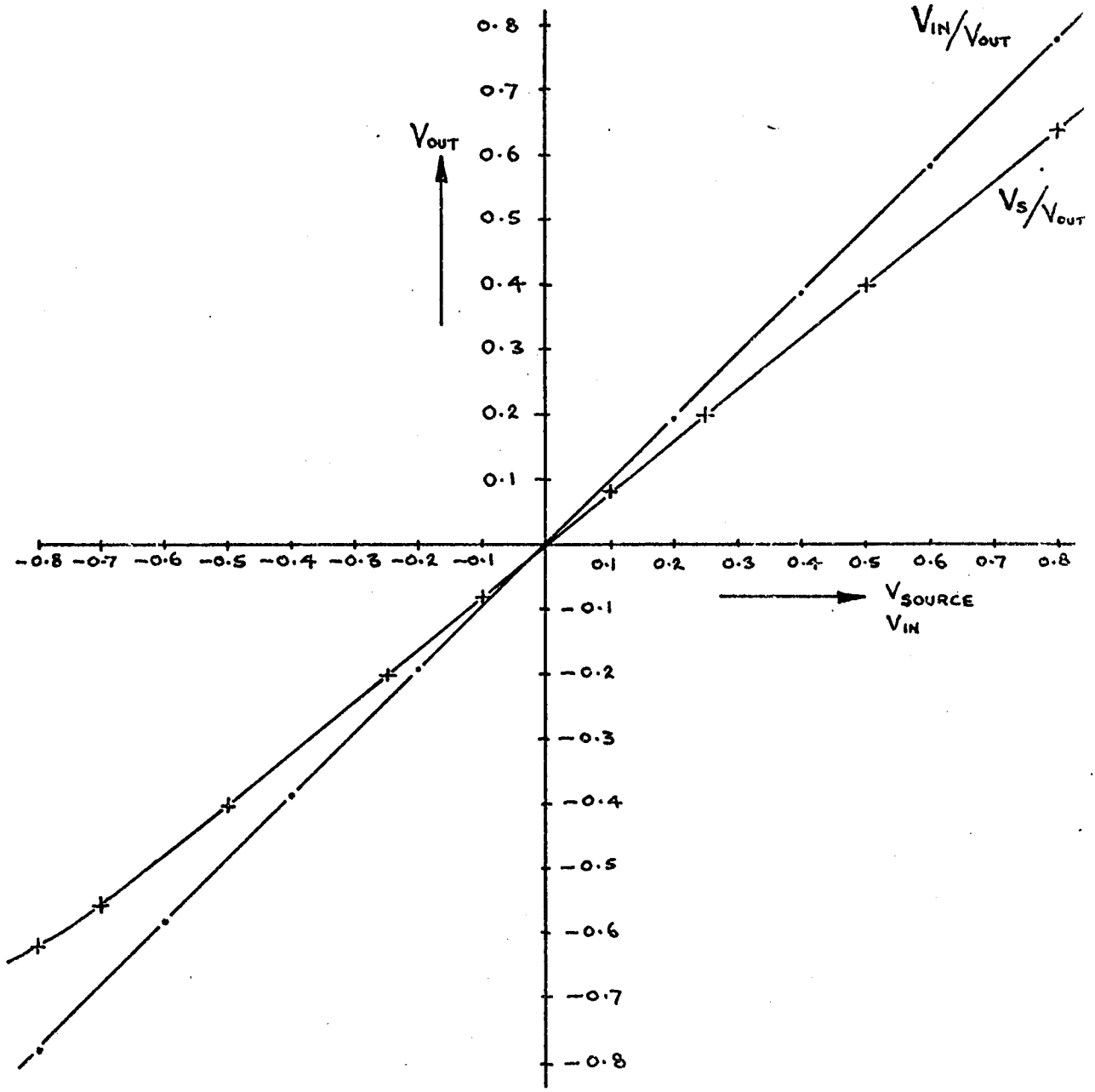

FIGURE 4·11. GATE VOLTAGE TRANSFER CHARACTERISTIC.

channel "on" resistance may be made from these measurements using the relationship:

$$r_{ds}(on) = R_L \left(\frac{V_{IN}}{V_{OUT}} - 1 \right) \qquad \ldots\ldots \quad 4.7$$

and is approximately 150 Ω.

4.5.2 Dynamic "off" Characteristics

The term "gate breakthrough" is defined in this application as,

$$\text{gate breakthrough} \equiv \frac{\text{signal voltage at load with gate "on"}}{\text{signal voltage at load with gate "off"}} \text{ dB's}$$

at constant signal source e.m.f.. It is a figure of merit for a sampling gate, including its source and load circuits, which indicates its ability to prevent the transmission of a signal of given frequency from its source to its load. A test circuit for the measurement of gate breakthrough, equivalent as far as possible to an image converter element, gate and load, is shown in figure 4.12 below.

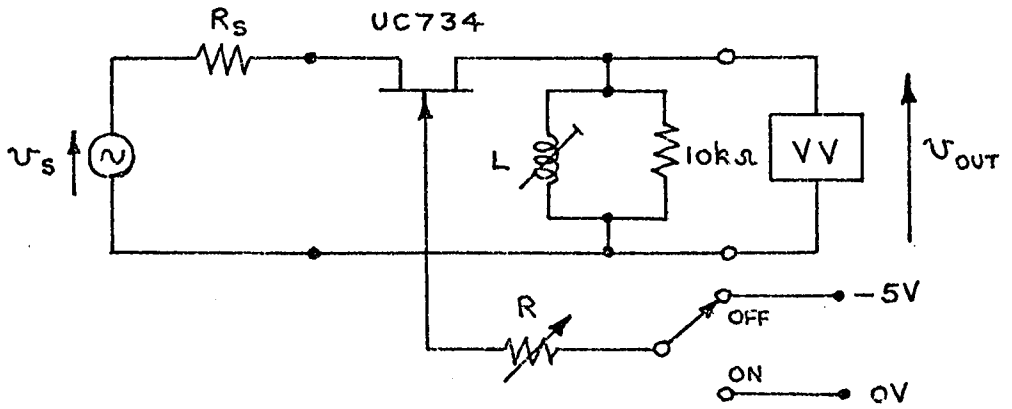

Figure 4.12 Test circuit for gate breakthrough measurements.

As before, R_s and V_s represent the transducer element source impedance and signal e.m.f. respectively. Circuit strays including the valve voltmeter

input and lead capacitance were used to tune the inductor L to a resonant frequency of 1 MHz. With R set to zero and with a signal source frequency of 1 MHz the gate breakthrough was 50 dB's. Increasing R up to 15 kΩ reduced this to 48 dB's, 5 kΩ giving a figure of approximately 49 dB's. It was found, as expected, that a 100 pF capacitor connected between the FET gate terminal and ground brought these back up to 50 dB's. The value of R had no effect on the "on" output voltage. The scanning matrix gates (figure 4.8) are driven by common emitter PNP transistor switching circuits whose emitters are grounded and collector circuits supplied via a 4·7 kΩ resistor from -5 V (see figure 4.14). Thus, unfortunately, the -5 V off drive to the sampling gates has an effective source resistance of 4·7 kΩ, causing an increase in signal breakthrough of around 1 dB per gate. Some improvement would therefore be expected if an NPN drive transistor arrangement were used with the emitters at -5 V. In many respects a better solution would have been to use p-channel FET sampling gates. These could then be driven directly by the TTL control circuits.

Since the breakthrough across an "off" gate is almost exclusively due to drain-source or channel capacitance, measurement of breakthrough at various frequencies was used as a means of estimating this capacitance. Due allowance had to be made in these measurements for the relatively large input and lead capacitance of the measuring instrument. In the equivalent circuit shown below (figure 4.13) C_{OFF} represents the FET source-drain coupling, C_s the total stray capacitance across the load and R the effective resistive load at the output. The relationship, may be derived,

$$C_{OFF} \simeq \frac{V_{OUT}(OFF)}{\omega R V_{IN}} \sqrt{1 + \omega^2 R^2 C_s^2} \quad \ldots\ldots \quad 4.8$$

assuming that $V_{OUT}(OFF) << V_{IN}$. ω is the angular frequency of the applied signal. It has been assumed that C_{OFF} may be considered constant over a

limited range of frequencies and from a series of breakthrough measurements between 10 kHz and 200 kHz a value of C_s was computed to make this so, giving an approximate value for C_{OFF} of 0·10 pF.

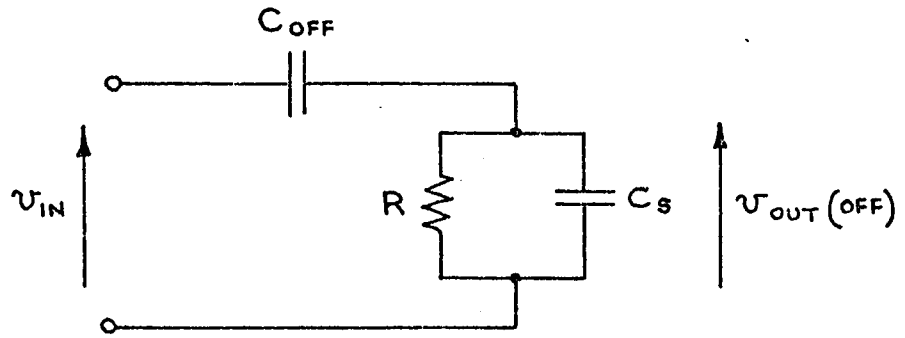

Figure 4.13 Measurement of C_{OFF}.

4.6 Control Circuits

This section describes the shift registers and buffer circuitry used to control the FET switching matrix or multiplexer unit. Details of the specific control circuits required for the complete camera systems are given in chapters 5 and 6.

Figure 4.2 shows in a block schematic form the converter electronic gating with its shift register control. A reset input to the two 11 stage shift registers sets stage 1 in each to a "0" and all other stages to "1". Clock pulses shift this "0" through the horizontal stages, the output of horizontal stage 11 being used as the source of shift pulses for the vertical register. Thus after every 11 clock pulses the vertical register will be shifted by one stage, and 121 clock pulses will complete the cycle leaving a single "0" in stage 1 of each register. Circuit details for one shift register unit are given in figure 4.14. Two of these are required for the system, interconnected as indicated above. Each uses two Texas

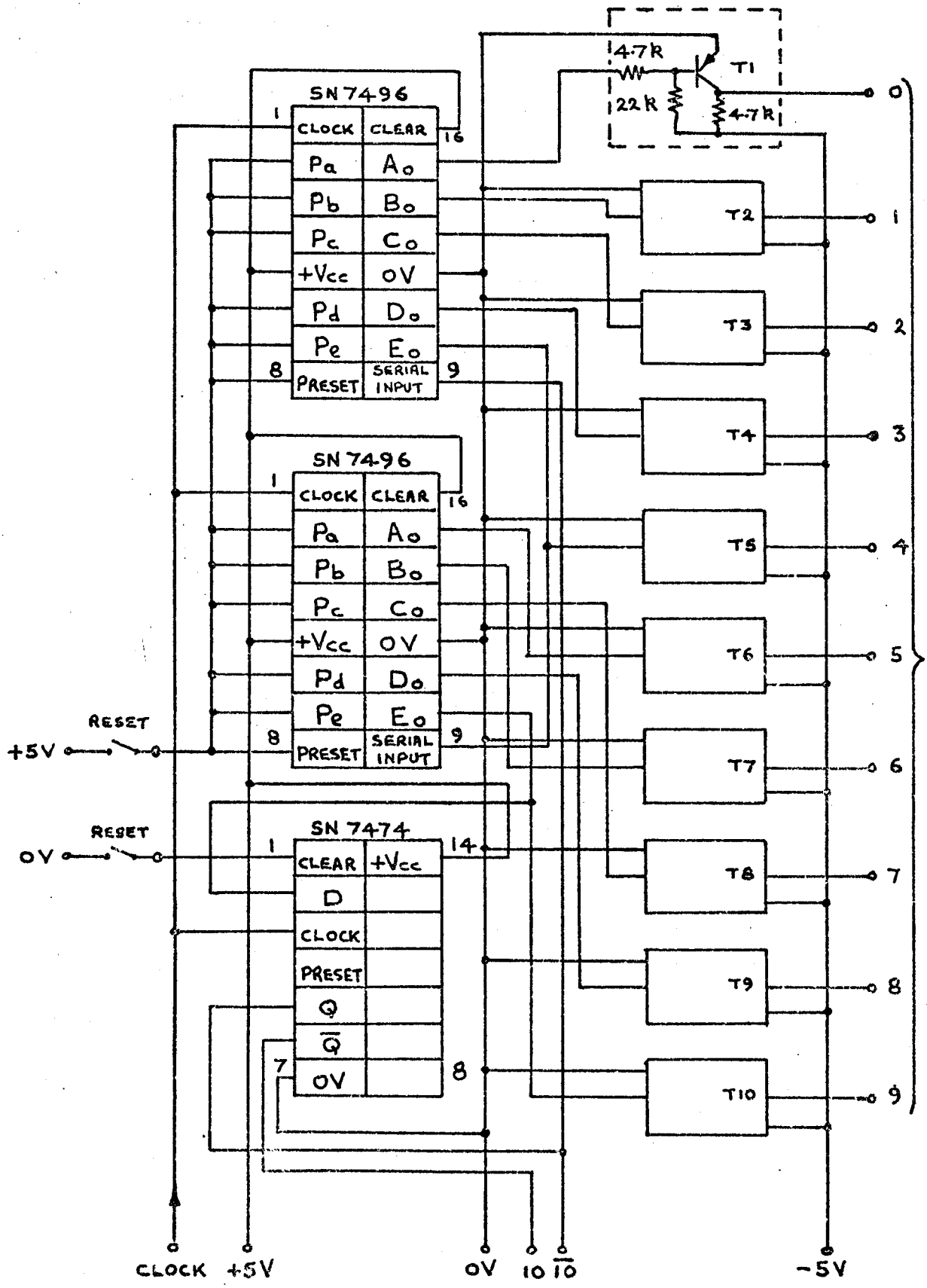

T1 → T10 - 2N3702

FIGURE 4·14 . SHIFT REGISTER CONTROL CIRCUIT.

Instruments SN7496 5 stage shift registers plus one half of an SN7474 D type flip flop. For each of the ten outputs a buffer circuit is included in order to provide the analogue sampling gates with a suitable control signal, the resulting outputs having a base level of -5 V and a peak level of around -200 mV (V_{ce} sat).

4.7 Converter Performance

4.7.1 System Noise

There are four main sources of noise within the solid state ultrasonic image converter; namely:

(i) thermal noise,

(ii) cross-coupling between elements (both electrical through the FET's and acoustic through the transducer and backing),

(iii) unequal element sensitivities,

and, (iv) switching spikes.

Whilst sources (i), (ii) and (iii) are inherent to the system, (iv) may be overcome relatively satisfactorily and very easily by sampling the output at a high enough level between the switching times (see chapter 5, section 5.3.3). The majority of the thermal noise present in the measured output is generated from within the amplifier used (see chapter 5, section 5.3.2) which has a very poor noise figure, 40 dB's, representing 17 μV at its input. Connection of the transducer matrix to the amplifier's input only increases this figure to 20 μV. Source (ii), whilst being relatively significant, is virtually impossible to quantify. The over-all electrical cross-coupling (or cross talk) is measurable but is only meaningful for a specific transducer plate spatial acoustic intensity pattern. This was measured under the condition of equal acoustic intensity over the whole

image plate, and was 40 dB's down on the average direct signal amplitude. This was an inaccurate figure, however, since the cross-talk was only just above the thermal noise level. Source (iii) may be virtually eliminated by careful manufacture of the converter, since it would appear that the unequal element sensitivities must be caused by unequal back-face acoustic loading on the transducer elements. In the present converter most elements lie within a ± 10% range around the average level (see figure 4.15). This introduces a form of noise into the system which can be up to 10 times the thermal noise level.

Wideband noise, which in this case is all thermal, will be affected by the system bandwidth. Since most of the thermal noise is generated within the bandpass amplifier, it is desirable for this unit to possess as narrow a bandwidth as possible, whilst still passing, without significant amplitude distortion, the upper and lower sidebands of the amplitude modulated output wave. Details of this amplifier are given in chapter 5, section 5.3.2. Its measured bandwidth is 140 kHz and any reduction of this is not acceptable if the system is to operate using pulses (see chapter 5).

4.7.2 Sensitivity

The converter sensitivity is directly proportional to the thermal noise in the absence of any sensitivity threshold. The limiting sensitivity is based on a measurement of the output of an average sensitivity transducer element, and will be defined as the acoustic intensity necessary on the converter image plate to produce an electrical output just discernable above the thermal noise. A more practically useful sensitivity figure, however, is the acoustic intensity necessary to produce an output 5 times the thermal noise level. Measuring at the output of the bandpass amplifier gave figures of 20 μV at the transducer for the limiting value and 100 μV for the 5 to 1 signal to noise ratio.

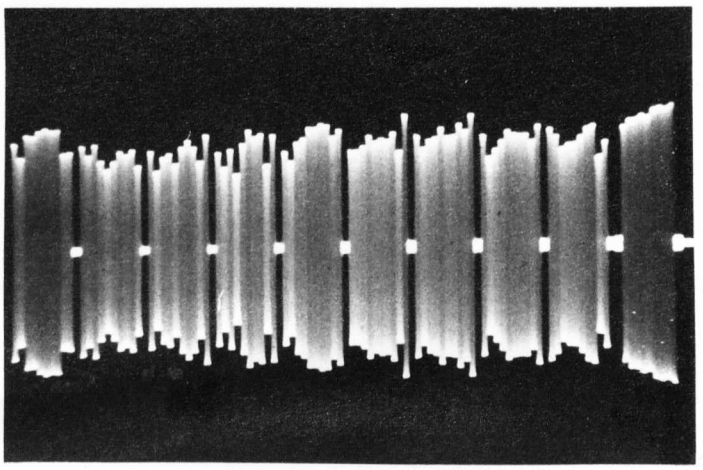

Figure 4.15 Complete 100 element serial output of converter for uniform "illumination"

An estimate of the sensitivity of the converter may be made by using the equation relating the piezoelectric voltage to the acoustic intensity at the transducer surface. Assuming equal front and back face loading (the back-face loading is variable from element to element and incalculable) the piezoelectric voltage, V_s, is given by:

$$V_s = \frac{2\ h_{33}}{\omega_s} \sqrt{\frac{2\ J_x}{\rho\ C}} \quad \text{Volts} \qquad \ldots\ldots \quad 4.9$$

Where h_{33} is a piezoelectric constant giving the electric field produced per unit strain in V m^{-1}, ω_s the ultrasonic angular frequency, J_x the sound intensity at the transducer surface in W m^{-2}, and ρ C the acoustic impedance of the water in kg m^{-2} s. Re-arranging gives:

$$J_x = \frac{V_s^{\,2}\ \omega_s^{\,2}}{8\ h^2{}_{33}} \cdot \rho\ C \cdot \ W\ m^{-2} \qquad \ldots\ldots \quad 4.10$$

A simplified equivalent circuit, figure 4.16, may be drawn representing at resonance the transducer element, the FET channel resistance, $r_{ds}(on)$, and the load R_L:

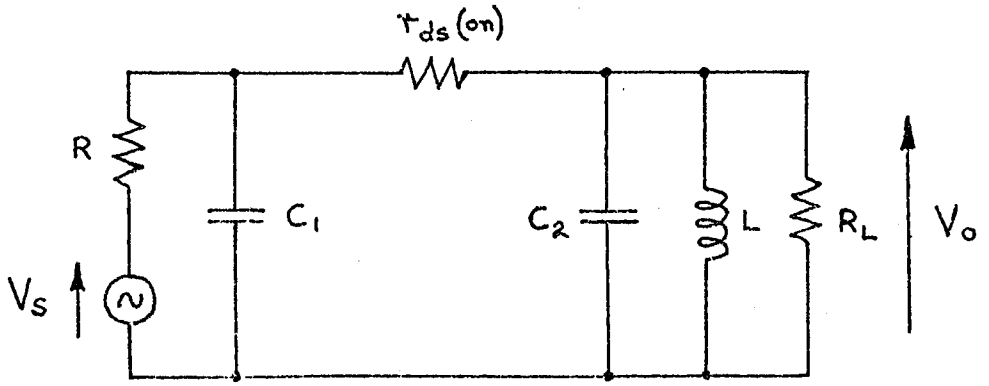

Figure 4.16 Equivalent circuit of transducer element, FET and load.

In practice $r_{ds}(on) << R$ and R_L, so that C_1 and C_2, representing the transducer C_o and various circuit strays, may be considered as a single capacitor $(C_1 + C_2)$. L and $C_1 + C_2$ are made to resonate at the natural mechanical resonant frequency of the transducer, so that the circuit becomes purely resistive. V_o is then given by:

$$V_o = V_s \frac{R_L}{R + R_L} \qquad \ldots\ldots \quad 4.11$$

For the experimental converter, R_L = 10 kΩ and R = 4 kΩ (see section 4.4). Hence $V_o \simeq 0{\cdot}7\ V_s$. Thus equation 4.10 may be rewritten:

$$J_x \simeq 0{\cdot}245 \cdot \frac{V_o^2\ \omega_s^2}{h^2_{33}} \cdot \rho\ C \quad W\ m^{-2} \qquad \ldots\ldots \quad 4.12$$

For PZT5A, $h_{33} = 21{\cdot}5 \times 10^8\ V\ m^{-1}$, $\omega_s = 2\pi \times 10^6$ radians s^{-1} and the acoustic impedance of water $\rho\ C = 1{\cdot}5 \times 10$ kg m^{-2} s.

Using these figures and equation 4.12, the limiting sensitivity, i.e. that acoustic intensity to produce an output voltage of 20 μV, will be,

$$J_x \text{ min} \simeq 1{\cdot}3 \times 10^{-13}\ W\ cm^{-2} \qquad \ldots\ldots \quad 4.13$$

and for a 5:1 signal to noise ratio,

$$J_x \simeq 3{\cdot}2 \times 10^{-12}\ W\ cm^{-2} \qquad \ldots\ldots \quad 4.14$$

4.8 Future Development of the FET Scanned Solid State Converter

The use of a single silicon slice within which a complete 100 x 100 scanning matrix including shift registers is built appears very attractive. Using MOS techniques it would provide a compact, reliable and comparatively cheap system. There are however, two inherent problems which seemingly prevent this method from being practically realisable at present. If a single homogeneous transducer plate is to be used then 10,000 connections

between its electrode matrix and the integrated circuit have to be made where no access is available. Ultrasonic bonding of a such a large number of points over the comparatively large area required is likely to be both difficult and unreliable.

A further problem arises from the fact that conduction paths to carry the gated electrical signals are required to pass from one side of the slice to the other. Some of these paths would be provided by diffusions and these would act as lossy transmission lines at the frequencies required, creating differential attenuation between the various gates and their common output terminal. Mixing at each gate to form a lower or intermediate frequency[11] could reduce the losses to an acceptable level, and if serious attenuation of the oscillator signals supplied to the gates occurred, then the gate circuits could each include a limiting amplifier. Alternatively if phase information is not required then each gate could rectify the signal, but this solution would be at the expense of limiting the applications of the converter.

A hybrid technique involving the use of integrated and film processes could be a satisfactory answer. However, the problem of bonding the 10,000 electrical connections still presents the same difficulties as those expected using large scale integration. Maginness[22] has apparently successfully constructed a converter using this arrangement. Full details on the manufacturing method have not as yet been published but it is clear that a hybrid technique is used.

An ideal solution would appear to involve the use of film transducers. If these could be reliably deposited to the required thickness on the top of a single silicon slice containing all 100 x 100 MOS gates and their associated control circuitry, then connection problems would be completely solved. A further advantage arising from the possibility of discrete

transducer elements would be a reduction of acoustic cross-coupling. Unfortunately, at the present time, film transducers in the 1 to 6 MHz range are difficult to fabricate owing to the thickness required. Overcoming this difficulty, if it is possible, should be the subject of future work.

4.9 Conclusions

Resolution limitations are clearly imposed on the FET scanned converter by the 10 x 10 matrix form, but two other factors have been shown to affect this also; namely, acoustic cross-coupling between adjacent transducer elements and electrical cross-talk caused by signal breakthrough in the "OFF" FET gates. Measurements indicate that the acoustically cross-coupled signal from one element to the next is around -13 dB's, and that the resolution limitation imposed by this is equivalent to a distance marginally less than the transducer plate thickness. Electrical breakthrough is not restricted to adjacent gates but affects a complete line and, to a lesser extent, the common output. For a single typical UC734 gate this was measured as -50 dB's up to 6 MHz, and at 1 MHz in the complete converter, with an evenly spread acoustic intensity over the transducer image plate, a figure of -40 dB's at the amplifier output was obtained. This was near the system thermal noise level.

By far the largest "noise" component in the converter output is that caused by the unequal transducer element sensitivities. For even image plate insonification most element outputs lie within ± 10% of the average signal level. It is thought that this is almost certainly caused by unequal back-face acoustic loading and would be almost entirely overcome in a well designed, carefully manufactured device. Only 15% of the total thermal noise at the amplifier output is generated from within the FET scanned converter. The remaining 85% originates from the amplifier used. Using this

amplifier a limiting sensitivity of $1{\cdot}3 \times 10^{-13}$ W cm^{-2} was estimated, and with a less noisy amplifier this figure would be still lower. The converter, even with the existing amplifier is thus 5 orders more sensitive than published measurements of tube converters.

The further development of this form of converter in which all the FET analogue gates and control circuitry are on a single silicon slice is at present not practically feasible owing to the multiple connections required between this and the transducer matrix. LSI, film hybrid circuitry is one answer but the ultimate solution appears to await the technology to enable the fabrication of suitable film transducers.

5. Ultrasonic Camera Using the FET Scanned Converter with an Acoustic Lens

5.1 System Description

Figure 5.1 shows in a schematic form the acoustic section of the system. To achieve efficient acoustic coupling the transmitter, object, lens and image converter are all suspended in a water filled standard glass fibre water storage tank (approximate dimensions: 4 ft. x 2 ft. x 2 ft.). A photograph of the experimental arrangement is given in figure 5.2. For the majority of tests through transmission is used, continuous or pulsed ultrasound at 1 MHz from the transmitting transducer insonifying the object, which, if of different acoustic impedance to that of water, will introduce discontinuities into the otherwise plane wave front. The object, in effect, may be considered as a re-radiating body and the convergent acoustic lens will focus, if positioned correctly, an acoustic diffraction image of the object on to the face of the image converter.

The overall camera system is outlined in figure 5.3. As may be seen, apart from the image converter, several additional functional blocks are required, the most important of these being the timing unit. This is composed of four delay circuits arranged in series each triggering the next and generating a set of timing waveforms of the form indicated in figure 5.4. The sequence of operation is as follows:

(i) The transmitter monostable is triggered and opens the transmitter gate for approximately 60 μS allowing a burst of ultrasound at 1 MHz to be transmitted down the water tank.

(ii) The rear edge of the transmitter monostable pulse triggers the delay monostable. This delay is adjustable between certain limits and allows time

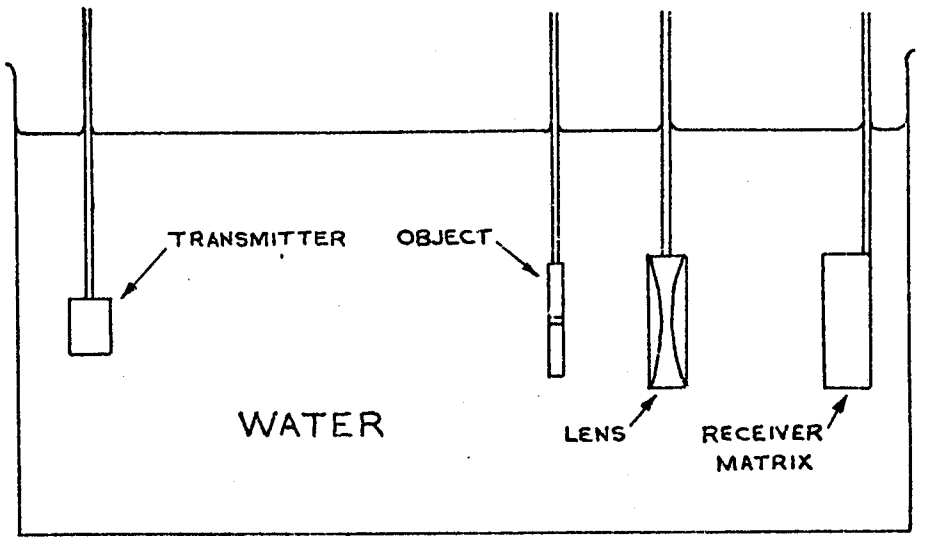

FIGURE 5.1 CAMERA SYSTEM WITH ACOUSTIC LENS

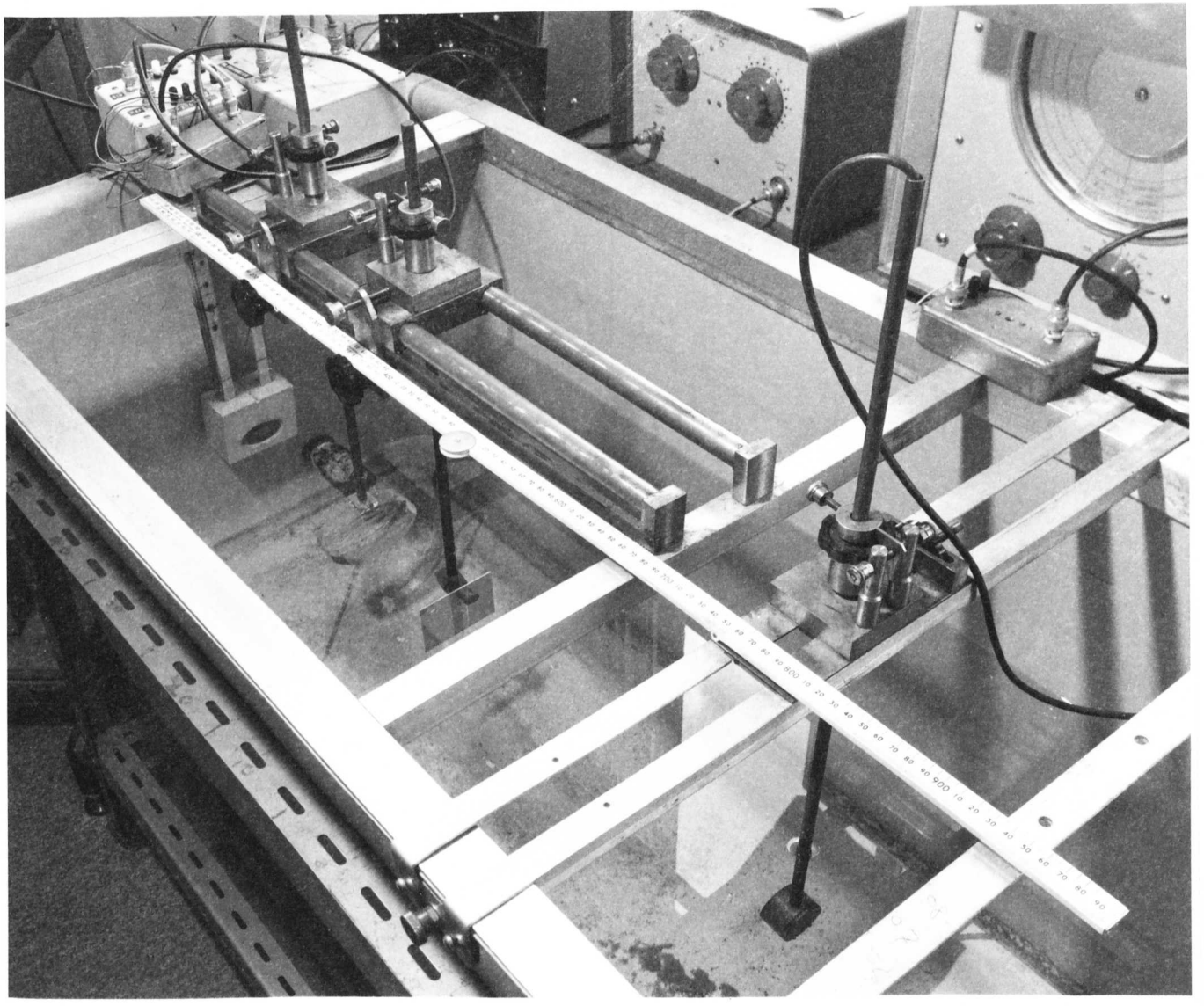

Figure 5.2 The experimental system arrangement.

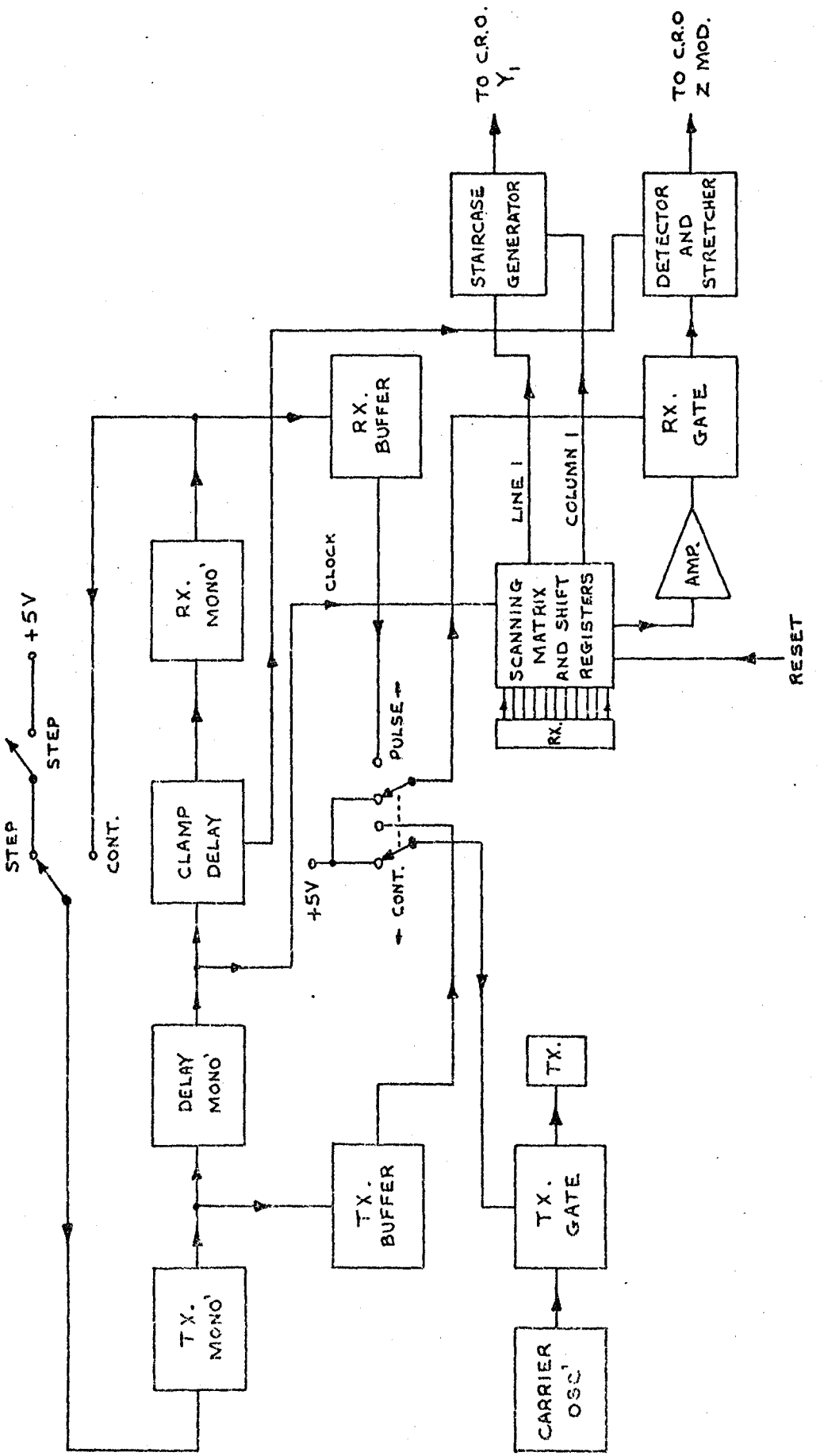

FIGURE 5.3 OVERALL CAMERA SYSTEM

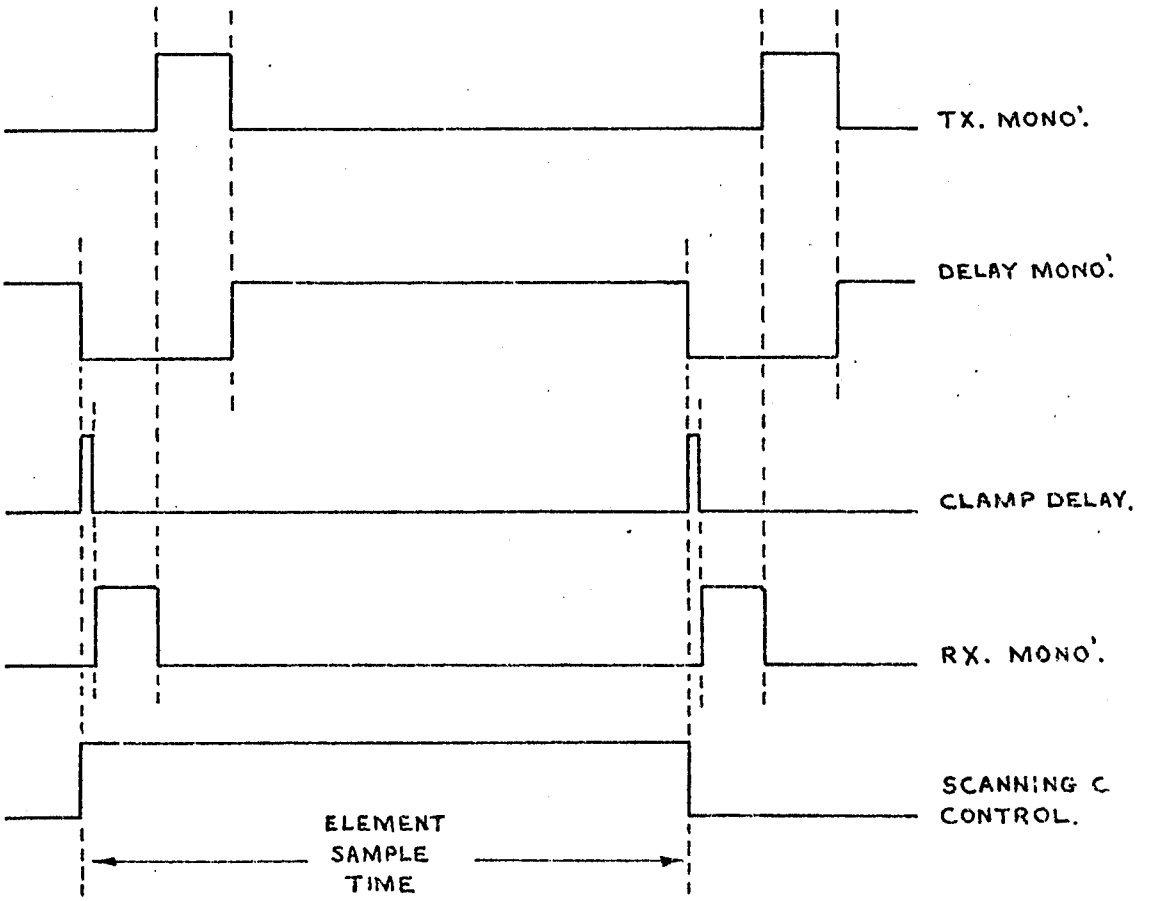

FIGURE 5.4 TIMING WAVEFORMS

for the transmitted pulse of ultrasound to reach the image converter (or receiver). The trailing edge of this timing pulse shifts the matrix scan to the next transducer element and also generates a clamping pulse of approximately 5 μS duration. This clamping pulse is used to reset the detector output to zero and to allow a settling time before sampling the output of the transducer element.

(iii) The trailing edge of the clamp delay pulse triggers the receiver monostable which generates a 30 μS pulse and is used to open the receiver gate. The delay monostable is adjusted until the receiver gate passes only the centre portion of the received transmitter signal and thus largely overcomes any problems which may otherwise arise due to slow rise time, switching spikes, spurious signals, etc. on the received pulse.

(iv) The rear edge of the receiver monostable pulse retriggers the transmitter monostable so that continuous element by element pulsing, scanning and sampling results.

A single shot or stepping facility is provided by breaking the loop connecting the four delay circuits between the receiver monostable and the transmitter monostable, and arranging that a press switch when operated produces a single positive edge so that one complete set of timing pulses is generated. Under continuous operation a minimum element scanning rate

of around 2 kHz results and this will clearly increase as the transmitter-receiver distance is reduced. As a consequence a complete scan of all 100 elements is completed in a maximum time of approximately 60 mS, a resulting picture rate of just under 20 Hz. Continuous wave rather than pulsed operation is achieved by simply holding both the receiver and transmitter gates permanently open.

The bandpass amplifier following the multiplexer unit provides a gain of 70 dB's with a 3 dB bandwidth of 140 kHz. The bandpass characteristic, achieved by means of tuned resonant filters at the input and output of a wide band video amplifier (see section 5.3.2), is used in order to reduce the broad band noise content of the output signal. A bandwidth sufficient to allow the upper and lower side bands of the amplitude modulated 1 MHz carrier is required. This means that in order to retain an acceptable output transient response for pulsed operation a bandwidth of at least 140 kHz is necessary. Since transmitted pulses are of 60 μS duration and are best sampled by the receiver gate over their centre 30 μS, a maximum of 45 cycles at 1 MHz may therefore be allowed for the output to reach its steady state value.

Under pulsed operation only 30 cycles of the 1 MHz signal are available at the output of the receiver gate and therefore the detector must also have a rapid response time. It is followed by a holding or stretching circuit so that a d.c. level, proportional to the incident ultrasonic signal on the sampled matrix element, is maintained until the next element is sampled. This is applied to the intensity modulation input of a cathode ray oscilloscope and a picture is produced by forming a rastor using its own internally triggered time-base together with a specially generated staircase waveform applied to its Y input. In addition to the latter, spot wobble is included so that the resulting ten line picture properly fills the screen area.

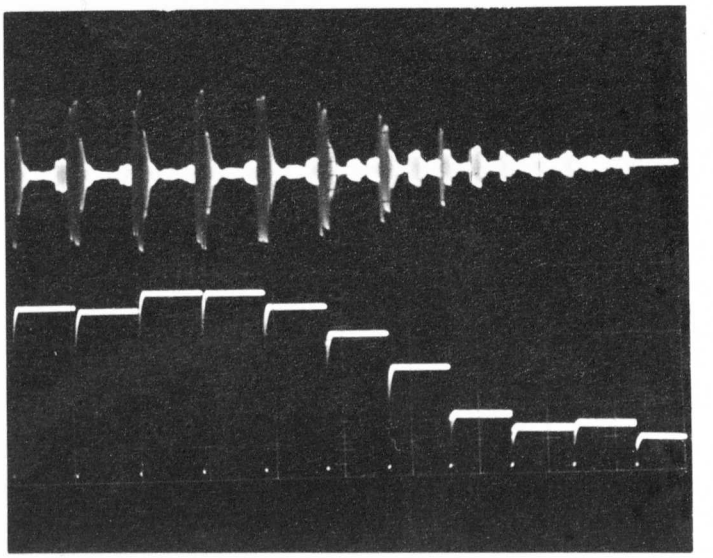

Figure 5.5 (a) Upper trace - Typical output of bandpass amplifier (pulsed mode).

(b) Lower trace - Output of detector for above input.

Figure 5.5(a) shows a typical pulsed mode output of the bandpass amplifier, while 5.5(b) is the receiver gate sampled and detected and stretched result of this signal.

5.2 The Acoustic System

5.2.1 Transmitter Units

A 10 mm disc of PZT-4 (Vernitron Ltd.), of thickness resonance nominally 1 MHz, forms the basis of the transmitter unit, and this is backed by a 3 mm thick disc of expanded polystyrene so that operation is effectively under air backed conditions. A coaxial cable is soldered to the two silvered faces of the transducer and the whole assembly, including a brass support rod, is encapsulated in an epoxy resin. In operation the transmitter has a measured far field 3 dB beam width of around 8^{o}, and a forward to backward transmit ratio of 37 dB's measured on axis at a distance of 200 mm from each face.

A second and larger transmitter unit (described in Appendix A) was used for many of the results included in this and later chapters. This is a 25 mm disc, air backed and mounted in a brass housing. It has the advantage of producing a higher ultrasonic field strength for a given electrical input than the 10 mm transmitter, but owing to the relatively narrow beam illumination of the target is less uniform.

5.2.2 Acoustic Lens

Perspex, readily available and easily formed, was considered, in conjunction with its acoustic properties (see table 5.1), to be the most suitable material for the acoustic lens. The ratio of the acoustic velocities in water and in perspex provides an effective refractive index to ultrasound of 1.8 and requires that for a convergent lens it should be of concave form. The specific acoustic impedance of perspex, however, is just over double that for water and as a result reflections of around 10% at

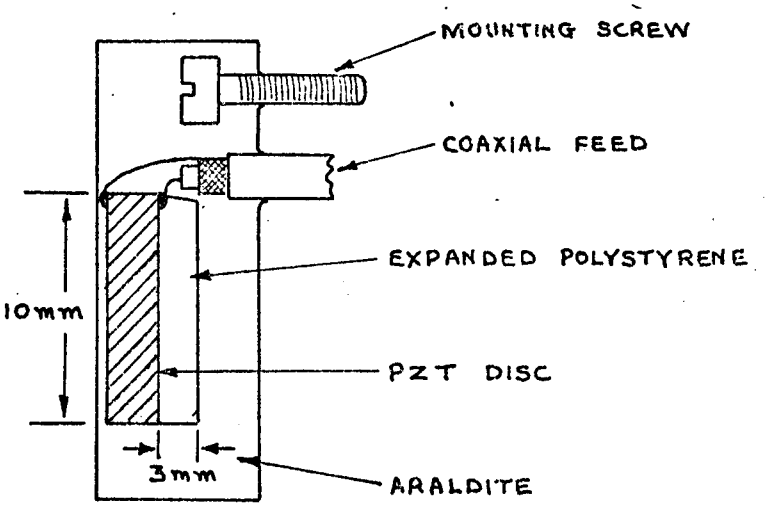

10 mm ENCAPSULATED TRANSDUCER

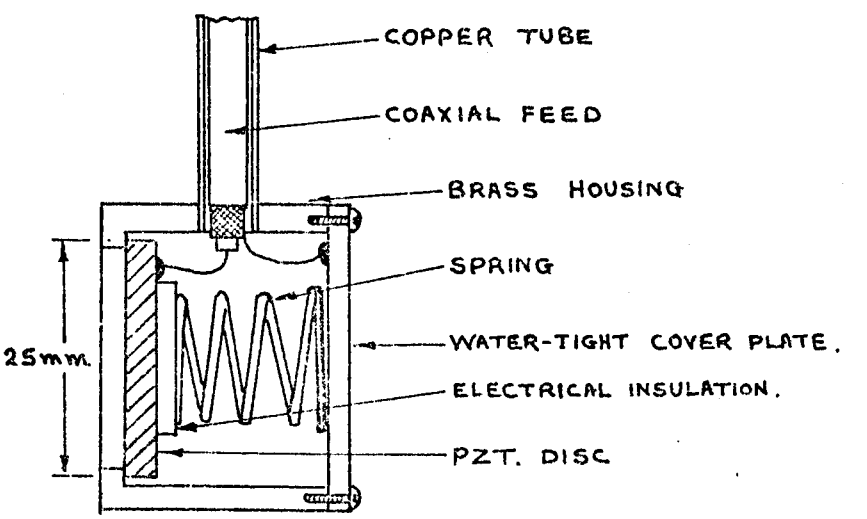

25 mm. AIR BACKED TRANSDUCER

FIGURE 5.6 THE ULTRASONIC TRANSMITTERS (NOT TO SCALE)

both the water-perspex and perspex-water interfaces are to be expected. The design procedure is based on the lens makers' formula and is detailed in Appendix A. A wide aperture is desirable in order to get maximum image "illumination", and using an "F" number of 1.1 and a focal length of 90 mm a radius of curvature of 79 mm and a diameter of 80 mm is found to be required. An aperture larger than this approaches close to the limit set by total internal reflection. The simple spherical design, although introducing considerable image degradation, is relatively easily manufactured using a lathe and an axially mounted tool.

Table 5.1

Material	Specific acoustic impedance m^{-2}, kg, $s^{-1} \times 10^{-6}$	Velocity m, s^{-1}
Carbon tetrachloride	1·48	928
Water	1·49	1,490
Glycerol	2·5	1,986
Mercury	19·6	1,450
Polyethylene	1·75	1,950
Perspex	3·16	2,680
Magnesium	10·0	5,770
Aluminium	17·3	6,420
Iron and steel	46	6,000

Abbe[49] developed a working rule for calculating the resolving power of optical lenses where two points on an object are reflecting largely coherent light. Namely,

$$s = \frac{\lambda}{2 \sin i} \qquad \ldots\ldots \quad 5.1$$

where s is the linear distance separating the two points to be resolved

and i the angle whose tangent is given by the radius of the lens divided by the object-lens distance. Equation 5.1 is based on the assumption that two points will be resolved when the central maximum of the diffraction pattern produced by one falls on the first of the Airy dark rings of the other. Assuming this rule to be applicable to the acoustic case, the resolving power of the acoustic lens used at various magnifications may be calculated. For a magnification of unity the resolution is found to be 2·32 λ or approximately 3·5 mm at 1 MHz. For a magnification of 2 times it becomes 1·76 λ or 2·64 mm, and this approaches a minimum of 1·23 λ as the magnification approaches infinity. According to Sayers[17] the diffraction unsharpness of the image, however, is a relatively small part of the total image degradation caused by an uncorrected lens. Since the lens used is uncorrected spherical aberration alone accounts for an unsharpness of around 3 times that due to diffraction and coma causes serious additional off axis aberrations. Apart from the "optical" effects mentioned above there is a further source of image degradation; that caused by mode conversion as the waves enter and leave the lens. This creates two focal lengths for the lens since the shear waves travel more slowly than do longitudinal waves. The image produced by the shear waves will be relatively weak, and in any case, in a different plane to that produced by the longitudinal waves.

5.2.3 Reflection Tests

A special pulsed oscillator (see Appendix C) was used to investigate the reflections occurring within the acoustic system. This produced, at an adjustable repetition frequency, an acoustic pulse at 1 MHz of duration approximately 8 μS. The test object, lens and converter were positioned as for normal imaging at distances of 515 mm, 670 mm and 855 mm respectively from the transmitter. These distances correspond, at the velocity

of sound in water, to times of 340 μS, 450 μS and 570 μS respectively. Figure 5.7(a) is a photograph of the CRO display of the output of one converter transducer element; the graticule shown represents 100 μS for each major division. Thus the first pulse is positioned at a time corresponding approximately to 575 μS after the start of trace (i.e. 575 μS after the transmitted pulse), and is clearly the direct signal. The second pulse of any consequence occurs at a time of around 780 μS and was found to be caused by the test object (an aluminium plate through which a cross had been cut). By calculating the total transit time it can be shown that this signal is the result of the transmitted pulse passing through the test object, reflecting off the lens back to the test object and off the test object and back through the lens to the converter. Referring to figure 5.7(a) again it will be noted that next there is a pair of pulses about 15 μS apart and positioned at approximately 840 μS after the transmitted pulse. It was determined experimentally that these were caused by the lens, and again by estimating the total transit time it is evident that a reflection back off the converter transducer reflects again off the lens back to the converter. It is not clear why a double pulse occurs here, since the 15 μS represents 40 mm in perspex and the second pulse is therefore not likely to be a reflection off the other surface of the lens, which in any case if it were would be expected to be of lower amplitude than the first. A reflection from the back of the tank to the lens and back to the converter transducer is likely, but again does not correspond to the observed time difference between the two pulses.

Figure 5.7(b) is the result of a similar test, but with the lens and object removed and the transmitter moved nearer to the converter. The first pulse is the direct signal while the second and third pulses are reflections from the transmitter of pulses reflected off the converter and the tank back-wall respectively.

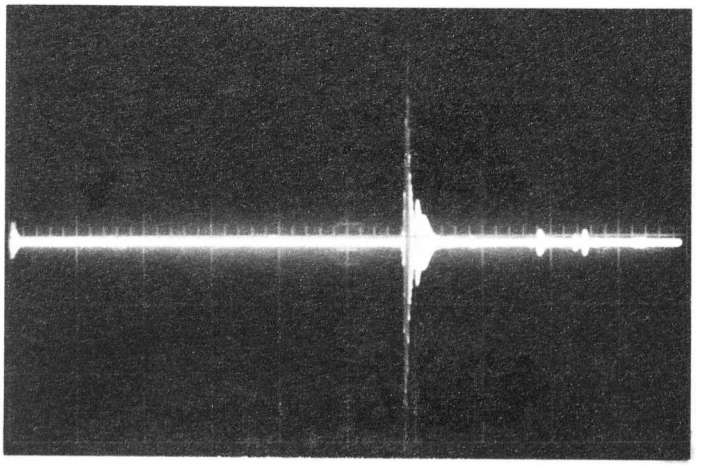

Figure 5.7(a) Reflections, with lens and test object positioned as for normal imaging.

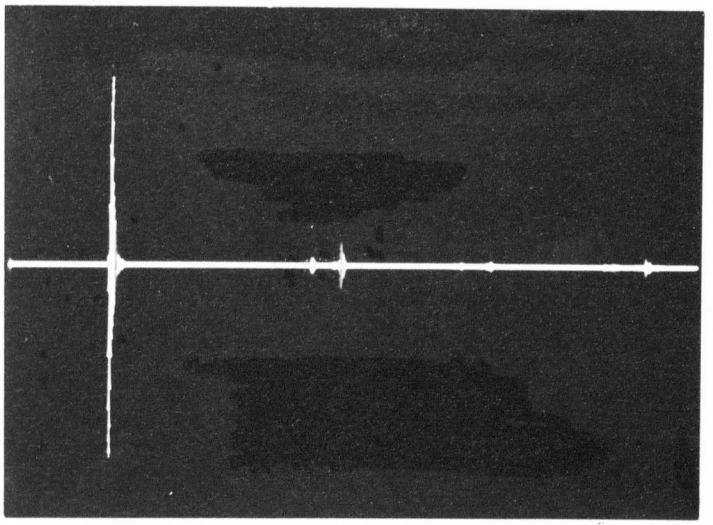

Figure 5.7(b) Reflections, with lens and test object removed.

The significance of these results in the context of the camera system is that they confirm experimentally the order of magnitude of the various reflections which occur. Continuous wave operation, and pulsed operation where these are of longer duration than the time separation of interfaces within the acoustic system, will generate standing waves and interference effects causing a general loss of image definition. The results show that observable reflections arriving back at the converter are less than 10% of the amplitude of the direct pulse, but they do not show the effect of reverberations within the test object, lens and converter. To investigate this experimentally would require a considerably shorter pulse in order to provide sufficient resolution.

5.3 Circuit Details

5.3.1 Timing Unit

Three SN74121 TTL monostables form the major part of this unit, the circuit of which is shown in figure 5.8. Between the delay and the receiver monostables is interposed the clamp pulse generator. This is basically a single transistor switch, T_2, biased "off" by R_5 to +5 V followed by a d.c. restorer (C_4, D_4 and R_8) to 0 V and an emitter follower T_3. D_3 prevents T_2 base from being more positive than approximately 500 mV and allows the negative spike, formed by the back edge of the delay monostable output and C_3, R_6, etc., to drive T_2 into saturation for around 5 µS. T_2 collector therefore produces a 5 µS pulse based on -5 V and rising to nearly 0 V, a level required for the clamping necessary in the detector unit (see 5.3.3). Restoration to normal TTL levels is required before this can be used as an input to the receiver monostable. Thus the pulse at T_3 emitter is of 5 µS duration based on approximately 0 V and rising to around +5 V. Transistors T_1 and T_4 buffer the outputs of the transmitter and receiver monostables respectively and create a level shift

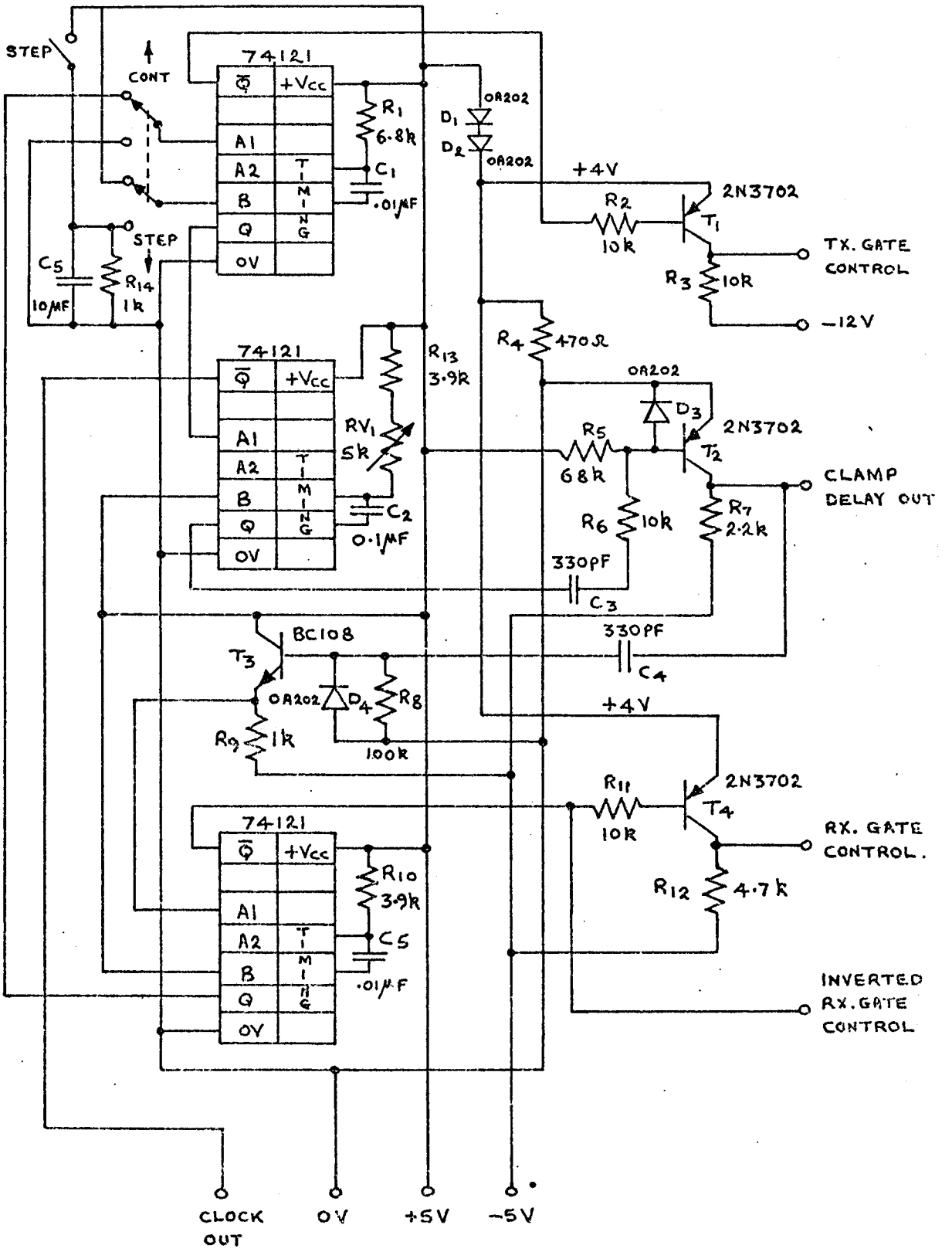

FIGURE 5.8 TIMING UNIT CIRCUIT DIAGRAM.

so that they may effectively drive the transmitter and receiver n-channel FET gates (see 5.3.3). D_1, D_2 and R_4 provide a supply rail of approximately +3·8 V to which T_1 and T_4 emitters are connected thus ensuring that the latter are properly switched "off" by a "1" output from their respective monostables. With switch S_1 in the "step" position the feedback loop around the timing circuits is broken. At the same time the positive Schmitt B input to the transmitter monostable is connected to a circuit designed to produce slow positive edges when press switch S_2 is closed. The recovery time of this circuit is slow (approximately $\frac{1}{10}$ S) in order to minimise the effect of any switch bounce. Potentiometer RV1 provides the necessary adjustment to the delay monostable pulse duration.

5.3.2 Bandpass Amplifier

Figure 5.9 is the circuit diagram of the bandpass amplifier. It is essentially a video amplifier with a gain of approximately 70 dB's from 10 Hz to 10 MHz with an input bandpass L.C. filter tuned nominally to 1 MHz. Two cascaded Texas SN7510 wide band video amplifiers are used to provide the overall gain, while T_2, D_1 and T_3, D_2 form the d.c. level shifting circuits necessary in order to bring the output approximately to 0 V when the input terminals are short circuited. Considerable d.c. feedback, provided by R_4 and R_7 decoupled by C_1, and R_{11} and R_{14} decoupled by C_3, around the two amplifier sections maintains this to within 16 mV. R_8 and C_2 form a simple lag network and are included to assist high frequency stability. They introduce an additional ~~pole~~ break point into the ~~transfer function~~ frequency response at 10·6 MHz, this being sufficiently low to prevent oscillation yet high enough not to reduce the bandwidth below that required (a design requirement on bandwidth of 10 MHz was used so that this amplifier could be used for possible future experimental work at higher frequencies). T_1, R_2 is an emitter follower which increases the effective input resistance of

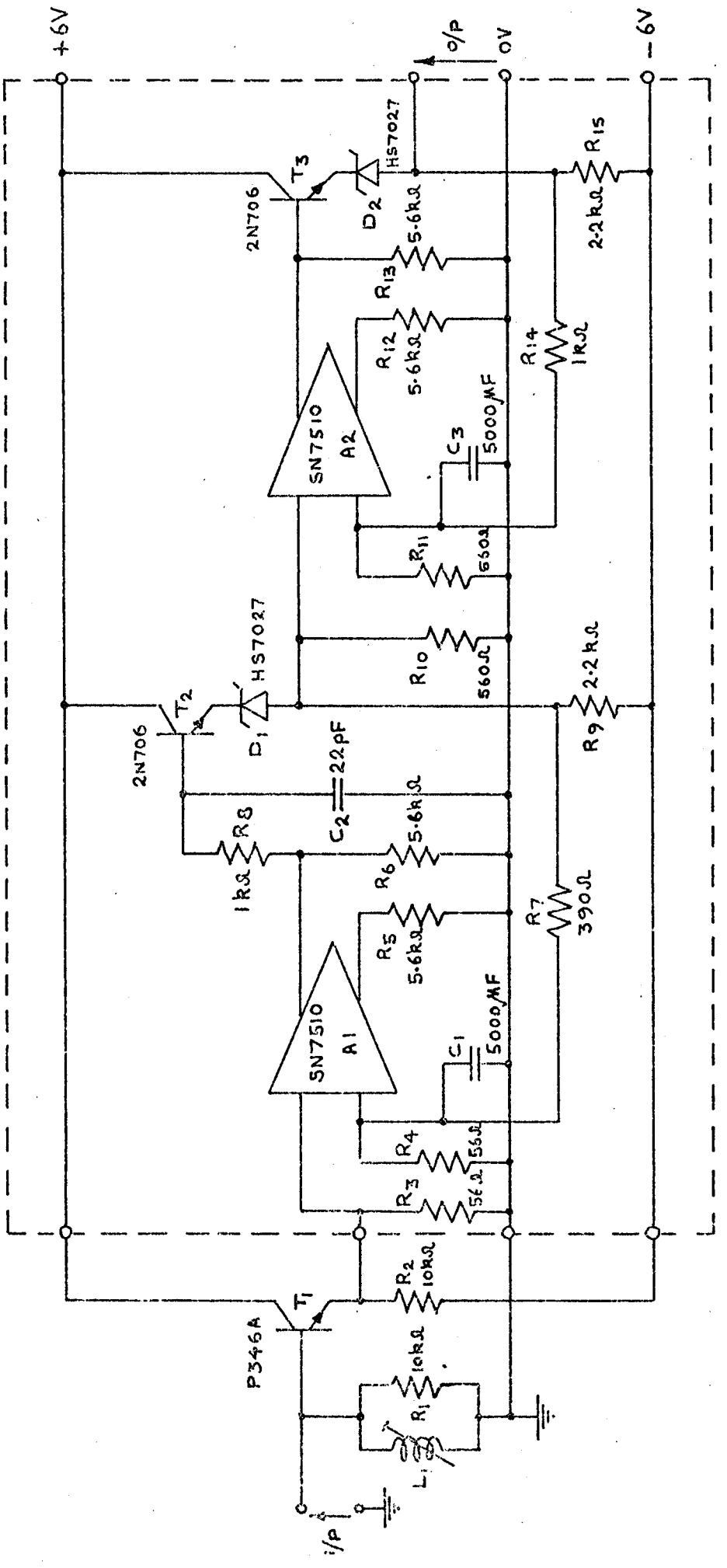

FIGURE 5.9 BANDPASS AMPLIFIER CIRCUIT DIAGRAM

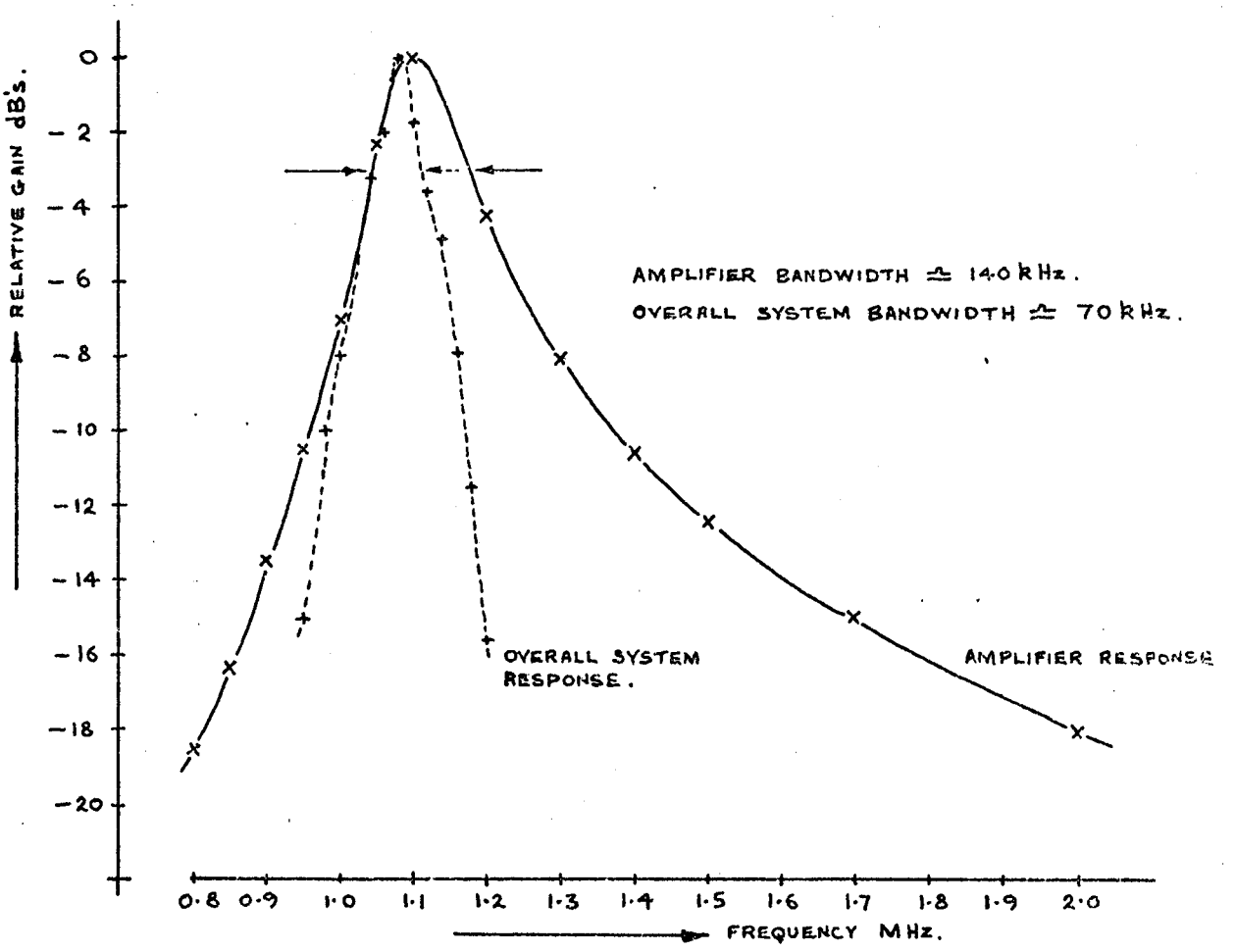

FIGURE 5.10 FREQUENCY RESPONSE OF BANDPASS AMPLIFIER.

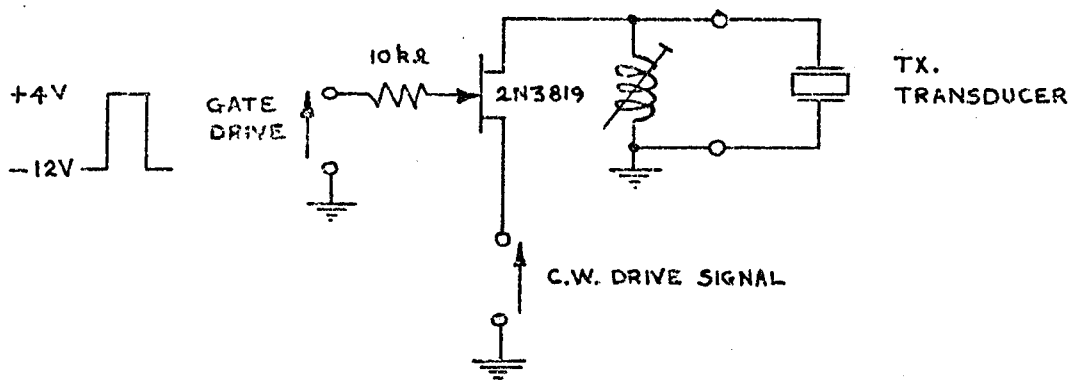

FIGURE 5.11 TRANSMITTER GATE CIRCUIT.

the amplifier to approximately 5 kΩ, reducing to a satisfactory level the transducer element and input filter loading. Power line decoupling (not shown in figure 5.9) is included at each stage of the amplifier using 0·1 μF capacitors, and the complete unit was constructed on a double sided printed circuit board mounted in a metal box. An output bandpass L.C. filter is also included within the overall amplifier but is physically located, for reasons of stability, in the detector unit (see 5.3.3). The frequency response, including both bandpass filters, is shown in figure 5.10, and it may be noted that maximum gain, 46 dB's, is provided at 1·1 MHz this being the apparent resonant frequency of the receiving transducer elements. The 3 dB bandwidth is 140 kHz, and the measured noise figure 40 dB's, representing 17 μV at the input.

5.3.3 Transmitter and Receiver Gates and Detector Unit

Both the transmitter and receiver gates each consist primarily of an n-channel junction FET operated in either its "on" or "off" state. Figure 5.11 shows the transmitter gate circuit including the transmitting transducer. The inductor L is arranged to resonate with the circuit strays and self capacitance, C_o, of the transducer and it thus presents a high impedance at the operating frequency whilst maintaining a near short circuit at d.c. This assists towards the production of a good transmitted pulse shape, particularly the trailing edge, where otherwise a long fall time would result. The gate drive, provided by the timing unit, is a 60 μS pulse based at -12 V and rising to approximately +3·8 V. This means that signals with a peak amplitude of approaching 4 V may be successfully gated by the circuit.

The detector unit may be considered as comprising of three main sections: a bandpass filter (really part of the bandpass amplifier - section 5.3.2), a sample and hold detector and a d.c. amplifier. The

complete circuit is given in figure 5.12. The simple bandpass filter, L_1 C_1, rejects noise outside its pass band which has been introduced by the video amplifier. D_1 and D_2 in series with L_1 and fed by R_1 cause a d.c. offset voltage of around +1·2 V on the base of T_1. T_1 is an emitter follower included in order to provide both a low impedance source to the diode detector which follows and a high impedance load to the filter. T_1 emitter is offset by +600 mV and, assuming negligible drop across the receiver gate, will give a forward bias to D_3 sufficient to ensure that it is on the verge of significant conduction. In this way the detector is made to respond to very low level signals. The measured input-output voltage transfer characteristic is given in figure 5.13a, from which it can be seen that although somewhat non-linear at low levels, it will respond to input signals in the order of 10 to 20 mV. Attempts were made to overcome the diode offset voltage and inherent non-linearity by including it in the feedback loop of an operational amplifier, but the transient response and in particular the slew rate was not fast enough to enable this arrangement to function effectively at 1 MHz. The receiver gate T_2 between T_1 and the peak detector circuit D_3 C_3 is driven by a gating pulse provided by the timing unit of duration 30 μS, based at -5 V and rising to +3·8 V. The maximum expected signal level at this point is approximately 1·5 V peak and will thus be adequately handled by the gate. T_3 is the clamping transistor which discharges C_3 before the next element is sampled and in effect therefore performs the function of resetting the detector. It is driven via R_5 by the 5 μS clamp delay pulse generated in the timing unit. T_4, a source follower, reduces the effect of any loading on the circuit which would otherwise significantly discharge C_3 during the hold period. An integrated circuit d.c. amplifier (741) with shunt feedback follows T_4 and provides an adjustable gain (RV2) of up to approximately 10 and an adjustable d.c. level facility (RV1).

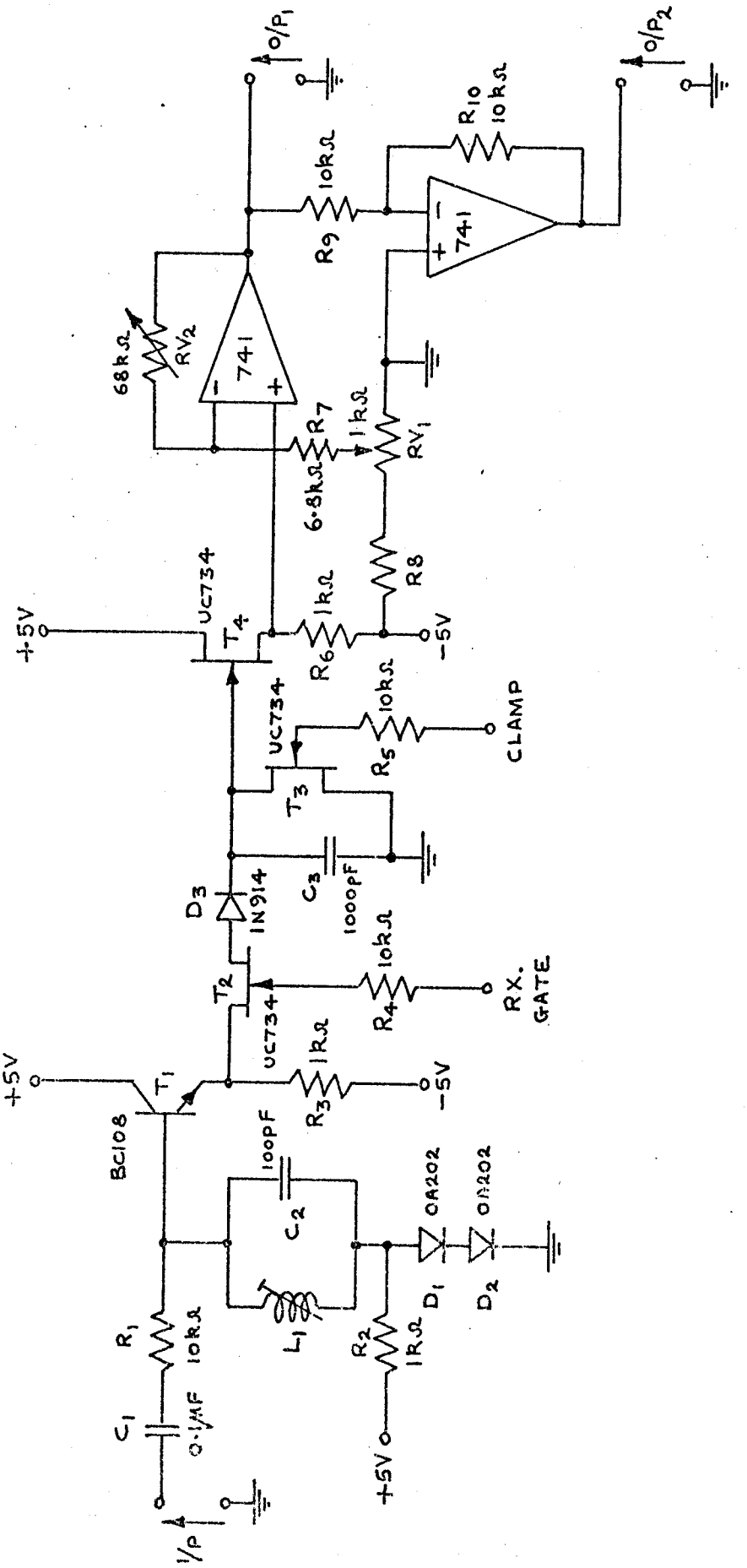

FIGURE 5.12 DETECTOR UNIT CIRCUIT DIAGRAM.

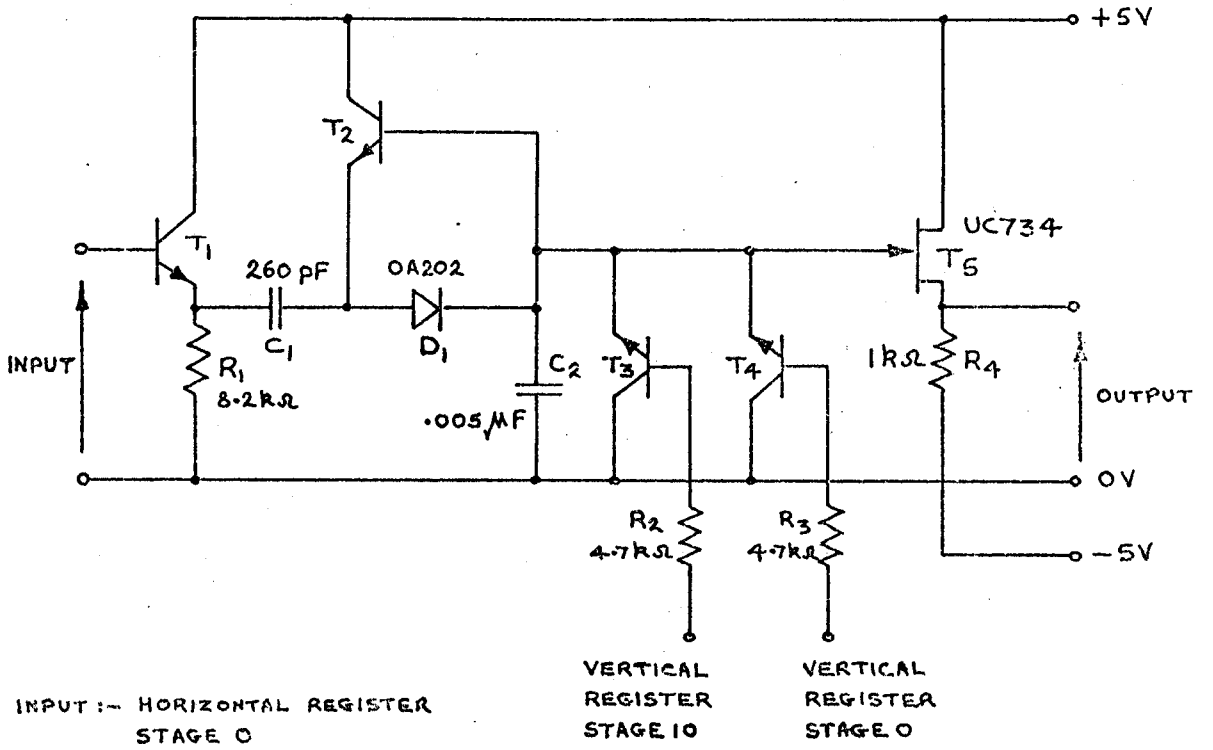

FIGURE 5.13 STAIRCASE GENERATOR CIRCUIT.

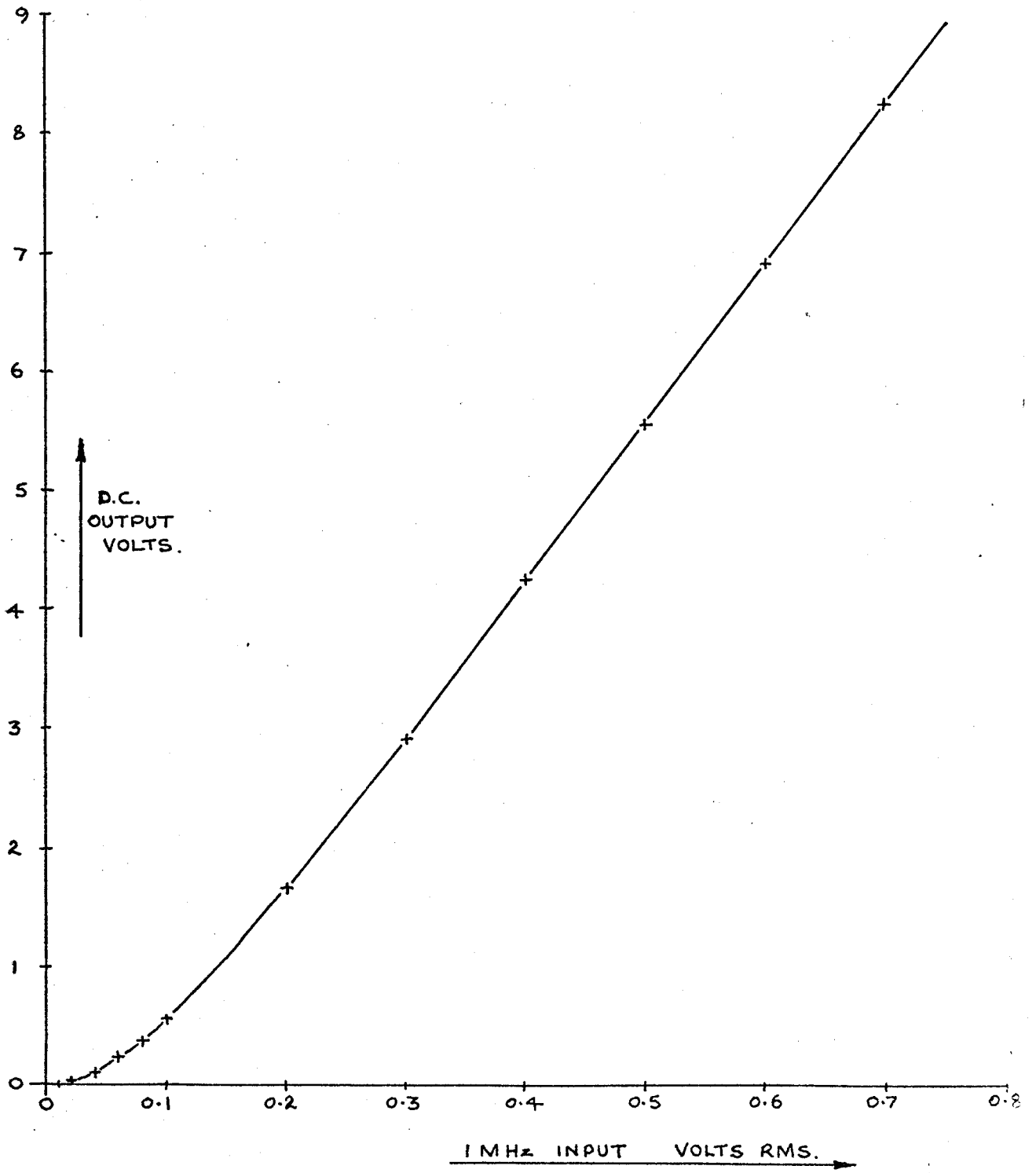

FIGURE 5.13 a. DETECTOR CALIBRATION CURVE

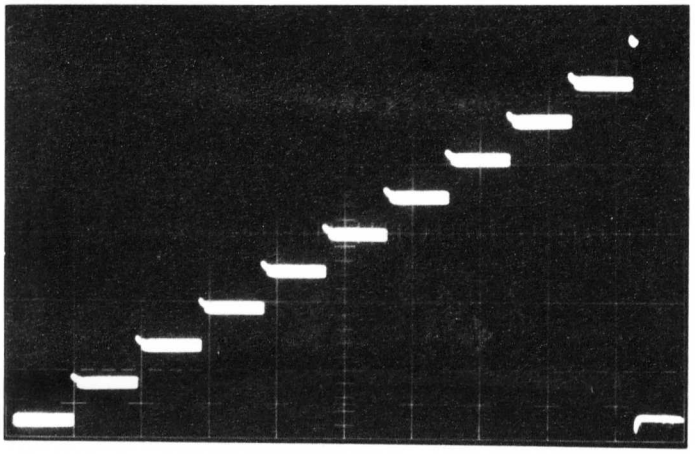

Figure 5.14 Staircase generator output waveform.

5.3.4 Staircase Generator

Operation of the circuit, figure 5.13, is basically similar to that of a diode storage counter, except that in this case when T_2 conducts it clamps the anode of D_1 to the voltage on C_2. This causes the next input pulse, via the emitter follower T_1, to be added to the existing voltage on C_2 resulting in a reasonably linear staircase voltage waveform at the output of the source follower T_5. Ten steps are required in order to produce the ten line oscilloscope raster, after which resetting is carried out by the clamping transistors T_3 and T_4 using the vertical shift register stage outputs 0 and 10. The output step amplitude V_s is given by,

$$V_s = V_i (1 - x) \qquad \ldots\ldots \quad 5.2$$

where V_i is the input pulse height, and x is given by,

$$x = \frac{C_2}{C_1 + C_2} \qquad \ldots\ldots \quad 5.3$$

5.4 Results

Figures 5.15(a) and (b) are results for a uniformly "illuminated" converter face plate, the former showing the amplitude modulated serial output signal for the 100 transducer elements, and the latter the visual picture produced by these signals on the CRO display. Although the serial output is shown for clarity using continuous waves, the visual picture, figure 5.15(b), was produced using pulsed transmission in order to reduce possible reverberations. Once again the transducer element sensitivity variations are clearly demonstrated, but a more important use to which these pictures may be put is that of accounting for some of the visible "noise" present on the images of the various test objects. They also provide an indication of the sensitivity and dynamic range of the electrical

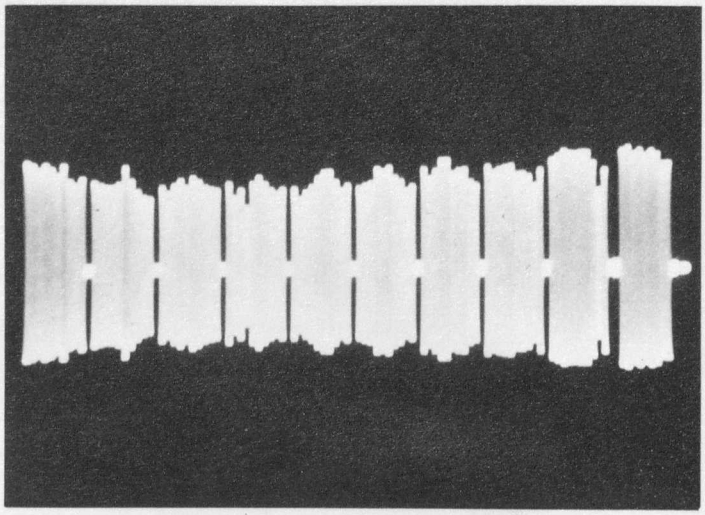

Figure 5.15(a) Output signal for a uniformly "illuminated" converter plate.

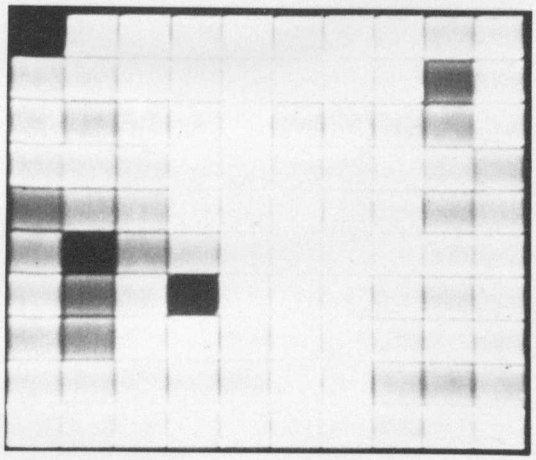

Figure 5.15(b) Final picture resulting from uniform "illumination".

to visual conversion. This may be set up within limits by the gain and output d.c. level controls of the amplifier following the detector, and also to some extent by the brilliance control on the CRO. For most of the results presented below these controls were optimised to produce the best visual picture. Scanning in figure 5.15(b) is from left to right and from bottom to top, and the serial output signal, figure 5.15(a), follows this sequence. Thus it may be noted that the top left hand transducer element produces no measurable output signal. When comparing figures 5.15(a) and (b) it is clear that the dynamic range is low, corresponding to high sensitivity. This gives a rather worse impression of the result of a uniformly "illuminated" converter plate than would have been the case for a lower sensitivity setting. It was, unfortunately, not possible to obtain satisfactory results with a lower sensitivity because a form of threshold at present exists in the detector caused by the spikes generated in the receiver gate. These very narrow positive and negative spikes are rectified and, owing to the necessarily small value of smoothing capacitor, create a d.c. offset voltage which effectively prevents the detection of signals which lie below a level of approximately 20% of the maximum output.

Figure 5.16(a) and (b) further demonstrate the dynamic range performance of the camera system, and shows also that acoustic shadows may be cast in the same manner as with light. In this case the shadow, as would be expected with the relatively long wavelength of the acoustic wave, is shown to be far less precise. A piece of folded waxed paper was placed 3 mm in front of the converter image plate so as to obscure approximately half of it from the incident and uniformly distributed ultrasonic waves. Again, for the visual picture, figure 5.16(b), pulsed transmission was used to reduce reverberations. It has been shown in chapter 4 that lateral acoustic wave-spread between adjacent transducer elements produces a

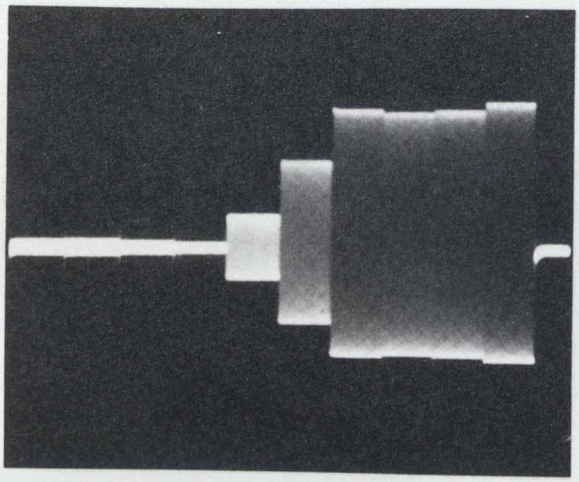

Figure 5.16(a) Converter serial output for half "shaded" plate.
(line 1 only shown)

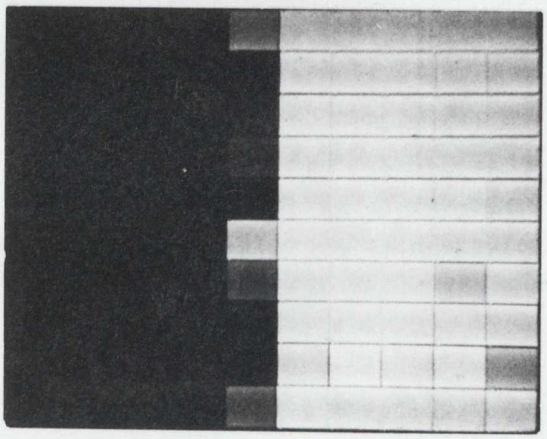

Figure 5.16(b) Final picture for half "shaded" converter plate.

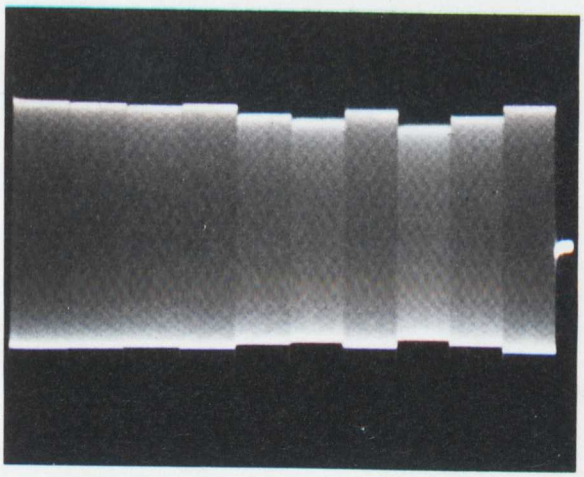

Figure 5.16(c) Converter serial output for "unshaded" plate.
(line 1 only shown)

cross-coupled component with an amplitude of somewhat less than 25% of the main signal. Assuming that columns 1 to 5 are totally obscured and that columns 6 to 10 are totally unobscured, it is evident that diffraction unsharpness is present in the cast shadow, since, referring to figure 5.16(a) it will be seen that the signal on element 5 is at least 75% of that on element 6. Figure 5.16(c) is a photograph of the signals from the same line of transducer elements (line 1) with the waxed paper removed, so that element signal amplitudes may be compared.

Figures 5.17 to 5.20 are the visual pictures resulting from the imaging of a cross cut through an 18 SWG sheet of aluminium. The arms of the cross more than filled the object plane and the width of each arm was approximately 1·5 mm, equivalent to 1 wavelength at 1 MHz in water. The magnification, set by the object and lens positions in relation to the converter plate, was in all cases approximately 1·2 times. Considerable improvement in picture quality resulted from setting the aluminium plate at an angle of around 10° to the proper object plane. It would appear that this causes reflections, which would otherwise clutter and blur the image, to be deflected off the axis. Figure 5.17 shows the cross centrally placed, (a) using continuous wave transmission, and, (b) using pulsed transmission. No significant difference is detectable except for a slight false image in the lower left hand sector for the continuous wave picture. With a magnification of 1.2 times the width of the arms of the imaged cross should have been approximately 2 mm. As can be seen the image is blurred to the extent that these occupy two transducer elements, or 5 mm. This confirms the lens difficiencies outlined in section 5.2.2. Figure 5.18(a) and (b), and figure 5.19(a) and (b) are images produced by pulsed transmission of the cross offset low, high, left and right respectively from the centre. They tend to show in a more pronounced manner the effects of unequal transducer element sensitivities, but on the other hand do not

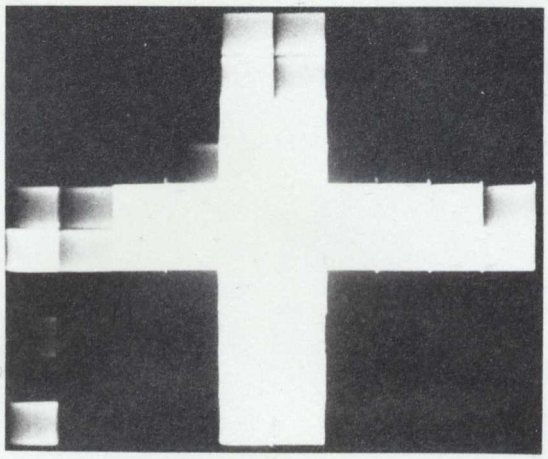

(a) Continuous wave transmission.

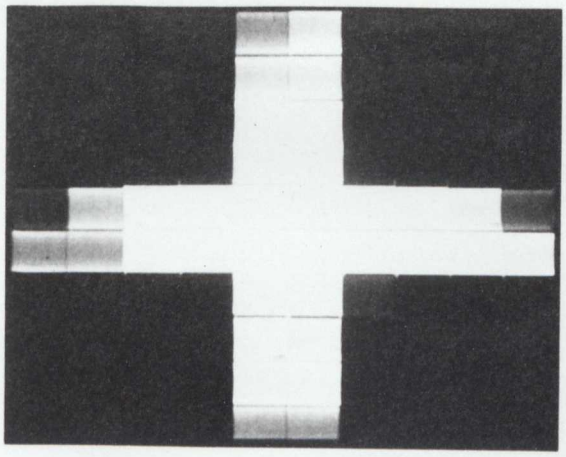

(b) Pulsed transmission.

Figure 5.17 Image of 1·5 mm cross cut through 18 SWG aluminium sheet.

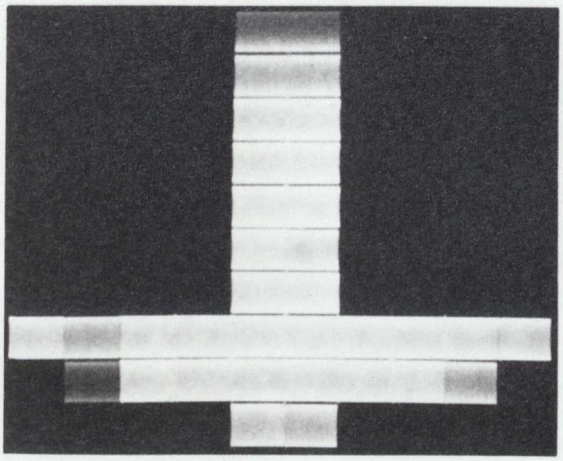

(a) Offset low.

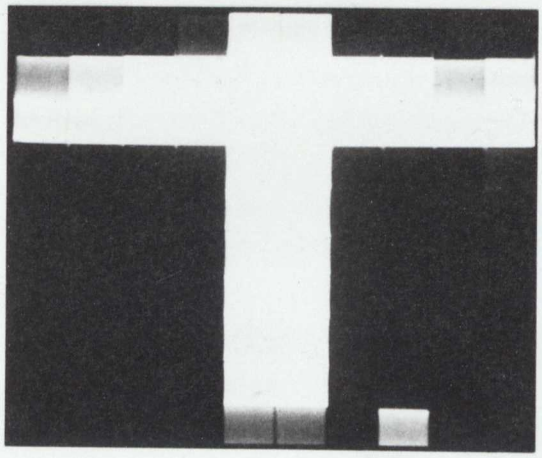

(b) Offset high.

Figure 5.18 Image of 1·5 mm cross cut through 18 SWG aluminium sheet, using pulsed transmission.

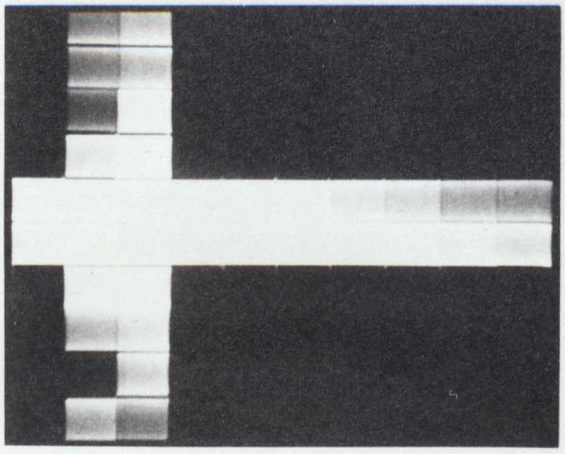

(a) Offset left.

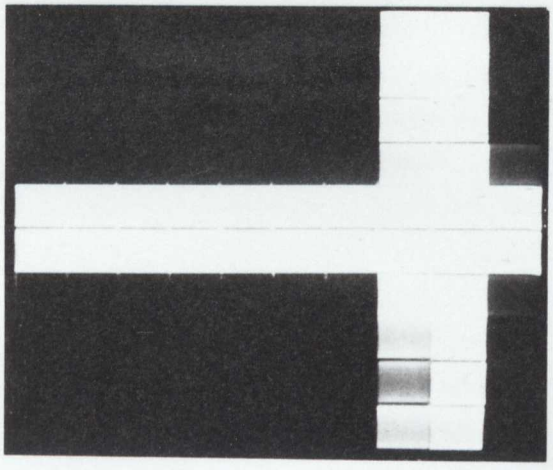

(b) Offset right.

Figure 5.19 Image of 1·5 mm cross cut through 18 SWG aluminium sheet, using pulsed transmission.

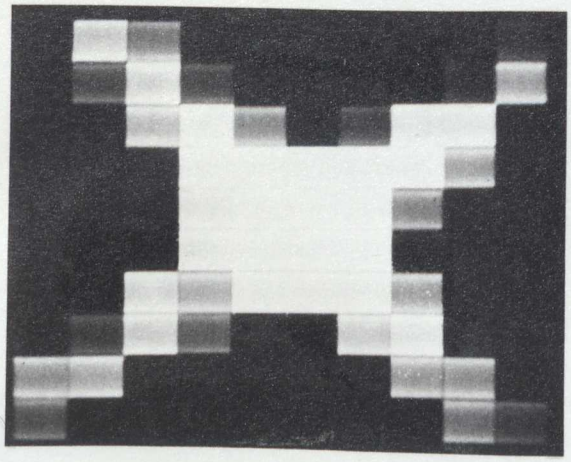

(a) Centrally placed.

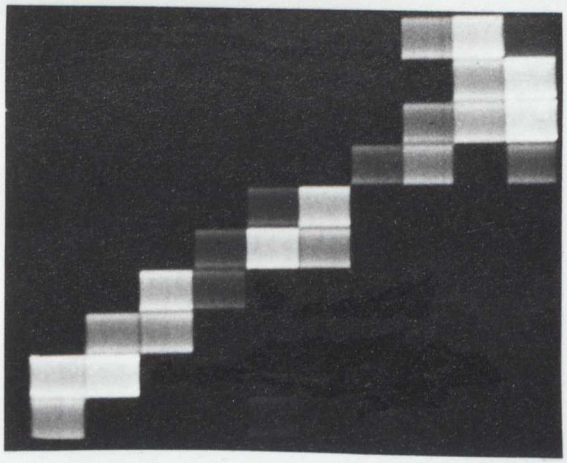

(b) Offset so that one arm only imaged.

Figure 5.20 Image of 1·5 mm cross cut through 18 SWG aluminium sheet, with arms at 45^{o} to x-y converter matrix axes. Pulsed transmission used.

indicate a noticeable worsening of resolution off the system axis, as might be expected with the simple uncorrected lens. The cross is set for figure 20(a) and (b) at an angle of 45°, centrally placed for (a) and moved off axis so that only one arm is imaged in (b). The image no longer naturally fits the rectangular pattern of the transducer matrix and therefore appears much degraded.

Figures 5.21(a) and (b) and 5.22(a) and (b) show images of solid crosses with arm widths equivalent at 1 MHz in water to 2 wavelengths for figure 5.21 and 1 wavelength for figure 5.22. Pulsed transmission was used. The 2 wavelength cross is imaged relatively well with a magnification of 1·9 times for (a) and 1·4 times for (b), although in both cases the imaged arm width covers 2 transducer elements, but within the limits of the transducer matrix resolution of 2·54 mm, this is the best that can be expected. Figure 5.22 compares for the 1 wavelength cross the transmission image with that obtained by reflection. The magnification was in both cases approximately 2·7 times; a magnification of 2 or less did not produce a recognisable image. As would be expected one image is the inverse of the other, for transmission the ultrasound being prevented from passing by the cross, whereas for reflection it is bounced back towards the lens. Owing to the necessity for the axial positioning of lens, object and converter, the transmitter position for reflection had to be offset and was placed in approximately the same plane as the lens, but angled so that the ultrasound was directed towards the object. The latter also required to be angled, being cut from a plane sheet of material, so that the reflected waves travelled along the lens-converter axis.

Figure 5.23 is a good demonstration of the resolving power of the ultrasonic camera. It shows the image resulting from an object consisting of two 2·5 mm diameter holes through a 16 SWG aluminium sheet, with a spacing between their adjacent edges of 1·5 mm (1 wavelength in water).

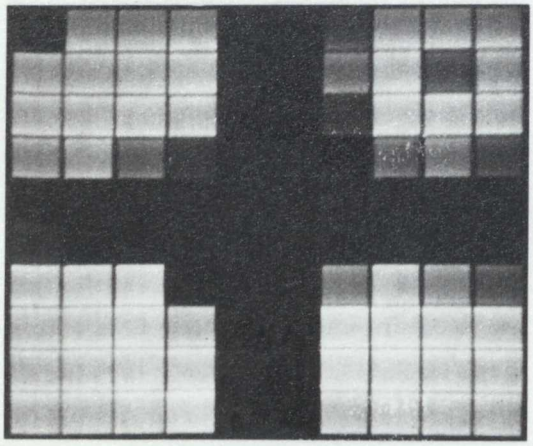

(a) Magnification 1·9 times.

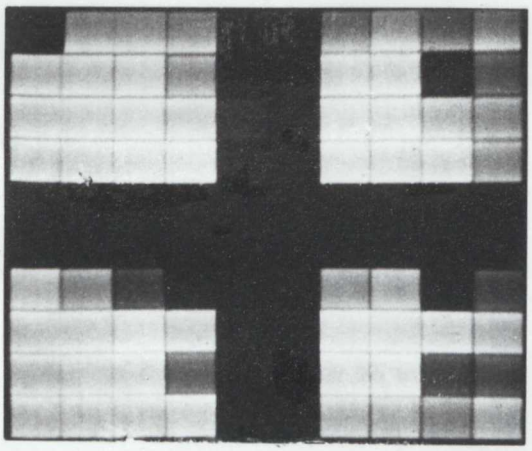

(b) Magnification 1·4 times.

Figure 5.21 Image of 3 mm solid cross, using pulsed transmission.

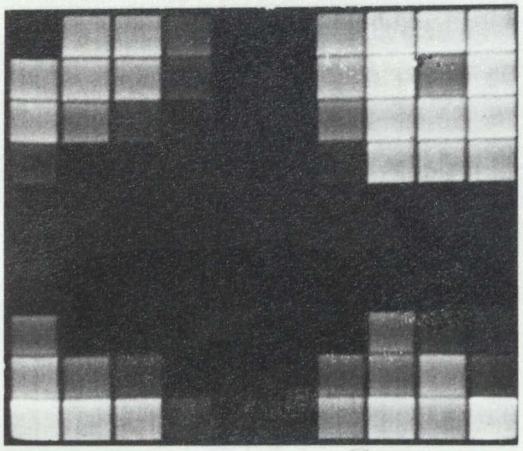

(a) Using pulsed transmission.

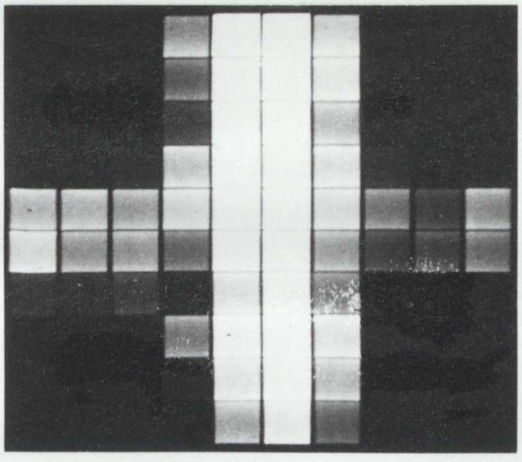

(b) Using pulsed reflection.

Figure 5.22 Image of 1·5 mm solid cross, with a magnification of 2·7 times.

The magnification given by the acoustic lens is approximately 2 times, and under these conditions the limiting resolution for two point sources is greater than 2·6 mm (see section 5.2.2). The centres of the two holes are separated by approximately 4 mm, and if these are considered as point sources then the Airy disc which each produces in the image plane, neglecting aberrations, will theoretically be resolvable one from the other. This seems to indicate that, in spite of the uncorrected lens used, spherical aberration near the axis is not affecting the resolution noticeably more than that caused by diffraction unsharpness.

The visualisation of spot welds using an ultrasonic camera would be a very useful application if it were possible to detect the difference between good and bad welds. Figure 5.24 shows the image of two spot welds between two 16 SWG steel plates. Unfortunately no noticeable difference was observed between good and suspected bad welds, but with a significant reduction of the "noise" caused by unequal transducer element sensitivities this may become possible.

Figure 5.25 shows the effect of attempting to obtain an image by reflection from a curved object. The object used was a brass rod of diameter 10 mm, positioned in conjunction with the acoustic lens to give a magnification of 1.7. Figure 5.25(a) shows the image produced by transmission and figure 5.25(b) that produced by reflection. For the latter, the transmitter was placed as before in approximately the same plane as the lens, and angled so as to direct the ultrasound at the object to be imaged. It will be noticed that whereas with transmission the imaged object is approximately the correct size (a little smaller because of diffraction, etc.), with reflection only the "highlights" of the cylindrical surface are imaged. This demonstrates a fundamental limitation of ultrasonic imaging when a reflection mode of operation is employed. Smooth (i.e. having a surface roughness less than a wavelength) contoured objects cannot be meaningfully imaged.

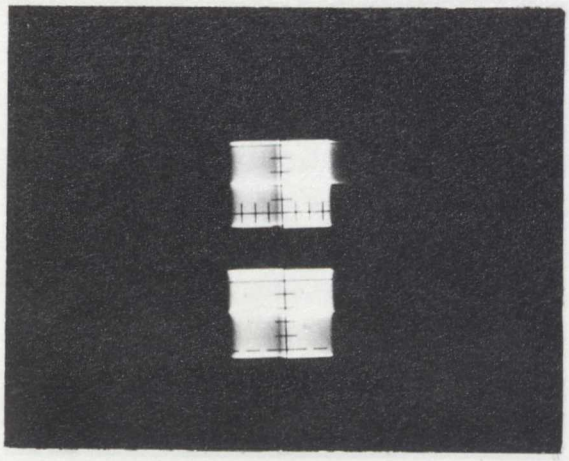

Figure 5.23 Image of two 2·5 mm diameter holes through a 16 SWG aluminium sheet. Spacing between adjacent edges 1·5 mm. Magnification 2 times.

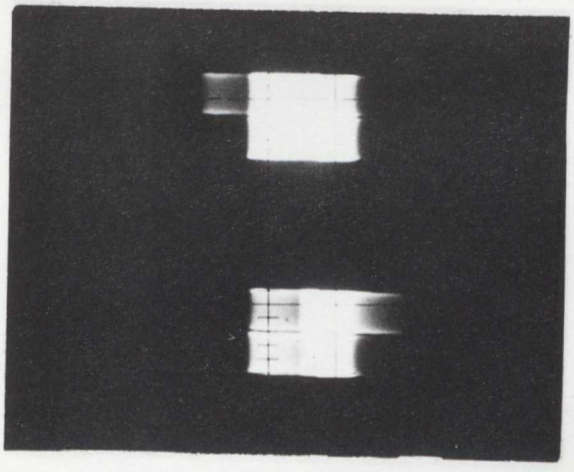

Figure 5.24 Image of two 3 mm electric spot welds between 16 SWG steel plates.

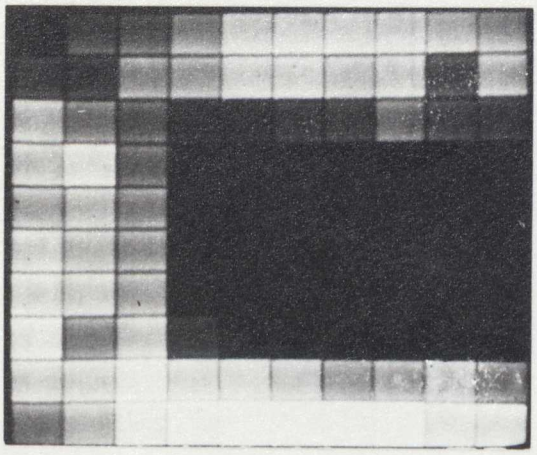

(a) By pulsed transmission.

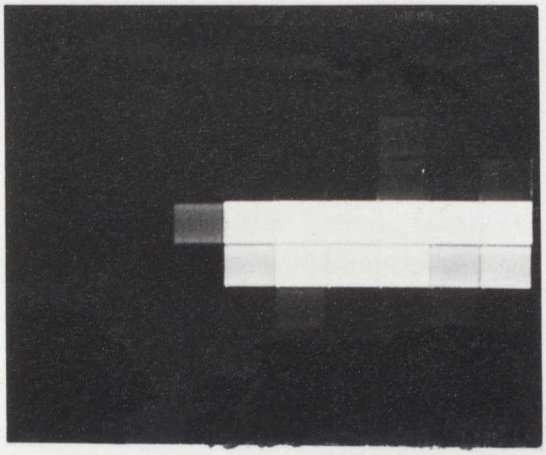

(b) By pulsed reflection.

Figure 5.25 Image of 10 mm diameter brass rod, with a magnification of 1·7 times.

5.5 Discussion

Resolution limitations in the ultrasonic camera may be attributed to two main sources, the acousto-electric converter and the acoustic lens. The former has a square matrix structure which imposes an ultimate resolution limit, but acoustic cross-coupling within the transducer and its surrounding assembly introduces a practical limit which is discussed in some detail in chapter 4. In the present converter it is the matrix pitch which limits the resolution, but if this were reduced to the transducer thickness and the operating frequency increased, then the limit would be set by the satisfactory maximum operating frequency of the FET analogue gates. Electrical breakthrough in these gates, again discussed in detail in chapter 4, increases with frequency and would appear to have a practical upper limit of between 6 and 10 MHz. In the acoustic section of the camera system, resolution is again inversely proportional to frequency and is limited finally by the fact that absorption of the ultrasonic waves in the materials through which they pass increases with frequency. Most successful ultrasonic inspection systems, in order to achieve a satisfactory acoustic resolution and at the same time operate within acceptable signal losses, use frequencies between 2 and 10 MHz. A compromise choice of 6 MHz would therefore appear to satisfy both the majority of likely applications and the electrical limitations imposed by the FET analogue gates. If higher operating frequencies were required, a frequency mixing arrangement[11] could be used.

The resolving power of the acoustic lens is proportional to its diameter. There is, however, a practical limit to the lens aperture, or F number, of near unity, and thus for best resolution the lens should have as long a focal length as the inspection system will allow. The lens used has an aperture of 1·1 and a focal length of 90 mm, and with the available 4 ft. test tank, cannot be improved upon in this respect. Results do not

indicate significant spherical aberration so that with the present system a corrected lens may not noticeably improve the image quality. A more obvious improvement would be apparent if the resolution of the converter was increased by raising the operating frequency and reducing the element pitch. Sayers[17] estimated that "spherical aberration of the lens used, if uncorrected, would be five times greater than the diffraction unsharpness". His system, however, operated at an ultrasonic frequency of 4 MHz.

Operation of the camera using pulsed ultrasound is, in principle, advantageous, but it appears to be doubtful from experimental evidence whether pulses of the duration used in the present system, 70 μS, really offer a noticeable improvement over continuous waves. It is very probable that any improvement is, in any case, masked by the high "noise" level introduced by the unequal transducer element sensitivities. It is clear, referring to figure 5.5(a), that a great deal of clutter which would otherwise cause loss of image definition is removed by the receiver gate. Very short pulses would prevent most reverberations from developing within the object, lens and converter, but the detector and sample and hold circuit (figure 5.8) would require considerable modification if pulses were reduced to less than ten cycles. In particular a much lower drive impedance to the smoothing capacitor C_3 would be needed in order that the pulse amplitude would be sampled accurately in one or two cycles. A further advantage to be gained from short pulse operation is that when the camera is operated in a reflection mode range gating would provide a third dimension. At present the 70 μS pulse gives a range resolution of approximately 100 mm which, at the ranges used, is of no special value.

Transient noise, which is present in the amplifier output in the form of switching spikes of considerable amplitude, is detected by the peak rectifying circuit of figure 5.8. Clearly this is a serious defect in the noise performance of the system, and would be made worse if the drive

impedance to the smoothing capacitor C_3 were reduced as was suggested in the preceding paragraph. An average detector is called for, although this becomes an increasingly difficult operation as the pulse duration is reduced.

5.6 Conclusions

The solid state ultrasonic camera at its operating frequency of 1 MHz has an object plane resolution limit, using the acoustic lens, of approximately 1·5 wavelengths in water, and an image plate resolution limited by the transducer matrix. Choice of operating frequency is the prime factor which determines the limiting resolution of the system. Transducer element pitch, it has been demonstrated, may be made somewhat less than half the ultrasonic wavelength in the transducer material, and both this and the acoustic lens diffraction unsharpness are inversely proportional to frequency. A practical limit with the FET analogue gates in their present form restricts the satisfactory operating frequency to 6 MHz and below, although this may be increased further if mixing were to be used in the gate circuits. At this higher frequency, the acoustic lens should be corrected for spherical aberration, since if uncorrected this would now be considerably greater than the diffraction unsharpness for the same aperture.

Operating with short pulses, although making accurate signal detection difficult, should improve the image definition and provide a useful third dimension. The relatively long pulses used in the present camera system do not give a noticeably better performance than continuous waves, but inequality of transducer element sensitivities makes serious judgement of small performance changes difficult.

6. On-Line Computer Lens

6.1 Introduction

The basic principles underlying the use of a computer as a synthetic lens in conjunction with an acousto-electric converter have been outlined in chapter 3. The specific application of a PDP8-E computer to the FET scanned solid state converter will be described here. The objective is on-line real time imaging, using a single frequency for processing simplicity and speed (i.e. continuous wave or long pulse operation of the converter), the final visual picture being an intensity modulated CRO TV type display. The results described below are those obtained by processing applied to only a single ten element linear transducer array (line 1 of the solid state converter), and although a 10 x 10 two dimensional matrix would require considerably more computer time, the processing becomes a relatively simple extension to the existing program. In any case the 1 dimensional results provide most of the information needed to establish the characteristics and likely performance of a complete 2 dimensional system.

6.2 Processing Principles

6.2.1 Focused Operation

Focused operation is advantageous when measureable path length differences exist between the various elements of the converter array and the point in the object plane to be imaged. These differences should be significant in relation to the system's overall accuracy. It has been found experimentally that focusing well inside the Fraunhofer zone, or far field, of the converter array still provides an improvement in angular resolution.

In order to focus the ultrasonic energy eminating from a point source in the object plane to an equivalent point in the image plane, the phase of all signals reaching the array elements from that point must be

modified, before summation, so that they are identical. A lens performs this by, in effect, imparting a spherical (or aspherical) spatial time delay function to the signals as they pass through its aperture. It is essentially this operation which the computer must be programmed to carry out on the array signals, the array in this case being equivalent to the aperture of a synthetic lens. The computer must first calculate the fractional path length differences which exist between each array element and that point in the object plane to be imaged, using as a reference length, for example, the perpendicular distance between the array and object planes (see program 6.1). After conversion to radians, with respect to the ultrasonic wavelength in the transmission medium, these differences represent the increments of phase which must be subtracted from the phases of the appropriate array element signals in order to achieve a focusing action. The resulting modified signals are then summed, producing a total magnitude which will represent electrically the intensity of ultrasound radiating from the chosen point in the object plane. The signals from all points other than that being imaged will, upon summation, tend to destructively interfere owing to their unequal phases and the resulting image magnitudes will be low. The process is repeated for each point in the object plane to be imaged, so that to image a line of X points in the object plane using a linear array of N elements requires NX basic computer operations (see program 6.2), excluding those required for the phase increment calculations.

Figure 6.1 represents the linear array of N equally spaced elements positioned at a distance L from a parallel object plane in which a point source P is placed. In order to demonstrate the form of the processing action carried out by the computer, consider the following:-

Let point P radiate a sinusoidal acoustic signal equivalent to an electrical voltage,

$$v_s = V_s \sin (\omega t + \phi_s) \qquad \ldots\ldots \quad 6.1$$

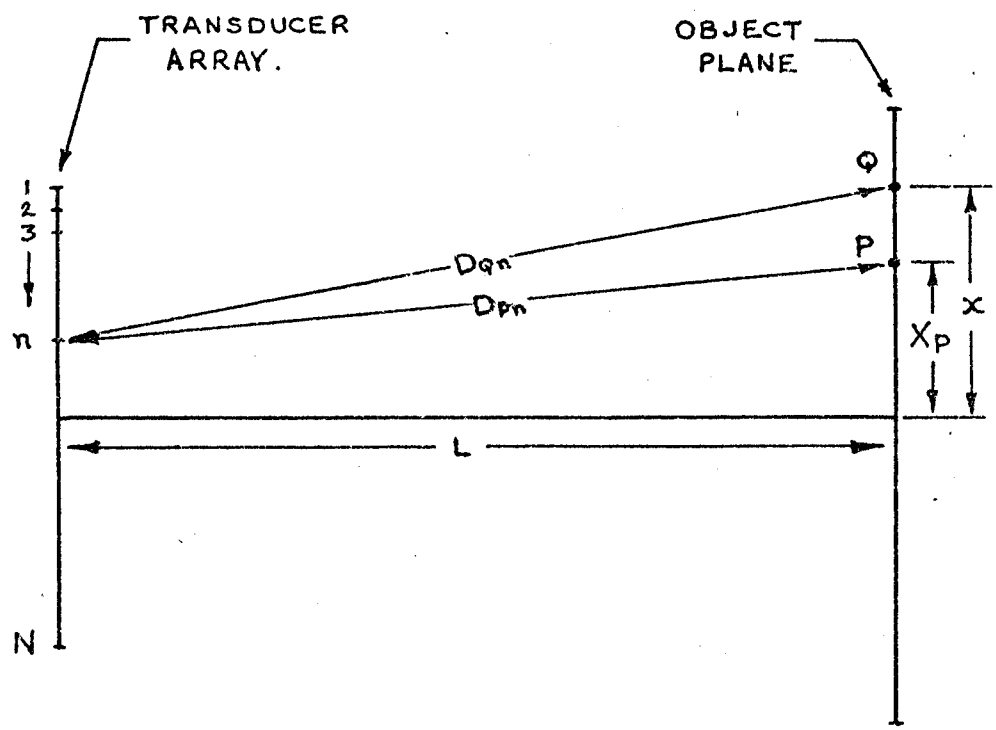

FIGURE 6.1 PATH LENGTHS BETWEEN ARRAY AND OBJECT PLANE

The signal received by element n of the array would then be of the form,

$$v_n = k_{Pn} V_s \sin (\omega t + \phi_s + \frac{2\pi D_{Pn}}{\lambda}) \quad \ldots\ldots \quad 6.2$$

where D_{Pn} is the path length between points P and n, λ the wavelength in the transmission medium, and k_{Pn} a constant determined by the radiation patterns of point P and element n along the line Pn. In practice the phase of the array element signals is measured with respect to a reference signal of the same frequency. Let this reference signal have a phase ϕ_R. Then the measured phase, ϕ_n, of element n may be expressed as,

$$\phi_n = (\phi_s - \phi_R) + \frac{2\pi D_{Pn}}{\lambda} \quad \ldots\ldots \quad 6.3$$

Let the computer focus to a point Q in the object plane, as shown in figure 6.1. The array element signal phases will now be modified so that all signals eminating from point Q will be in phase. Thus ϕ_n will now be given by,

$$\phi_n = (\phi_s - \phi_R) + \frac{2\pi}{\lambda} (D_{Pn} - D_{Qn}) \quad \ldots\ldots \quad 6.4$$

where D_{Qn} is the path length between points Q and n.

The computer, having calculated ϕ_n from n = 1 to n = N, is then programmed to compute the magnitude of the resultant summation of all N modified array element signals, when focused at point Q. It does this by first separating the signals into their real and imaginary parts (see program 6.2), forming real and imaginary totals and finally calculating the resultant magnitude. The imaginary part of the modified signal at array element n may be expressed as,

$$J_n = k_{Pn} V_s \cos \left[(\phi_s - \phi_R) + \frac{2\pi}{\lambda} (D_{Pn} - D_{Qn}) \right] \quad \ldots\ldots \quad 6.5$$

and, similarly, the real part as,

$$R_n = k_{Pn} V_s \sin\left[(\phi_s - \phi_R) + \frac{2\pi}{\lambda} (D_{Pn} - D_{Qn}) \right] \quad \ldots\ldots \quad 6.6$$

Their respective totals will then be,

$$J_T = k V_s \sum_{n=N}^{n=1} \cos\left[(\phi_s - \phi_R) + \frac{2\pi}{\lambda} (D_{Pn} - D_{Qn}) \right] \quad \ldots\ldots \quad 6.7$$

$$\text{and,} \quad R_T = k V_s \sum_{n=N}^{n=1} \sin\left[(\phi_s - \phi_R) + \frac{2\pi}{\lambda} (D_{Pn} - D_{Qn}) \right] \quad \ldots\ldots \quad 6.8$$

assuming that k_{Pn} may be approximated to a constant, k, for all elements. The resultant magnitude of the image of the signal from Q is then,

$$V_T = \sqrt{J_T^2 + R_T^2} \quad \ldots\ldots \quad 6.9$$

$$\text{or,} \quad V_T = k V_s \sqrt{\left[\sum_{n=N}^{n=1} \cos \phi_Q \right]^2 + \left[\sum_{n=N}^{n=1} \sin \phi_Q \right]^2} \quad \ldots\ldots \quad 6.10$$

where $\phi_Q = (\phi_s - \phi_R) + \frac{2\pi}{\lambda} (D_{Pn} - D_{Qn})$.

Referring to figure 6.1 it will be seen that D_{Pn} and D_{Qn} may be written,

$$D_{Pn} = \sqrt{\left[L^2 + X_P + (n - \tfrac{N}{2})a \right]^2} \quad \ldots\ldots \quad 6.11$$

$$\text{and,} \quad D_{Qn} = \sqrt{\left[L^2 + x + (n - \tfrac{N}{2})a \right]^2} \quad \ldots\ldots \quad 6.12$$

Thus ϕ_Q may be written,

$$\phi_Q = \frac{2\pi}{\lambda}\left[\sqrt{L^2 + \left[X_P + (n - \frac{N}{2})a\right]^2} - \sqrt{L^2 + \left[x + (n - \frac{N}{2})a\right]^2}\right] \quad \ldots\ldots 6.13$$

neglecting the constant phase term $(\phi_s - \phi_R)$.

Substituting equation 6.13 into equation 6.10 gives the complete expression for the image magnitude of point Q, and the computer uses this expression for each of the X points in the object plane.

When Q is coincident with the point source P, $x = X_P$, and thus $\phi_Q = 0$. Then V_T is a maximum and given by,

$$V_T = N\,k\,V_s \quad \ldots\ldots 6.14$$

6.2.2 Response of a Focused Continuous Receiving Aperture to a Point Source

The previous section, although demonstrating the processing action performed by the computer, does not show the general form of the image response to a point source in the object plane. By considering the array as a continuous aperture[33] and integrating, a more meaningful result is obtained.

When the aperture, A in figure 6.2, of the transducer is small compared to its focal length, L, then the focused transducer may be represented as a plane transducer in which the waveform impinging on it, before being integrated over the aperture, is first multiplied by the phase function,

$$e^{j\frac{\pi}{\lambda L}(x - a)^2} \quad \ldots\ldots 6.15$$

Consider a point source situated centrally in the object plane at 0 and radiating towards the receiving aperture. The wave arriving at point a

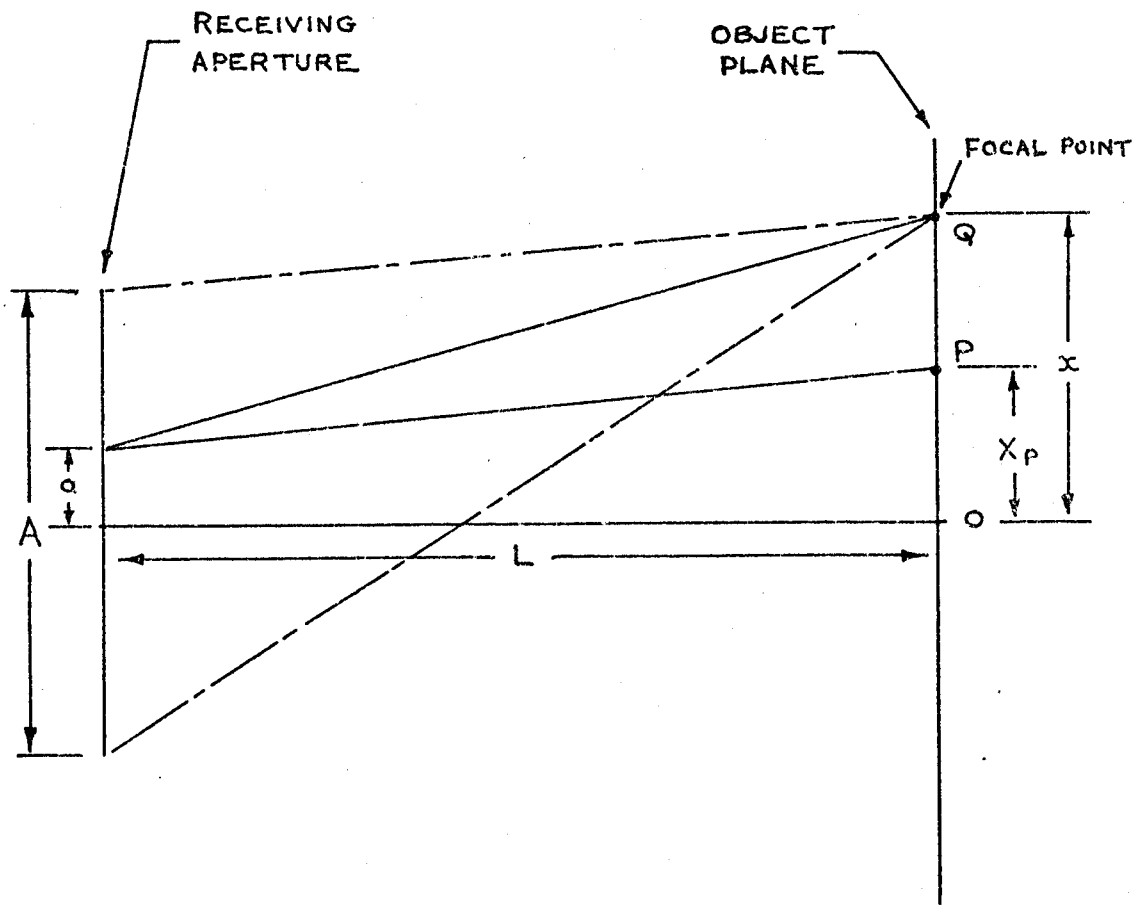

FIGURE 6.2 FOCUSED CONTINUOUS APERTURE.

will then be,

$$\frac{1}{L} \; e^{j(\omega t - \frac{2\pi L}{\lambda})} \cdot e^{-j \frac{\pi a^2}{\lambda L}} \qquad \ldots\ldots \; 6.16$$

and after multiplication by the phase function the transducer output will be,

$$\frac{1}{L} \; e^{j(\omega t - \frac{2\pi L}{\lambda})} \int_{-A/2}^{A/2} e^{-j \frac{\pi a^2}{\lambda L}} \cdot e^{j \frac{\pi}{\lambda L} (x - a)^2} \cdot da \quad \ldots. \; 6.17$$

This equals,

$$\frac{1}{L} \; e^{j(\omega t - \frac{2\pi L}{\lambda} + \frac{\pi}{\lambda L} x^2)} \cdot \left[\frac{\sin \frac{\pi A}{\lambda L} x}{\frac{\pi}{\lambda L} x} \right] \qquad \ldots\ldots \; 6.18$$

The second, bracketed, term represents the amplitude and approximates to a delta function positioned at x equals zero. The first zeros of the expression 6.18 occur when,

$$x = \pm \frac{\lambda L}{A} \qquad \ldots\ldots \; 6.19$$

If the point source was positioned at any point P in the object plane instead of centrally at 0, expression 6.16 would become,

$$\frac{1}{L} \; e^{j(\omega t - \frac{2\pi L}{\lambda})} \cdot e^{-j \frac{\pi}{\lambda L} (X_P - a)^2} \qquad \ldots\ldots \; 6.20$$

After multiplying by the phase function, 6.15, and integrating over the

aperture, the result would be,

$$\frac{1}{L}\, e^{j\left[\omega t - \frac{2\pi L}{\lambda} + \frac{\pi}{\lambda L}(x^2 - X_P{}^2)\right]} \cdot \left[\frac{\sin \frac{\pi A}{\lambda L}(x - X_P)}{\frac{\pi}{\lambda L}(x - X_P)}\right] \quad \ldots\ldots \quad 6.21$$

This has the same form as expression 6.18, but has its central maximum and first zeros displayed by X_P from the centre.

6.2.3. Unfocused or Far Field Operation

Whereas operation in the near field, when focusing was performed, required a spherical phase function, operation in the far field requires only a linear phase function. The array signal processing becomes the application of a simple linear phase taper. In practice the computer processing does not distinguish between focused and unfocused operation, since if it were to do so, the flexibility of the system, a very important attribute of the computer lens, would be reduced.

The phase function becomes,

$$e^{j \frac{2\pi}{\lambda} a \sin \Theta} \quad \ldots\ldots \quad 6.22$$

where Θ is the angle of the incident parallel plane wave front to the aperture normal. Assuming, again, a point source on the axis, the wave arriving at point a will be,

$$\frac{1}{L}\, e^{j(\omega t - \frac{2\pi}{\lambda} L)} \quad \ldots\ldots \quad 6.23$$

and after multiplication by the phase function the transducer output

will be,

$$\frac{1}{L} e^{j(\omega t - \frac{2\pi}{\lambda} L)} \int_{-A/2}^{A/2} e^{j \frac{2\pi}{\lambda} a \sin \Theta} \cdot da \quad \ldots\ldots \quad 6.24$$

which after integration, equals,

$$\frac{1}{L} e^{j(\omega t - \frac{2\pi}{\lambda} L)} \left[\frac{\sin (\frac{\pi A}{\lambda} \sin \Theta)}{\frac{\pi}{\lambda} \sin \Theta} \right] \quad \ldots\ldots \quad 6.25$$

This again approximates to a delta function centred at $\Theta = 0$. The first zeros of the expression occur when,

$$\Theta \simeq \pm \frac{\lambda}{A} \quad \ldots\ldots \quad 6.26$$

For small angles this is virtually identical to the equivalent result, expression 6.19, for a focused aperture. So, also, the second terms in expressions 6.18 and 6.25 become almost identical.

For a source incident at an angle of ϕ to the array normal, equation 6.25 becomes,

$$\frac{1}{L} e^{j(\omega t - \frac{2\pi}{\lambda} L)} \left[\frac{\sin \frac{\pi A}{\lambda} (\sin \Theta - \sin \phi)}{\frac{\pi}{\lambda} (\sin \Theta - \sin \phi)} \right] \quad \ldots\ldots \quad 6.27$$

which represents, for small angles, a shift in the pattern of expression 6.25 by ϕ radians.

6.3 The Computer

6.3.1 Introduction

The Digital Equipment Corporation PDP8-E computer is a small general purpose machine, with expansion capabilities to suit almost any requirement. Basically a 4,000 word store machine, it can be increased to 32,000 words within the same cabinet, and disk and magnetic bulk storage peripherals are available. The basic processor is a single-address, fixed

word length, parallel transfer computer using 12 bit, two's complement arithmetic. The cycle time of the random access memory is around 1·2 μS, and each addition requires 2·6 μS while a subtraction requires 5 μS. The KE8-E Extended Arithmetic Element option greatly increases the speed of multiplication and division, by parallel operation, with a result that 40 μS is a typically required time. Inputting is achieved via a teletype, a low speed paper tape reader or directly via the console switch register. A variety of optional input devices may be interfaced, such as a high speed paper tape reader, analogue to digital converters, or a magnetic tape reader. The output facilities provided as standard are the teletype and low speed paper tape punch, but again optional devices, such as a high speed paper tape punch, digital to analogue converters, etc., may be interfaced relatively simply.

The computer extensions and peripherals included for the experimental work involved with the on-line ultrasonic imaging were:

(i) Extended Arithmetic Element, KE8-E.

(ii) Additional 4,000 word core store. (making a total of 8,000 words)

(iii) Positive 1/0 Interface board, KA8-E.

(iv) High speed paper tape reader.

(v) Two analogue to digital converters.

Future requirements will include three digital to analogue converters for CRO display control.

6.3.2 Programming Languages

Many languages are available[47] for use on the PDP-8E computer, the two used here for the signal processing and associated work being PAL III and FOCAL. The former is an assembly language, using English-like mnemonics for the binary numbers which are interpreted by the computer as

the program instructions. It is thus virtually a machine code. Focal, on the other hand, is a conversational, relatively high level language, requiring a form of compiler. It is therefore simpler to use, but uses considerably more core area and is much slower. It enables the computer to be used as a simple but powerful desk calculator or for problems requiring long and sophisticated programs.

An assembly language, such as PAL III, has the advantage that once the binary tape of the program has been generated, the core need no longer hold the assembler, thus leaving it free to store the program and any data required. The process of assembly, using PAL III, involves the loading of the assembler tape into the store followed by two passes (with an optional third for program listing) of the symbolic program tape, after which a binary translation is punched out. This is then loaded and used in the normal way. A Floating Point Package[46] may be additionally loaded after the program has been assembled with PAL III, and this provides many useful mathematical routines which may be called up in the program by an appropriate mnemonic.

PAL III together with the Floating Point Package have been used exclusively for the signal processing required for image reconstruction (see programs 6.1, 6.2 and 6.3). FOCAL has been used for certain mathematical off-line calculations and for the simulated point source image construction shown later in figure 6.9 and program 6.4.

6.3.3 Interfacing Principles

Peripherals may be interfaced[45] directly with the Omnibus or indirectly via the Positive I/O Bus or external bus. Optional peripherals in the experimental system developed are all interfaced using the latter. The main external bus signals are:

(i) BAC 00-11. These represent the buffered content

of the Accumulator and are the signals to be outputted.

(ii) AC 00-11. These signals represent the contents of a register in an input peripheral which are to be transferred into the computer.

(iii) BIOP 1, 2 and 4. These pulses generate further pulses in an addressed peripheral and cause it to perform certain functions, as directed by the program.

(iv) SKIP. When a peripheral grounds this line it causes the next sequential instruction of the program to be skipped. Normally a Jump instruction in a waiting loop is skipped when the peripheral is ready to output or input.

(v) B INITIALIZE 1. A pulse generated by the computer at power turn-on and by the "Clear All Flags" instruction which clears the Accumulator, Link and peripheral flags.

BIOP pulses are allocated certain specific primary functions; BIOP 1 for sampling flags and skipping, BIOP 2 for clearing flags and clearing the Accumulator, and, BIOP 4 for reading, loading and clearing buffers.

Figure 6.3 shows the basic device selection and data transfer logic. Device selection is achieved by gate A, high and low buffered memory lines BMB 03 to 08 carrying the various codes, so that when selected gates C, E and G are ready to pass BIOP pulses 1, 2 and 4 respectively. These pulses are generated within the computer when called for by the program. Gates I to P transfer the data stored in the output buffer of the peripheral to the Accumulator when the gated BIOP 2, IOTXX2, is applied to

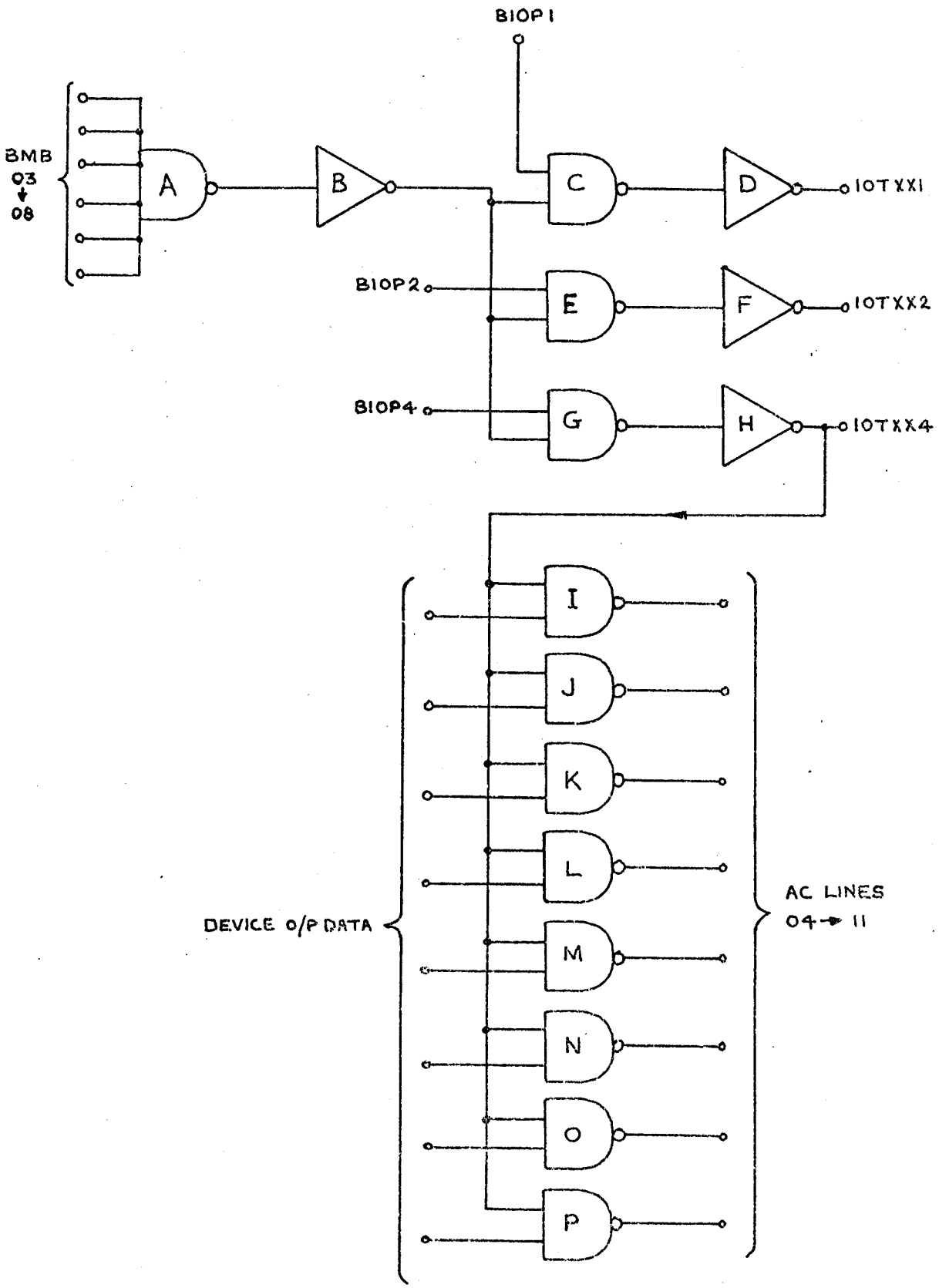

FIGURE 6.3 INPUT PERIPHERAL DEVICE SELECTION AND DATA TRANSFER LOGIC.

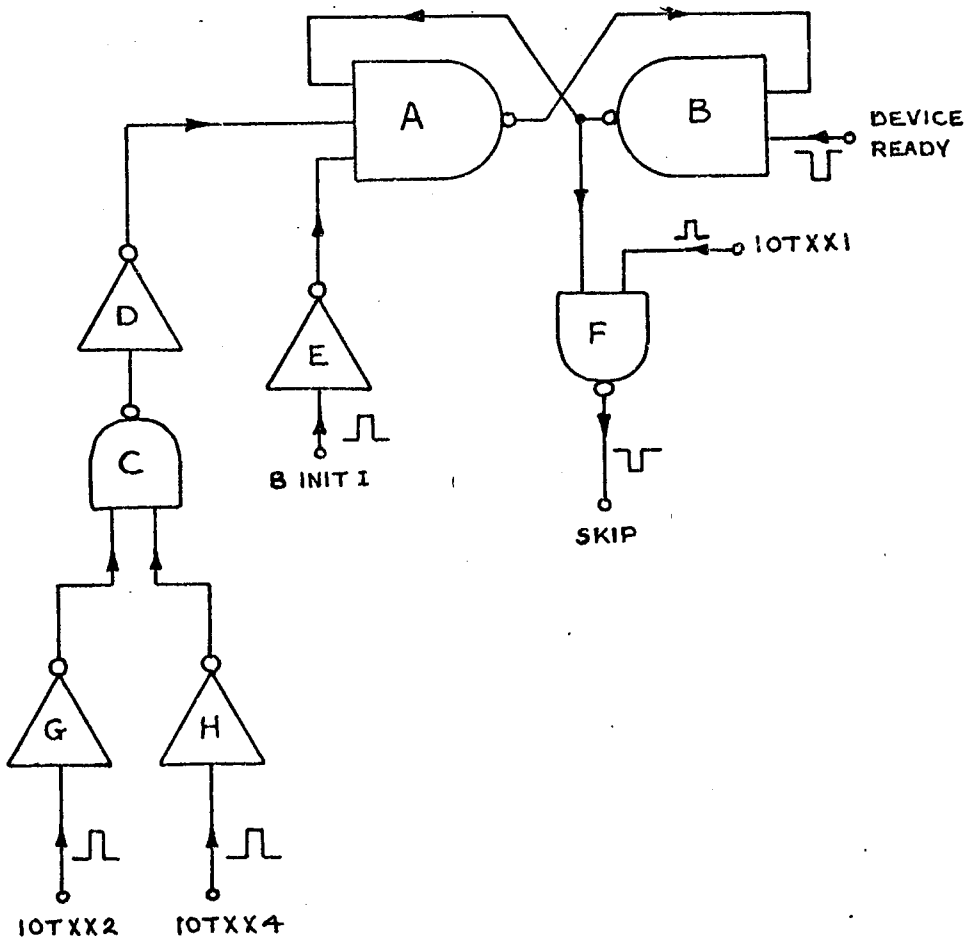

FIGURE 6.4 PERIPHERAL FLAG LOGIC

each of them. These gates require open collector outputs so that they may form a "wired or" arrangement with the interface logic of other peripherals.

The flag logic cannot be so specifically described since each device may require a slightly different form. It must, however, conform to the basic requirements outlined in figure 6.4. Here gates A and B are cross-coupled to form a flip flop, and a low signal on any input to this will ensure that the output of the triggered side is at a "1". The flag is cleared by both IOTXX2 and IOTXX4, causing the SKIP bus to remain high and thus inoperative. When a device ready pulse is received from the peripheral the flip flop changes its state and gate F is made ready so that IOTXX1 will pull the SKIP bus down, thus allowing the program to proceed, for example, with device buffer reading. IOTXX4 performs the data transfer operation and also clears the flag in order to prevent a further reading until the device is again ready.

6.4 The Experimental System

6.4.1 General Description

The experimental system used is shown in outline in figure 6.5. The solid state converter with its scanning control, bandpass amplifier, receiver and transmitter gates, and amplitude detector are arranged as for the conventional ultrasonic camera system described in chapter 5. Additional units, apart from the computer, are the phase detector and the two analogue to digital converters (ADC's), including their computer interfacing circuitry. At present the system operates on line 1 only of the converter, and the phase and amplitude of the signals from these ten elements are detected, converted into a suitable digital form and transferred to the computer store, via its accumulator. Data acquisition is controlled by the computer and the program directs its processing so that the

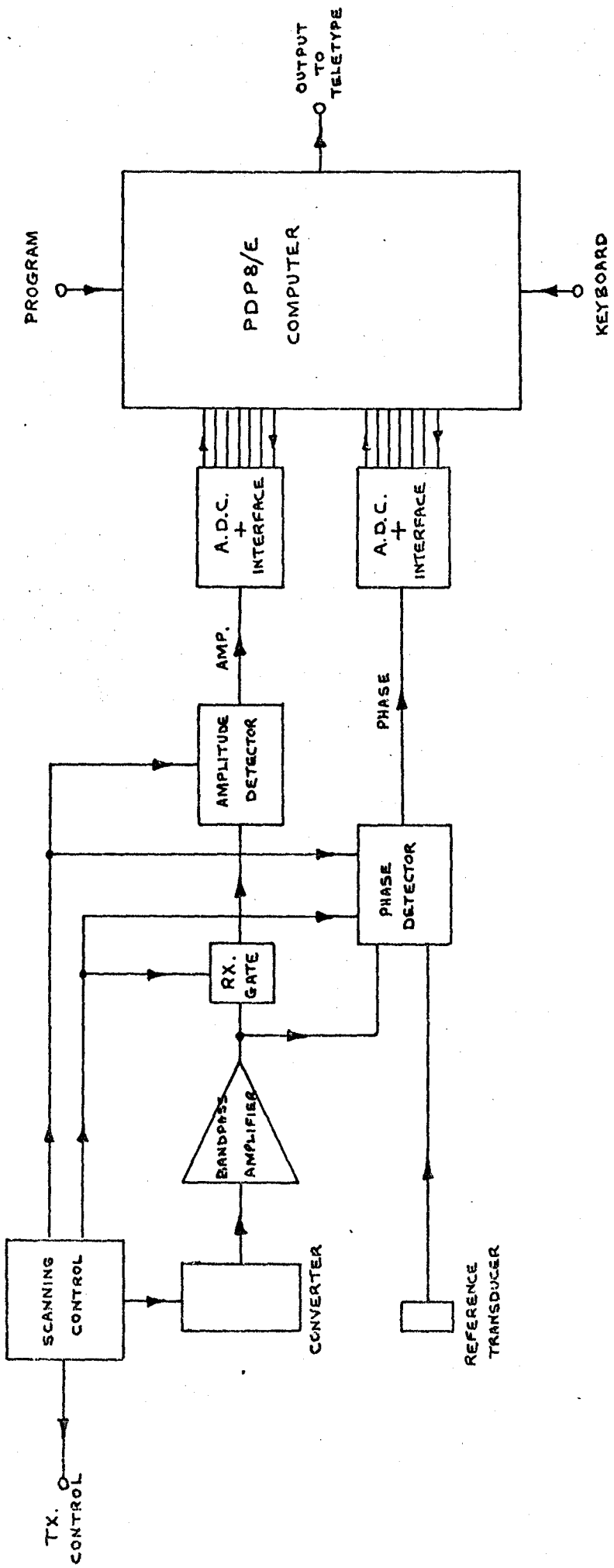

FIGURE 6.5(a) OUTLINE OF EXPERIMENTAL SYSTEM.

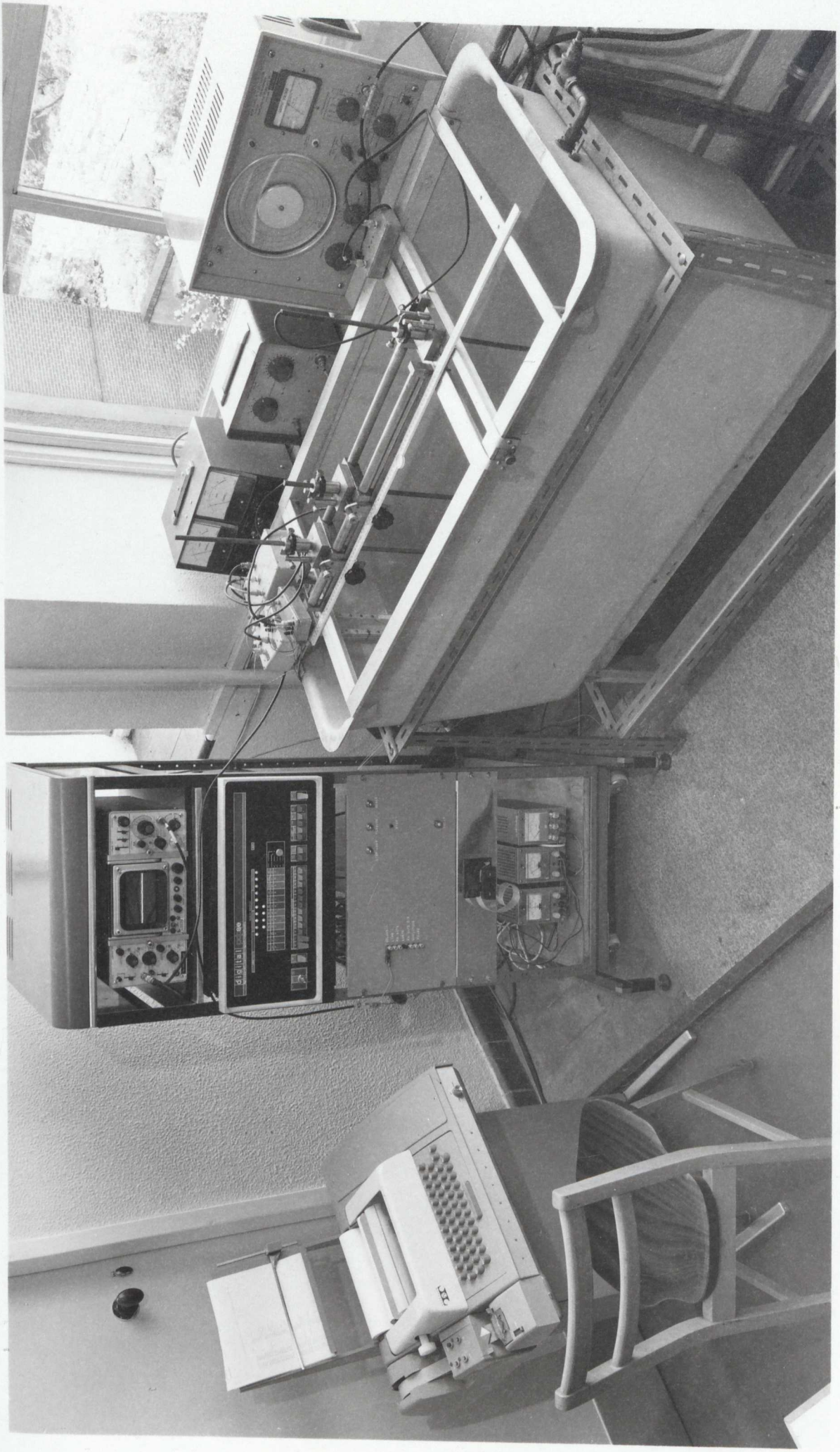

Figure 6.5(b) The experimental system.

computed image amplitudes of desired points in the object plane (a single line) are printed by the teletype. The reference signal required by the phase detector is derived either from a separate receiving transducer situated near the transducer matrix, or directly from the transmitter drive oscillator. It is advantageous to use the former method since this ensures that any small changes of frequency or of transmitter converter distance do not alter the measured phase of the signal. An additional feature is provided in the scanning control; a single frame may be scanned so that once a complete set of data has been transferred to the computer, scanning stops.

6.4.2 Phase Detector

The Motorola MC 4044 (see data sheet in Appendix B) is intended primarily for use in phase locked loop circuits, and is therefore not normally required to indicate absolute phase. In order to provide a complete range of phase measurement from 180° lag to 180° lead a special logic circuit was developed (see figure 6.6) so that as the output switches from U1 to D1 an inverter is introduced giving an additional 180° phase shift to the output from D1. Signal routing is controlled by the SN7470 D type flip flop, triggered appropriately by the phase detector U1 and D1 outputs.

The μA 710 comparators are used to amplify and square the reference and test signals. Figure 6.7(a) shows how these are connected.

Figure 6.7(b) is the diagram of the sample and hold circuit. T_1 is the receiver gate which is opened at the appropriate time by the gate control signal allowing approximately 30 complete periods of the phase detector output through. T_2 being open circuit, C_2 charges up to a level

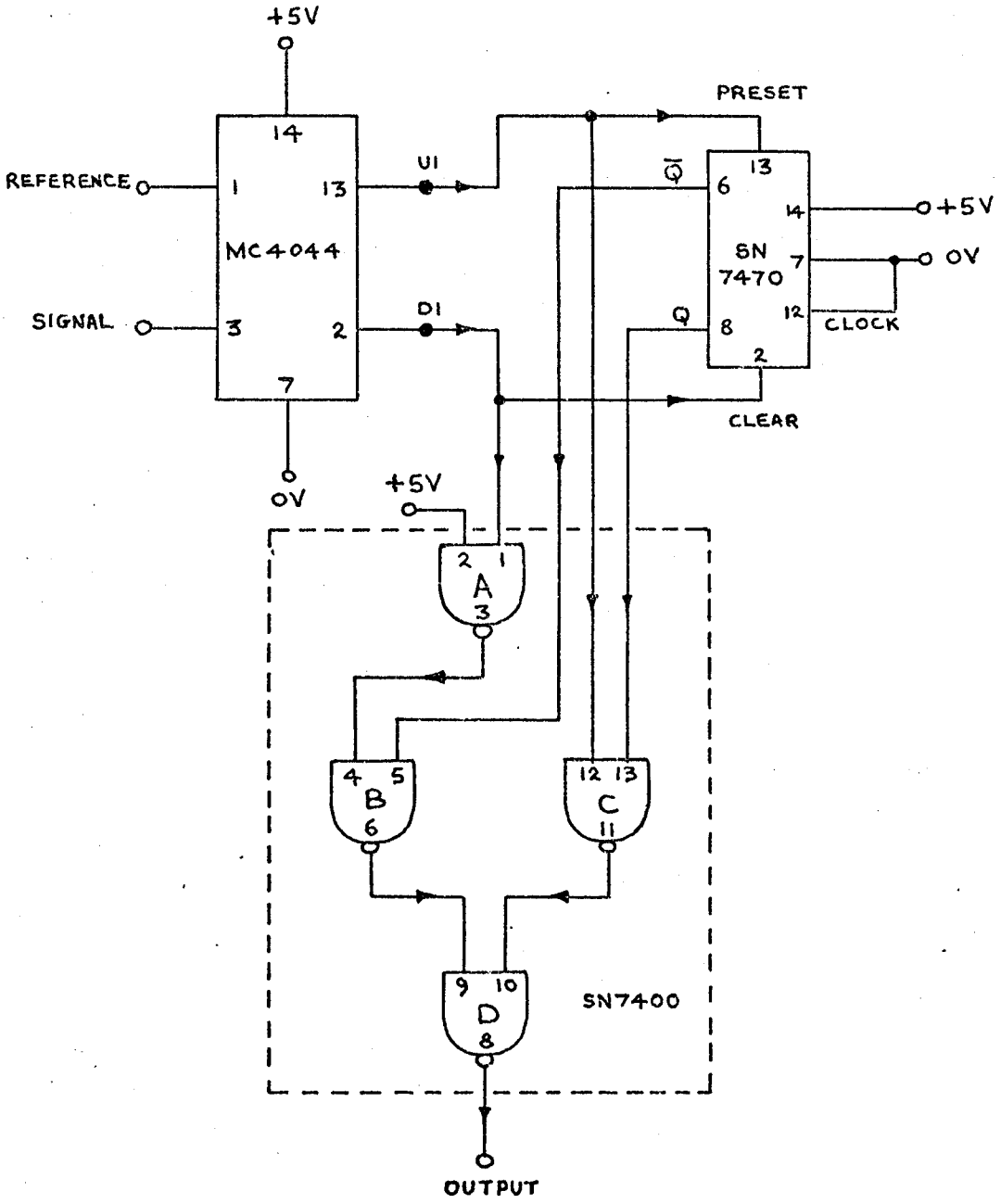

FIGURE 6.6 PHASE DETECTOR AND ADDITIONAL LOGIC.

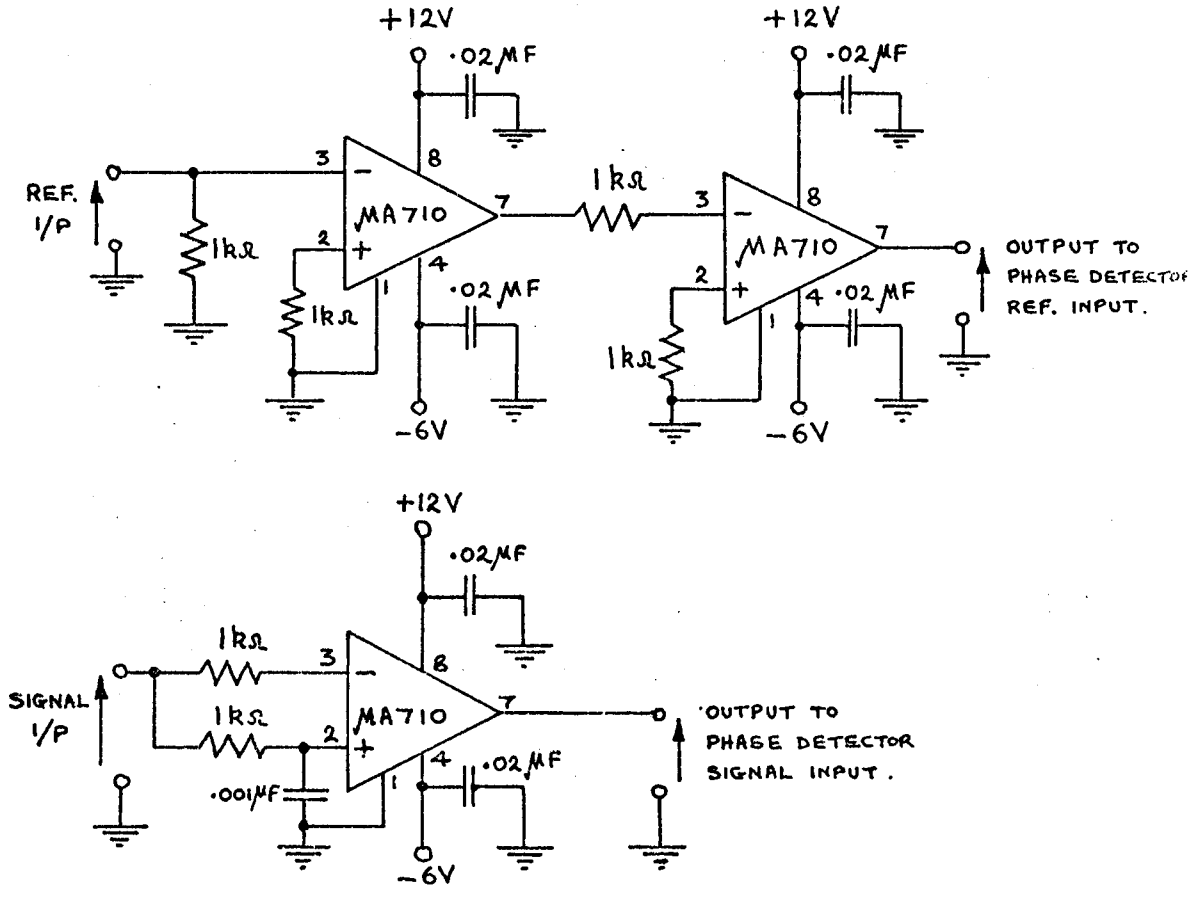

FIGURE 6.7(a) REFERENCE AND SIGNAL COMPARATOR CIRCUITS.

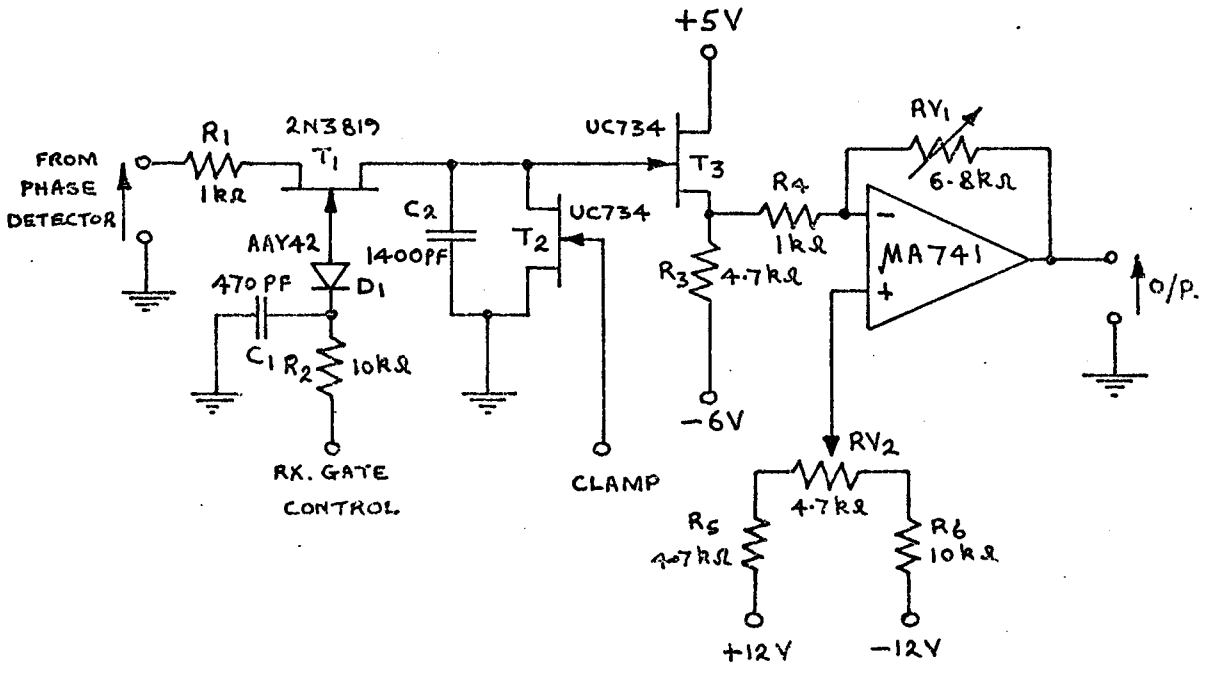

FIGURE 6.7 (b) PHASE DETECTOR OUTPUT SAMPLE AND HOLD CIRCUIT.

equal to the average value of the phase detector waveform. This level is proportional to the phase and after passing through source follower T_3, is amplified so that the range 0^o to 360^o corresponds to 0 V to +10 V at the output. RV1 and RV2 set the gain and output d.c. level respectively. Before the next phase sample, C_2 is discharged by switching T_2 on with a "clamp" pulse. Capacitor C_1 reduces the rise and fall times of the drive at T_1 gate, and by doing so, reduces the spike amplitude appearing across C_2 which may otherwise cause significant phase errors.

6.4.3 Analogue to Digital Converters

The Hybrid Systems ADC 540-8 module (see Appendix B for manufacturer's data) forms the basis of the analogue to digital converter unit. It produces an 8 bit binary coded output in a conversion time of under 5 μS, with a unipolar input range of 0 V to +10 V. Figure 6.8 shows how this unit is interconnected to the rest of the system. The interfacing flag logic is included in this circuit diagram, but the device selection and data transfer circuitry is as indicated in figure 6.3. Strobing of the ADC is performed, when the flag has been cleared, by the back edge of the receiver gate pulse, since it is at this time that both the amplitude and phase of the sampled signal have been properly detected. The flag flip flop consists of two cross-coupled 3 input NAND gates, and this is cleared by B INIT I via inverter E, and $\overline{\text{IOTXX2}}$ and $\overline{\text{IOTXX4}}$ via the OR gate formed by diodes D_1 and D_2. The back edge of the ADC busy bit, which corresponds to conversion complete, sets the flag by triggering the SN74121 monostable circuit which then triggers the flip flop. When this occurs the SKIP bus is grounded by IOTXX1 passing through gate F and diode D_3. D_3 is included in series with the SKIP output in order to effectively form an OR gate with similar SKIP outputs of other peripherals. Alternatively an open collector NAND gate could be used for gate F.

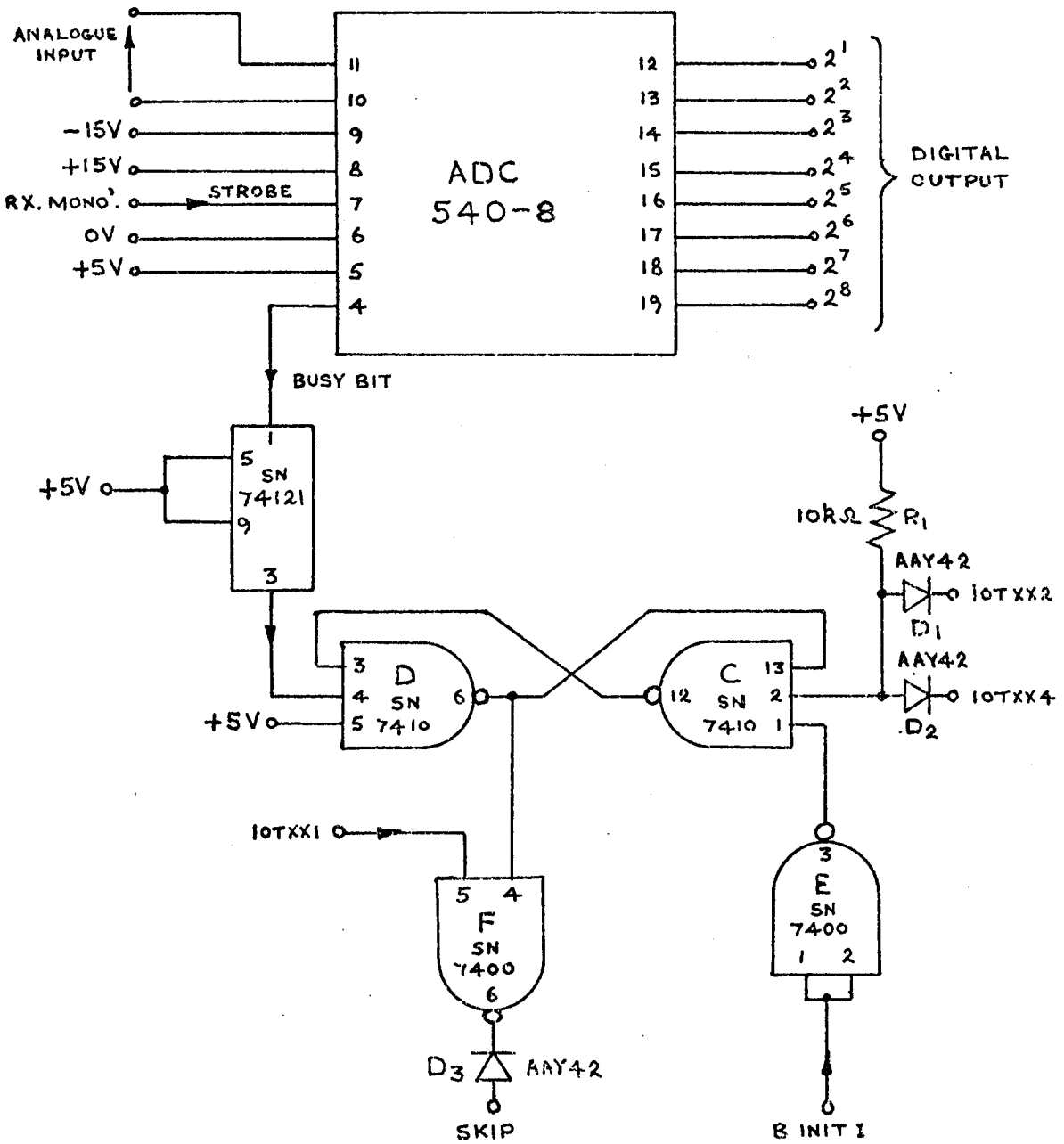

FIGURE 6.8 ADC INTERCONNECTIONS

The two converters are identical, the device codes being determined by the socket interconnections to the BMB high and low 03 to 08 lines. The amplitude ADC uses the code 14 and the phase ADC, 15.

6.5 The Computer Program

The program may be considered in three parts, Computation for Path Length Phase Increments, program 6.1, Image Reconstruction Routine, program 6.2, and, Phase and Amplitude Data Acquisition, program 6.3.

The calculation of path length phase increments has already been outlined in a general way in section 6.2.1 by equation 6.12. In practice the problem becomes a little more involved in order to account for the actual number of array elements and to allow for the inputting of any desired object plane dimension as the program proceeds. Figure 6.9(a) defines most of the important symbols used in the program. Distances O, L, X and H are all in wavelengths. The 10 array elements are spaced on 0·1 inch or 2·54 mm, centres and the wavelength of the 1 MHz ultrasound in water is 1·5 mm. Thus each element is spaced the equivalent of 1·69 wavelengths between centres. Assuming, as shown in figure 6.9(a), that the array and object planes are parallel and that their centres are on the same perpendicular axis, an element in the array line may be referenced about this axis, in wavelengths, by the expression,

$$1{\cdot}69(A - 4{\cdot}5) \qquad \ldots\ldots \quad 6.28$$

Similarly the distance in wavelengths of a point in the object plane from the centre line will be given by,

$$\frac{O}{N_{MAX}} \left(N - \frac{N_{MAX}}{O}\right) \qquad \ldots\ldots \quad 6.29$$

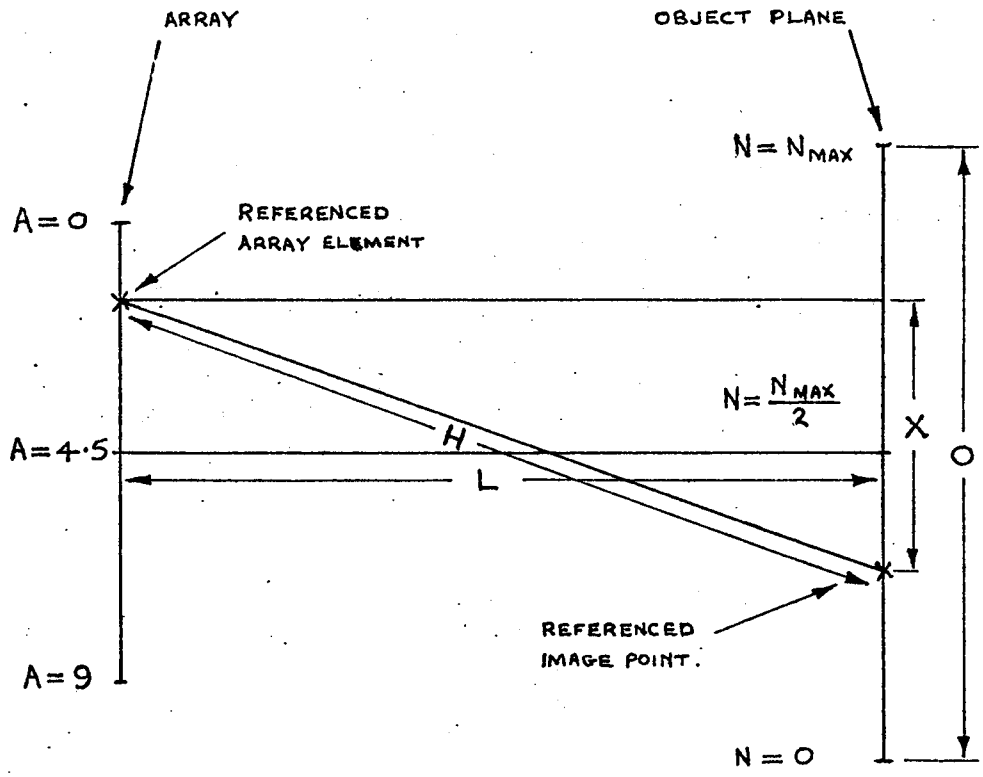

FIGURE 6.9 (a) DEFINITIONS OF SYMBOLS USED IN PROGRAM 6.1

Hence the magnitude of the distance X will be given by,

$$X = \left| \frac{O}{N_{MAX}} \left(N - \frac{N_{MAX}}{2}\right) - 1{\cdot}69(A - 4{\cdot}5) \right| \quad \ldots\ldots \quad 6.30$$

The program begins by setting up auto index registers R10, R11 and R13, which when indirectly referenced automatically address, for reading or depositing, consecutive locations in stores areas A and B. Then there follows the calculation and storage of the values of expression 6.28 for array elements A = 0 to A = 9. At the same time A is checked by the program so that when the calculations for all 10 elements have been made, the program moves to the next stage. This involves the inputting, via the teletype keyboard, and storing of the object plane dimension O and the object - array distance L, the latter being squared ready for use in the next section. Auto index register R13 is then reset so that the stored values of expression 6.28 may be used in the next calculation. This determines the values of X, as a first step, using equation 6.30, for array elements A = 0 to A = 9, and object elements N = 0 to N = N_{MAX}. There are thus, for N_{MAX} = 19, 200 values of X and these are squared before storage in locations controlled by auto index register R10. H may be calculated using the expression,

$$H = \sqrt{L^2 + X^2} \quad \ldots\ldots \quad 6.31$$

Using the value of L^2 stored earlier and the values of X^2 as they are calculated, the program next computes the 200 values of H, and, before storage in locations set by auto index register R11, converts these to fractions of 2π radians. The last part of this first section of the complete program counts the number of repetitions of the above so that the program is stopped when completed.

COMPUTATION FOR PATH LENGTH PHASE INCREMENTS 3/7/74

```
*200
        CLA CLL
        KCC
        TLS
        JMS I 7
        FGET INDXA
        FPUT R13
        FGET INDXB
        FPUT R10
LOOPA,  FGET A
        FSUB FOURP5
        FMPY ONEP7
        FPUT I R13
        FGET A
        FADD ONE
        FPUT A
        FSUB TEN
        FSZA
        FJMP LOOPA

        FIN             /READ O FROM KEYBOARD
        FPUT O
        FIN             / READ L FROM KEYBOARD
        FPUT L
        FSQU
        FPUT STORE
LOOPB,  FGET INDXA
        FPUT R13

LOOPC,  FGET N
        FSUB HFNMAX
        FMPY O
        FDIV NMAX
        FSUB I R13
        FSQU    / X SQUARED AND Y SQUARED
        FPUT I R10
        FADD STORE      / H SQUARED
        FSQR
        FSUB L
        FMPY TWOPI      / PHASE INCREMENT D IN RADIANS
AGAIN,  FPUT SAVE
        FSUB TWOPI      /
        FSNA
        FJMP AGAIN      /REDUCE TO FRACTION OF 2PI
        FJMP CONT       /
CONT,   FGET SAVE
        FPUT I R11      /STORE IN REGISTER 11
        FGET A
        FSUB ONE
        FPUT A
        FSZA
        FJMP LOOPC
        FGET TEN
        FPUT A          / RESET A TO 10
        FGET N
        FADD ONE
        FPUT N
        FSUB NMAXP1
        FSZA
        FJMP LOOPB
        FEXT
        HLT
```

Program 6.1

```
A,      0
        0
        0
N,      0
        0
        0
STORE,  0
        0
        0
SAVE,   0
        0
        0
L,      0
        0
        0
TWOPI,  3
        3122
        0000

ONE,    1
        2000
        0000

FOURP5, 3
        2200
        0000

ONEP7,  1
        3314
        0000

TEN,    4
        2400
        0000

0,      0
        0
        0

NMAX,   5       / DECIMAL 19
        2300
        0000

HFNMAX, 4       / DECIMAL 9.5
        2300
        0000

NMAXP1, 5       / DECIMAL 20
        2400
        0000

STOREA=1000
STOREB=1040
STOREC=2200


INDXA,  STOREA-3
        0
        0
INDXB,  STOREB-3
        STOREC-3
        0
*10
R10,    0
R11,    0
R12,    0
R13,    0
R14,    0
R15,    0

$
```

Program 6.1 (Cont.)

```
/ IMAGE RECONSTRUCTION ROUTINE  11/4/74


*400
        CLA CLL
        TLS
        TAD N20
        DCA TALLYB      /SET UP TALLY B TO -20
        JMS I 7
        FGET STORB      /   SET UP AUTO
        FPUT R16        /INDEX REGISTER R16
        FEXT
LOOPC,  TAD N10
        DCA TALLYA      /SET UP TALLY A TO -10
        JMS I 7
        FGET STORC      /   SET UP AUTO
        FPUT R10        /INDEX REGISTER R10
        FEXT
LOOPB,  JMS I 7
        FGET I R11      /GET PHASE DATA
        FSUB I R16      /P(N)-D(N,M)=Q(N)
        FPUT STOREQ     /STORE Q(N)
        FCOS            /COSQ(N)
        FMPY I R10      /J(N)=A(N)COSQ(N)
        FPUT STOREJ
        FADD JTOT       /TOTAL IMAGINARY PART
        FPUT JTOT
        FGET STOREQ
        FATN            /TANQ(N)
        FMPY STOREJ     /A(N)SINQ(N)=A(N)COSQ(N)*TANQ(N)
        FADD RTOT
        FPUT RTOT       /TOTAL REAL PART
        FEXT
        ISZ TALLYA      /INCREMENT TALLY A
        JMP LOOPB       /IF NOT ZERO, THEN JUMP TO LOOP B
        JMS I 7         /IF ZERO SKIP JUMP INSTRUCTION
        FGET JTOT       /GET J TOTAL
        FSQU            /J TOTAL SQUARED
        FPUT TEMP
        FGET RTOT       /GET R TOTAL
        FSQU            /R TOTAL SQUARED
        FADD TEMP
        FSQR            /SQRT (J TOT SQRD + R TOT SQRD)
        FOUT
        FGET ZERO
        FPUT JTOT       /RESET J TOTAL TO 0
        FPUT RTOT       /RESET R TOTAL TO 0
        FEXT
        ISZ TALLYB      /INCREMENT TALLY B
        JMP LOOPC       /IF NOT ZERO JUMP TO LOOP C
        HLT             /IF ZERO SKIP JUMP AND HALT

STORB,  STORED-3
        0
        0
STORC,  STOREA-3
        STOREP-3
        0
ZERO,   0
        0
        0
STOREQ, 0
        0
        0
STOREJ, 0
        0
        0
JTOT,   0
        0
        0
RTOT,   0
        0
        0
TEMP,   0
        0
        0
TALLYA, 0
TALLYB, 0
N10,    -12
N20,    -24

*2200
STORED, 0
*10
R10,    0
R11,    0
R12,    0
$
```

Program 6.2

```
/ PHASE AND AMPLITUDE DATA ACQUISITION    11/4/74


*200
        CLA CLL
        6140
        6150
        JMS I 7
        FGET STORA          /    SET UP AUTO
        FPUT R16            / INDEX REGISTER R16
LOOPA,  FEXT
        JMS AMP             /READ AMPLITUDE DATA
        DCA 044
        JMS I 7
        FLOT                /CONVERT AMP DATA TO F.P. FORM
        FPUT I R16          /STORE IN R16
        FEXT
        JMS PHASE           /READ PHASE DATA
        DCA 044
        JMS I 7
        FLOT                /CONVERT PHASE DATA TO F.P. FORM
        FDIV PCONST         /CHANGE TO RADIANS
        FPUT I R17          /STORE IN R17
        FISZ R20            /
        FJMP LOOPA          /REPEAT DECIMAL 10 TIMES
        FEXT
        JMP I RECON         /THEN JUMP TO IMAGE RECONSTRUCTION

AMP,    0
        6141
        JMP .-1
        6146
        JMP I AMP

PHASE,  0
        6151
        JMP .-1
        6156
        JMP I PHASE

STORA,  STOREA-3
        STOREP-3
        -12
COUNT,  0
PCONST, 6
        2424
        0000
RECON,  400

*16
R16,    0
R17,    0
R20,    0

*3400
STOREA, 0

*4000
STOREP, 0
```

Program 6.3

Program 6.3 is the next section which the computer follows. This performs the phase and amplitude data acquisition and transfer from the two ADC's to the computer store. Auto index registers are again used to route the data to sequential store locations, and the program is arranged to repeat 10 times so that the data from all 10 array elements is inputted. Phase data has to be converted into radians by dividing by an appropriate phase constant, P_{CONST}. After completing this section the program jumps to the next, program 6.2.

The image reconstruction routine, program 6.2, follows in outline the procedure given in section 6.2.1, and in particular equations 6.5 to 6.10. The symbols used are different, however, owing to the limited teletype keyboard. The main theme of the computer procedure is explained in program 6.2, data for the path length phase increments and the array element phase and amplitude signals being taken out of the store when required, using, once again, auto index registers. The resultant image amplitudes of the 20 object points are finally printed out and the program halts when this is completed.

6.6 Results

Before the computer peripheral interfacing had been completed single line 1-dimensional results for both simulated and real point sources were obtained using the FOCAL image reconstruction program 6.4. Phase measurements were made using a laborious Lissajous figure method and were in consequence not very accurate due to phase drift during the time required to measure the 10 element signals. In spite of this, these results, which are not included here, did demonstrate quite effectively the validity of the processing principles. The array element phases were calculated, based on path lengths, for a simulated point source offset by 7·5 wavelengths or 3 object line elements from the array central axis, and at a

```
 WRITE ALL
C-FOCAL, 1969

01.10 S K=1.7; S PI=3.142
01.20 S C=50
01.30 S L=200
01.40 S N=21
01.70 F I=-10,10; DO 2.0
01.80 QUIT

02.10 F A=0,9; DO 3.0
02.20 T " "%2.00,"I"I
02.30 T %6.03,"  VT"FSQT(JT*JT+RT*RT),!

03.10 S H(A)=FSQT[<(I*C/N)-(A-4.5)*K>*<(I*C/N)-(A-4.5)*K>+L*L]
03.20 S D(A)=[H(A)-L]*2*PI;
03.30 S P(0)=3.41; S P(1)=2.67; S P(2)=2.02; S P(3)=1.46
03.40 S P(4)=0.99; S P(5)=0.61; S P(6)=0.33; S P(7)=0.13
03.50 S P(8)=0.02; S P(9)=0
03.60 S V(A)=1
03.80 S Q(A)=P(A)-D(A)
03.90 S J(A)=V(A)*FCOS(Q(A)); S R(A)=V(A)*FSIN(Q(A));
03.91 S JT=J(0)+J(1)+J(2)+J(3)+J(4)+J(5)+J(6)+J(7)+J(8)+J(9)
03.92 S RT=R(0)+R(1)+R(2)+R(3)+R(4)+R(5)+R(6)+R(7)+R(8)+R(9)
*


 GO

 I=-10  VT=    1.285
 I=- 9  VT=    1.402
 I=- 8  VT=    0.973
 I=- 7  VT=    0.078
 I=- 6  VT=    1.021
 I=- 5  VT=    1.928
 I=- 4  VT=    2.233
 I=- 3  VT=    1.640
 I=- 2  VT=    0.066
 I=- 1  VT=    2.305
 I=  0  VT=    5.044
 I=  1  VT=    7.587
 I=  2  VT=    9.374
 I=  3  VT=   10.000
 I=  4  VT=    9.324
 I=  5  VT=    7.507
 I=  6  VT=    4.961
 I=  7  VT=    2.244
 I=  8  VT=    0.093
 I=  9  VT=    1.653
 I= 10  VT=    2.253
*
```

Program 6.4 FOCAL program for simulated offset point source.

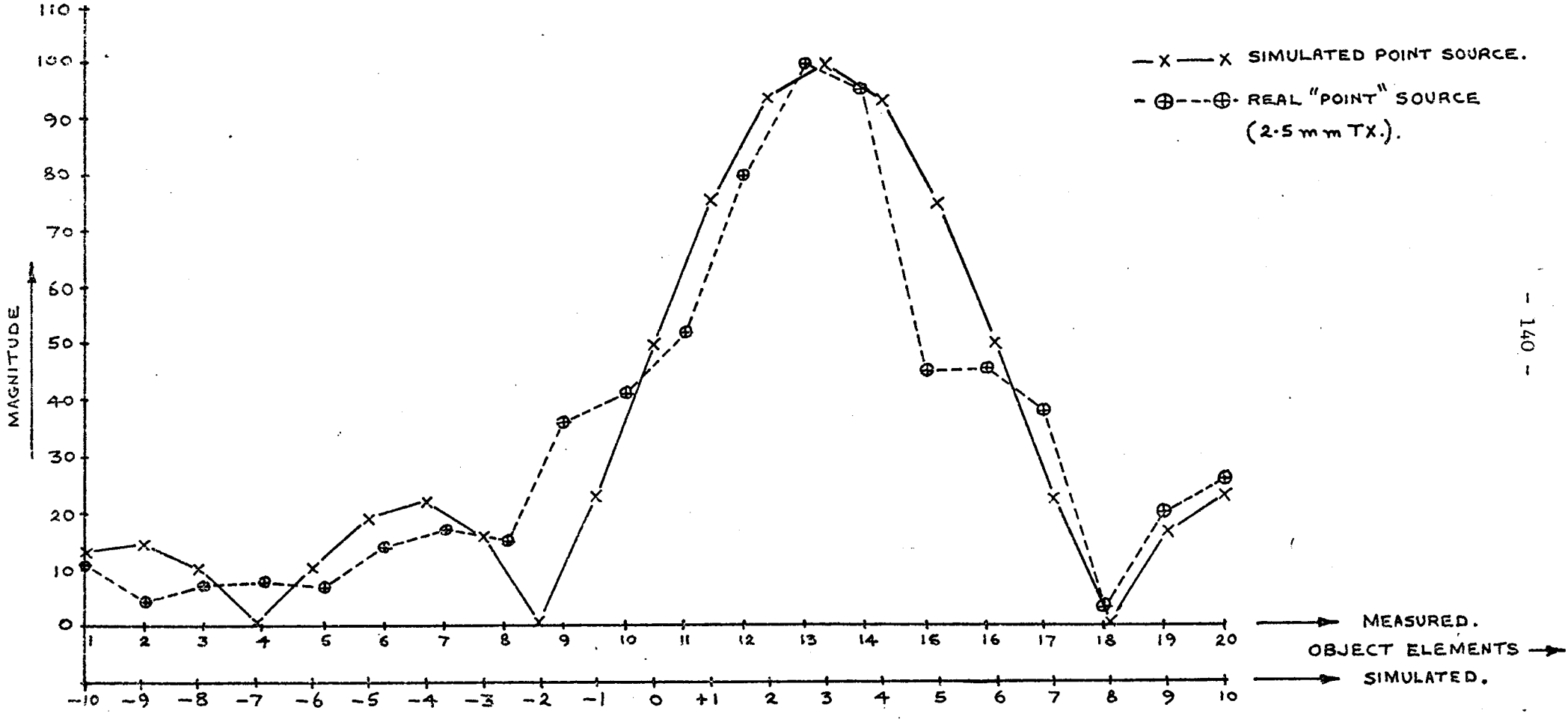

FIGURE 6.9 SIMULATED POINT SOURCE COMPARED WITH REAL "POINT" SOURCE.

distance of 300 mm. It was assumed that the amplitudes of the signals reaching all 10 array elements would be identical and these were therefore made equal to unity. The ten calculated phases and the single value of the amplitude were included in the program 6.4 as shown, and the resulting plot of the computed signal magnitude along the chosen object line is given in figure 6.9. It will be noted that it has the distinctive $\frac{\sin x}{x}$ form, as would be expected if reference is made to the relevant expression 6.21. From this expression the first zeros should be situated at approximately +29 mm and -6·5 mm, corresponding to +7·7 and -1·7 object line elements about the centre. Referring to figure 6.9 again, the zeros in fact occur at +8 and -2 elements, and within the errors caused by the effective sampling of the object line compare well with those predicted by expression 6.21. The results for a real "point" source, placed in the same position as the simulated source, have been calculated using the on-line system and are presented for comparison in figure 6.9. The amplitudes of the simulated and real results have been normalised so that they are equal at the central maximum to make the comparison easier. The number of object line elements in the on-line program is unfortunately one less than that used for the off-line program, so that two horizontal scales are given. The two results compare very favourably, even to the extent that the ripples are of a somewhat similar form. Two points should be born in mind when considering this comparison; firstly the real "point" source was a 2·5 mm square transducer which may easily have had an asymmetric radiation pattern, and secondly, no account has been taken of the normal spherical radiation patterns of the array elements and "point" source. The latter probably causes the real result to indicate a better resolution than that shown by the simulated results.

Figure 6.10 shows an on-line computer reconstructed image of a 10 mm

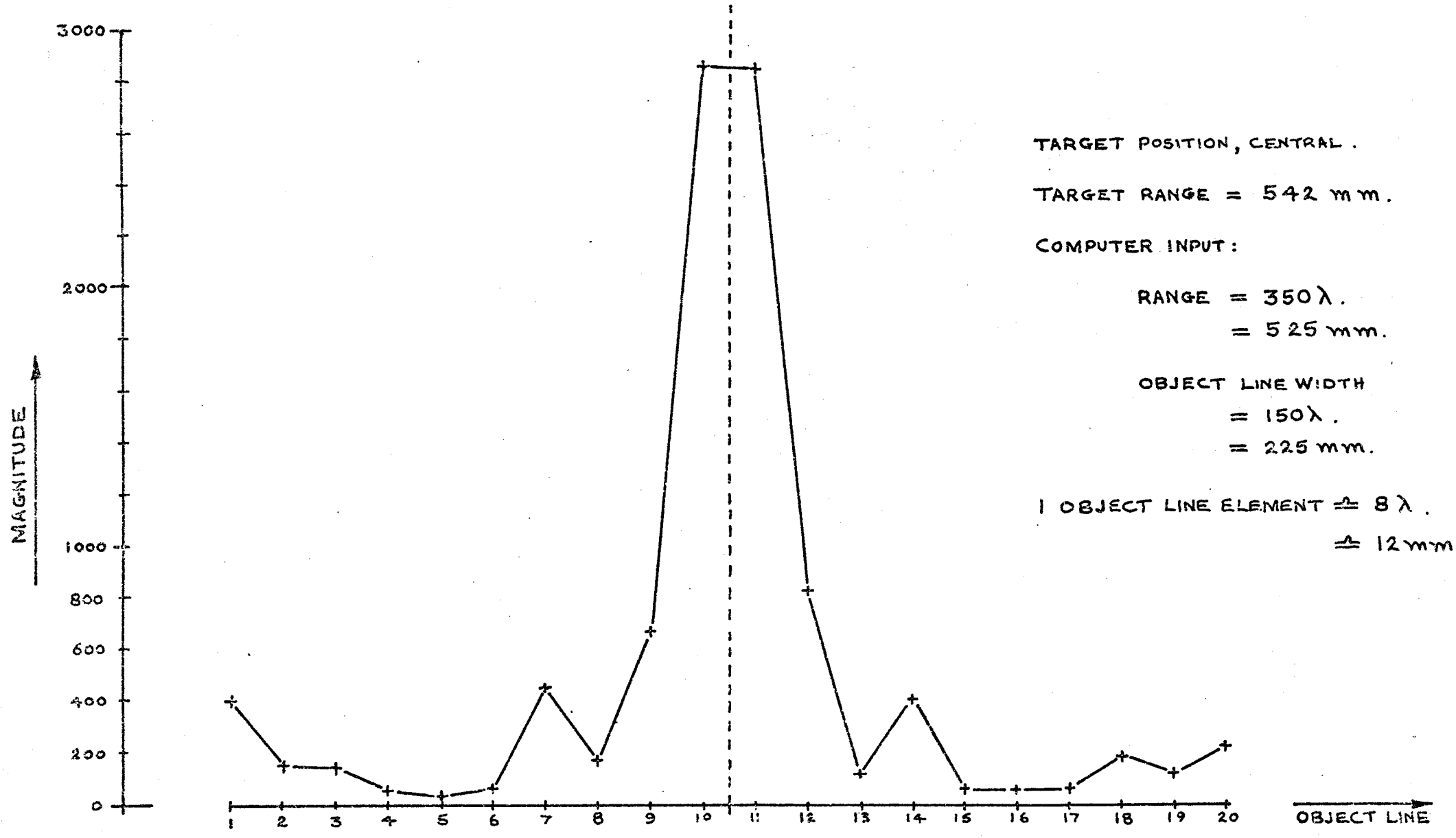

FIGURE 6·10 COMPUTER RECONSTRUCTED IMAGE OF 10mm. TRANSMITTER

transmitter situated on the system axis at a range of 542 mm. The computer was programmed with a range of 350 wavelengths, or 525 mm, and an object line width of 150 wavelengths, or 225 mm. The difference between the actual range and that given to the computer was intended to allow for the near field region of the transmitter. In practice at ranges of that order the focusing action of the computer is almost negligible, resulting in a very large depth of field. The result is a strikingly symmetrical response with a well defined central maximum and with the predicted zeros on each side. Again using expression 6.21 these would be expected at ± 32 mm about the centre, or ± 2·7 object line elements. Referring to figure 6.10 it will be seen that the zeros occur near ± 2·5 elements about the centre, which again provides a good agreement with the predicted positions. The maximum side-lobe level is nearly 16 dB's down on the main signal.

In order to demonstrate that major side-lobes were present as expected in the radiation pattern of the array, the object line width was extended to 500 wavelengths with the range set to 440 wavelengths. A 25 mm transmitter, used as the target, was positioned approximately 50 wavelengths to the left of the central axis. The on-line computer reconstructed results for this test are presented in figure 6.11, and show very clearly the right hand major side-lobe. The array has an element pitch of 2·54 mm (0·1 inch) and this should produce major side-lobes at angles of approximately 36^{o} each side of the array normal. Using this figure and converting it into an object line distance gives an estimated separation between the main and side-lobe of approximately 415 mm. From figure 6.11 the separation is 11 elements, which corresponds to 435 mm. Bearing in mind that the object line sampling may not have located the exact positions of the two maxima, this result compares very reasonably with the predicted figure.

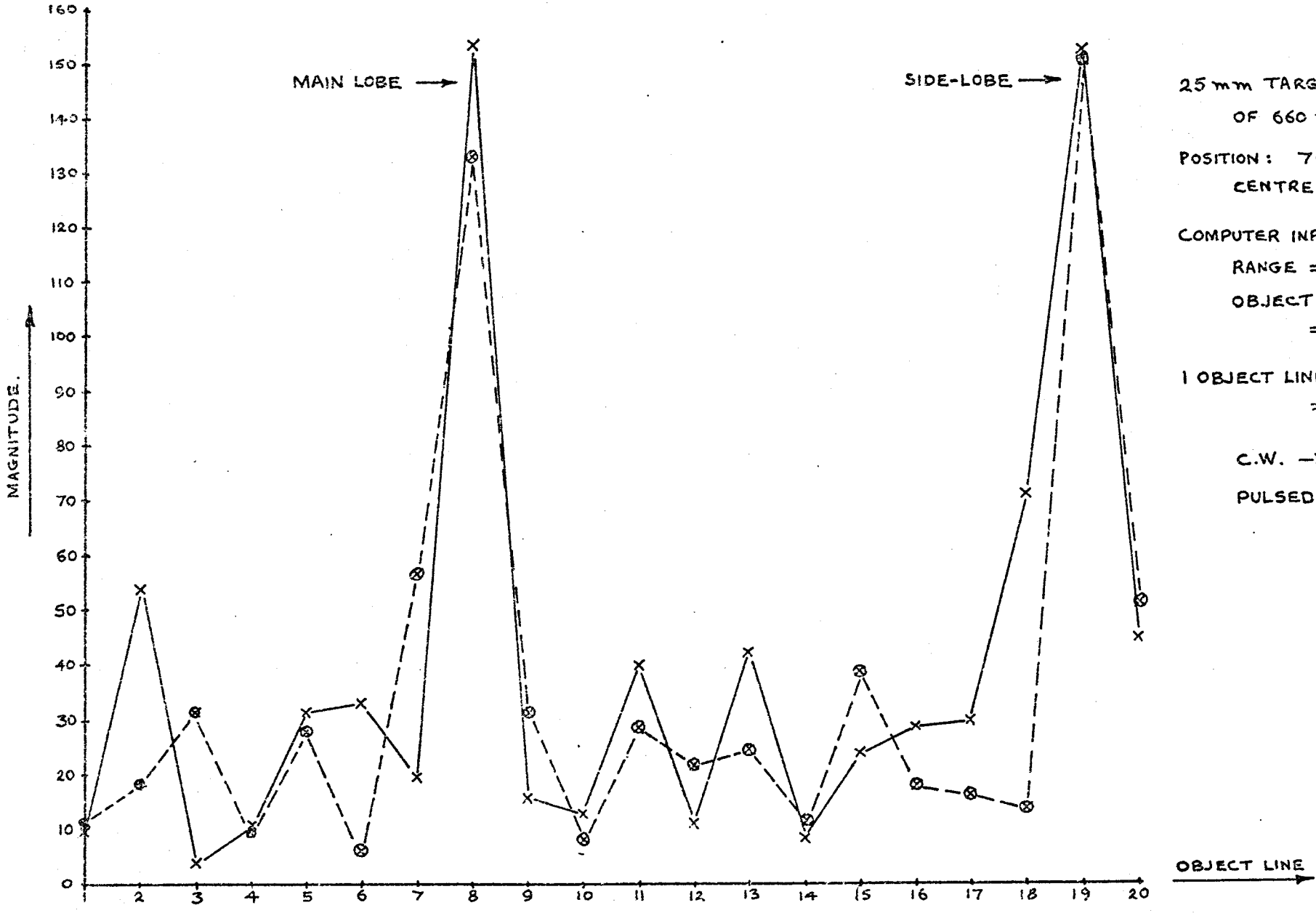

25 mm TARGET (TX.) AT RANGE OF 660 mm.

POSITION: 75 mm LEFT OF CENTRE (50λ) APPROX.

COMPUTER INPUT:

RANGE = 440λ.

OBJECT LINE WIDTH = 500λ.

1 OBJECT LINE ELEMENT ≙ 26λ.

C.W. —X——X—

PULSED. -⊗---⊗-

FIGURE 6.11 COMPUTER RECONSTRUCTED IMAGE SHOWING EFFECT OF MAJOR SIDELOBE.

The approximate 50 wavelength offset of the target, is represented by 2·5 object line elements in figure 6.11, corresponding to 65 wavelengths, based on the object line width of 500 wavelengths. Two plots are shown in the figure, one the result of using continuous wave transmission and the other that for pulsed operation. For the former a rather large spurious peak appears in the position of element number 2 which under pulsed operation is no longer present. This suggests that it is caused by a reflection, and it seems likely that this was the water surface (left in practice being high and right, low). Neglecting the spurious signal, the ripple level is approximately 11 dB's down on the two main signals.

Figures 6.12 and 6.13 show the results of focused near field operation. The object line width has to be kept to within certain limits otherwise the major side-lobes will appear. For figure 6.12 the separation between the main lobe and the first major side-lobes would be approximately equivalent to 50 object line elements, so that the side-lobes will be well off the picture. In the case of figure 6.13, however, the separation between these would be very approximately 15 object line elements, and the effect of the right hand major side-lobe can be clearly seen for the result when the target is positioned 5 wavelengths to the left. The target, when intended to be positioned 5 wavelengths to the right of centre, was evidently only approximately 4 wavelengths to the right. Thus the side-lobe for this response is not quite detectable. Figure 6.12 demonstrates a resolution, based on 50% amplitude, of around 6 wavelengths, and this does not significantly reduce when the focal point is deflected to the left or right, although interesting and symmetrical kinks begin to appear on the lower slopes of the responses. Surprisingly, the resolution given by the results shown in figure 6.13, where the target is positioned only 33 mm from the array, is considerably better, being approximately 4·5

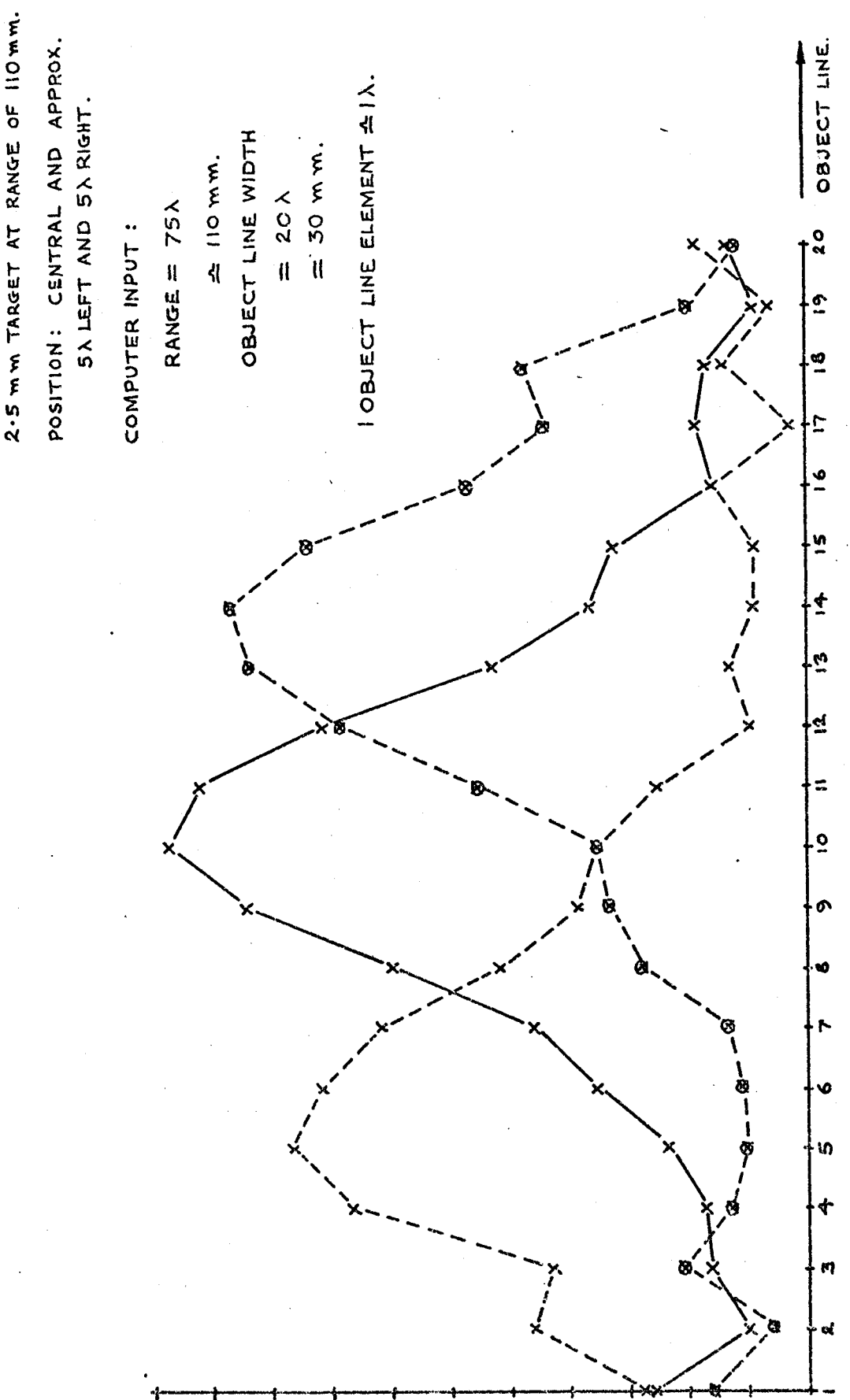

FIGURE 6.12 FOCUSED NEAR FIELD IMAGES.

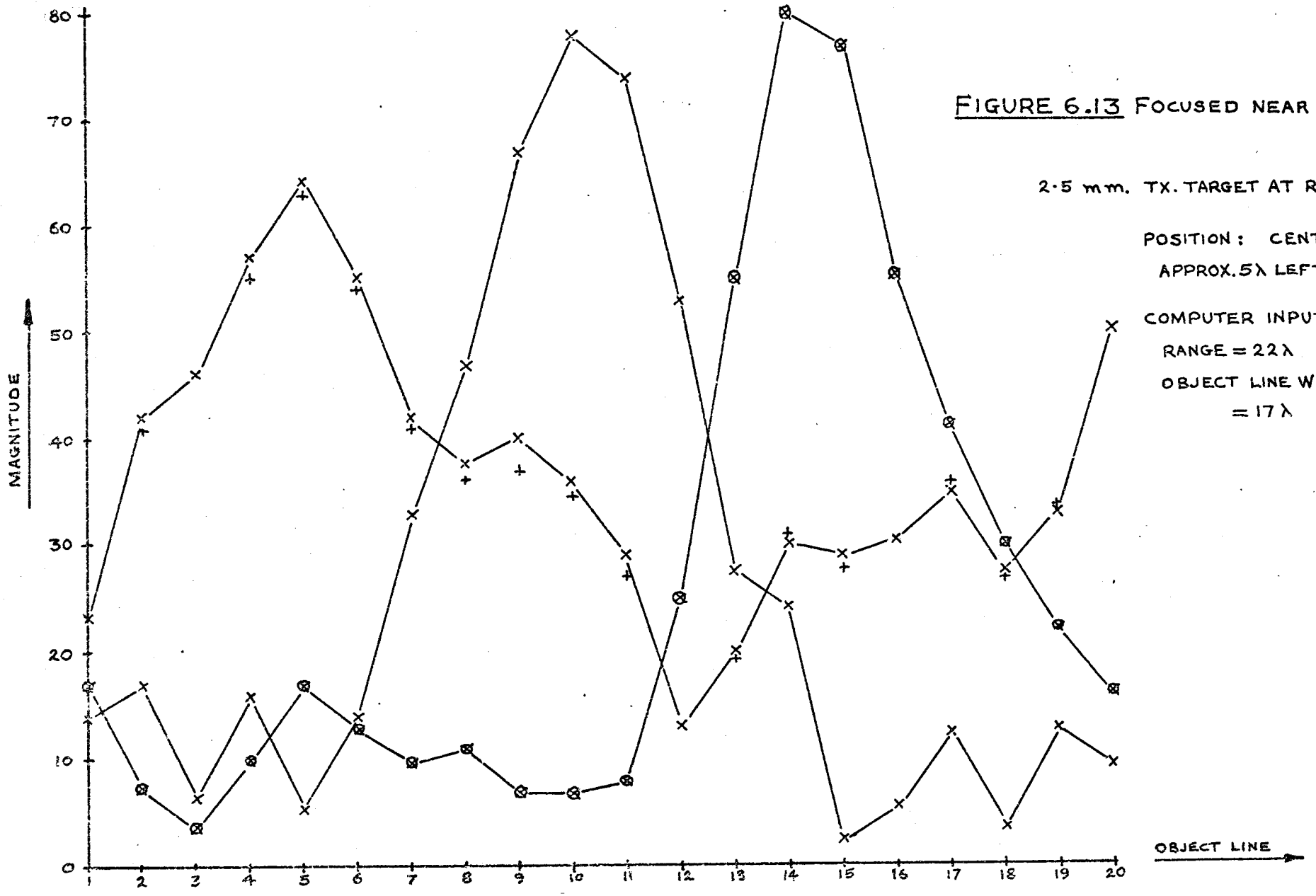

FIGURE 6.13 FOCUSED NEAR FIELD IMAGES.

2·5 mm. TX. TARGET AT RANGE OF 33 mm.

POSITION: CENTRAL AND APPROX. 5λ LEFT AND 5λ RIGHT.

COMPUTER INPUT:
RANGE = 22λ
OBJECT LINE WIDTH = 17λ

wavelengths. Although the targets were only positioned approximately 5 wavelengths left and right of centre, the ability of the system to deflect its focal point without a significant loss of resolution is well demonstrated by these last results. In figure 6.13 a check is shown on the consistency of the results for the response with the target at 5 wavelengths left of centre. A repeat run was made of the computer processing and array element data reading and these additional results are shown by small plus signs, where they are not identical to the previous results. The agreement is very close and demonstrates that the somewhat strange shape of this particular response is not the effect of random noise.

Ultimately a practical imaging system needs to be able to operate in a reflection mode. Although in principle there is no real difference as far as a receiver is concerned between an ultrasonic transmitter and a reflecting object, apart from the possibly less coherent form of the waves received from the latter, it was considered to be a useful demonstration to carry out such a test. A small piece of expanded polystyrene, approximately 10 mm square, was supported on the central axis at a distance of 310 mm from the array, and insonified by a transmitter placed off axis and between the array and the target. The angle of one of the faces of the polystyrene target was carefully adjusted so that the maximum signal was directed towards the receiving array. Figure 6.14 shows the resulting plot of the computer reconstructed "image" of this and also with the target offset by approximately 10 wavelengths left and 10 wavelengths right. When offset the target was not readjusted to maximise the array output, and this is the probable reason why the peak amplitudes of the responses for the off axis positions are so much smaller than that for the centrally placed target. One object line element corresponds to approximately 2·6 wavelengths and with a target size of around 10 mm, or 7 wavelengths,

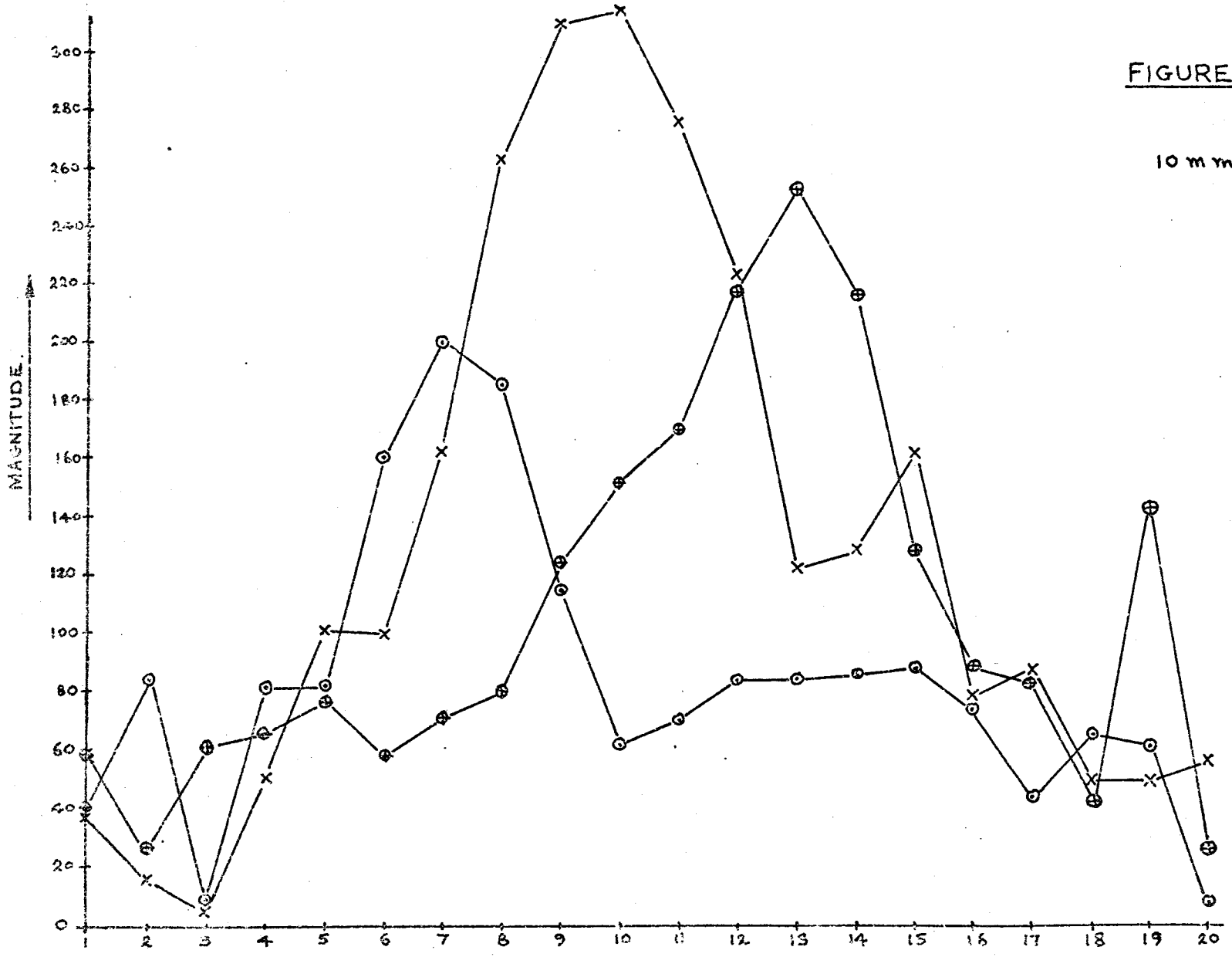

FIGURE 6.14 IMAGES BY REFLECTION.

10 m m. SQUARE TARGET AT RANGE OF 310 m m

POSITION : APPROX CENTRAL
10λ LEFT AND 10λ RIGHT.

COMPUTER INPUT :

RANGE = 200λ
OBJECT LINE WIDTH
= 50λ.

1 OBJECT LINE ELEMENT ≙ 2·6λ.

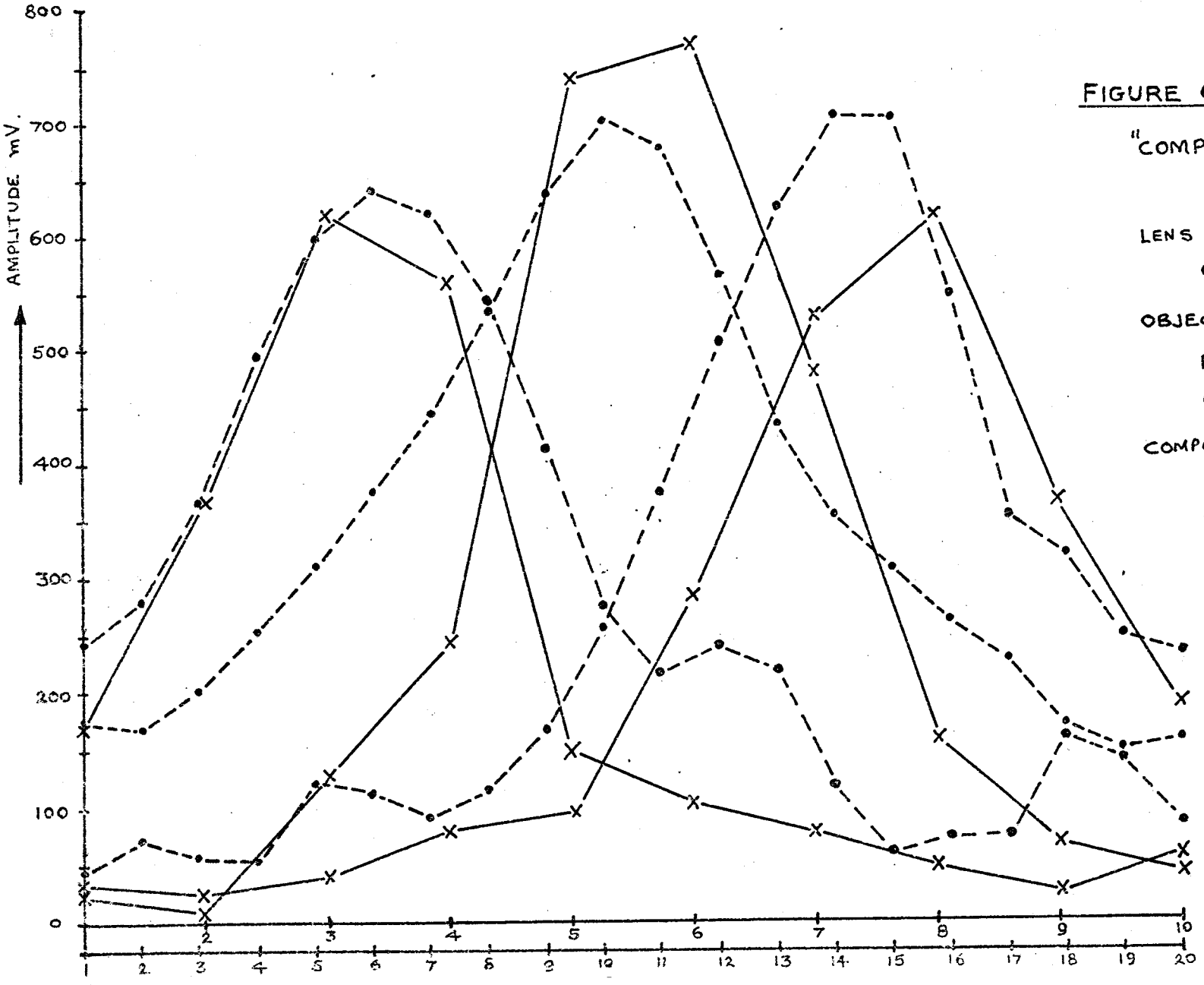

FIGURE 6.15 PERSPEX LENS AND "COMPUTER LENS" COMPARISON

LENS : MAGNIFICATION UNITY.
OBJECT LENS DISTANCE = 100 mm.

OBJECT : 2·5 mm TX.
POSITIONED CENTRALLY AND
APPROX 5 λ LEFT AND 5 λ RIGHT.

COMPUTER INPUT :
RANGE = 67 λ
OBJECT LINE WIDTH = 17 λ.

PERSPEX LENS —x——x—

COMPUTER LENS —•——•—

ARRAY ELEMENT.
IMAGE ELEMENT.

square it is evident the latter is far from a point source, and this, plus the fact that it had irregular contours, accounts to some extent for the rather poor response shape.

Lastly, a comparison was made between a perspex lens (that used for the ultrasonic camera system described in chapter 5) and a computer "lens". The lens was positioned to provide unity magnification and was used to image a 2·5 mm transmitter at a lens-transmitter distance of 100 mm. The transmitter was placed in three positions, centrally and 5 wavelengths left and 5 wavelengths right, and the array element signal amplitudes of the matrix line 1 were measured using a valve voltmeter. The results of this test are shown in solid lines in figure 6.15. In order to as nearly as possible simulate the same conditions for both lens and lensless tests, when the computer was used the target was positioned at a distance of 100 mm from the array, and the computer was programmed to produce an object line width equal to the array length of 17 wavelengths. The results of this test are shown in figure 6.15 using dashed lines. Accurate positioning of the target was very difficult and accounts for the differences in the image positions for the two processing methods. The most important point to be made from these results is that in spite of the perspex lens aperture being more than three times that of the array, the resolution is not significantly better, particularly off axis. Spherical aberration should not be present in the computer "lens" but is certainly present in the uncorrected spherical perspex lens, and this may account for its rather poor relative performance.

6.7 Future Work

The results obtained up to the present have been in one dimension only and an impressive but relatively simple step will be the extension of the processing to produce images in two dimensions. The same approach

will be used, the programs merely requiring extension in terms of the number of operations performed rather than the addition of any special steps. It is expected that the computing time may become quite long, and this will have to be carefully watched and the program optimised for minimum time. There are two important aspects of the work on which it is felt considerably more time could be usefully spent. The first of these is to determine what effect using an incomplete matrix of transducers[50] has on the imaging properties and performance of the system. The second is a thorough investigation into the near field focusing action of the array or matrix.

Practical improvements should be made to the programming to enable the inherent system flexibility to be fully realised, so that, for example, the range and object plane dimensions are controllable, whilst processing proceeds, from the keyboard. Also, a relatively simple step should be made by interfacing three digital to analogue converters to the computer so that the image may be displayed on a CRO.

6.8 Conclusions

The 1-dimensional results obtained using point source transmitters demonstrate the effectiveness of the computer processing of array signals for both beam deflection in the far field and, more significantly, focusing in the near field. The results adequately confirm the theory presented and compare very favourably with those achieved using the much wider aperture perspex acoustic lens. Off axis resolution is maintained to a greater extent with the computer "lens" than is apparent in the case of the acoustic lens, and it is suggested that this is caused by the absence of spherical aberration in the former. Images in 1-dimension of a reflecting target have been successfully produced. Near field focusing appears to be very effective and results with a point source as near as 33 mm to the

array are better than those obtained at 100 mm, the former demonstrating a resolution of around 4 wavelengths with an aperture of 17 wavelengths and a range of 22 wavelengths.

The on-line facility has proved to be very effective, its flexibility being its main attribute. The computation time involving 10 transducer array elements and 20 object line elements is virtually unnoticeable.

7. Scanned Array Doppler System

7.1 Introduction

The basic principles of this processing method have already been outlined in chapter 3. Here more theoretical details and an account of the experimental work and its results will be given. The investigations described are only of a preliminary nature, however, and were intended to show the feasibility of such a method of signal processing. The principle is undoubtedly well demonstrated by the results obtained and there is clearly much further work to be done on what may prove to be an extremely simple yet effective underwater imaging system.

The fact that a scanned receiving aperture produces an output whose harmonic content contains information on the bearings of insonified and reflecting targets was first considered as being possibly applicable to electron beam scanned ultrasonic image converter tubes. The velocity of the scanning beam in conjunction with the incident plane waves on the transducer face would produce a Doppler shifted frequency at the secondary electron collector output. Later the principle was experimentally investigated using a sampled array of transducers, and although this did not use the solid state ultrasonic image converter, because the operating frequency of the latter was too high for the underwater application in mind, it was a basically similar FET scanned array. Figure 7.1 shows the basis of the system, which relied on adherence to the sampling principle in order that it may be considered to act as a continuous aperture. The low pass filter formed the demodulator so that the sampling frequency was effectively removed, leaving only the frequencies of interest in the output f_R. These may be either above or below the ultrasonic frequency, dependent on which side of the array normal the reflecting target is situated. For the incident wave shown in figure 7.1 the resultant frequency will be less than the ultrasonic frequency.

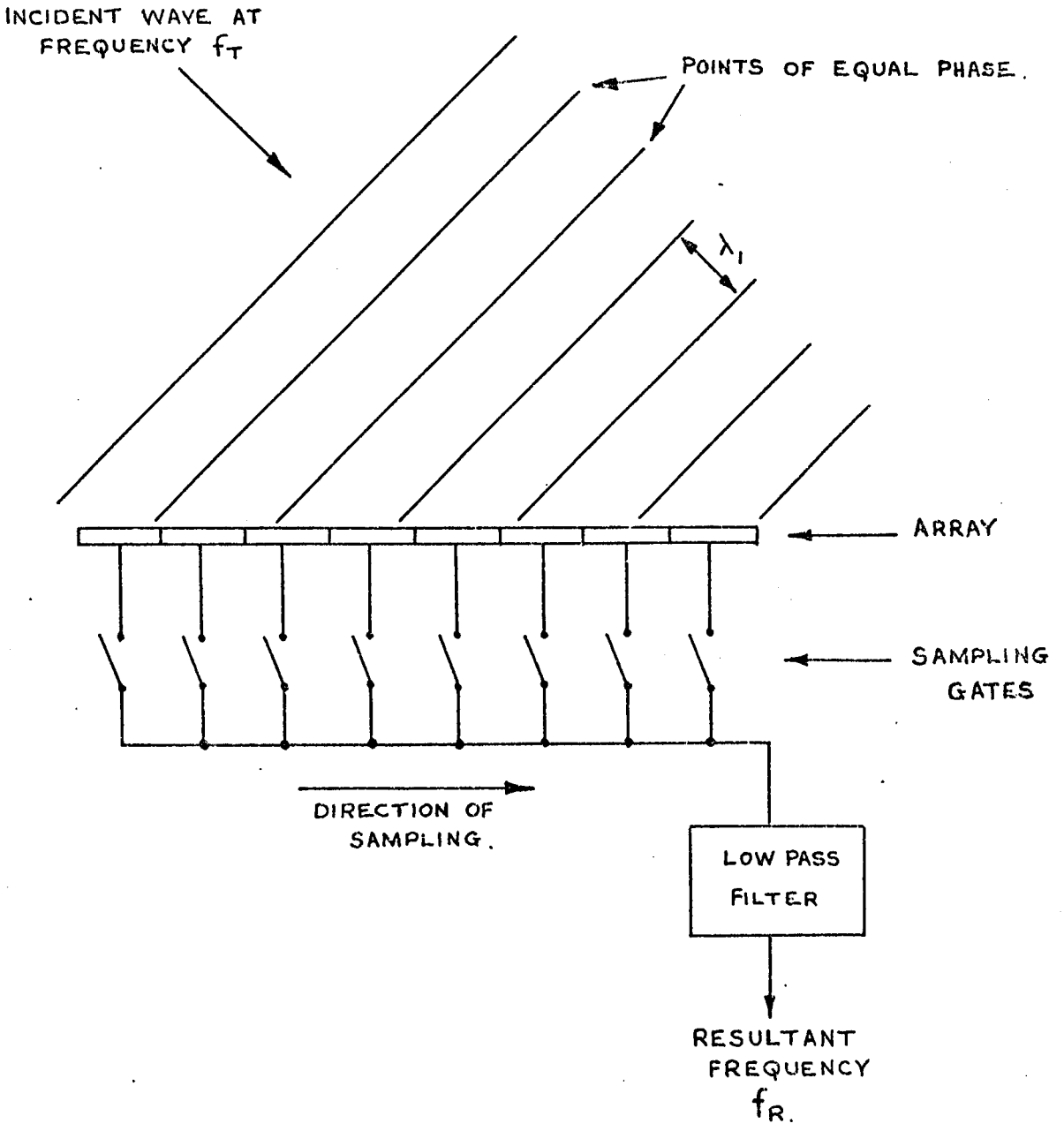

FIGURE 7.1 BASIC PRINCIPLE OF SYSTEM.

7.2 System Principles

An echo returning from an insonified target situated in the far field of an array of ultrasonic transducers will strike this array at an angle dependent on the target bearing. If the array is linear and consists of equally spaced elements which are sampled sequentially at a known and fast enough rate, the resultant electrical samples, after appropriate demodulation, will produce a sinusoidal signal whose Doppler shifted frequency is a function of the angular bearing of the target. Figure 7.2 shows diagrammatically how this frequency component is formed from the sequential samples.

Consider the array to be of infinite length and consisting of an infinite number of infinitely small elements. Referring to figure 7.3, the velocity of a point of constant phase along the array is seen to be $C_1/\sin\theta$, where C_1 is the longitudinal wave velocity in water and θ the angle of incidence of beam to receiver array, and the resulting apparent velocity, C_R, of a point of constant phase to the sampling position is given by,

$$C_R = \frac{C_1}{\sin\theta} - C_S \qquad \ldots\ldots \quad 7.1$$

where C_S is the sampling velocity.

This gives a resultant output frequency, $f_{R\theta}$, of

$$f_{R\theta} = f_T \left[1 - \frac{C_S}{C_1} \sin\theta \right] \qquad \ldots\ldots \quad 7.2$$

where f_T is the transmitted ultrasonic frequency. In practice the elements will be of finite size and spaced at finite distances so that each element must be sampled for a short period sequentially. Thus a series of amplitude samples will be obtained and these require demodulation using a suitable low pass filter in order to recover the frequency $f_{R\theta}$.

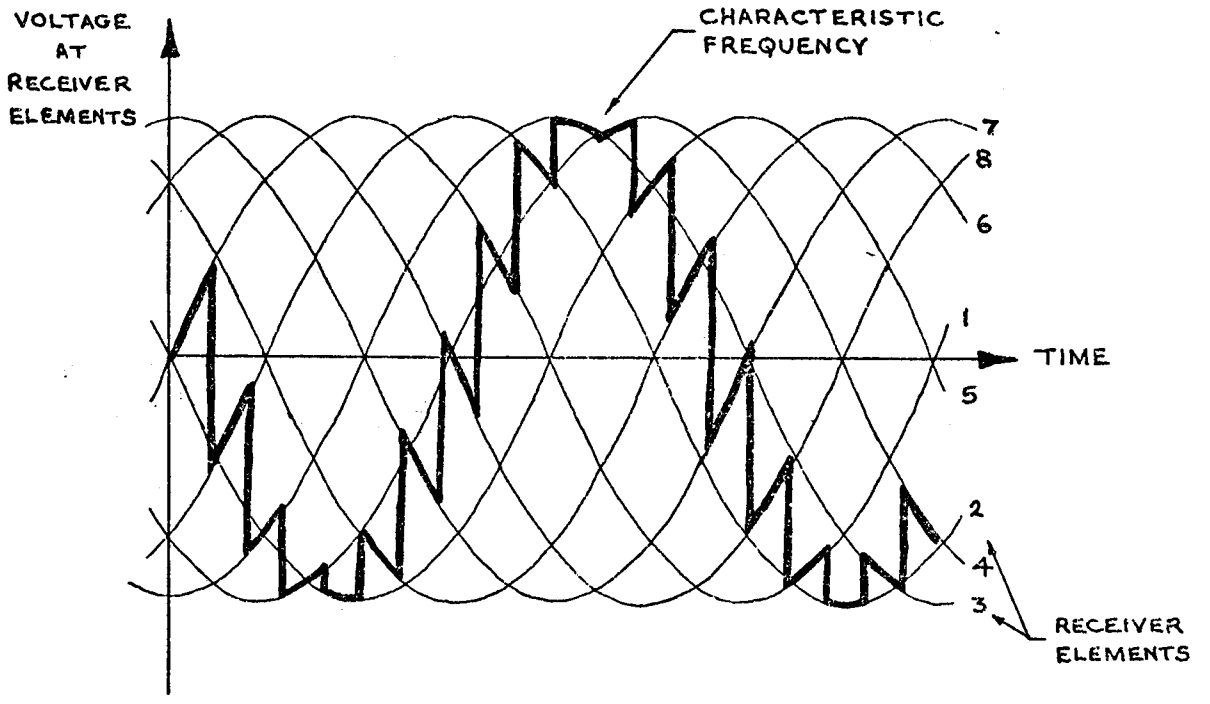

FIGURE 7.2 How sequential sampling builds up the characteristic frequency.

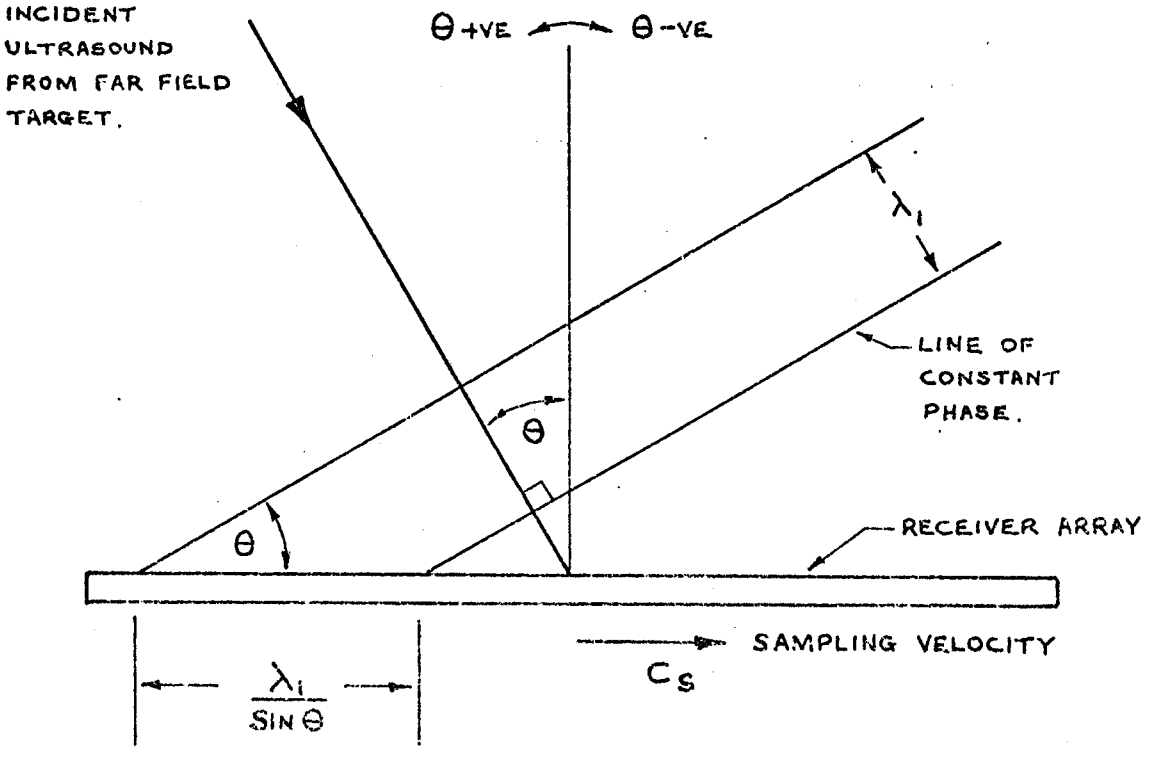

FIGURE 7.3 Diagram used for derivation of theory.

In practice then

$$f_{R\theta} = f_T \left[1 - \frac{f_s\, d}{C_1} \sin \theta \right] \qquad \ldots\ldots \quad 7.3$$

where d is the distance between centres of adjacent receiver elements. This may be written

$$f_{R\theta} = f_T \left[1 - \frac{p\, d}{\lambda_1} \sin \theta \right] \qquad \ldots\ldots \quad 7.4$$

where p is the ratio $\frac{f_s}{f_T}$ and λ_1 is the wavelength of longitudinal waves in water. Figure 7.4 shows plots of equation 7.4 for various values of p and with $\frac{d}{\lambda_1} = 1$. The theoretical limit to the target bearing, θ, is given by the sampling principle requirement that $f_s > 2\, f_{R\theta}$.

In order to use continuous sampling for a finite array length, the equality

$$n\, \phi = 2\pi q \qquad \ldots\ldots \quad 7.5$$

must apply, where n is the total number of elements in the array, ϕ is the phase difference between adjacent elements for angle of incidence θ, and q is any integer. Therefore only discrete resultant frequencies can be obtained and these are given by

$$f_{R\theta} = f_T \left[1 - \frac{p\, q}{n} \right] \qquad \ldots\ldots \quad 7.6$$

These will be referred to as characteristic frequencies.

The corresponding discrete target bearings will then be given by

$$\theta = \sin^{-1} \left[\frac{q\, \lambda_1}{dn} \right] \qquad \ldots\ldots \quad 7.7$$

If q = 1 in equation 7.7 the first suitable angle for continuous sampling is given. The second suitable, or discrete, angle when q = 2 will be

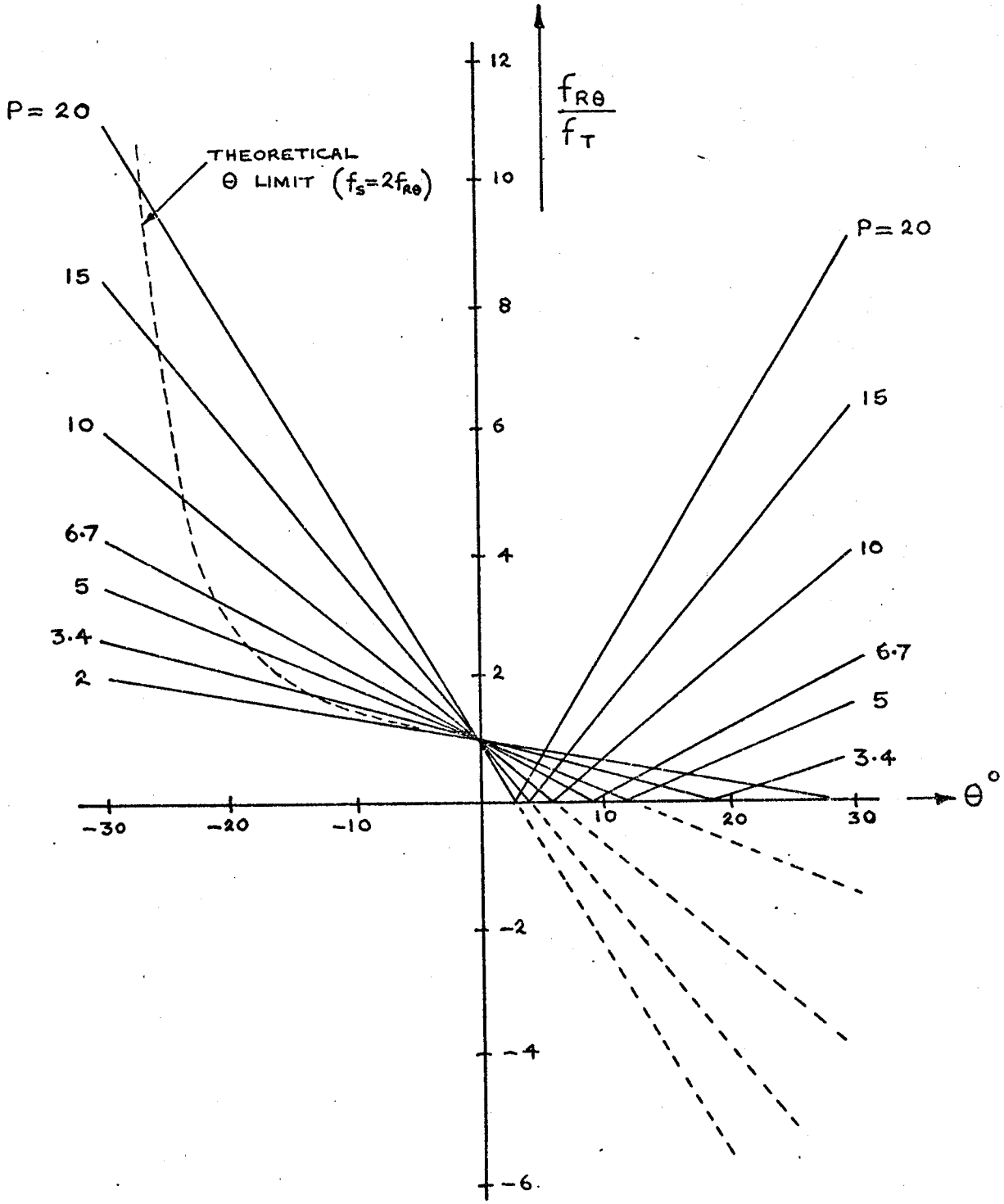

FIGURE 7.4 PLOT OF $f_{R\theta}$ AGAINST TARGET BEARING FOR $d/\lambda_1 = 1$.

virtually twice the first, these angles being small. Thus a measure of the angular "resolution", θ_{Res}, of this system will be the angle θ given when $q = 1$. That is

$$\theta_{Res} \simeq \frac{\lambda_1}{dn} \qquad \ldots\ldots \quad 7.8$$

The beam width of the array is also given by equation 7.8, since the first zero in the polar plot will occur when the angle of the incident wave causes one complete half cycle to appear across the array. The "resolution" given by equation 7.8 however means that the polar plot will take the form of a set of fingers whose positions are fixed, leaving "blind" areas between each finger. It should be pointed out that bearing information about targets within the whole sector can however be present in the samples obtained from a single scan of the array elements, but that the extraction of this information is more complex.

7.3 Experimental Work

7.3.1 The Transducer Array and Sampling Electronics

The transducer array used in the experimental system consisted of one 20 element line of a 500 kHz circular transducer multielement matrix. Acoustic cross-coupling was reduced somewhat by grooves cut between adjacent elements, and the resulting pitch was 2·4 mm. Insulated but unscreened wires were soldered to the silvered electrode of each element and the connections and electrodes were covered by a thin layer of epoxy resin to both insulate and to provide some mechanical support for the wires. Scanning of the 20 transducer elements used 20 UC734 n-channel junction FET sampling gates (see figure 7.5), with commoned outputs, driven by a 20 stage shift register through which a single "1" was shifted stage by stage by an astable multivibrator clock generator. The shift register comprised of four TTL SN7496 five stage registers, and because the suitable FET's were n-channel devices the gate control circuitry had to be

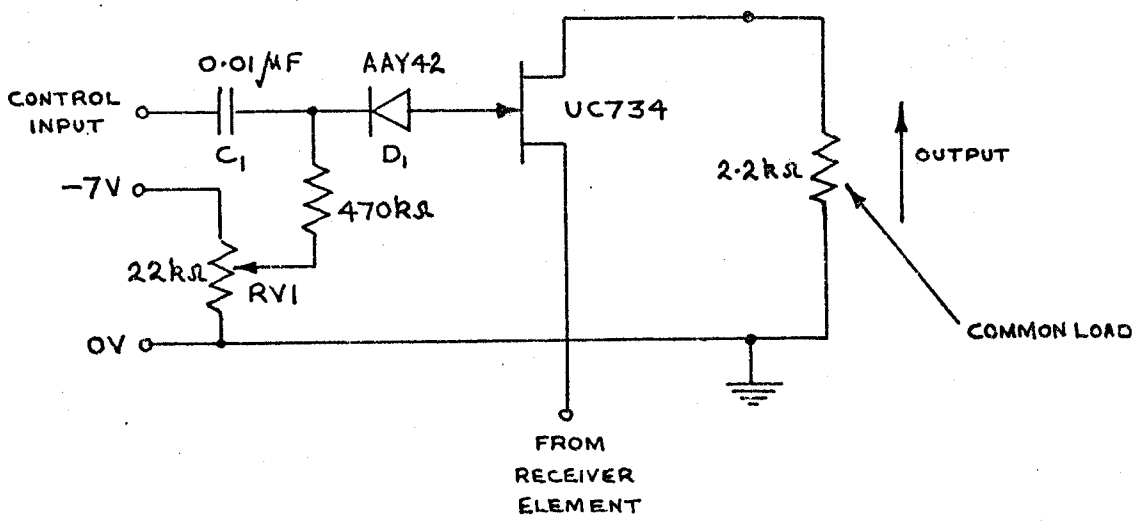

FIGURE 7.5 BASIC F.E.T. SWITCH UNIT.

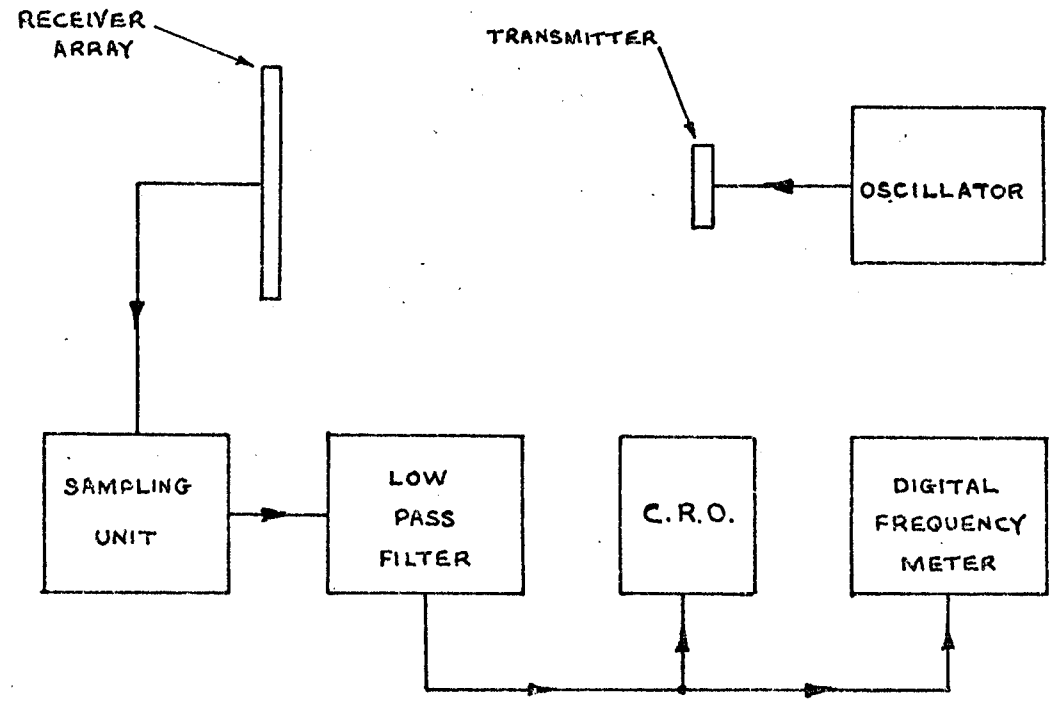

FIGURE 7.6 EXPERIMENTAL SYSTEM FOR MEASUREMENT OF CHARACTERISTIC FREQUENCIES.

much more complex than would otherwise have been the case had suitable p-channel devices been available. A special negative supply was provided to hold the gates off (adjustable using RV1), and the positive shift register pulses were a.c. coupled via C_1 to the gate circuit. D_1 prevented the gate-channel junction from becoming forward biased, with C_2 included to speed up the switching action.

7.3.2 Measurement of the Characteristic Frequencies

The experimental system used for the measurement of the characteristic frequencies is shown in a block schematic form in figure 7.6. The acoustic lens, which was the same as that described in chapter 5, included between the transmitter and the receiving array brought the spherical wave front leaving the transmitter into a relatively plane form. This allowed a simple rotation of the array about its axis to provide the complete range of incident wave angles required. The low pass filter was of a constant k, π section form, using two equal capacitors and an inductor. It had an approximate cut-off frequency of 800 kHz and a flat response up to 600 kHz. A CRO monitored the low pass filter output so that the waveforms could be observed and, if desired, recorded, and a digital frequency meter was used to measure the resulting characteristic frequencies.

7.3.3 Target Range and Bearing Tests

A tank for model ship testing was used for these tests, and for convenience, small transmitters took the place of insonified targets. The experimental system is shown in figure 7.7. A gating unit and a power amplifier were included in the transmitter circuit, the former to enable ranging tests to be made and the latter in order to provide sufficient transmitted acoustic power so that the received signals were well above the inherent noise level. Since the output of the scanned array contained

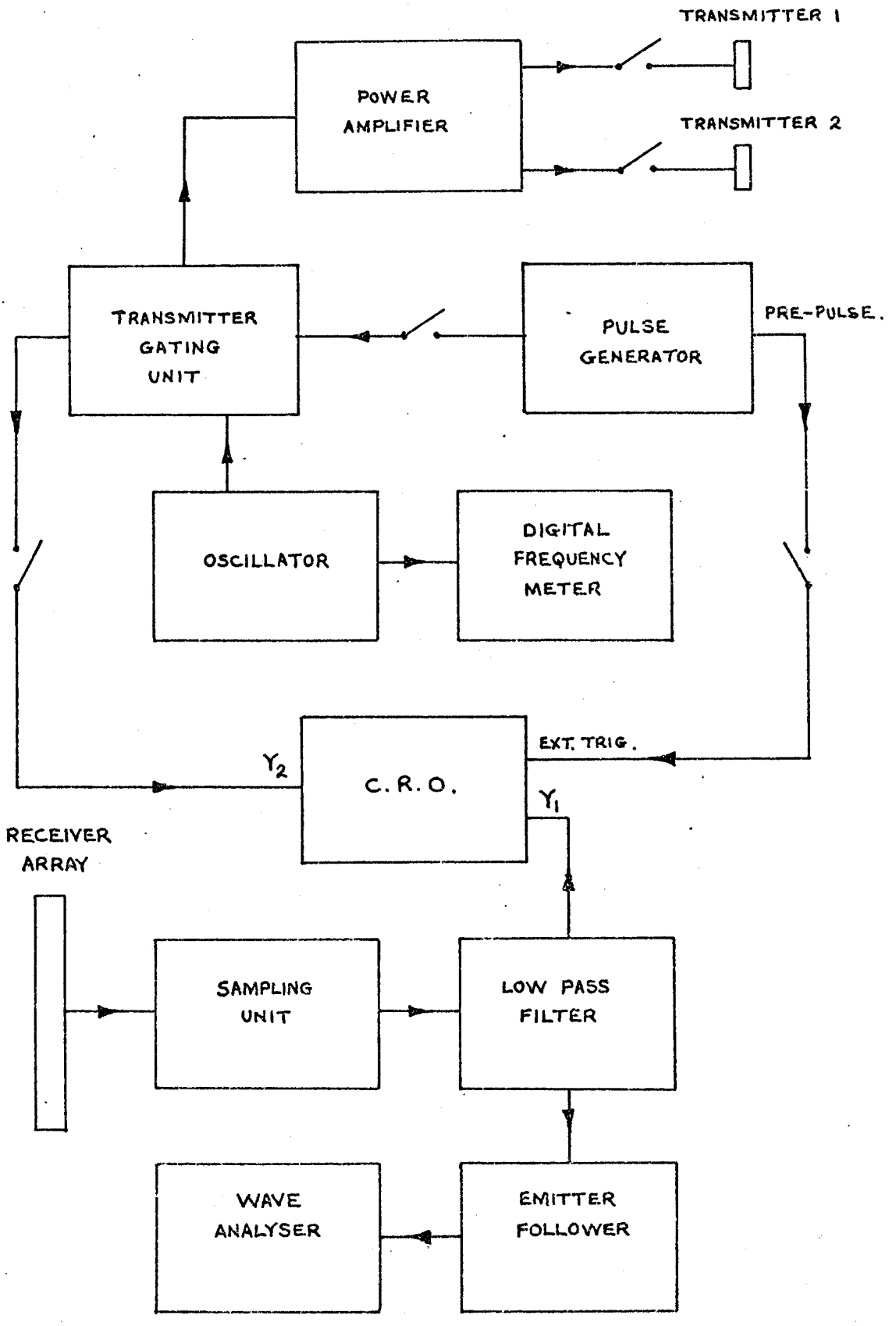

FIGURE 7.7 EXPERIMENTAL SYSTEM FOR TARGET RANGE AND BEARING TESTS

many signals, a wave analyser was used to accurately determine their frequencies. The two transmitter-targets were 8 mm diameter discs of PZT-4, encapsulated in epoxy resin, having a nominal thickness resonance of 500 kHz. They were arranged so that their angular positions and range relative to the receiving array could be independently varied. Switches S_1 and S_2 allowed either one or both of the transmitters to be energised as desired. For the ranging tests the low pass filter was replaced by a tunable resonant bandpass filter, so that the signal from a target on a particular bearing, and hence a particular characteristic frequency, could be selected and the signal from the other target rejected.

7.4 Results

The measured characteristic frequencies agreed very closely with those calculated using equation 7.6. These were checked using both sampling frequencies, 2·26 MHz and 4·52 MHz, and the results are presented in tables 7.1 and 7.2. The two characteristics for the experimental system are plotted in figure 7.4, that for $\frac{p\ d}{\lambda_1} \simeq 6{\cdot}7$ corresponding to a sampling frequency of 4·52 MHz, and $\frac{p\ d}{\lambda_1} \simeq 3{\cdot}4$ corresponding to a sampling frequency of 2·26 MHz. The apparent anomoly accurring in table 7.2, where the characteristic frequencies for 10^o and 13^o are higher than that for 7^o, may be explained by referring to figure 7.4. It will be seen that the appropriate characteristic passes through the zero frequency point at an angle of just over 8^o, and thus frequencies at angles greater than this will rise with increasing angle, whereas at angles less than this they will fall with increasing angle.

Using the system described by figure 7.7 and with a single target set on the array normal and at a range of 1·18 M, the harmonic content of the sampled array output, for continuous wave operation, was determined. The

Table 7.1

f_s = 2·26 MHz; f_T = 534 kHz

Experimental Results		Predicted Values	
θ(Degrees)	$f_{R\theta}$ (kHz)	θ(Degrees)	$f_{R\theta}$ (kHz)
0	534 on D.F.M.	0	534
3	420 on D.F.M.	3·3	421
7	307 on D.F.M.	6·7	308
10	194 on D.F.M.	10·0	195
13	80	13·4	82·2

Table 7.2

f_s = 4·52 MHz; f_T = 534 kHz

Experimental Results		Predicted Values	
θ(Degrees)	$f_{R\theta}$ (kHz)	θ(Degrees)	$f_{R\theta}$ (kHz)
0	534	0	534
3	290	3·3	306
7	75	6·7	77·9
10	145	10·0	150
13	360	13·4	378

major signals are given in table 7.3, and it will be seen that the largest spurious signal, that equivalent to a target at 10^{o}, was 22 dB's down on the 0^{o} signal. The component at one twentieth of the sampling frequency is of interest, since this corresponds to the discontinuity which occurs in the output as sampling switches from the last to the first array element. The more accurately the target bearing equals the bearing corresponding to a characteristic frequency the smaller this component should become. Any inequality in performance of the 20 sampling gates would also tend to show up as a component at this frequency, since each individual element is sampled at this rate.

The same single target was then moved across the tank on a line parallel to the array to positions which were suitable for the continuous sampling of the array; i.e. those positions which produced the characteristic frequencies. The bearings and the frequencies for these various positions were recorded for ultrasonic frequencies of 528 kHz and 547 kHz (within the system bandwidth) and are presented in table 7.4, together with, for comparison, those predicted from theory using equation 7.6. These results confirmed the close agreement between theory and practice already shown in tables 7.1 and 7.2.

A second transmitter-target was then placed in the tank at a range of 2·69 M (see figure 7.8), so that tests could be made on the ability of the system to resolve two targets. Some of the many results taken are given in tables 7.5 and 7.6. For table 7.5, transmitter 1 was positioned on a bearing of 7^{o} and transmitter 2 on a bearing of 10^{o}, and the table shows the output levels at the various characteristic frequencies with their corresponding bearings with each individually on, and, finally, with both switched on. The output levels are all relative to the largest output; i.e. that for transmitter 2 when both transmitters are switched on.

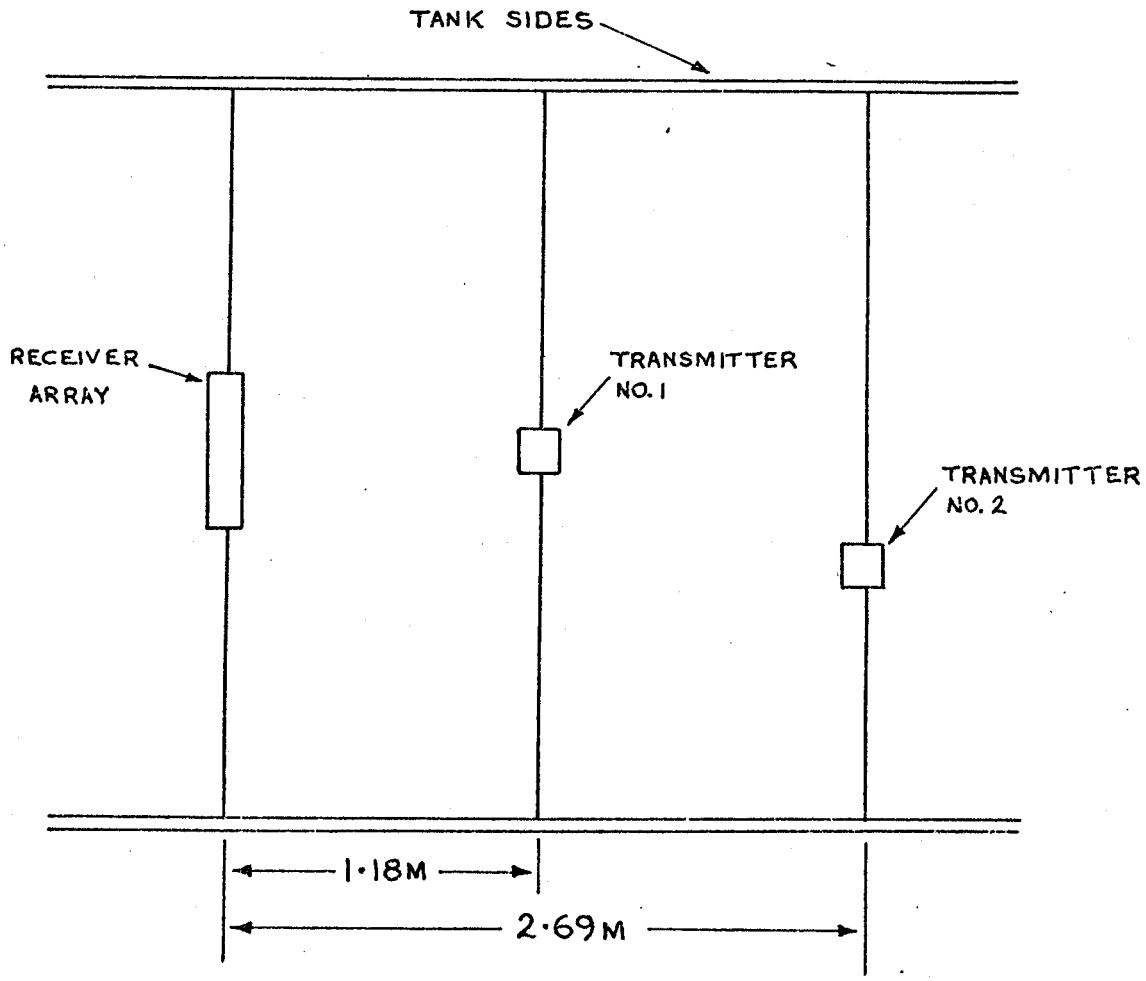

FIGURE 7.8 POSITIONS OF TRANSMITTERS AND THE RECEIVING ARRAY.

Table 7.3

f_s = 4·52 MHz; f_T = 547 kHz

Frequency (kHz)	Amplitude (dB)	Frequency Component
95·1	- 31	$f_R\ 7^o$
130	- 22	$f_R\ 10^o$
225	- 24	$f_S/20$
322	- 26	$f_R\ 3^o$
547	0	$f_R\ 0^o$

Table 7.4

f_s = 4·52 MHz

	Experimental Results		Predicted Values	
	θ(Degrees)	$f_{R\theta}$ (kHz)	θ(Degrees)	$f_{R\theta}$ (kHz)
f_T = 547 kHz	0	547	0	547
	3	322	3·3	321
	7	94·0	6·5	95·1
f_T = 528 kHz	0	528	0	528
	3	304	3·4	302
	7	76·2	6·8	76·0

Table 7.5

Transmitter No. 1 at 7^{o}; Transmitter No. 2 at 10^{o}

f_s = 4·52 MHz; f_T = 542 kHz

		Relative amplitudes (dB's)		
Frequency (kHz)	Corresponding angle θ	Tx. No. 1 on	Tx. No. 2 on	Tx. No. 1 and Tx. No. 2 on
87	7^{o}	- 4	- 7	- 4
136	10^{o}	- 30	+ 1	0
316	3^{o}	- 19	- 10	- 15
542	0^{o}	- 16	- 16	- 17

Table 7.6

Transmitter No. 1 at 0^{o}; Transmitter No. 2 at 10^{o}

f_s = 4·52 MHz; f_T = 542 kHz

		Relative amplitudes (dB's)		
Frequency (kHz)	Corresponding angle θ	Tx. No. 1 on	Tx. No. 2 on	Tx. No. 1 and Tx. No. 2 on
87	7^{o}	- 23	- 10	- 12
136	10^{o}	- 10	- 2	0
316	3^{o}	- 18	- 13	- 11
542	0^{o}	- 1	- 19	- 1

This also applies to table 7.6, which shows a similar set of results for transmitter 1 at 0^{o} and transmitter 2 at 10^{o}. Although the expected signals have fairly consistent levels with one or both transmitters on (all within ± 1 dB), the spurious signals vary considerably. The relatively high levels of these unexpected components may have been caused by reflections, since no real effort was made to reduce side or back-wall reflections, although a brief investigation into this proved inconclusive at the time.

Figures 7.9 to 7.13 are photographed CRO displays of the output of the low pass filter with either one or both transmitters on and at various bearings. Transmitters 1 and 2, however, were always at perpendicular ranges of 1·18 M and 2·69 M respectively. The characteristic frequencies are clearly visible for the single transmitter tests, and where two are used, the addition of the two expected frequencies is evident. Figures 7.14 and 7.15 show the output of the tuned bandpass filter when the two transmitters are pulsed. The lower trace of both figures is the transmitted signal and it will be noticed that before this reaches the receiver array an electrical breakthrough signal is present. Figures 7.14 and 7.15 show the results when the resonant bandpass filter was tuned to the near and the far target respectively. The Q of the filter was inadequate as can be seen by reference to figure 7.15, where ideally only a single step in amplitude at a time of approximately 3·5 mS should have occurred.

7.5 Conclusions and Suggestions for Further Work

The foregoing sections have demonstrated the simplicity of this method for obtaining the bearing of targets within a specified sector. It has been shown both experimentally and theoretically that the angular resolution may be considered to be approximately the array beam width, $\frac{\lambda_1}{dn}$, and results have indicated that the resolution in range and bearing

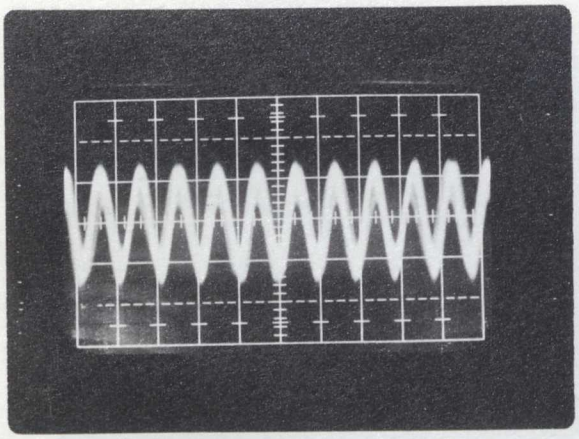

Figure 7.9 Transmitter No. 2 at 0^{o}.
Horizontal scale: 2 μS/cm, Vertical scale: 20 mV/cm.

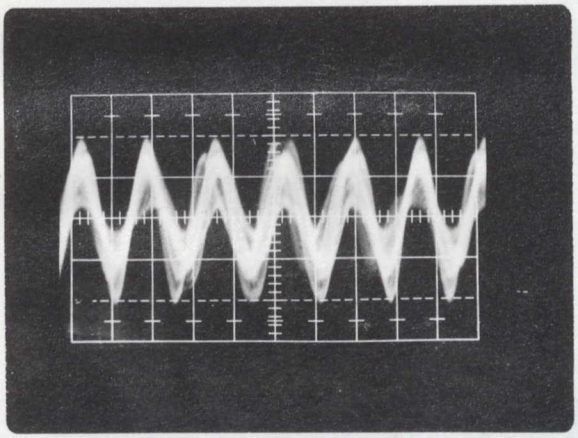

Figure 7.10 Transmitter No. 2 at 3^{o}.
Horizontal scale: 2 μS/cm, Vertical scale: 20 mV/cm.

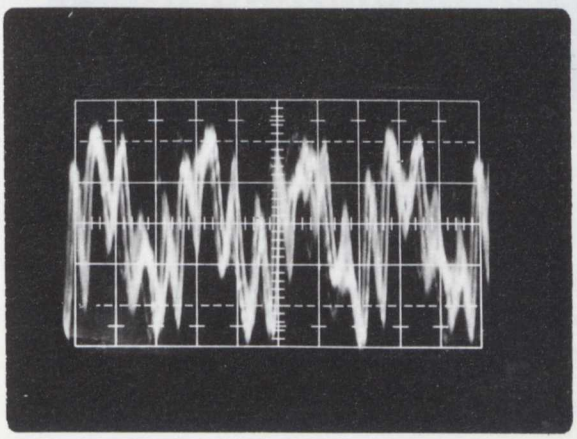

Figure 7.11 Transmitter No. 2 at 7^{o}.
Horizontal scale: 5 μS/cm, Vertical scale: 10 mV/cm.

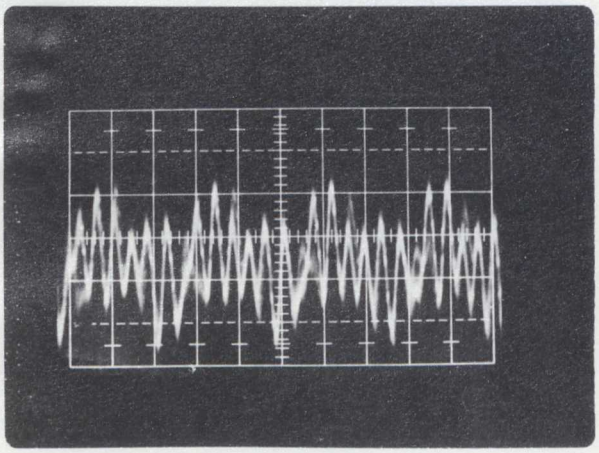

Figure 7.12 Transmitter No. 1 at 0^{o}, Transmitter No. 2 at 7^{o}.
Horizontal scale: 5 µS/cm, Vertical scale: 10 mV/cm.

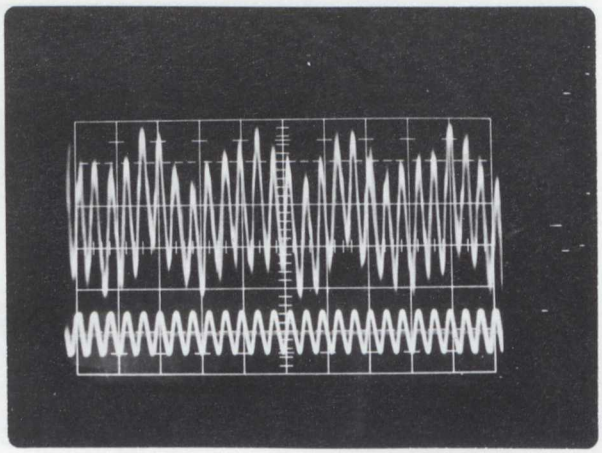

Figure 7.13 Transmitter No. 1 at 0^{o}, Transmitter No. 2 at 7^{o}.
(pulsed transmission)
Horizontal scale: 5 µS/cm.

Upper trace: Output from low pass filter.

Lower trace: Input to power amplifier.

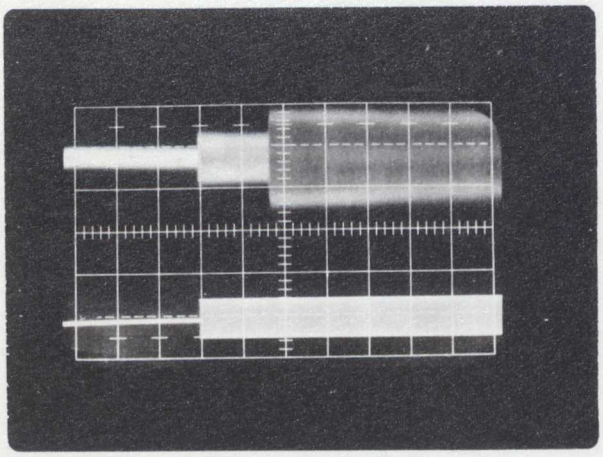

Figure 7.14 Transmitter No. 1 at 0^{o}, Transmitter No. 2 at 7^{o}.
Horizontal scale: 500 µS/cm.

Upper trace: Output from resonant filter tuned to f_R 0^{o}.

Lower trace: Input to power amplifier.

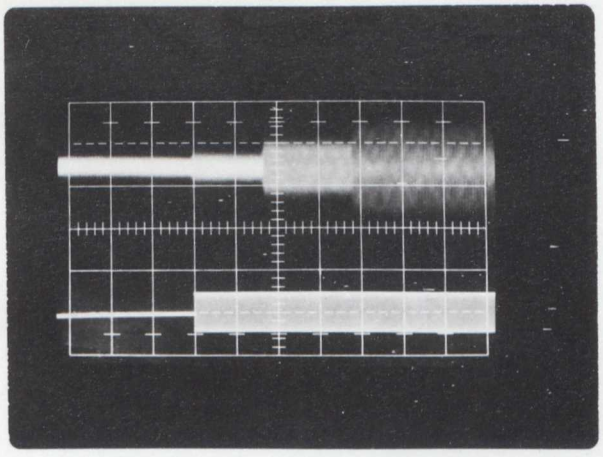

Figure 7.15 Transmitter No. 1 at 0^{o}, Transmitter No. 2 at 7^{o}.
Horizontal scale: 500 µS/cm.

Upper trace: Output from resonant filter tuned to f_R 7^{o}.

Lower trace: Input to power amplifier.

of more than one target is practically feasible.

Clearly much more fundamental work is required. In particular the problems of noise, resolution and usable sector in relation to sampling frequency, etc., must be more fully investigated. A system using a fixed narrow band filter and a variable sampling frequency (and hence scanning velocity) should be considered, since this may prove to be less complex and therefore less expensive. It would seem, however, that the array would require to be offset at a certain angle, since no bearing resolution is available using this method for targets lying on or near the normal to the array. The sampling frequency would then be approximately inversely proportional to the target bearing, when the resultant velocity along the array of the incident waves is in the opposite direction to the scanning velocity.

The outline of a proposed system using a controlled bandpass filter is given in figure 7.16, in which it is shown how information from the sampling circuits could be processed to give a sector PPI display of targets. Again only "positive" angles of θ are considered but a complete sector is formed by scanning the array first in one direction and then the other. Use of "negative" angles requires that $f_{R\theta} > f_T$ and in consequence f_s must be high. A high value for f_s limits the range of "positive" θ, assuming that only characteristic frequencies up to the zero or "reflection" point are used (see figure 7.4). The mixer included after the right to left sampling unit will frequency shift the output of the latter upwards by f_T to give the required frequencies for the "negative" angles. The angular control circuitry sets both the centre frequency of the bandpass filter, the desired beam direction, and the angular position of the display.

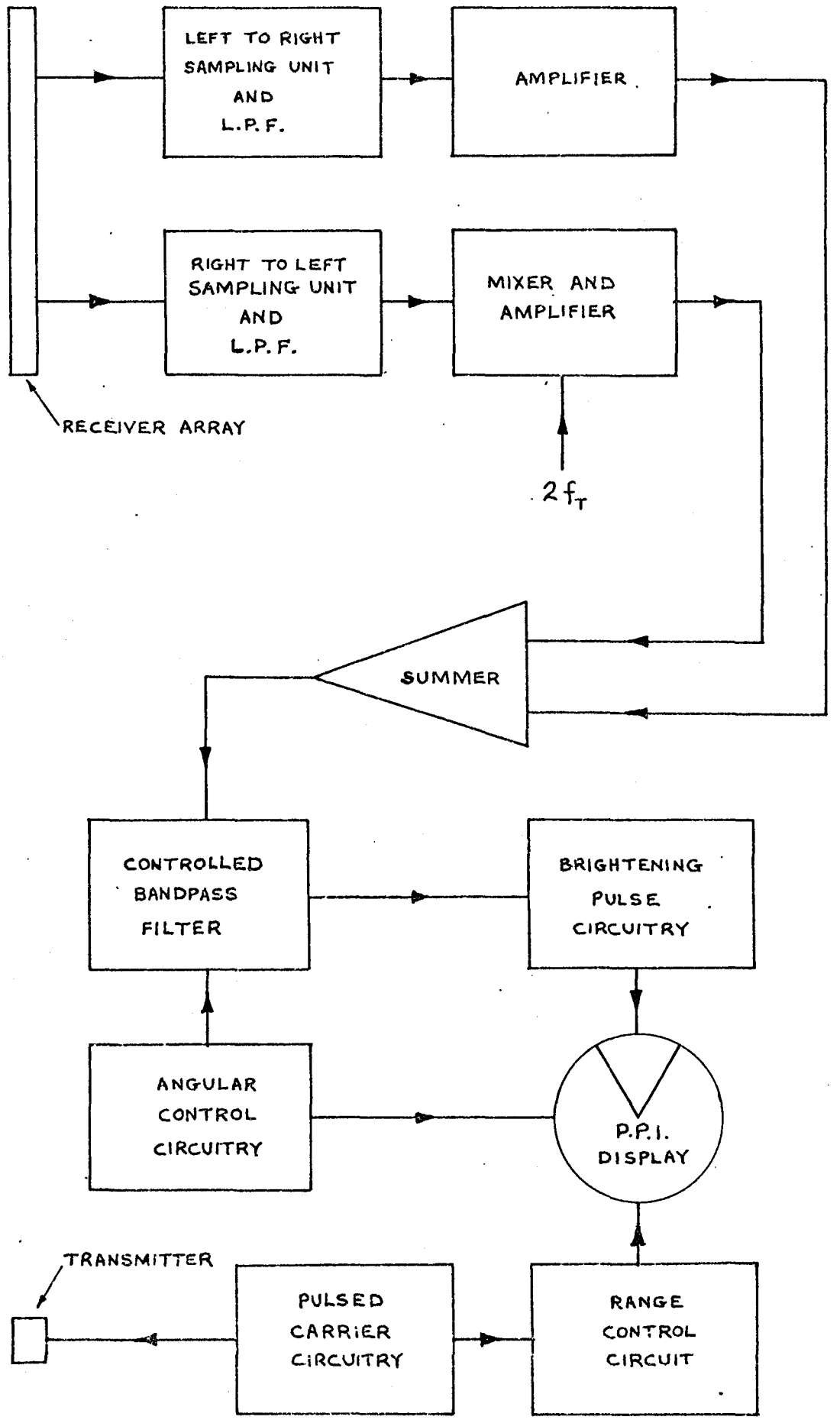

FIGURE 7.16 PROPOSED SYSTEM TO PROVIDE A P.P.I. DISPLAY OF TARGET POSITIONS

8. General Conclusions

The research programme may be divided into two main sections; the development of a new form of ultrasonic image converter, and an investigation into the signal processing which may be used with this in order to create a complete ultrasonic camera system. The two are interrelated in so far as the performance of the former affects the results of the latter.

Considering, firstly, the solid state converter, it may be concluded that there are two problems that are carried with it, as with any converter, which seriously affect its performance; noise and resolution. The former, in the case of the solid state converter, is mainly generated by what would appear to be unequal transducer element sensitivities causing a form of spatial sampling noise as the matrix is scanned. Thermal noise introduced by the converter itself is only approximately 15% of the total thermal noise, the rest being produced within the bandpass amplifier. Not withstanding this a limiting sensitivity for the converter of $1{\cdot}3 \times 10^{-13}$ W cm^{-2} was estimated, based on thermal noise only. This figure means that the solid state ultrasonic image converter is 5 orders more sensitive than the equivalent published measured sensitivities for tube converters. The spatial sampling noise should be virtually eliminated in a properly manufactured device. Experimentally the resolution is shown to be limited to marginally less than the transducer thickness. It is thus a function of the operating ultrasonic frequency and consequently is limited in practice by the maximum effective frequency which the FET analogue gates will satisfactorily block. This imposes a maximum ultrasonic frequency of around 6 MHz, resulting in a limiting resolution in the image plane of approximately $\frac{1}{3}$ mm.

Three processing techniques have been experimentally investigated; the acoustic lens, the on-line computer "lens" and a scanned array

Doppler system. The perspex acoustic lens, a simple spherical design, produced excellent pictures in conjunction with the solid state converter of simple objects using both transmission and reflection, and resolution in the object plane was between 1·5 and 2 wavelengths. A transmission image of electric spot welds, although very clear, did not present any observable difference between good and suspected bad welds. Using pulsed transmission only marginally improved the image quality and it is concluded that the pulses were too long and that in any case small improvements would be masked by the converter sampling noise. If a higher ultrasonic frequency is to be used then a corrected lens is required, but at 1 MHz spherical aberration does not appear to significantly degrade the image. The system is, however, fundamentally inflexible since unless the object can be moved with respect to the converter matrix it is not possible, without changing to a lens of different focal length, to alter the magnification.

The on-line computer "lens", in contrast, is inherently extremely flexible, the field of view and range being readily adjustable by inputting the new information through the teletype keyboard. Results using on-line computer image reconstruction have demonstrated that far field beam deflection and near field focusing is possible using the specially written programs. A comparison between the performance of the perspex acoustic lens, with an aperture of 60 wavelengths, and the computer "lens", with an aperture of 17 wavelengths, shows the resolution achieved by the latter as being surprisingly near that of the former.

The scanned array Doppler system employs an extremely simple processing technique and the preliminary results presented show how one or more targets may be located both in range and bearing. The resolution limitations are as for any linear array; bearing resolution is directly proportional to aperture, or array, width.

The future development of the solid state converter depends upon whether technology can develop a suitable production technique to either enable the bonding of multiple connections on an upturned silicon slice to a multi-element transducer electrode pattern, or to manufacture thin film transducers at a low enough frequency. With the latter technique, film transducers would ideally be deposited through a mask directly onto the scanning circuit silicon slice (or slices), and it is felt that this offers the best chance for the production of a device which may at last become accepted as a useful tool in the materials' testing, medical diagnostics and underwater fields.

References

1. Sokolov, S. Ya., British Patent No. 477, 139, 13th May 1937.

2. Prokhorov, V.G., "The problem of converting an ultrasonic image into a visible one", Soviet Physics - Acoustics, 3, No. 3, pp. 272-80, 1958.

3. Semennikov, Yu. B., "A study of acoustic image converters", Soviet Physics - Acoustics, 4, No. 1, pp. 72-83, 1958.

4. Freitag, W., "Investigations of an electronic ultrasonic image converter", Jenaer Jahrbuch, Vol. 1, Part 1, pp. 228-74, 1958.

5. Smyth, C.N., Poynton, F.Y., Sayers, J.F., "The ultrasound image camera", Proc. I.E.E., 110, No. 1, pp. 16-23, 1963.

6. Haslett, R.W.G., "An ultrasonic to electronic image converter tube for operation at 1·20 M c/s", The Radio and Electronic Eng., pp. 161-170, March 1966.

7. Jacobs, J.E., Collis, W.J., Berger, H., "An evaluation of an ultrasonic inspection system employing television techniques", Materials Evaluation, May 1964.

8. Pigulevskii, E.D., "The sensitivity and resolution of acousto-optical image conversion at a liquid surface", Soviet Physics - Acoustics, 4, p. 359, 1958.

9. Pohlman, R., "Internal examination of material by ultrasonic optical pictures", Z. Angew, Physik, 1, p. 181, 1948.

10. Suckling, E.E., Maclean, W.R., "Sonic images", Journal of the Acoustical Society of America, Vol. 29, p. 146, 1957.

11. Knollman, G.C. et al., Final Report on Underwater Acoustic Imaging, Lockheed Research Laboratory, June 1967.

12. Rozenberg, L.D., "Survey of methods used for the visualization of ultrasonic fields", Soviet Physics - Acoustics, 1, p. 105, 1955.

13. Berger, H., Dickens, R.E., "A review of ultrasonic imaging methods, with a selected, annotated bibliography", Argonne National Laboratory, July 1963.

14. Jones, H.W., Miles, H.T., "The development of ultrasonic image converters for underwater viewing and other applications", Journal of Ocean Engineering, Vol. 1, pp. 479-96, 1969.

15. Sokolov, S. Ya., "An ultrasonic microscope", C.R. Acad. Sci. USSR, No. 46, p. 333, 1949. (In Russian).

16. Smyth, C.N., "The ultrasound camera - recent considerations", Ultrasonics No. 4, pp. 15 - 20, January 1966.

17. Sayers, J.F., "The ultrasound camera, Part I: The instrument constructed at A.E.R.E.", Harwell report No. AERE - R4356, November 1963.

18. Sayers, J.F., "The ultrasound camera", Physics and Non-Destructive Testing, pp. 97 - 127, 1964.

19. Harrold, S.O., "Solid state ultrasonic camera", Ultrasonics, pp. 95 - 101, April 1969.

20. Knollman, G.C., et al., "Experimental hydroacoustic imaging system", Journal of Applied Physics, Vol. 42, No. 6, pp. 2168-2180, May 1971.

21. Knollman, G.C., Brown, A.E., "Hydroacoustic image transducer", The Review of Scientific Instruments, Vol. 42, No. 8, pp. 1202-1214, August 1971.

22. Maginness, M.G., Plummer, J.D., Meindl, J.D., "An acoustic image sensor using a transmit-receive array", Presented at the 5th Int. Symp. on Acoustical Holography and Imaging, Palo Alto, July 1973.

23. Mavlice, J.F., Kino, G.S., Quate, C.F., "Electronically focused acoustic imaging device", App. Phys. Lett. Vol. 23, No. 11, December 1973, pp. 581 - 583.

24. Kennedy, J.A., Muenow, R., "Practical improvements and applications for the ultrasonic image converter", I.E.E.E. Trans. Sonics and Ultrasonics, Vol. SU-14, No. 2, pp. 47 - 52, April 1967.

25. Grasyuk, D.S., et al., "An ultrasonic introscope with the new U-55 electronic-acoustic image converter", Soviet Physics - Acoustics, Vol. 11, No. 4, pp. 376 - 380, April-June 1966.

26. Schätzer, E., "An electronic to ultrasonic image converter with enlarged image field", Ultrasonics, pp. 233 - 234, October 1967.

27. Muenow, R.A., "Image conversion cathode ray tube with piezo-electric face element provided with rigidifying means", United States Patent No. 3, 431 - 462, 1969.

28. Whymark, R.R., "Ultrasonic imaging apparatus", United States Patent No. 3, 567 - 990, 1971.

29. Jacobs, J.E., Peterson, D.W., "The use of discrete, shaped matching sections to increase the aperture of the Sokoloff tube", Ultrasonic International 1973, Conference Proceedings.

30. Green, P.S., Bellin, J.L.S., Knollman, G.C., "Acoustic imaging in a turbid underwater environment", The Journal of the Acoustical Society of America, Vol. 44, No. 6, pp. 1719 - 1730, 1968.

31. Wells, P.N.T., "The medical applications of ultrasonics", Reports on Progress in Physics, 33, p. 88, January 1970.

32. Haslett, R.W.G., et al., "The underwater acoustic camera", Acustica, Vol. 17, No. 4, pp. 187-203, 1966.

33. Aldridge, E.E., "Acoustical holography", A Merrow Monograph, 1971.

34. Tomlinson, J., Alves, N.H.J., "Ultrasonic holography", EMI Electronics Ltd., Wells Division, 1969.

35. Halstead, J., "Ultrasound holography", Ultrasonics, pp. 79 - 87, April 1968.

36. Massey, G.A., "Acoustic imaging by holography", I.E.E.E. Trans. or Sonics and Ultrasonics, Vol. SU-15, No. 3, pp. 141-146, July 1968.

37. Milder, D.M., Wells, W.H., "Acoustic holography with crossed linear arrays", I.B.M. J. Res. Development, pp. 492 - 500, September 1970.

38. Knollman, G.C., Weaver, J.L., "Acoustical holography with a scanned linear array", J. Appl. Phys. Vol. 43, No. 10, pp. 3906 - 3913, October 1972.

39. Maginness, M.G., Kay, L., "Ultrasonic imaging in solids", The Radio and Electronic Engineer, Vol. 41, No. 2, pp. 91-93, February 1971.

40. Sondhi, M.M., "Reconstruction of objects from their sound diffraction patterns", The Journal of the Acoustical Society of America, Vol. 46, No. 5 (Part 2), pp. 1158 - 1164, 1969.

41. Maginness, M.G., "The reconstruction of elastic wave fields from measurements over a transducer array", Journal of Sound and Vibration, No. 20 (Part 2), pp. 219-240, 1972.

42. Maginness, M.G., et al., "A small scale model for seismic imaging systems", Proceedings of the 4th Int. Symp. on Acoustical Holography, Santa Barbara, April 1972.

43. Harrold, S.O., West, R.C., "Far-field sector scanning using a sampled multielement ultrasonic receiving array", Electronic Letters, Vol. 7, No. 4, pp. 100 - 101, February 1971.

44. West, R.C., Harrold, S.O., "Control of acoustic beam angle by harmonic analysis of sequential samples from a multi-element linear array", Ultrasonics, September 1974.

45. Digital Equipment Corporation, PDP8-E Small Computer Handbook, 1973.

46. Digital Equipment Corporation. PDP-8E Introduction to Programming, 1973.

47. Digital Equipment Corporation. PDP8-E Programming Languages, 1972.

48. Pigott, M.T., Whitmarsh, D.C., Brown, J.L., "Scanned line hydrophone method of determining angle of arrival of sound in water", Journal of the Acoustical Soc. of America, Vol. 34, No. 3, March 1962.

49. Jenkins, F.A., White, H.E., "Fundamentals of optics", Chapter 15, McGraw Hill, 1951.

50. Cook, G.B., Johnson, D.A.H., "Pseudo-random selection of elements in a multi-element array", The Radio and Electronic Engineer, Vol. 38, No. 2, pp. 82-88, August 1969.

APPENDIX A

Reprint of paper published in Ultrasonics,
April 1969.

"Solid state ultrasonic camera"

Solid state ultrasonic camera

S. O. HARROLD*

A solid state ultrasonic image converter has produced photographs which compare favourably with results from tube converters. In appendices, the designs of the acoustic lens, the receiver and the transmitter are discussed, and detailed circuits are given for the linear switch, the master oscillator and pulse generator, the bistable multivibrator, the video amplifier and detector, and the staircase generator. The solid state ultrasonic camera will be further developed by the use of thin film and integrated circuit techniques.

INTRODUCTION

Ultrasound has for sometime been used for the detection of flaws in materials and, at low intensities, for the inspection of living tissues. Many elaborate methods have been devised to enable a visual two-dimensional picture to be built up of an object 'illuminated' by ultrasound. Most of these require some form of mechanical movement of a transducer, relative to the object under observation. Clearly, this movement must be slow to produce a picture. So far, the only practically effective, non-mechanical system has a form like a television camera tube, the photoelectric plate being replaced by an acoustoelectric transducer. The image of an 'illuminated' object is focussed (or a shadow is cast) on to the front face of the transducer whose rear face is then scanned by an electron beam within the tube. A serial output of the voltage, and hence the acoustic pressure across the transducer surface, is obtained and this, after amplification, may be used to reproduce the object image on a display tube.[1-6, 8]

It is clearly an advantage, and for many uses a necessity, to produce a visual picture at the same time as the acoustic examination is being made. In other words an 'on-line' system is distinctly preferable. In addition, the picture build-up time must be as short as possible to enable, if required, large sheets of material to be rapidly inspected. The electron scanning method would, at first glance, appear to answer both these requirements. It does, however, suffer from certain limitations, namely:

a low sensitivity (in comparison with echo location systems),

b tendency to implode, if either transducer area too large or operating frequency too high,

c not particularly rugged, requiring careful setting up procedure, etc,

d not easy to use under pulsed conditions.

It is suggested that the system described in this paper, which is essentially another method of scanning the back face of the transducer, is superior in most respects. Is has a sensitivity which is nearly two orders higher, an undoubted ruggedness, no physical restrictions on transducer area, no complex setting up procedure, and is comparatively simple to operate under pulsed conditions. In addition the system promises to give a limiting sensitivity several orders higher—using metal oxide silicon devices.

ACOUSTIC SYSTEM ARRANGEMENT

Fig 1 is a diagram of the acoustic arrangement. Continuous wave, unmodulated ultrasound, at 1MHz, from the transmitting transducer 'illuminates' the object. Diffraction occurs and all points on the object radiate in a spherical fashion. The acoustic lens is concave and is machined with spherical surfaces from a piece of perspex. The acoustic lens focusses a diffraction image on to the surface of the receiving transducer. (See Appendix A for details on the design of the acoustic system.)

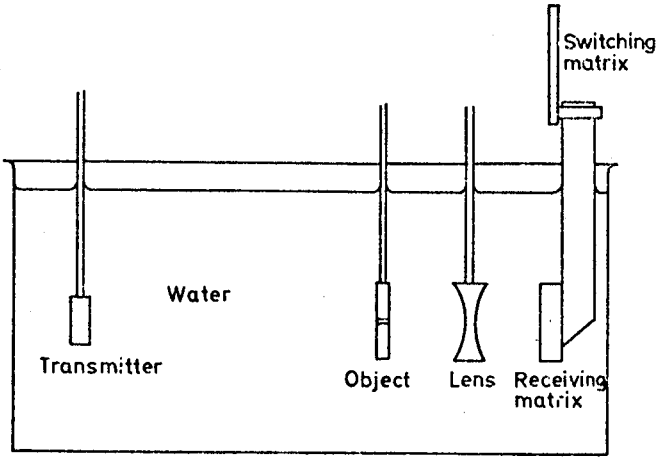

Fig 1 Arrangement of acoustic system. The object is illuminated by ultrasound from the transmitter. The acoustic lens focusses the diffraction image on the receiving matrix

RECEIVING MATRIX

The transducer used is a lead zirconate titanate disc, thickness resonant at 1MHz: its diameter is three inches and both faces are silvered. The back face is not in contact with the water and has one hundred separate equi-area elements formed on the silver surface by cutting ten horizontal and ten vertical lines through the silver, each twenty thousandths of an inch wide. This means that each elemental area of silver is square with dimensions eighty by eighty thousandths of an inch. The effective area of the transducer is a square, one inch by one inch, which is subdivided into a hundred elemental areas.

Electrical connection is made by means of compression spring arrangements (see Appendix A); the output of each element is passed via a coaxial lead to the switching matrix mounted at the top of the receiver unit (Fig 1).

SWITCHING MATRIX

Fig 2 shows the linear gate circuit: a hundred of these are used, one for each element, to transmit the signals sequentially to the common output line. The transistors have to

* Department of Electrical Engineering, Portsmouth College of Technology, Hampshire Terrace, Portsmouth, Hampshire, England

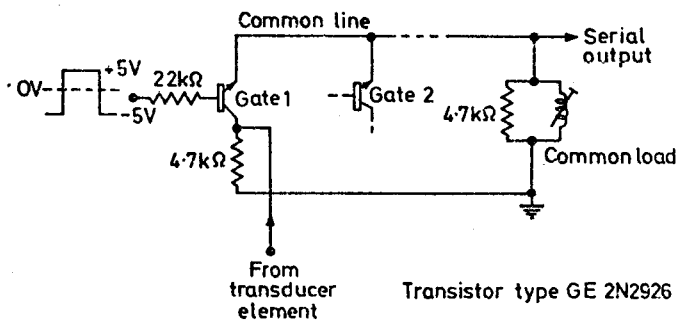

Fig 2 Linear gate circuit and load. In the switching matrix, a hundred of these are used to transmit signals

work in a bidirectional mode and require to be fully saturated to pass signal currents in either direction without loss. Switching is essentially at low levels: the voltages from the transducer elements are usually less than 100mV. Fig 3a shows that the relationship between input and output voltages for a single switch is almost perfectly linear for input voltages up to 300mV for the 2N2926 transistor used. Figs 3b and 3c show that no noticeable crossover distortion occurs at micro-volt levels as the input polarity reverses. For economic reasons, the gate circuit must be simple and the chosen transistor was one of the cheapest available at the time and is not symmetrical.

The major problem has been that of break-through via the open transistor switches. The transistor type used has a collector-emitter capacitance when 'off' of between 4.5 and 12pF, and at 1MHz this presents a reactance of between 35 and 13kΩ. Clearly, from each individual transducer element there will be a component of the signal developed across the common tuned load; only one component will be from the selected element. However, these components do not add directly since they appear in parallel via the source impedance of each transducer element. Choice of a transistor with a high-cut-off frequency would improve the situation—but only marginally—and effort has been concentrated into producing a composite switch-clamp arrangement. At present, surprisingly, results indicate that this offers no advantage over the basic switch.

Theoretical considerations to give minimum break-through/signal ratio require that the load impedance should be as small as possible. This, however, is in direct opposition to requirements for sensitivity and clearly a compromise, must be made.

CONTROL CIRCUITS

Control of the matrix gates is achieved by the use of two shift registers, one controlling the columns and the other the lines, as shown in Fig 4. Thus, a form of scanning is obtained by allowing a '1' to be shifted through each register in a cyclic manner. The overall system is shown in Fig 5 and needs little explanation. A master clock generator decides the scanning rate—at present 6,000 elements/s. This means that the complete matrix is scanned in approximately 16ms. A staircase generator, suitably driven, provides a synchronized raster for the display oscilloscope.

The serial output of the switching matrix is a form of amplitude modulated carrier: the carrier frequency is ultrasonic (1MHz) and the modulation frequency is the element scanning rate (6kHz). The signal is tuned by an inductance, which resonates with the self capacitance of each transducer element in turn. This has the advantage of producing a greater output from the transducer and also—and this is very important—it provides a low dc resistance in the output side of each gating element, thus minimizing dc fluctuations on the output line caused by:

a variations in the gate control voltages;

b variation from transistor to transistor of the transistor saturation voltages.

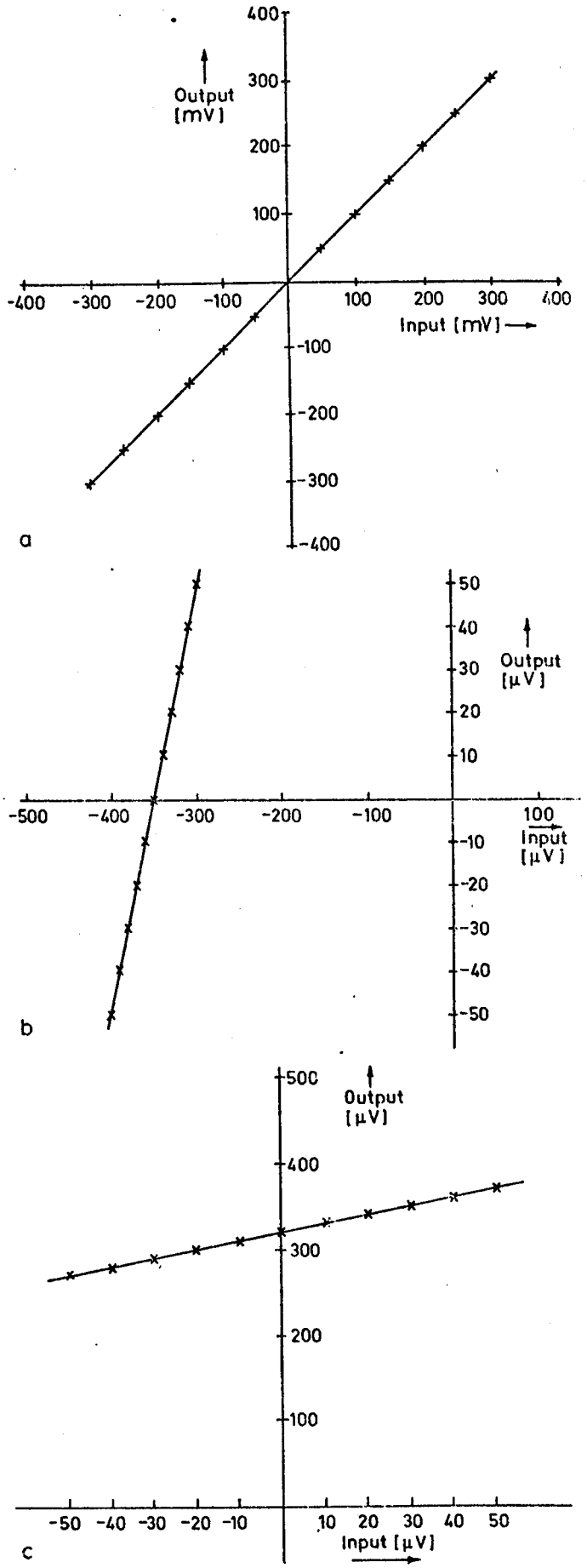

Fig 3 Input/output voltage relationships of a linear switch (with 4.7kΩ load). These relationships are almost perfectly linear and b and c show that there is no noticeable crossover distortion as the input polarity reverses

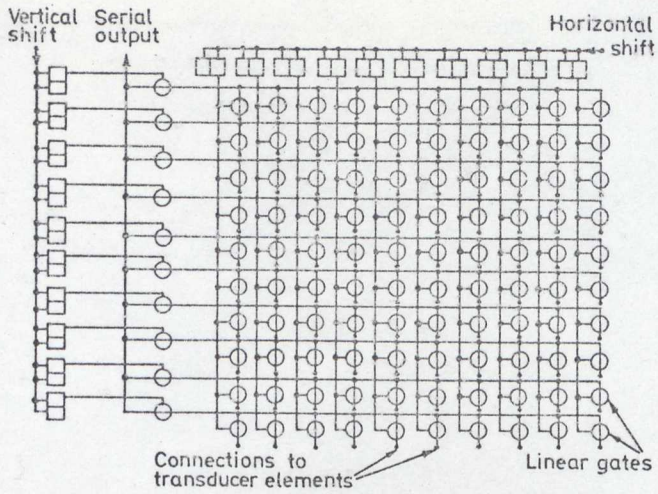

Fig 4 Switching matrix and shift register control of the columns and the lines

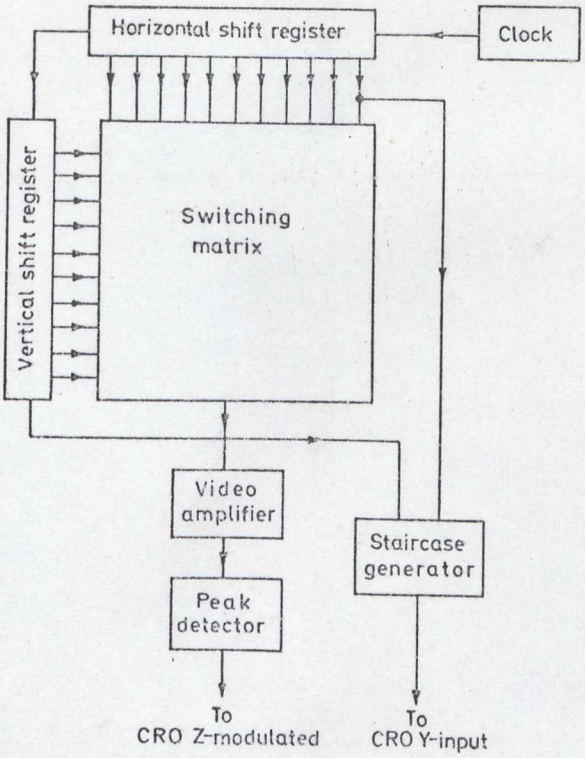

Fig 5 Block diagram of system. The master clock generator decides the scanning rate

Tuning the load has one disadvantage which could well cause more trouble as the system is generally improved. Each element will have a slightly different resonant frequency and therefore, with a fixed inductive load, each will give a different output voltage for a given input. The resonant frequency of an element is dependent on both dimensions and mechanical loading. It is possible to obtain a reasonable accuracy on thickness and area, but mechanical loading will vary with the physical position of the element in the complete matrix and with the electrical connection to the back face.

RESULTS

The photographs (Figs 6 to 11) leave a good deal to be desired, but, as a first step, they compare very favourably with many results obtained from tube converters. The resolution,

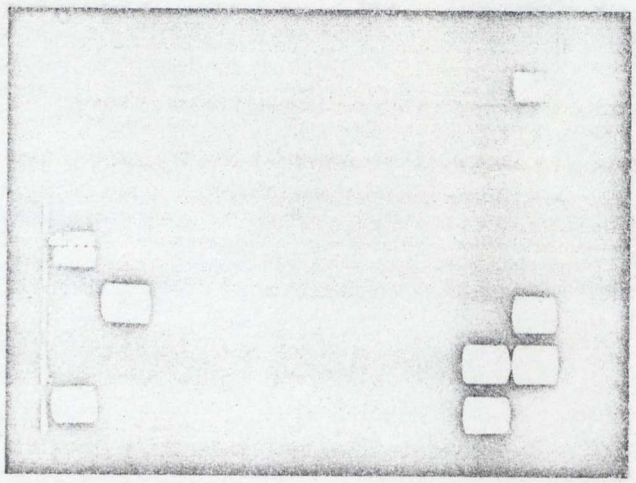

Fig 6 Image obtained when no object or lens is present. This shows those transducer elements which have failed to make an electrical connection to the switching matrix

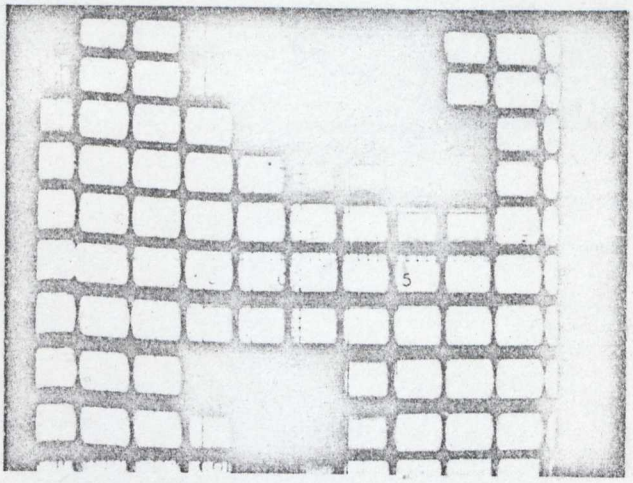

Fig 7 A shadowgraph formed by a sheet of $\frac{1}{8}$in Al through which two holes are drilled. The upper hole is 0.3in in diameter and the lower hole is 0.2in in diameter. The space between the holes is 0.35in

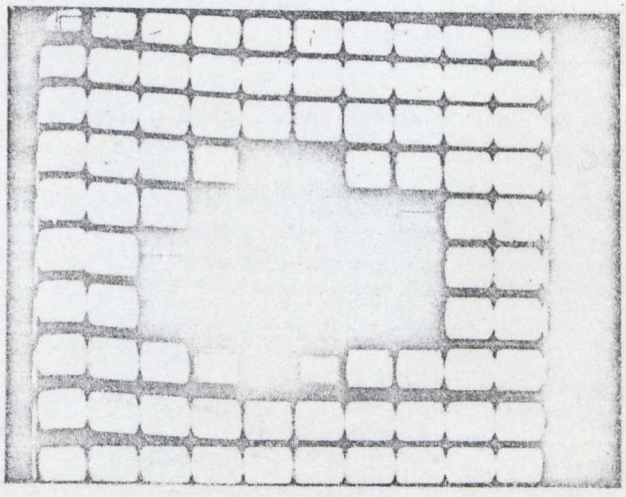

Fig 8 Image of the 0.3in diameter hole in the Al sheet. An acoustic lens has been used to give an approximate magnification of $1\frac{1}{2}$

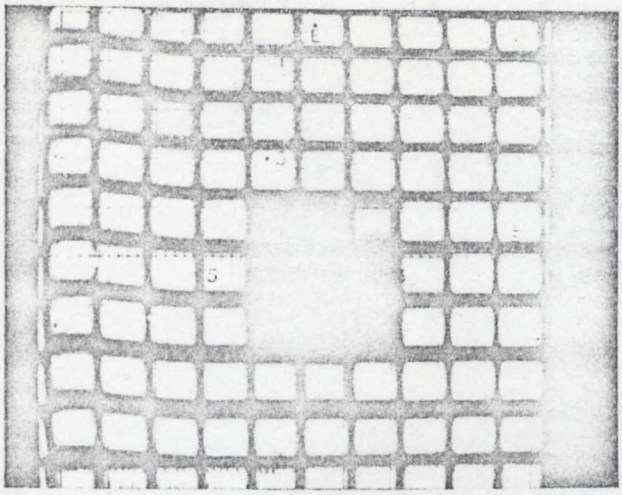

Fig 9 As in Fig 8, except that the hole in the Al sheet is 0.2in diameter

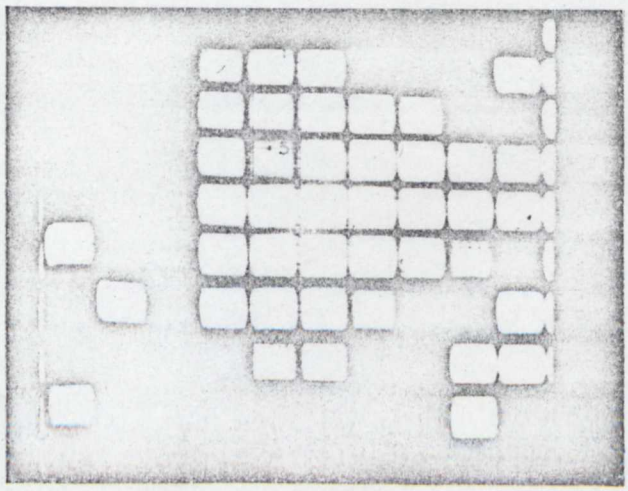

Fig 10 Image of a 2BA cheesehead screw. An acoustic lens gave an approximate magnification of 1½

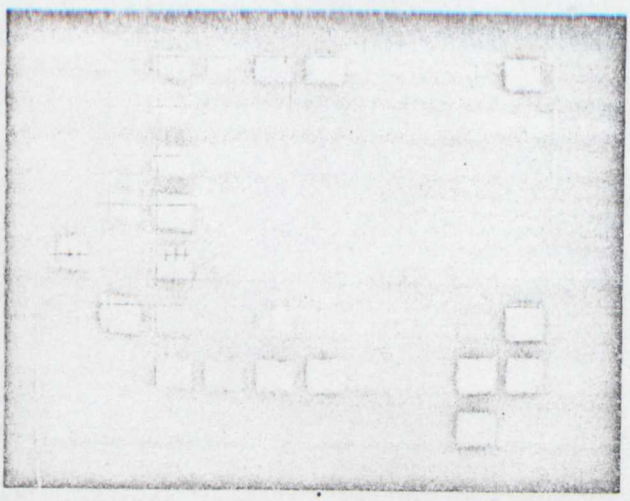

Fig 11 Image of a hook formed by a piece of wire 0.08in in in diameter. An acoustic lens gave an approximate magnification of 1½

shown in Figs 10 and 11 is better than 2 wavelengths in water (3mm) but clearly cannot be better than one transducer matrix element. The various blank areas seen in the photographs, other than those obviously caused by the object image, are caused by failure to make proper electrical contact with the back face of some of the transducer elements.

FUTURE WORK

With the continued fall in the cost of thin film and integrated circuits, coupled with the advances in their constructional techniques, the further development of this solid state converter is now economically possible. In the immediate future the use of field effect transistors will be investigated and the system will be converted to pulsed operation in order to minimize the effect of reverberations and reflections within the various ultrasonic media. This conversion is expected to produce a marked improvement in the image quality, although it will inevitably take longer to scan a complete frame. Before moving into the full solid state converter system, improvements must be made to the method of electrical connection to the back face of the transducer elements. The existing arrangement (see Appendix A) is unsatisfactory, and it is hoped that a low temperature soldering technique may be used.

After proving the feasibility of the discrete component system when the above improvements have been included, the next step would be towards the use of thin film and integrated circuit units, a number of units forming a complete multi-element array. The ultimate aim is an array of at least 100 by 100 elements in units of 10 by 10, using an ultrasound frequency of around 6MHz.

Appendix A

ACOUSTIC LENS DESIGN

Considerations

The design of an acoustic lens may follow the same procedure and use the same formulae as that used for an optical lens. There are, however, two points which should be mentioned that limit the application of optical design methods:

> The length of the wave-front is comparable with the wave-length. Hence, diffraction cannot be ignored.
>
> Mode transformation will occur at any boundary, that is, longitudinal waves will be transformed, as they strike the lens, into other modes; the major secondary mode is shear.

The choice of material, however, is less limited in the acoustic case, but has to be made with due consideration of the following points:

a The acoustic impedance should be as near as possible to that of the water to minimize reflections;

b The sound transmission velocity should differ widely from that of the water to achieve a high refractive index;

c It should be relatively simple to form the lens into the required shape.

The final choice is inevitably a compromise and it was decided to use perspex, as this satisfied most requirements reasonably—particularly c (See Table 1).

Procedure

Since the lens was to be machined in a standard lathe by simple techniques, a spherical design was followed, although it is hoped later to produce one of aspheric form to counteract the spherical aberration present in the resulting image.

Table 1 Acoustic properties of various media

Material	Specific acoustic impedance [$m^{-2}.kgs^{-1} \times 10^{-6}$]	Velocity [ms^{-1}]
Carbon tetrachloride	1.48	928
Water	1.49	1,490
Glycerol	2.5	1,986
Mercury	19.6	1,450
Polyethylene	1.75	1,950
Perspex	3.16	2,680
Magnesium	10.0	5,770
Aluminium	17.3	6,420
Iron and steel	46	6,000

Fig 12 shows the ray diagram used to calculate the final design figures of the acoustic lens.

The lens makers' design formula is:

$$\frac{n}{s} + \frac{n}{s^{11}} = (n^1 - n)\left(\frac{1}{r_1} - \frac{1}{r_2}\right) \quad 1$$

where n = acoustic impedance of water
n^1 = acoustic impedance of lens material
F and F^{11} are the two foci
M the object
M^{11} the image

Also:

$$\frac{\sin\phi}{\sin\phi^1} = \frac{n^1}{n} \quad 2$$

and:

$$\frac{\sin\phi}{\sin\phi^1} = \frac{c}{c^1} \quad 3$$

where ϕ and ϕ^1 are the angles of incidence in the materials n and n^1 respectively, and c and c^1 the acoustic velocities (longitudinal mode) in materials n and n^1 respectively.

From equations 2 and 3:

$$\frac{n^1}{n} = \frac{c}{c^1} \quad 4$$

Dividing equation 1 by n gives:

$$\frac{1}{s} + \frac{1}{s^{11}} = \left(\frac{n^1}{n} - 1\right)\left(\frac{1}{r_1} - \frac{1}{r_2}\right) \quad 5$$

Substituting 4 into this gives:

$$\frac{1}{s} + \frac{1}{s^{11}} = \left(\frac{c}{c^1} - 1\right)\left(\frac{1}{r_1} - \frac{1}{r_2}\right) \quad 6$$

Now, $\frac{1}{s} + \frac{1}{s^{11}} = \frac{1}{f}$ 7

where f = focal length

Therefore, from 6 and 7:

$$\frac{1}{f} = \left(\frac{c}{c^1} - 1\right)\left(\frac{1}{r_1} - \frac{1}{r_2}\right) \quad 8$$

The sign convention for the radii is as follows:

All convex surfaces encountered are taken as having a positive radius and all concave surfaces encountered have a negative radius. Thus, for convenience, if $|r_1| = |r_2| = r$,

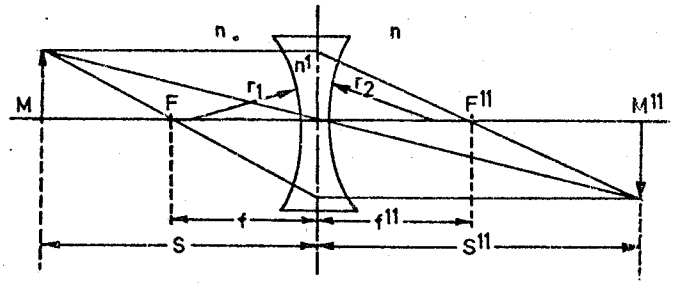

Fig 12 Ray diagram used to calculate final design figures of acoustic lens

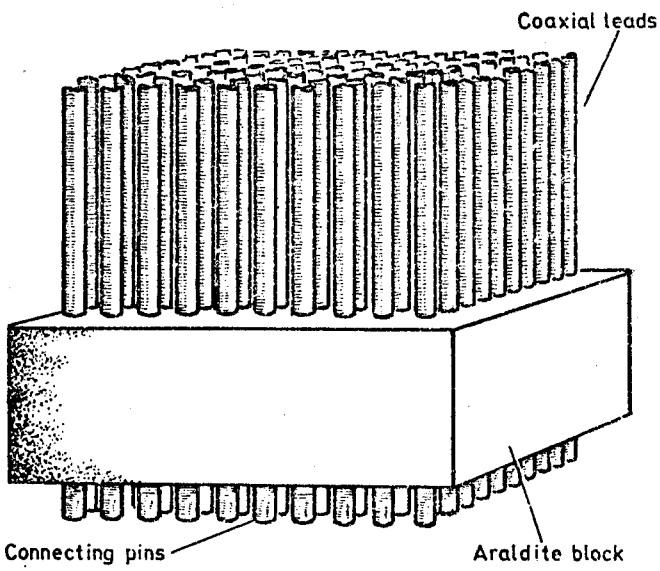

Fig 13 Electrical connections to transducer elements are made using 100 compression spring arrangements

r_1 will be $-r$ and $r_2 + r$. The ratio c/c^1 becomes 0.56, since c = 1,490m/s and c^1 = 2,680m/s. Hence, equation 8 is:

$$\frac{1}{f} = (-0.44)\left(-\frac{2}{r}\right) = \frac{0.88}{r}$$

Let f = 9cm, then r = 7.9cm.

It is clearly desirable to have the widest possible aperture, that is, make the value of 'F' approach unity. A diameter of 8cm was chosen to make F = 1.1.

The final design figures are therefore:

f = 9cm

r = 7.9cm

Diameter 8cm

Material - perspex

MECHANICAL DESIGN OF RECEIVER

Transducer

The material used is Brush Clevite PZT5; this is a modified lead zirconate titanate ceramic with a high electromechanical coupling coefficient and high charge sensitivity. It is in the form of a disc of diameter 3in, thickness resonant at 1MHz and silvered on both faces; the face away from the water is cut as described in the section on receiving matrix, so that 100 electrically isolated areas are formed.

The transducer is fitted to a brass mount using Clear Bostic to both hold and seal it against water.

Electrical connection to transducer elements

Fig 13 shows the main features of the method used at present. Essentially it comprises 100 compression spring

arrangements each of which presses on to a transducer element. These spring arrangements are modified watch strap retaining pins; one end has a feed-out wire soldered to it and the other is used to make contact with the transducer. The complete array of pins with attached wires is potted in Araldite, and is accurately spaced by a drilled paxolin panel of 0.1in pitch. Sufficient pressure is applied to the back of this system to make all the pins connect to their respective transducer elements. The whole is sealed by a rubber 'O' ring to prevent water from penetrating to the electrical connections. The wires are fed out via a copper tube with its upper end held above the water line and its lower end soldered to the brass transducer mount. A single pin is shown in Fig 14.

MECHANICAL DESIGN OF TRANSMITTER

The transmitter is a 2.5cm diameter disc of Plessey PC5 material (a lead zirconate titanate ceramic); both faces are silvered and thickness resonant at 1MHz. The disc is fixed in a brass mount using Clear Bostic as a seal. The electrical connection is achieved by a spring arrangement on to the back face of the transducer; the coaxial wire is passed out through a copper tube which is fixed and sealed to the brass mount and with its upper end held above the water.

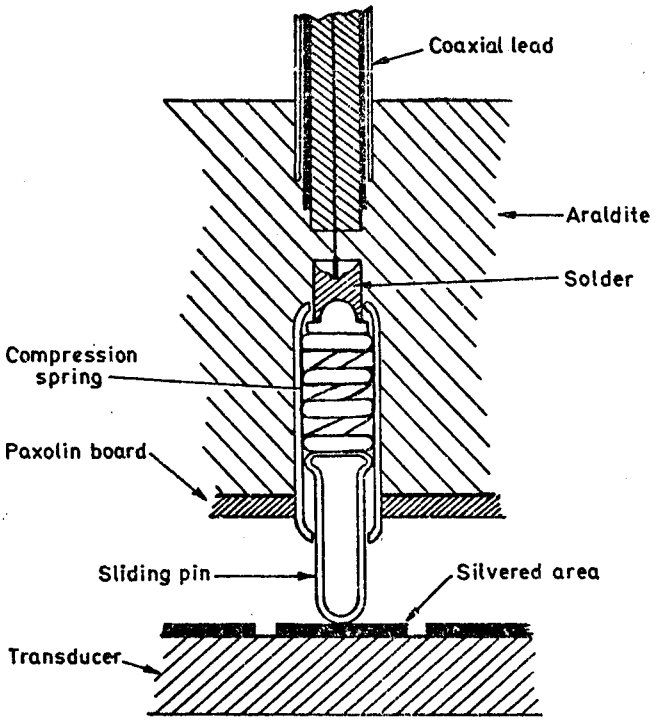

Fig 14 Enlarged cross-section through a single pin assembly, which is accurately spaced from its neighbours

Appendix B

LINEAR SWITCH

Fig 2 shows the circuit of a single linear switch or gate, 110 of these being used to gate the outputs of the 100 transducer element matrix, as indicated in Fig 4. The transistor used is a General Electric 2N2926 plastic planar passivated type, which maintains a reasonable current gain at low current levels. At collector currents of around 40μA, the reverse current gain over five samples varied between 0.5 and 2.8; the forward gain for the same transistors was 80 to 280 respectively. By using a base drive resistor of 22kΩ, an adequate degree of saturation is maintained over the range of expected forward and reverse currents; which clearly depend on many factors, although a figure of 100 μA has been used as a basis for design.

MASTER OSCILLATOR AND PULSE GENERATOR

A circuit diagram of the master oscillator and pulse generator is given in Fig 15. An astable multivibrator provides the basic clock frequency of around 6kHz. Diodes D1 and D2 provide isolation of the collector loads from the capacitors C1 and C2 when their respective transistors are switching from saturation to cut-off, thus speeding up the positive edge of the output waveform. D3 and D4 guard against breakdown of the reverse biased transistor emitter-base junctions during their respective 'off' periods.

C3 and R3 differentiate the multivibrator output wave, the resulting positive spikes being shaped by T4 to form a square pulse. T3, an emitter follower, is included to reduce the loading of the output stage T4 on the timing circuit C3, R3. D5 removes the unwanted negative spike.

The final output is a pulse of amplitude approximately 10V, duration 1μS and with rise and fall times of <10ns when unloaded.

BISTABLE MULTIVIBRATOR

The bistable multivibrator (Fig 16) forms the basic unit used in the two shift registers. It is of the conventional Eccles Jordan form; diodes D1 and D2 are included to allow for resetting the registers. By connecting the relevant diode cathode to −5V the bistable may be set to the desired state.

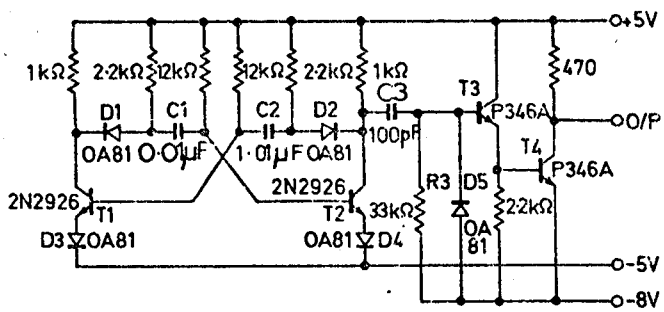

Fig 15 Master oscillator and pulse generator circuit. The basic frequency is 6MHz, the final output is a pulse of around 10V, duration 1μs, with rise and fall times <10ns when unloaded

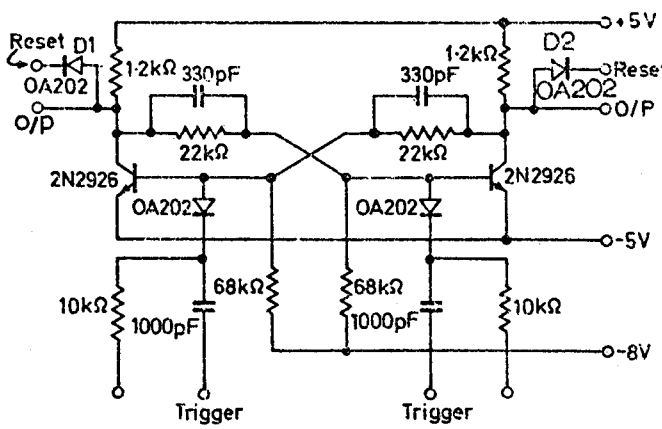

Fig 16 Bistable multivibrator circuit is set to the desired state by connecting the relevant diode cathode to −5V

VIDEO AMPLIFIER AND DETECTOR

The complete circuit is given in Fig 17.
The video amplifier is directly coupled with a voltage gain of approximately 3, 000 from 50Hz to 2MHz. The feedback loop R1 and R2 provides dc stability, the ac gain being maintained by decoupling the loop via C1. The peak detector D1, R3, and C2, is followed by a single stage of amplification—introduced to enable a voltage swing equal to the full supply voltage to be achieved. This is necessary in order to adequately control the brilliance of the oscilloscope used (a Tektronix Type 536).

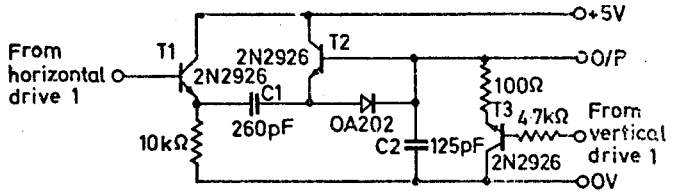

Fig 17 Video amplifier and detector circuit. All transistors are 2N2926

STAIRCASE GENERATOR[9]

The circuit diagram for the staircase generator is shown in Fig 18. T1 is an emitter follower which acts as a buffer to reduce the loading of the circuit on the horizontal shift register. T3 is merely a clamp arrangement to reset the conditions of the circuit at the beginning of each scan. The operation of the generator is similar to a diode storage counter, except that, when the transistor T2 conducts, it clamps the anode of the diode to the voltage at the top end of C2 instead of earth potential. This means that the following input pulse is added to the existing output voltage; the result is a linear staircase voltage waveform with steps of equal magnitude.

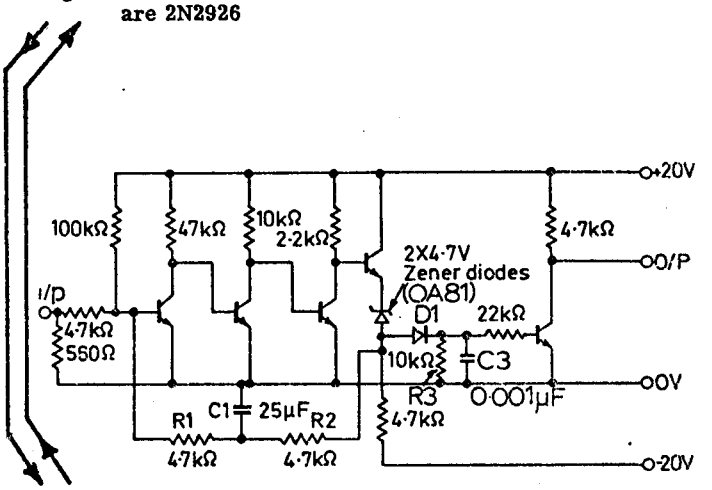

Fig 18 Staircase generator circuit which produces a linear staircase voltage waveform with steps of equal amplitude

ACKNOWLEDGEMENT

The author wishes to thank Dr D. I. Crecraft for much useful advice and support and Mr H. McKinnon for his great help in the mechanical design and construction of the system and, in particular, of the acoustic receiver.

REFERENCES

1 Sokolov, S. Ia. 'Contemporary problems in the use of ultra-sound', Uspekhi Fizicheskikh Nauk, Vol 40 (1950) pp 20-27

2 Freitag, W. 'Investigations of an ultrasonic image converter', Jenaer Jahrbuch, Vol 1, Part 1 (1958) pp 228-274 (translated from German by E. Kolm)

3 Prokhorov, V. G. 'The problems of converting an ultrasonic image into a visible', Soviet Physics—Acoustics, Vol 3 (1958) pp 272-280

4 Smyth, C. N., Poynton, F. Y., Sayers, J. F. 'The ultrasound image camera', Proceedings of the IEE, Vol 110, No 1 (January 1963) pp 16-28

5 Jacobs, J. E., Collis, W. J., Berger, H. 'An evaluation of an ultrasonic inspection system employing television techniques', Materials Evaluation, (May 1964)

6 Kennedy, J. A., Muenow, R. 'Practical improvements and applications for the ultrasonic image converter', IEEE Transactions on Sonics and Ultrasonics, Vol SU-14, No 2 (April 1967) pp 47-52

7 Jenkins and White 'Fundamentals of optics'

8 Sayers, J. F. 'The ultra-sound camera', Research report for AERE Harwell (November 1963)

9 Bolton, B. A. 'A staircase generator', BSc Project Report (1966), Lanchester College of Technology

APPENDIX B

Manufacturers' data on the following:-

Union Carbide n-channel field effect transistor UC734.

Hybrid Systems Corporation A/D converter ADC540-8.

Motorola phase-frequency detector MC4044.

UC734

LOW COST N-CHANNEL FIELD EFFECT TRANSISTOR — FOR HIGH FREQUENCY AND GENERAL PURPOSE APPLICATIONS

Union Carbide UK Ltd Electronics Division
8 Grafton Street London W1 Tel: 01-629 8100

MAXIMUM RATINGS (25°C Unless otherwise noted)

Drain to Gate Voltage	V_{DGO}	30V
Drain to Source Voltage	V_{DSO}	30V
Source to Gate Voltage	V_{SGO}	30V
Gate Current	I_G	10mA
Device Diss. (free air)	P_D	300mW
Junction Temp. (oper)	T_j	200°C
Storage Temp. range	T_S	-55 to 200°C

DESCRIPTION

N-Channel, Junction Field Effect Transistor for VHF amplifier and mixer applications. LOW COST!

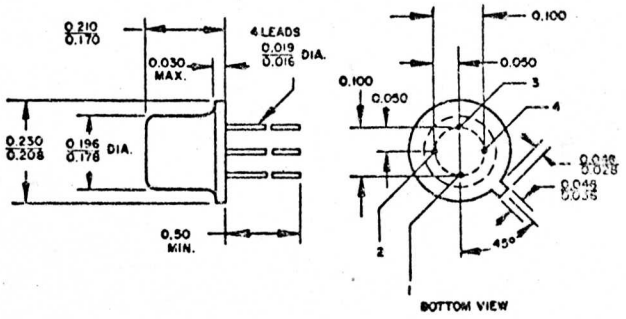

1=S 2=D 3=G 4=Case

ELECTRICAL CHARACTERISTICS @ 25°C unless otherwise noted

	SYM.	CONDITIONS	MIN.	MAX.	UNITS
Gate Breakdown Voltage	BV_{GSS}	V_{DS}=0, I_G=1μA	30		Volts
Gate Leakage Current	I_{GSS}	V_{GS}=20V, V_{DS}=0		5	nA
Gate Leakage Current @ 100°C	I_{GSS}	V_{GS}=20V, V_{DS}=0		1.5	μA
Drain (SAT) Current	I_{DSS}	V_{DS}=15V, V_{GS}=0	4	20	mA
Gate to Source Voltage	V_{GS}	V_{DS}=15V, I_D=400μA	-1	-7.5	Volts
Pinch-Off Voltage	V_P	V_{DS}=15V, I_D=10nA	-1	-8	Volts
Transconductance (1KC)	(Y_{fs})	V_{DS}=15V, V_{GS}=0	3500	6500	μmhos
Output Admittance (1KC)	(Y_{os})	V_{DS}=15V, V_{GS}=0		50	μmhos
Input Capacitance (1MC)	C_{iss}	V_{DS}=15V, V_{GS}=0		4	pF
Feedback Capacitance (1MC)	C_{rss}	V_{DS}=15V, V_{GS}=0		0.8	pF
Input Conductance (200MC)	RE(Y_{is})	V_{DS}=15V, V_{GS}=0		800	μmhos
Transconductance (200MC)	RE(Y_{fs})	V_{DS}=15V, V_{GS}=0	3000		μmhos
Output Conductance (200MC)	RE(Y_{os})	V_{DS}=15V, V_{GS}=0		200	μmhos

PARAMETER INTER-RELATIONSHIP

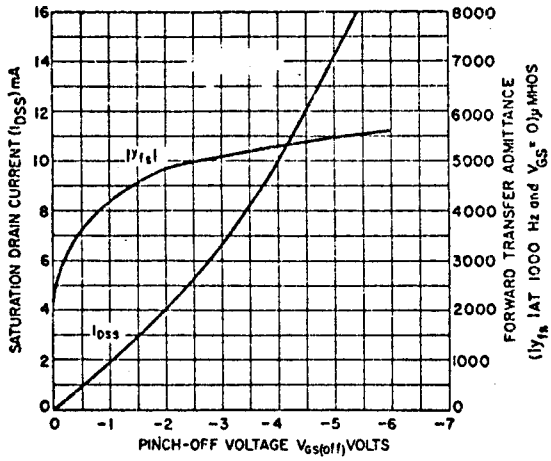

SATURATION DRAIN CURRENT
AND FORWARD TRANSFER ADMITTANCE
VS.
PINCH-OFF VOLTAGE

TRANSFER CHARACTERISTIC

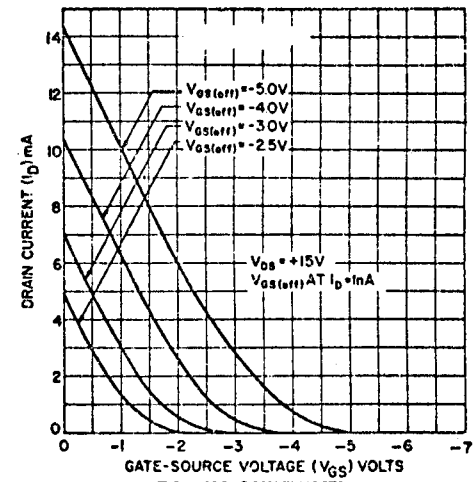

DRAIN CURRENT
VS.
GATE-SOURCE VOLTAGE

DRAIN CHARACTERISTIC

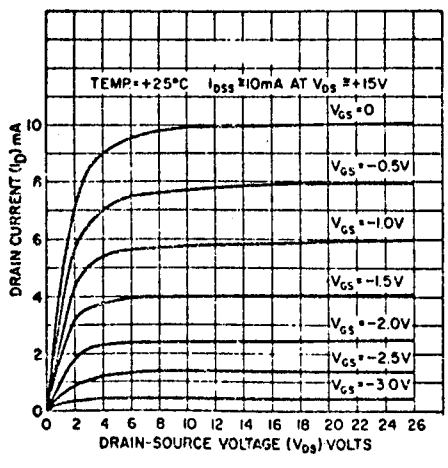

DRAIN CURRENT
VS.
DRAIN-SOURCE VOLTAGE

TRANSFER CHARACTERISTIC

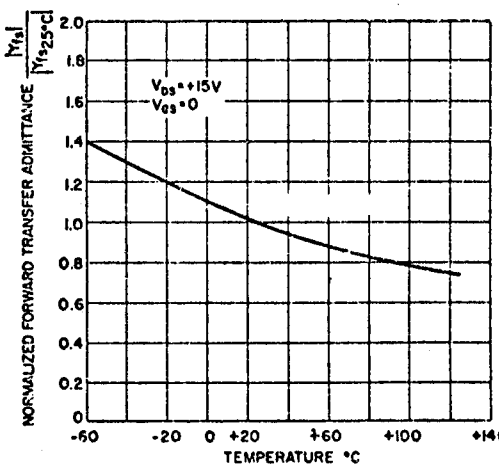

NORMALIZED FORWARD TRANSFER
ADMITTANCE
VS.
TEMPERATURE

HIGH FREQUENCY COMMON SOURCE CHARACTERISTICS

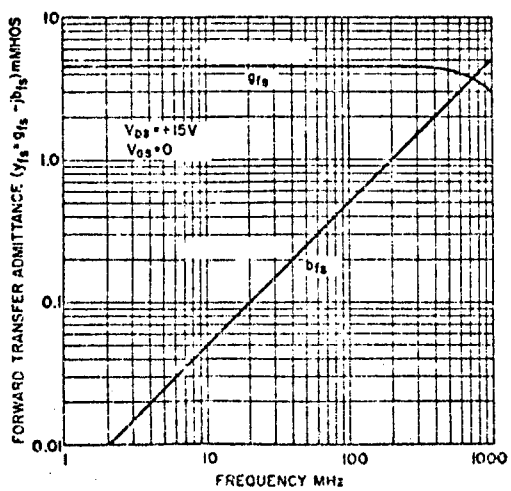

FORWARD TRANSFER ADMITTANCE
VS.
FREQUENCY

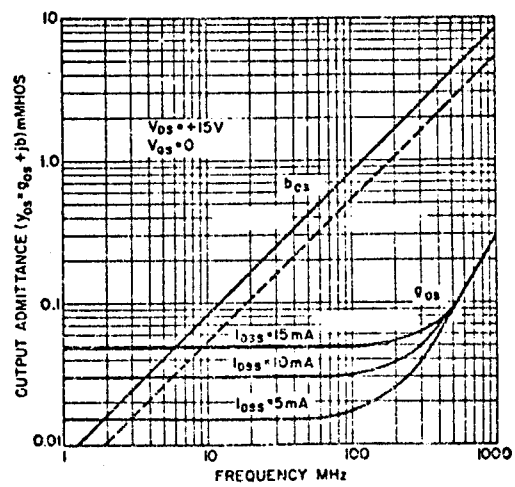

OUTPUT ADMITTANCE
VS.
FREQUENCY

ULTRA FAST, 8-BIT A/D CONVERTER

MODELS ADC 540-8, ADC 540WB-8

Leaflet No. 09-222

May 1972

Ultra Fast A/D Converter Now in Miniature Module - 2" x 2" x 0.4"

- FAST CONVERSION
- COMPACT – 2"X2"X0.4
- COMPLETE – READY TO USE
- PC MOUNTING
- DIP COMPATIBLE PIN SPACING
- ±15V, +5V POWER SUPPLY

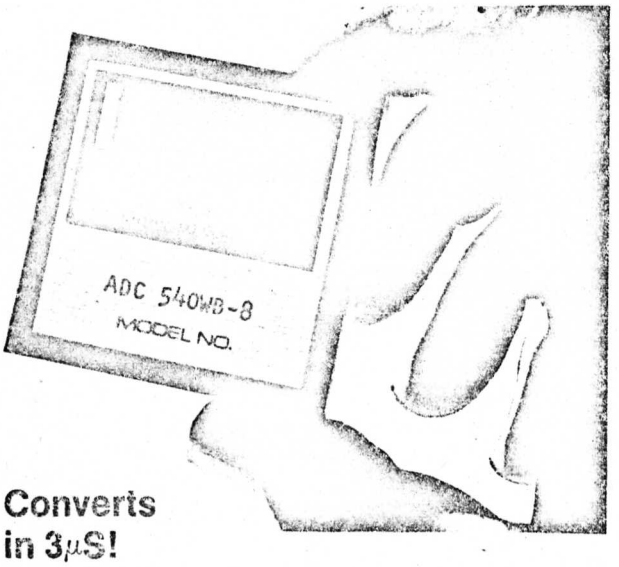

Converts in 3μS!

ADC 540 Series

The ADC 540 are a series of state of the art, ultra high speed, general purpose A/D converters packaged in a remarkably compact 2"X2"X0.4" module. The standard ADC 540-8 converts 8 bits in under 5μS and the extra fast ADC 540WB-8 converts them in under 3μS. The units are complete with all logic, references, clocks; no extra components are required for operation. The high speed and small size is achieved by a unique modification to the successive approximation technique combined with an extremely fast settling, proprietary D/A converter.

Special Reliability Features

To assure long life and good stability, all ADC 540 converters have these three important reliability features: all active components are hermetically sealed – no plastic transistors or IC's, all precision resistors are thin film type, all converters are burned in under power for 72 hours minimum – a real reliability bonus.

SUMMARY SPECIFICATIONS

MODEL	540-8	540WB-8
RESOLUTION	8	8
CONVERSION TIME	5μS Max	3μS Max
OUTPUT CODES	BINARY & BCD	
SAMPLING RATE	200KHZ	330KHZ
ACC. TEMPCO	50PPM/°C	50PPM/°C
INPUT RANGE	0 to +10V	*

* Same as Column on Left.

COMPLETE SPECIFICATIONS ON REVERSE SIDE

ORDERING INFORMATION

MODEL	CODE
ADC540-8	8 Bits Binary
ADC540WB-8	8 Bits Binary

Wide Temperature Option
−55°C to +125°C: Add suffix-MIL,

Guest International Limited
INDUSTRIAL ELECTRONIC COMPONENTS DIVISION
Nicholas House, Brigstock Road,
Thornton Heath, Surrey, CR4 7JA
01-689 2121
Sales Lines 01-684 5654/5 Telex 25649

Printed and designed by the Printing Division, Guest International Limited

NOTES ON USE

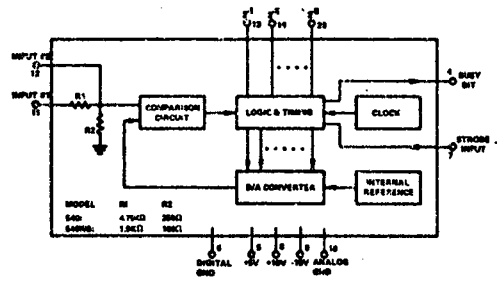

CAUTION: Maximum voltage at Input No. 2 is +5V

1. TIMING

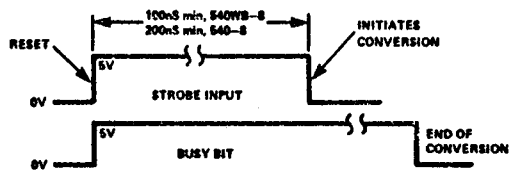

Both the Strobe Input and the Busy Bit are standard TTL levels. Rise Time of the Strobe Input should be 1μS min.

2. INPUT OVERLOAD

If the input signal exceeds the full scale, the output digital code becomes all "ones".

INPUT RANGES

a. Pin 11 is set for a 0 to +10V input range.

b. Pin 12 may be used for other ranges. Add an appropriate series resistor for a nominal +0.5V input to the comparison circuit.

3. CODING
–BINARY

ANALOG INPUT	MSB OUTPUT CODE							LSB
	2^{-1}	2^{-2}	2^{-3}	2^{-4}	2^{-5}	2^{-6}	2^{-7}	2^{-8}
+9.96	1	1	1	1	1	1	1	1
+7.50	1	1	0	0	0	0	0	0
+5.00	1	0	0	0	0	0	0	0
+2.50	0	1	0	0	0	0	0	0
+0.04V*	0	0	0	0	0	0	0	1
0.00V	0	0	0	0	0	0	0	0

*1LSB = 10V/256

MECHANICAL

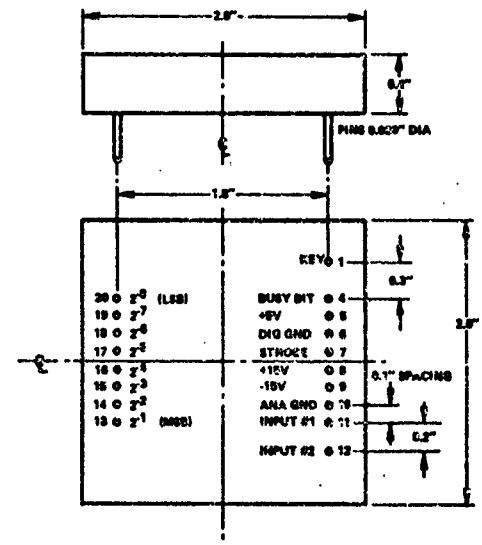

SPECIFICATIONS

MODEL	ADC 540-8	ADC 540WB-8
DIGITAL		
Conversion Type	Successive Approximation	
Resolution	8 Bits	8 Bits
Output Code	Binary, Parallel	"
Output Type	TTL, DTL Compatible	"
"0"	<+0.5V drives up to 4TTL loads	
"1"	>+2.5V	
Conversion Time	5μS Max	3μS Max
Max Sampling Rate	200K/SEC	330K/SEC
ANALOG		
Input Range	0 to +10V	"
Input Impedance	5K	2K
Reference	Internal	"
ACCURACY AND STABILITY		
Accuracy	0.2%**	"
Quantization	±1/2LSB	"
Accuracy vs Temp.	50PPM/°C	"
Linearity vs Temp.	20PPM/°C	"
Long Term Stability	0.05%/year	
Precision Network	Matched discrete thin film resistors	

RELIABILITY		
Construction	Encapsulated modules, factory repairable	
Active Components	All hermetically sealed - no plastics	
Factory Burn-In	72 Hour	
Warantee Period	3 years	
ENVIRONMENTAL		
Operating Temperature		
Standard Versions	0 to +70°C	
-MIL Versions	-55°C to +125°C	
Power Supply	+15V @ 25mA, -15V @ 20 mA, +5V @ 140 mA	
Power Supply Rej.	0.05%/%	"
Dimensions	2"x2"x0.4"	"
Weight	Under 2 oz	"

*Same as column on left

**Includes all effects due to offset, gain, and linearity

REPRESENTED BY

PHASE-FREQUENCY DETECTOR

MC4344 • MC4044

ISSUE A

The MC4344/4044 consists of two digital phase detectors, a charge pump, and an amplifier. In combination with a voltage controlled multivibrator (such as the MC4324/4024 or MC1648), it is useful in a broad range of phase-locked loop applications. The circuit accepts MTTL waveforms at the R and V inputs and generates an error voltage that is proportional to the frequency and/or phase difference of the input signals. Phase detector #1 is intended for use in systems requiring zero frequency and phase difference at lock. Phase detector #2 is used if quadrature lock is desired. Phase detector #2 can also be used to indicate that the main loop, utilizing phase detector #1, is out of lock.

F SUFFIX
CERAMIC PACKAGE
CASE 607
(TO-86)

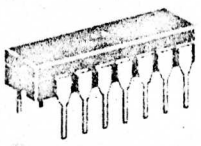

L SUFFIX
CERAMIC PACKAGE
CASE 632
(TO-116)

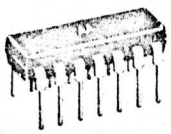

P SUFFIX
PLASTIC PACKAGE
CASE 646
(TO-116)
MC4044 only

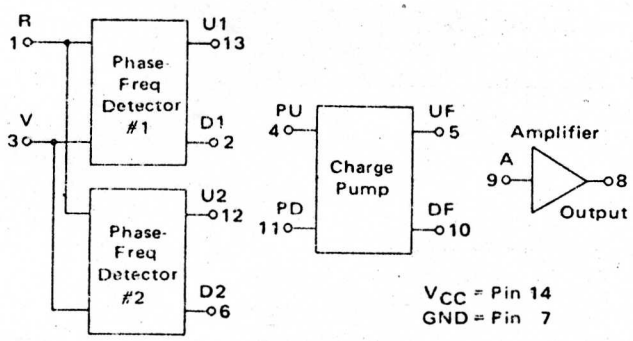

Input Loading Factor: R, V = 3
Output Loading Factor (Pin 8) = 10
Total Power Dissipation = 85 mW typ/pkg
Propagation Delay Time = 9.0 ns typ
(thru phase detector)

PHASE DETECTOR

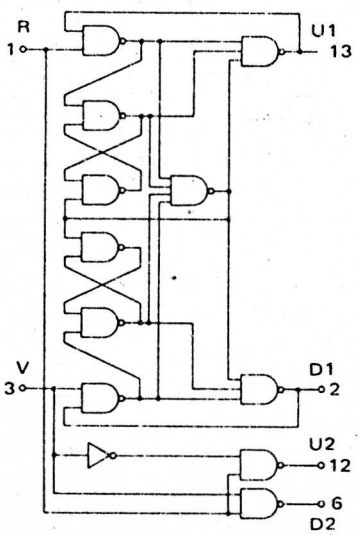

CHARGE PUMP

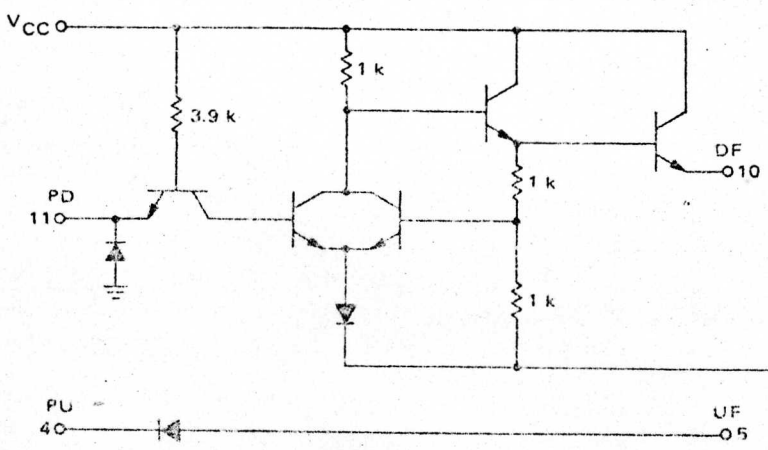

AMPLIFIER

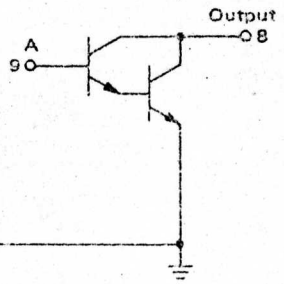

INPUT STATE	INPUT RI	INPUT VI	OUTPUT U1	OUTPUT D1	OUTPUT U2	OUTPUT D2
1	0	0	X	X	1	1
2	1	0	X	X	0	1
3	1	1	X	X	1	0
4	1	0	X	X	0	1
5	0	0	X	X	1	1
6	1	0	X	X	0	1
7	0	0	X	X	1	1
8	1	0	X	X	0	1
9	0	0	0	1	1	1
10	0	1	0	1	1	1
11	0	0	1	1	1	1
12	0	1	1	1	1	1
13	0	0	1	0	1	1
14	0	1	1	0	1	1
15	0	0	1	0	1	1
16	1	0	1	0	0	1
17	0	0	1	1	1	1

TRUTH TABLE

This is not strictly a functional truth table; i.e., it does not show all possible modes of operation. It is useful for dc testing.

1. X indicates output state unknown.
2. U1 and D1 outputs are sequential; i.e., they must be sequenced in order shown.
3. U2 and D2 outputs are combinational; i.e., they need only inputs shown to obtain outputs.

ELECTRICAL CHARACTERISTICS

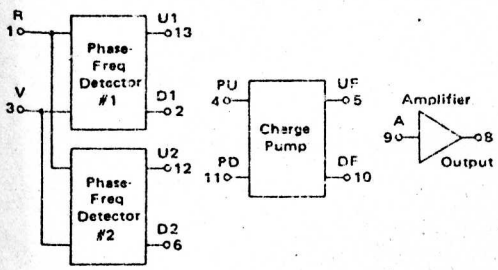

Test Temperature		I_{OL} mA	I_{OH1} mA	I_{OH2} mA	I_{in} mA	I_{IC} mA	I_A mA	V_{IL} Volts	V_{IH} Volts	V_{IHH} Volts	V_R Volts	V_{ILT} Volts	V_{IHT} Volts	V_{out} Volts	V_{CC} Volts	V_{CCL} Volts	V_{CCH} Volts
MC4344	-55°C	20	-1.6	-1.0	–	–	0.002	0.4	2.4	–	4.5	1.1	2.0	1.5	5.0	4.5	5.5
	+25°C	20	-1.6	-1.0	1.0	-10	0.002	0.4	2.4	5.5	4.5	1.1	1.8	1.5	5.0	4.5	5.5
	+125°C	20	-1.6	-1.0	–	–	0.002	0.4	2.4	–	4.5	0.9	1.8	1.5	5.0	4.5	5.5
MC4044	0°C	20	-1.6	-1.0	–	–	0.002	0.4	2.5	–	4.5	1.1	2.0	1.5	5.0	4.75	5.25
	+25°C	20	-1.6	-1.0	1.0	-10	0.002	0.4	2.5	5.5	4.5	1.1	1.8	1.5	5.0	4.75	5.25
	+75°C	20	-1.6	-1.0	–	–	0.002	0.4	2.5	–	4.5	0.9	1.8	1.5	5.0	4.75	5.25

Characteristic	Symbol	Pin Under Test	MC4344 Test Limits -55°C Min	-55°C Max	+25°C Min	+25°C Max	+125°C Min	+125°C Max	MC4044 Test Limits 0°C Min	0°C Max	+25°C Min	+25°C Max	-75°C Min	-75°C Max	Unit	TEST CURRENT/VOLTAGE APPLIED TO PINS LISTED BELOW: I_{OL}	I_{OH1}	I_{OH2}	I_{in}	I_{IC}	I_A	V_{IL}	V_{IN}	V_{IHH}	V_R	V_{ILT}	V_{IHT}	V_{out}	V_{CC}	V_{CCL}	V_{CCH}	Pulse 1	Gnd
Input																																	
Forward Current	I_{IL}	1	–	-4.8	–	-4.8	–	-4.8	–	-4.6	–	-4.8	–	-4.8	mAdc	–	–	–	–	–	–	1	–	–	–	–	–	–	–	–	14	–	7
		3	–	-4.8	–	-4.8	–	-4.8	–	-4.8	–	-4.8	–	-4.8		–	–	–	–	–	–	3	–	–	–	–	–	–	–	–		–	
		11	–	-1.6	–	-1.6	–	-1.5	–	-1.6	–	-1.6	–	-1.6		–	–	–	–	–	–	11	–	–	–	–	–	–	–	–		–	
Leakage Current	I_{IH}	1	–	120	–	120	–	120	–	120	–	120	–	120	μAdc	–	–	–	–	–	–	–	1	–	–	–	–	–	–	–	14	–	7
		3	–	120	–	120	–	120	–	120	–	120	–	120		–	–	–	–	–	–	–	3	–	–	–	–	–	–	–	14	–	7
		4	–	5.0	–	5.0	–	5.0	–	5.0	–	5.0	–	5.0		–	–	–	–	–	–	–	–	–	–	–	–	–	–	–	4	–	5,7
		11	–	40	–	40	–	40	–	40	–	40	–	40		–	–	–	–	–	–	–	11	–	–	–	–	–	–	–	14	–	7
	I_{IHH}	1	–	–	1.0	–	–	–	–	–	1.0	–	–	–	mAdc	–	–	–	–	–	–	–	–	1	–	–	–	–	–	–	14	–	7
		3	–	–	↓	–	–	–	–	–	↓	–	–	–	↓	–	–	–	–	–	–	–	–	3	–	–	–	–	–	–	↓	–	↓
		11	–	–		–	–	–	–	–		–	–	–		–	–	–	–	–	–	–	–	11	–	–	–	–	–	–		–	
Clamp Voltage	V_{IC}	1	–	–	–	-1.5	–	–	–	–	–	-1.5	–	–	Vdc	–	–	–	–	–	1	–	–	–	–	–	–	–	–	14	–	7
		3	–	–	–	-1.5	–	–	–	–	–	-1.5	–	–	Vdc	–	–	–	–	–	3	–	–	–	–	–	–	–	–	14	–	7
Output (Note 1)																																	
Output Voltage	V_{OH}	6	2.4	–	2.4	–	2.4	–	2.5	–	2.5	–	2.5	–	Vdc	–	6	–	–	–	–	–	–	–	–	1,3	–	–	–	14	–	–	7
		12	2.4	–	2.4	–	2.4	–	2.5	–	2.5	–	2.5	–	Vdc	–	12	–	–	–	–	–	–	–	–	1,3	–	–	–	14	–	–	7
	**	–	–	–	–	–	–	–	–	–	–	–	–	–	–	–	–	–	–	–	–	–	–	–	–	2	1	–	–	14	–	–	7
	V_{OL}	8	–	0.4	–	0.4	–	0.4	–	0.4	–	0.4	–	0.4	Vdc	6	–	–	–	–	–	–	–	–	–	–	1,3	–	–	–	14	–	–	7
	V_{OH}	12	2.4	–	2.4	–	2.4	–	2.5	–	2.5	–	2.5	–	Vdc	–	12	–	–	–	–	–	–	–	–	–	1,3	–	–	–	14	–	–	7
	**	–	–	–	–	–	–	–	–	–	–	–	–	–	Vdc	–	–	–	–	–	–	–	–	–	–	3	1	–	–	14	–	–	7
	**	–	–	–	–	–	–	–	–	–	–	–	–	–	Vdc	–	–	–	–	–	–	–	–	–	–	1,3	–	–	–	14	–	–	7
	V_{OH}	6	2.4	–	2.4	–	2.4	–	2.5	–	2.5	–	2.5	–	Vdc	–	6	–	–	–	–	–	–	–	–	–	3	1	–	–	14	–	–	7
	V_{OL}	12	–	0.4	–	0.4	–	0.4	–	0.4	–	0.4	–	0.4	Vdc	12	–	–	–	–	–	–	–	–	–	–	3	1	–	–	14	–	–	7
	**	–	–	–	–	–	–	–	–	–	–	–	–	–	–	–	–	–	–	–	–	–	–	–	–	1,3	–	–	–	14	–	–	7
	**	–	–	–	–	–	–	–	–	–	–	–	–	–	–	–	–	–	–	–	–	–	–	–	–	3	1	–	–	14	–	–	7
	V_{OH}	2	2.4	–	2.4	–	2.4	–	2.5	–	2.5	–	2.5	–	Vdc	–	2	–	–	–	–	–	–	–	–	–	1,3	–	–	–	14	–	–	7
	V_{OL}	13	–	0.4	–	0.4	–	0.4	–	0.4	–	0.4	–	0.4	Vdc	13	–	–	–	–	–	–	–	–	–	–	1,3	–	–	–	14	–	–	7
	V_{OH}	2	2.4	–	2.4	–	2.4	–	2.5	–	2.5	–	2.5	–	Vdc	–	2	–	–	–	–	–	–	–	–	–	1	3	–	–	14	–	–	7
	V_{OL}	13	–	0.4	–	0.4	–	0.4	–	0.4	–	0.4	–	0.4	Vdc	13	–	–	–	–	–	–	–	–	–	–	1	3	–	–	14	–	–	7
	V_{OH}	2	2.4	–	2.4	–	2.4	–	2.5	–	2.5	–	2.5	–	Vdc	–	2	–	–	–	–	–	–	–	–	–	1,3	–	–	–	14	–	–	7
		13	2.4	–	2.4	–	2.4	–	2.5	–	2.5	–	2.5	–	Vdc	–	13	–	–	–	–	–	–	–	–	–	1,3	–	–	–	14	–	–	7
	V_{OH}	2	2.4	–	2.4	–	2.4	–	2.5	–	2.5	–	2.5	–	Vdc	–	2	–	–	–	–	–	–	–	–	–	1	3	–	–	14	–	–	7
		13	2.4	–	2.4	–	2.4	–	2.5	–	2.5	–	2.5	–	Vdc	–	13	–	–	–	–	–	–	–	–	–	1	3	–	–	14	–	–	7
	V_{OL}	2	–	0.4	–	0.4	–	0.4	–	0.4	–	0.4	–	0.4	Vdc	2	–	–	–	–	–	–	–	–	–	–	1,3	–	–	–	14	–	–	7
	V_{OH}	13	2.4	–	2.4	–	2.4	–	2.5	–	2.5	–	2.5	–	Vdc	–	13	–	–	–	–	–	–	–	–	–	1,3	–	–	–	14	–	–	7
	V_{OL}	2	–	0.4	–	0.4	–	0.4	–	0.4	–	0.4	–	0.4	Vdc	2	–	–	–	–	–	–	–	–	–	–	1	3	–	–	14	–	–	7
	V_{OH}	13	2.4	–	2.4	–	2.4	–	2.5	–	2.5	–	2.5	–	Vdc	–	13	–	–	–	–	–	–	–	–	–	1	3	–	–	14	–	–	7
	V_{OL}	2	–	0.4	–	0.4	–	0.4	–	0.4	–	0.4	–	0.4	Vdc	2	–	–	–	–	–	–	–	–	–	–	1,3	–	–	–	14	–	–	7
	V_{OH}	13	2.4	–	2.4	–	2.4	–	2.5	–	2.5	–	2.5	–	Vdc	–	13	–	–	–	–	–	–	–	–	–	1,3	–	–	–	14	–	–	7
	V_{OL}	2	2.4	–	2.4	–	2.4	–	2.5	–	2.5	–	2.5	–	Vdc	2	–	–	–	–	–	–	–	–	–	–	1,3	–	–	–	14	–	–	7
	V_{OH}	13	2.4	–	2.4	–	2.4	–	2.5	–	2.5	–	2.5	–	Vdc	–	13	–	–	–	–	–	–	–	–	–	1,3	–	–	–	14	–	–	7
	V_{OL}	2	2.4	–	2.4	–	2.4	–	2.5	–	2.5	–	2.5	–	Vdc	2	–	–	–	–	–	–	–	–	–	–	3	1	–	–	14	–	–	7
	V_{OH}	13	2.4	–	2.4	–	2.4	–	2.5	–	2.5	–	2.5	–	Vdc	–	13	–	–	–	–	–	–	–	–	–	3	1	–	–	14	–	–	7
	V_{OH}	2	2.4	–	2.4	–	2.4	–	2.5	–	2.5	–	2.5	–	Vdc	–	7	–	–	–	–	–	–	–	–	–	1,3	–	–	–	14	–	–	7
		13	2.4	–	2.4	–	2.4	–	2.5	–	2.5	–	2.5	–	Vdc	–	13	–	–	–	–	–	–	–	–	–	1,3	–	–	–	14	–	–	7
Short-Circuit Current	I_{OS}	2	-20	-65	-20	-65	-20	-65	-20	-65	-20	-65	-20	-65	mAdc	–	–	–	–	–	–	–	–	–	–	–	1	–	–	–	–	14	2,3,7
		6	↓	↓	↓	↓	↓	↓	↓	↓	↓	↓	↓	↓	↓	–	–	–	–	–	–	–	–	–	–	–	–	–	–	–	14	–	1,3,6,7
		12														–	–	–	–	–	–	–	–	–	–	–	–	–	–	–	14	–	1,3,7,12
		13														–	–	–	–	–	–	–	–	–	–	–	1	–	–	–	–	–	3,7,13
Leakage Current	I_{OLK}	2	–	250	–	250	–	250	–	250	–	250	–	250	μAdc	–	–	–	–	–	–	–	–	–	–	–	–	1	–	–	7,14	–	3,7
		6	–	↓	–	↓	–	↓	–	↓	–	↓	–	↓	↓	–	–	–	–	–	–	–	–	–	–	–	–	–	–	–	6,14	–	1,3,7
		12	–		–		–		–		–		–			–	–	–	–	–	–	–	–	–	–	–	–	–	–	12,14	–	1,3,7
		13	–		–		–		–		–		–			–	–	–	–	–	–	–	–	–	–	–	1	–	–	13,14	–	–	3,7
Collector-Emitter Voltage	V_{CE}	5	–	–	0.5	–	–	–	–	–	0.5	–	–	–	Vdc	–	–	–	–	5	–	–	–	–	–	–	–	–	–	–	–	–	4,7
Output Voltage	V_{EH}	10	1.5	–	1.5	–	1.5	–	1.5	–	1.5	–	1.5	–	Vdc	–	–	–	10	–	–	–	–	–	–	–	1.5	–	–	–	14	–	–	7
Output Current	I_O	8	0.2	–	0.8	–	1.0	–	0.8	–	1.0	–	–	–	mAdc	–	–	–	–	–	8	–	–	–	–	–	–	–	–	–	–	8	–	7
Leakage Current	I_{OLK}	8	–	120	–	120	–	120	–	120	–	120	–	120	μAdc	–	–	–	–	–	–	–	–	–	–	–	–	–	–	–	–	8	–	7,9
		10	–	5.0	–	5.0	–	5.0	–	5.0	–	5.0	–	5.0	μAdc	–	–	–	–	–	–	–	11	–	–	–	–	10	–	–	14	–	7
Power Requirements (Total Device) Power Supply Drain	I_{CC}	14	–	40	–	40	–	40	–	40	–	40	–	40	mAdc	–	–	–	–	–	–	–	–	–	–	–	–	–	–	14	–	–	7

Note 1. The outputs of the device must be tested by sequencing through the indicated input states according to the truth table and functional diagram. All input, power supply, and ground voltages must be maintained between tests unless otherwise noted. Procedures identified by a double asterisk (**) in the Symbol column are necessary to change the state of the sequential logic.

Pulse 1: V_{CCL} ⌐ V_{CC} Used to change power supply voltage from previous test

MAXIMUM RATINGS

Rating		Value	Unit
Supply Operating Voltage Range	MC4344 MC4044	4.5 to 5.5 4.75 to 5.25	Vdc
Supply Voltage		+7.0	Vdc
Input Voltage		+5.5	Vdc
Output Voltage		+5.5	Vdc
Operating Temperature Range	MC4344 MC4044	-55 to +125 0 to +75	°C
Storage Temperature Range – Ceramic Package Plastic Package		-65 to +150 -55 to +125	°C
Maximum Junction Temperature	MC4344 MC4044	+175 +150	°C
Thermal Resistance - Junction To Case (θ_{JC}) Flat Ceramic Package Dual In-Line Ceramic Package Plastic Package		 0.06 0.05 0.07	°C/mW
Thermal Resistance - Junction To Ambient (θ_{JA}) Flat Ceramic Package Dual In-Line Ceramic Package Plastic Package		 0.21 0.15 0.15	°C/mW

CONTENTS

OPERATING CHARACTERISTICS

Operation of the MC4344/4044 is best explained by initially considering each section separately. If phase detector #1 is used, loop lockup occurs when both outputs U1 and D1 remain high. This occurs only when all the negative transitions on R, the reference input, and V, the variable or feedback input, coincide. The circuit responds only to transitions, hence phase error is independent of input waveform duty cycle or amplitude variation. Phase detector #1 consists of sequential logic circuitry, therefore operation prior to lockup is determined by initial conditions.

When operation is initiated, by either applying power to the circuit or active input signals to R and V, the circuitry can be in one of several states. Given any particular starting conditions, the flow table of Figure 1 can be used to determine subsequent operation. The flow table indicates the status of U1 and D1 as the R and V inputs are varied. The numbers in the table which are in parentheses are arbitrarily assigned labels that correspond to stable states that can result for each input combination. The numbers without parentheses refer to unstable conditions. Input changes are traced by horizontal movement in the table; after each input change, circuit operation will settle in the numbered state indicated by moving horizontally to the appropriate R-V column. If the number at that

FIGURE 1 – PHASE DETECTOR #1 FLOW TABLE

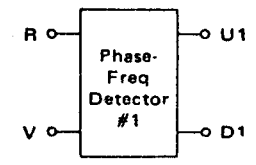

R-V 0-0	R-V 0-1	R-V 1-1	R-V 1-0	U1	D1
(1)	2	3	(4)	0	1
5	(2)	(3)	8	0	1
(5)	6	7	8	1	1
9	(6)	7	12	1	1
5	2	(7)	12	1	1
1	2	7	(8)	1	1
(9)	(10)	11	12	1	0
5	6	(11)	(12)	1	0

FIGURE 2 – PHASE DETECTOR #1 TIMING DIAGRAM

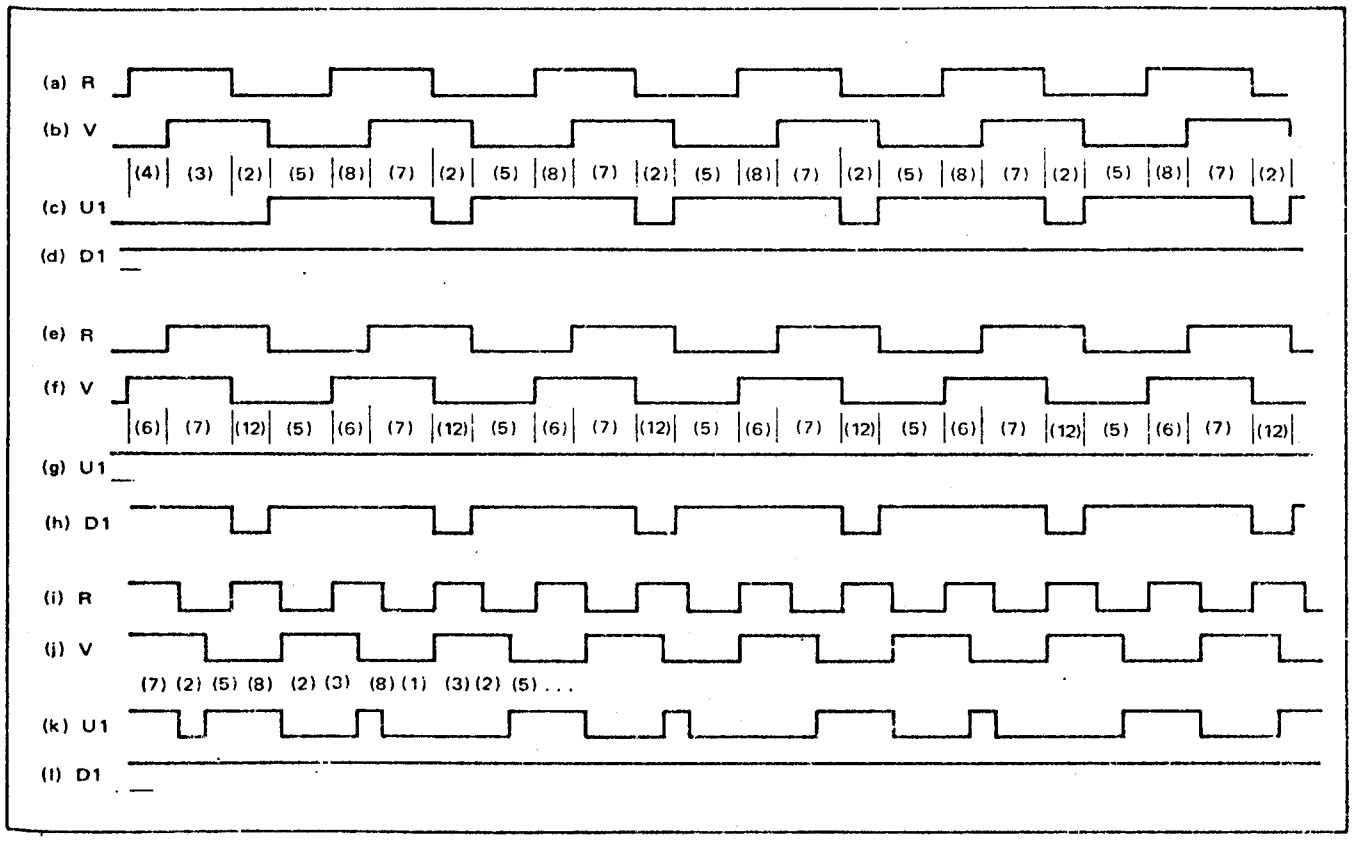

location is not in parentheses, move vertically to the number of the same value that is in parentheses. For a given input pair, any one of three stable states can exist. As an example, if R = 1 and V = 0, the circuit will be in one of the stable states (4), (8), or (12).

Use of the table in determining circuit operation is illustrated in Figure 2. In the timing diagram, the input to R is the reference frequency; the input to V is the same frequency but lags in phase. Stable state (4) is arbitrarily assumed as the initial condition. From the timing diagram and flow table, when the circuit is in stable state (4), outputs U1 and D1 are "0" and "1" respectively. The next input state is R-V = 1-1; moving horizontally from stable state (4) under R-V = 1-0 to the R-V = 1-1 column, state 3 is indicated. However, this is an unstable condition and the circuit will assume the state indicated by moving vertically in the R-V = 1-1 column to stable state (3). In this instance, outputs U1 and D1 remain unchanged. The input states next become R-V = 0-1; moving horizontally to the R-V = 0-1 column, stable state (2) is indicated. At this point there is still no change in U1 or D1. The next input change shifts operation to the R-V = 0-0 column where unstable state 5 is indicated. Moving vertically to stable state (5), the outputs now change state to U1-D1 = 1-1. The next input change, R-V = 1-0, drives the circuitry to stable state (8), with no change in U1 or D1. The next input, R-V = 1-1, leads to stable state (7) with no change in the outputs. The next two input state changes cause U1 to go low between the negative transitions of R and V. As the inputs continue to change, the circuitry moves repeatedly through stable states (2), (5), (8), (7), (2), etc. as shown, and a periodic waveform is obtained on the U1 terminal while D1 remains high.

A similar result is obtained if V is leading with respect to R, except that the periodic waveform now appears on D1 as shown in rows e-h of the timing diagram of Figure 2. In each case, the average value of the resulting waveform is proportional to the phase difference between the two inputs. In a closed loop application, the error signal for controlling the VCO is derived by translating and filtering these waveforms.

The results obtained when R and V are separated by a fixed frequency difference are indicated in rows i-l of the timing system. For this case, the U1 output goes low when R goes low and stays in that state until a negative transition on V occurs. The resulting waveform is similar to the fixed phase difference case, but now the duty cycle of the U1 waveform varies at a rate proportional to the difference frequency of the two inputs, R and V. It is this characteristic that permits the MC4344/4044 to be used as a frequency discriminator; if the signal on R has been frequency modulated and if the loop bandwidth is selected to pass the deviation frequency but reject R and V, the resulting error voltage applied to the VCO will be the recovered modulation signal.

Phase detector #2 consists only of combinatorial logic, therefore its characteristics can be determined from the

FIGURE 3 – PHASE DETECTOR #2 OPERATION

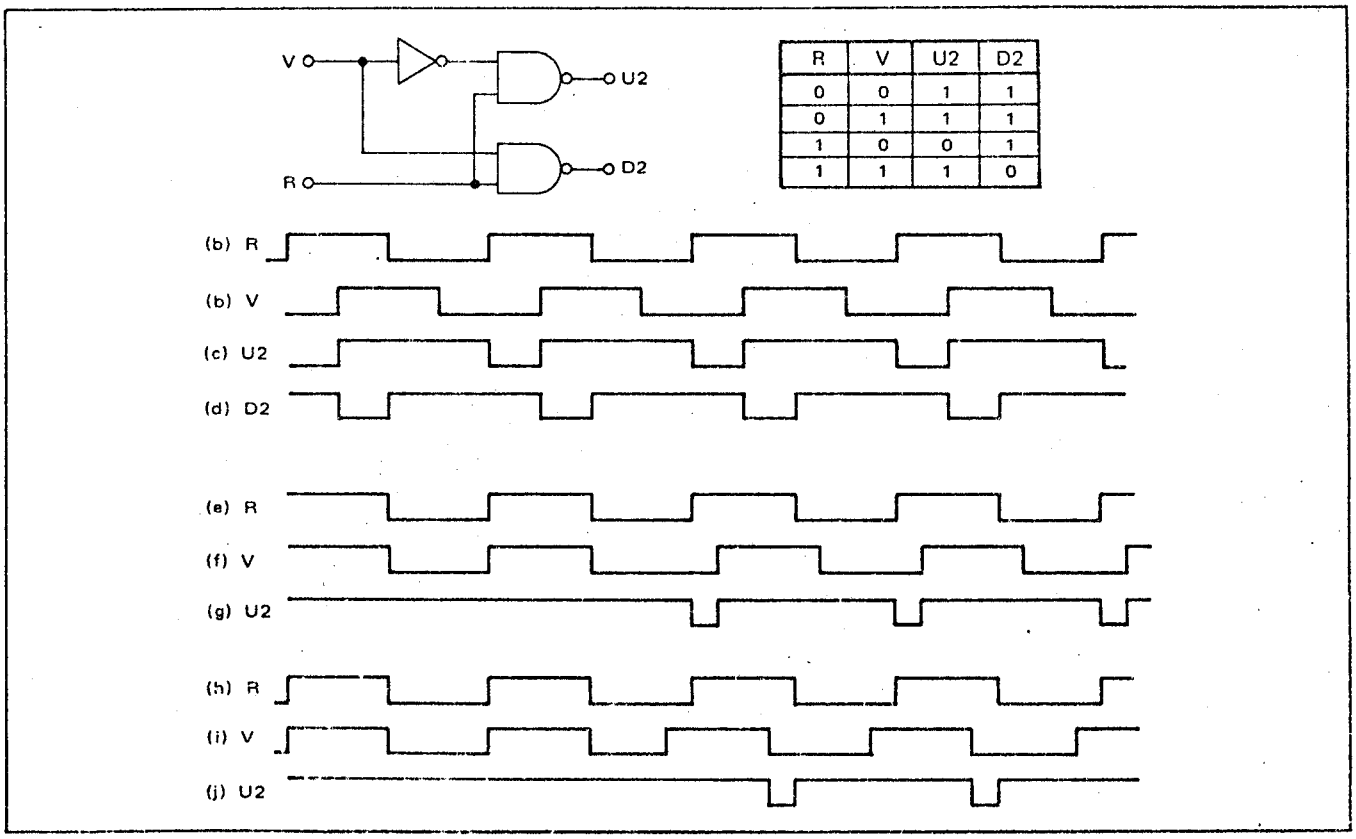

R	V	U2	D2
0	0	1	1
0	1	1	1
1	0	0	1
1	1	1	0

simple truth table of Figure 3. Since circuit operation requires that both inputs to the charge pump either be high or have the same duty cycle when lock occurs, using this phase detector leads to a quadrature relationship between R and V. This is illustrated in rows a-d of the timing diagram of Figure 3. Note that any deviation from a fifty percent duty cycle on the inputs would appear as phase error.

Waveforms showing the operation of phase detector #2 when phase detector #1 is being used in a closed loop are indicated in rows e-j. When the main loop is locked, U2 remains high. If the loop drifts out of lock in either direction a negative pulse whose width is proportional to the amount of drift appears on U2. This can be used to generate a simple loss-of-lock indicator.

Operation of the charge pump is best explained by considering it in conjunction with the Darlington amplifier included in the package (see Figure 4). There will be a pulsed waveform on either PD or PU, depending on the phase-frequency relationship of R and V. The charge pump serves to invert one of the input waveforms (D1) and translates the voltage levels before they are applied to the loop filter. When PD is low and PU is high, Q1 will be conducting in the normal direction and Q2 will be off. Current will be flowing through Q3 and CR2; the base of Q3 will be two V_{BE} drops above ground or approximately 1.5 volts. Since both of the resistors connected to the base of Q3 are equal, the emitter of Q4 (base of Q5) will be

FIGURE 4 – CHARGE PUMP OPERATION

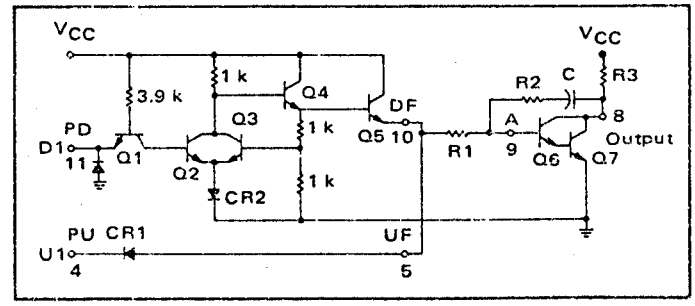

approximately 3.0 volts. For this condition, the emitter of Q5 (DF) will be one V_{BE} below this voltage, or about 2.25 volts. The PU input to the charge pump is high (> 2.4 volts) and CR1 will be reverse biased. Therefore Q5 will be supplying current to Q6. This will tend to lower the voltage at the collector of Q7, resulting in an error signal that lowers the VCO frequency as required by a "pump down" signal.

When PU is low and PD is high, CR1 is forward biased and UF will be approximately one V_{BE} above ground (neglecting the $V_{CE(sat)}$ of the driving gate). With PD high, Q1 conducts in the reverse direction, supplying base current for Q2. While Q2 is conducting, Q4 is prevented from supplying base drive to Q5; with Q5 cut off and UF low there is no base current for Q6 and the voltage at the

collector of Q7 moves up, resulting in an increase in the VCO operating frequency as required by a "pump up" signal.

If both inputs to the charge pump are high (zero phase difference), both CR1 and the base-emitter junction of Q5 are reverse biased and there is no tendency for the error voltage to change. The output of the charge pump varies between one V_{BE} and three V_{BE} as the phase difference of R and V varies from minus 2π to plus 2π. If this signal is filtered to remove the high-frequency components, the phase detector transfer function, K_ϕ, of approximately 0.12 volt/radian is obtained (see Figure 5).

FIGURE 5 – PHASE DETECTOR TEST

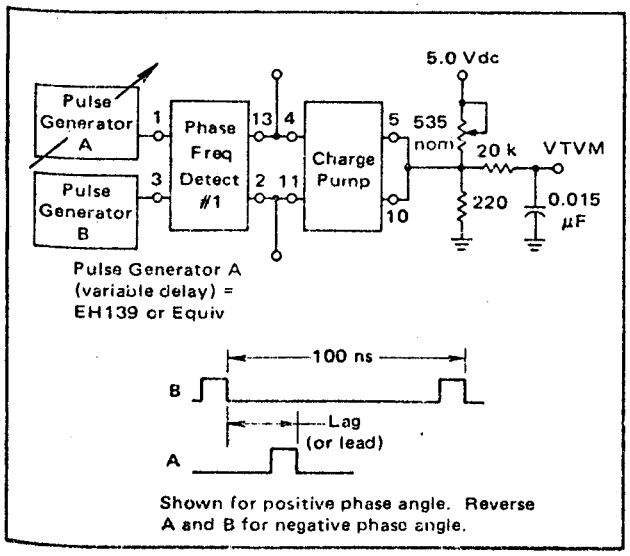

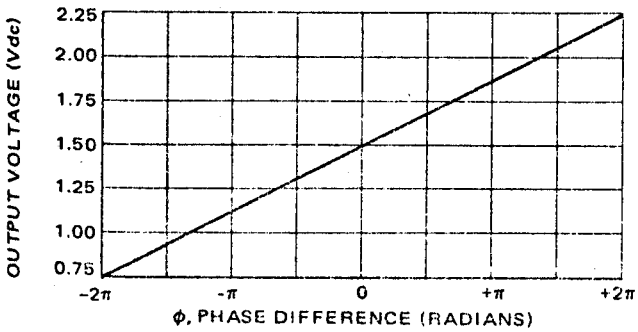

The specified gain constant of 0.12 volt/radian may not be obtained if the amplifier/filter combination is improperly designed. As indicated previously, the charge pump delivers pump commands of about 2.25 volts on the positive swings and 0.75 volt on the negative swings for a mean no-pump value of 1.5 volts. If the filter amplifier is biased to threshold "on" at 1.5 volts, then the pump up and down voltages have equal effects. The pump signals are established by V_{BE}'s of transistors with milliamperes of current flowing. On the other hand, the transistors included for use as a filter amplifier will have very small currents flowing and will have correspondingly lower V_{BE}'s – on the order of 0.6 volt each for a threshold of 1.2 volts. Any displacement of the threshold from 1.5 volts causes an increase in gain in one direction and a reduction in the other. The transistor configuration provided is hence not optimum but does allow for the use of an additional transistor to improve filter response. This addition also results in a non-symmetrical response since the threshold is now approximately 1.8 volts. The effective positive swing is limited to 0.45 volt while the negative swing below threshold can be greater than 1.0 volt. This means that the loop gain when changing from a high frequency to a lower frequency is less than when changing in the opposite direction. For type two loops this tends to increase overshoot when going from low to high and increases damping in the other direction. These problems and the selection of external filter components are intimately related to system requirements and are discussed in detail in the filter design section.

APPENDIX C

Details of the pulsed oscillator used for reflection tests.

The Pulsed Oscillator

General Description

T_1 and T_2 and their associated components form an astable multivibrator whose period is varied by means of RV_1. This circuit provides the clock drive to the 74121 monostable multivibrator whose output pulse duration may be set within certain limits by RV_2. The simple tuned collector oscillator is formed around T_4 and uses the transducer self capacitance as part of the tuned circuit shunt capacitance. T_3 effectively switches the oscillator on and off as it is driven into saturation and back to cut-off respectively by the monostable output. The loop gain of the oscillator circuit is less than one when pulsed and the large overdrive on T_3 base causes a large step of current through T_4, creating a ring in the collector output which decays to almost zero from maximum peak output in a few cycles. For C.W. operation the damping resistor RV_3 is removed to raise the loop gain above unity so that oscillations can commence.

Approximate Specification

Output frequency (nominal)	1 MHz
Minimum output pulse duration (electrical)	1 µS
Pulse repetition frequency	1 to 10 kHz
Output amplitude	11 V. r.m.s.

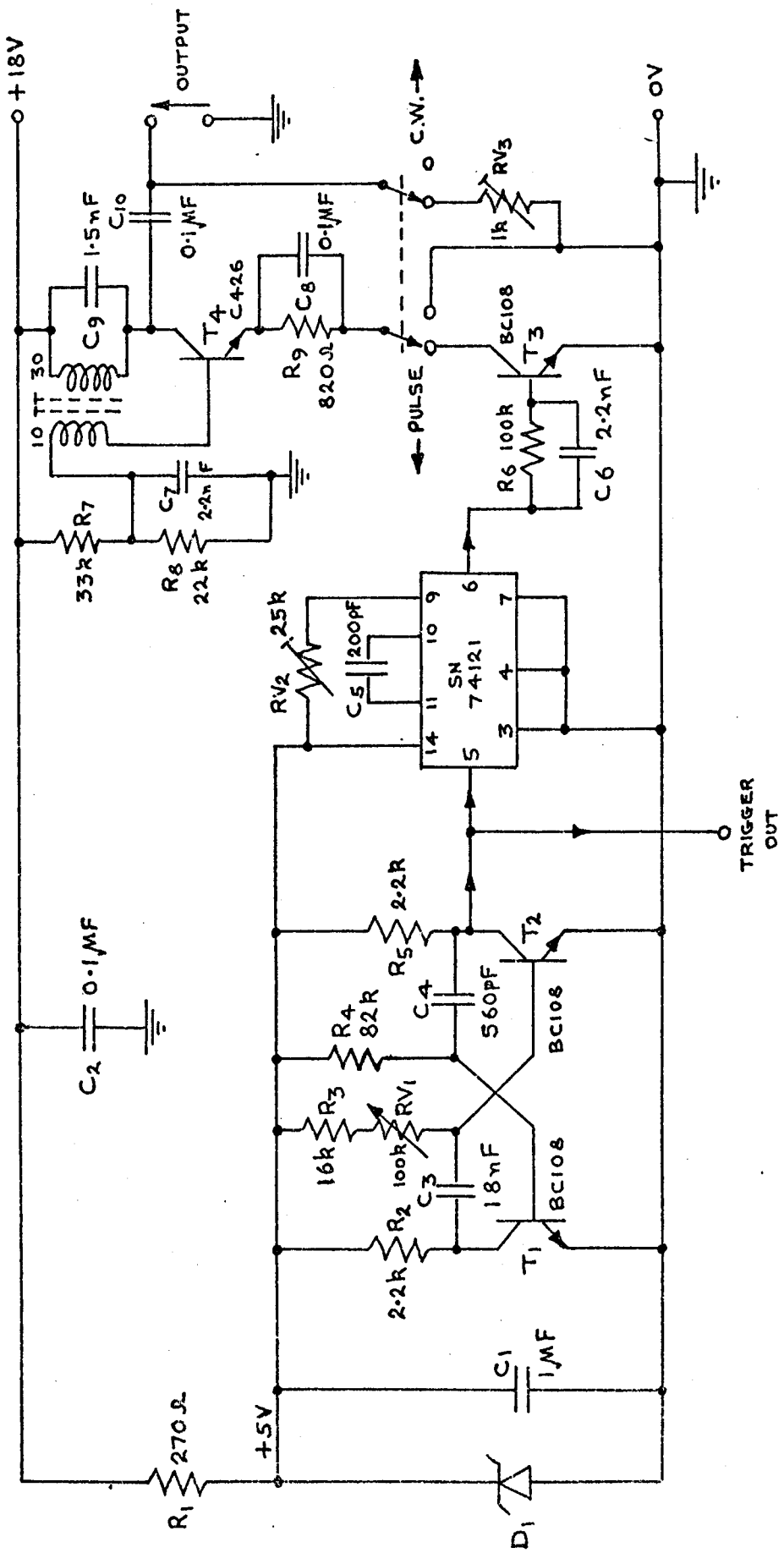

PULSED OSCILLATOR CIRCUIT.

APPENDIX D

Reprint of letter published in Electronics Letters,
25th February 1971, Vol. 7, No.4.

"Far-field sector scanning using a sampled multi-element ultrasonic receiving array"

FAR-FIELD SECTOR SCANNING USING A SAMPLED MULTIELEMENT ULTRASONIC RECEIVING ARRAY

Indexing terms: Ultrasonic devices, Ultrasonic applications

A technique which enables target bearing and range information to be obtained by sequential sampling of a multielement linear ultrasonic array is described. A resultant output frequency is extracted which is shown to be a function of the target angle, and results are given which confirm theoretical expectations.

An echo returning from an insonified target situated in the far field of an array of ultrasonic transducers will strike this array at an angle dependent on the target bearing. If the array is linear and consists of equally spaced elements which are sampled sequentially at a known and fast enough rate, the resultant electrical samples after demodulation will produce a sinusoidal signal whose frequency is a function of the angular bearing θ of the target. This resultant frequency is given by

$$f_R = f_T \left(1 - \frac{f_S d}{C_1} \sin\theta\right)$$

where

f_T = frequency of incident wave

d = distance between adjacent-element centres

C_1 = velocity of sound in transmission medium

f_S = sampling frequency

To satisfy the sampling theorem, f_S must clearly always be greater than $2f_R$, thus giving a boundary to the range of θ for a given f_S.

In practice, with a finite array and where sampling is continuous, only certain discrete characteristic frequencies corresponding to discrete bearings are reconstructable.

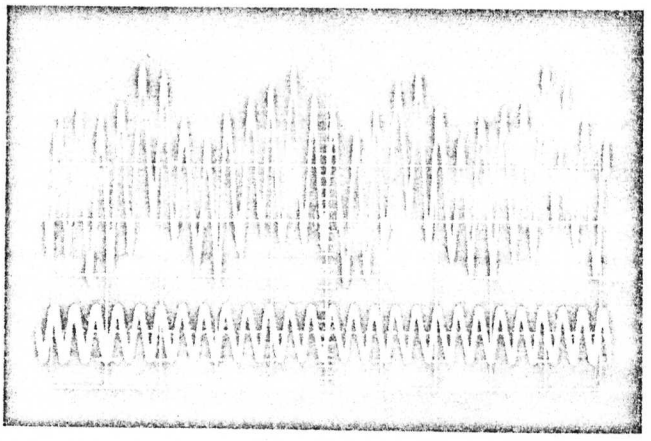

Fig. 1 *Oscilloscope trace*
Upper trace: demodulated signal produced by targets at 0° and 7°
Lower trace: signal applied to transmitters (targets)

For a continuous resultant sine wave to be produced, the phase of the signal from the last element should be $\Delta\phi$ behind the phase of the first, where $\Delta\phi$ is the phase difference between adjacent elements. The discrete bearings caused by this limitation are given by

$$\theta = \sin^{-1}\left(\frac{m\lambda_1}{dn}\right)$$

where m is an integer, and n is the total number of elements.

The limitation expressed by this equation is brought about only by the manner in which information is extracted from the resulting signal. A single set of n samples across the array contains all the required bearing information.

A 20-element 500 kHz array with a 2·4 mm element spacing was used in water, giving a set of discrete bearings separated by approximately 3·3°. A typical set of results is given in Table 1 for two simulated targets (these were small transmitting transducers), and the effect of one in the absence of the other is also shown. It can be seen that other characteristic frequencies were well down on the expected frequencies. Fig. 1 shows an oscilloscope display, the upper trace of which is the demodulated output when the targets were at bearings of 0° and 7°, the 7° target being at approximately twice the range of the other. The two frequency components can be clearly seen, the 7° target being represented by the lower frequency of 87 kHz, and the 0° target by the higher frequency of 542 kHz. The lower trace is the signal applied to the transmitters on a different voltage scale.

Table 1 TYPICAL RESULTS

Frequency	Amplitudes			Frequency component
	Transmitter 1 on	Transmitter 2 on	Transmitters 1 and 2 on	
kHz	dB	dB	dB	
90	−23	−10	−12	f_R 7°
136	−10	− 2	0	f_R 10°
316	−18	−13	−11	f_R 3°
542	− 1	−19	− 1	f_R 0°

Transmitter 1 at 0° position, transmitter 2 at 10° position;
f_S = 4·52 MHz, f_T = 542 kHz

Target range may be conveyed to the receiver without affecting the bearing information by gating a carrier oscillator to produce transmitted pulses containing many cycles of carrier. The time of arrival of edges at the various discrete frequencies will give the range of a target, if present, at each discrete angular position. Early results using this method of ranging have proved perfectly satisfactory. The accuracy would depend on the risetime of the transmitted pulse and the response time of the selective filter in the receiver.

Sector scanning should prove simple, since the only processing required is a single electronically tunable narrowband filter which will sweep through the range of frequencies corresponding to the swept sector. Sensitivity is a problem, however, since each sample is taken necessarily from a small transducer, and, in its simple form, no addition is carried out. In a normal phased array, all elements, after individual delays have been included, are finally added.

The authors wish to thank D. I. Crecraft, who, several years ago, suggested this method as a possible means of beam direction in a different context. Also much time and effort was saved by the Rocket Propulsion Establishment, Westcott, who kindly lent the multielement transducer which was used for these first tests.

S. O. HARROLD

Department of Electrical & Electronic Engineering
Portsmouth Polytechnic
Portsmouth, Hants., England

R. C. WEST
Plessey Co.
West Leigh, Havant, Hants., England

19th January 1971

APPENDIX E

Reprint of paper to be published in Ultrasonics, September 1974.

"Control of acoustic beam angle by harmonic analysis of sequential samples from a multi-element linear array"

Control of acoustic beam angle by harmonic analysis of sequential samples from a multi-element linear array

R. C. WEST and S. O. HARROLD

Frequency components contained within the sequential samples of a linear array of ultrasonic receiver transducers are shown to be a function of the angle of incidence of the received energy. The principle has been successfully confirmed by experimental results which provide both the range and bearing of multiple targets. The equipment used was operated at an ultrasonic frequency of 500 kHz and the array sampled at rates of 2.26 and 4.52 MHz. Finally, a system is proposed where the target information is given on a sector PP1 display.

List of Symbols

C_1	Velocity of longitudinal waves in water
λ_1	Wavelength of longitudinal waves in water
C_R	Resultant velocity along receiver array
C_S	Sampling velocity
d	Distance between centres of adjacent receiver elements
$f_{R\theta}$	Characteristic frequency obtained for angle of incidence θ
f_s	Sampling rate
f_T	Frequency of transmitted longitudinal wave
n	Total number of elements in receiver array
p	Ratio f_s/f_T
q	Any integer value
θ	Angle of incidence of beam to receiver array
Φ	Phase difference between adjacent elements in receiver array for angle of incidence θ
θ_{Res}	Approximate angular resolution obtainable

Introduction

A simple and inexpensive sector scanning sonar system is clearly a worthwhile objective since it would widen the economic field of use to include, for example, small fishing craft. The most successful sector scanning technique appears to be that known as modulation scanning[1-5] in which the beam is swung through the required sector within the duration of a single transmitted pulse. To ensure adequate angular resolution and to preclude any serious sidelobe problems, an array may consist, as in the bifocal equipment,[5] of 75 elements. Each receiver array element requires a channel unit consisting of at least one mixer unit,[4] and in practice it has been found desirable to have a pre-amplifier, two mixers and a second amplifier.[2,3]

In the system to be described[6] the same number of elements are required to obtain the same resolution and useable sector, but each element of the multi-element linear array requires only one sampling gate. The output of each sampling gate is connected to a common line so that all subsequent processing is applied to one resultant signal. A FET has been found to be an ideal sampling gate and the individual circuitry required for each of these is minimal as will be seen from Fig.1. The general system arrangement is shown in Fig.2 The transmitter radiates over the arc of interest and reflected signals from targets within this arc will be received by the elements of the array. By sampling the elements and applying comparatively simple processing to the resulting series of samples, the target bearings may be found. Using pulses allows target range information to be obtained in the usual way.

System principles

An echo returning from an insonified target situated in the farfield of an array of ultrasonic transducers will strike this array at an angle dependent on the target bearing. If the array is linear and consists of equally-spaced elements which are sampled sequentially at a known and fast enough rate, the resultant electrical samples, after appropriate demodulation, will produce a sinusiodal signal whose shifted frequency is a function of the angular bearing of the target. Fig.3 shows diagramatically how this frequency component is formed from the sequential samples.

Consider the array to be of infinite length and consisting of an infinite number of infinitely small elements. Referring to Fig.4, the velocity of a point of constant phase along the

Mr R. C. West is with the Plessey Company, West Leigh, Havent, Hampshire, and Mr S. O. Harrold is in the Department of Electrical and Electronic Engineering, Portsmouth Polytechnic, Portsmouth.
Paper received 17 April 1974.

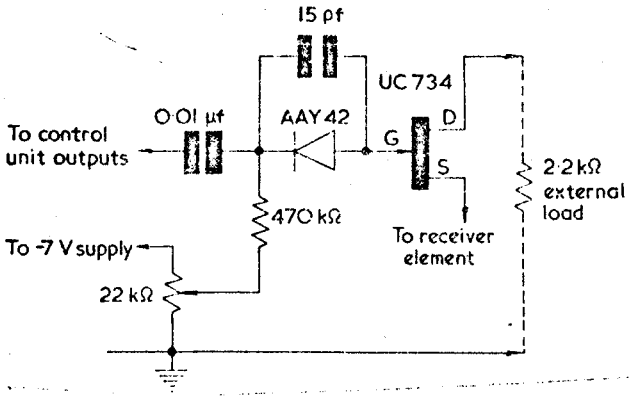

Fig.1 Basic FET switch unit

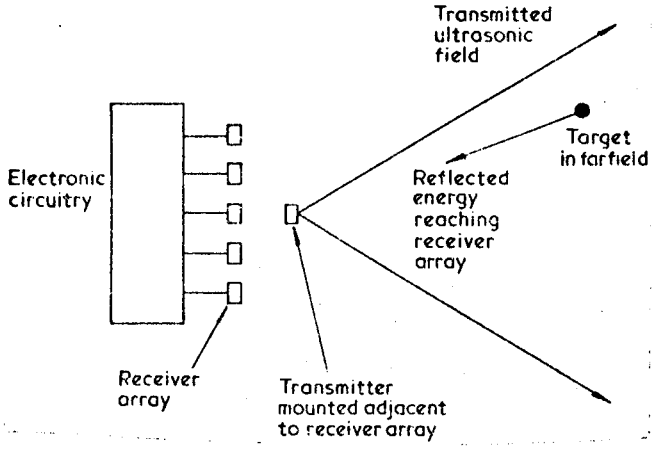

Fig.2 The basic sector scanning sonar system

array is seen to be $C_1/\sin\theta$, and the resulting apparent velocity of a point of constant phase to the sampling position is given by:

$$C_R = \frac{C_1}{\sin\theta} - C_S \qquad (1)$$

This gives a resultant output frequency of

$$f_{R\theta} = f_T \left[1 - \frac{C_s}{C_1} \sin\theta \right] \qquad (2)$$

In practice the elements will be of finite size and spaced at finite distances so that each element must be sampled for a short period sequentially. Thus a series of amplitude samples will be obtained and these require demodulation using a suitable low-pass filter in order to recover the frequency $f_{R\theta}$.

In practice then

$$f_{R\theta} = f_T \left[1 - \frac{f_s d}{C_1} \sin\theta \right] \qquad (3)$$

which may be written

$$f_{R\theta} = f_T \left[1 - \frac{pd}{\lambda_1} \sin\theta \right] \qquad (4)$$

Fig.5 shows plots of (4) for various values of p and with d and λ_1 having the values used in the experimental work

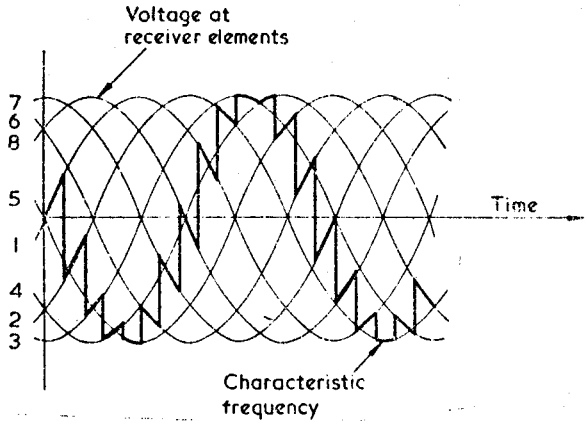

Fig.3 Diagram showing how sequential sampling builds up the characteristic frequency

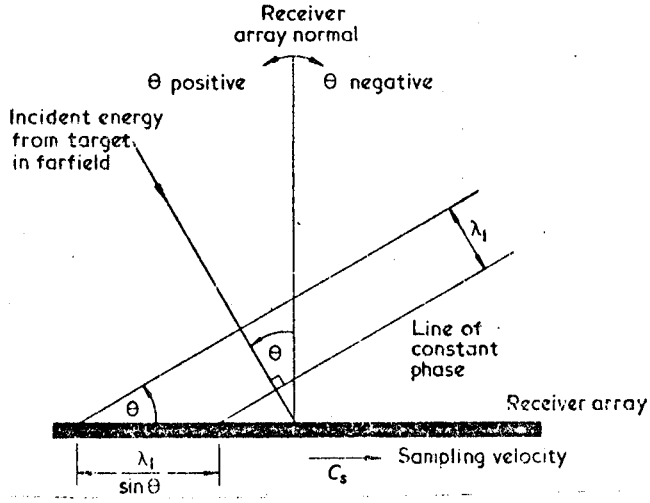

Fig.4 Diagram used for derivation of the theory. The array is considered to be of infinite length and consisting of an infinite number of infinitely small elements. The velocity of a point of constant phase along the array is seen to be $C_1/\sin\theta$

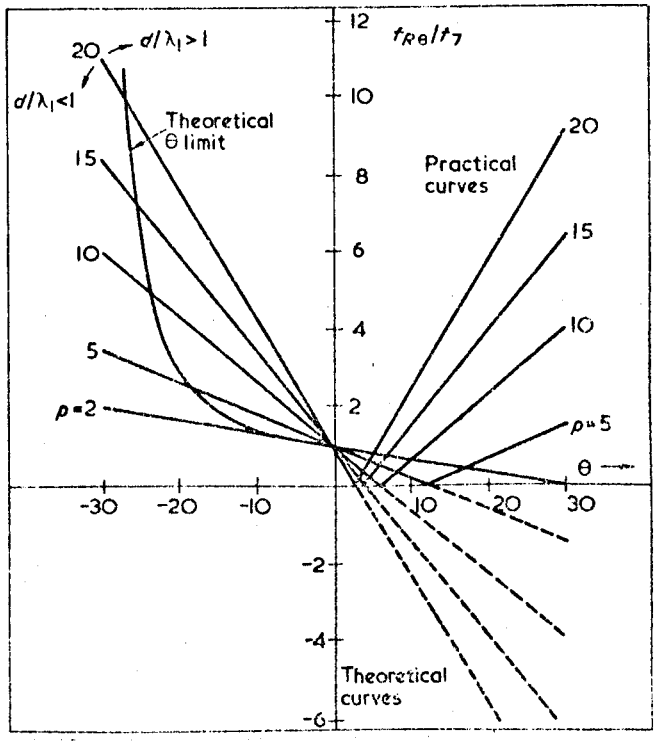

Fig.5 Plot of $f_{R\theta}$ against target angle for d/λ_1 unity

detailed below. It can be seen that there are limits to the range of target bearings acceptable to the system and these are clearly a function of the sampling frequency.

In order to use continuous sampling for a finite array length, the equality

$$n\phi = 2\pi q \tag{5}$$

must apply. Therefore only discrete resultant frequencies can be obtained and these are given by

$$f_{R0} = f_T \left[1 - \frac{pq}{n} \right] \tag{6}$$

The corresponding discrete target bearings will then be given by

$$\theta = \sin^{-1} \left[\frac{q\lambda_1}{dn} \right] \tag{7}$$

If $q = 1$ in (7) the first suitable angle for continuous sampling is given. The second suitable or discrete angle when $q = 2$ will be virtually twice the first, these angles being small. Thus a measure of the angular *resolution* θ_{Res} of this system will be the angle θ given when $q = 1$. That is

$$\theta_{Res} \simeq \lambda_1 / dn \tag{8}$$

The beam width of the array is also given by (8), since the first zero in the polar plot will occur when the angle of the incident wave causes one complete half cycle to appear across the array. The resolution given by (8), however, means that the polar plot will take the form of a set of fingers whose positions are fixed, leaving 'blind' areas between each finger. It should be pointed out that bearing information about targets within the whole sector is present in the samples obtained from a single scan of the array elements, but that the extraction of this information is more complex. By using pulsed transmission the range may be found of each target present, the strength of the signal received being a function of range and echo area of the respective targets.

The usual restrictions on element spacing apply regarding sidelobes in the array radiation pattern. Thus, for example, in order that the first major sidelobes lie 90 degrees each side of the array normal, the required element spacing would be one wavelength in the transmission medium.

Experimental equipment

In order to verify the expressions developed in the last section and to determine the practicability of a working system an experimental rig was constructed. This is shown diagramatically in Fig.6. In order to simplify investigations at this stage targets were simulated by small transmitters, these being 8 mm diameter discs of pzt having a nominal thickness resonance of 500 kHz. They were arranged so that their range and angular positions relative to the receiver array normal could be independently varied. The receiver array consisted of a horizontal line of 20 square elements

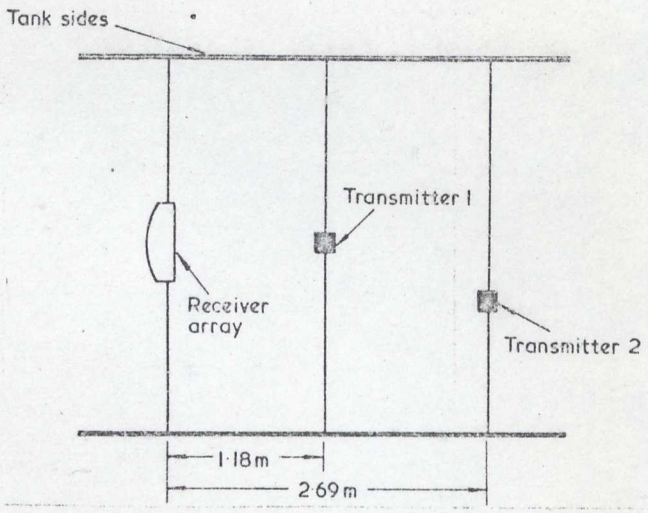

Fig 6 The experimental rig used for target simulations

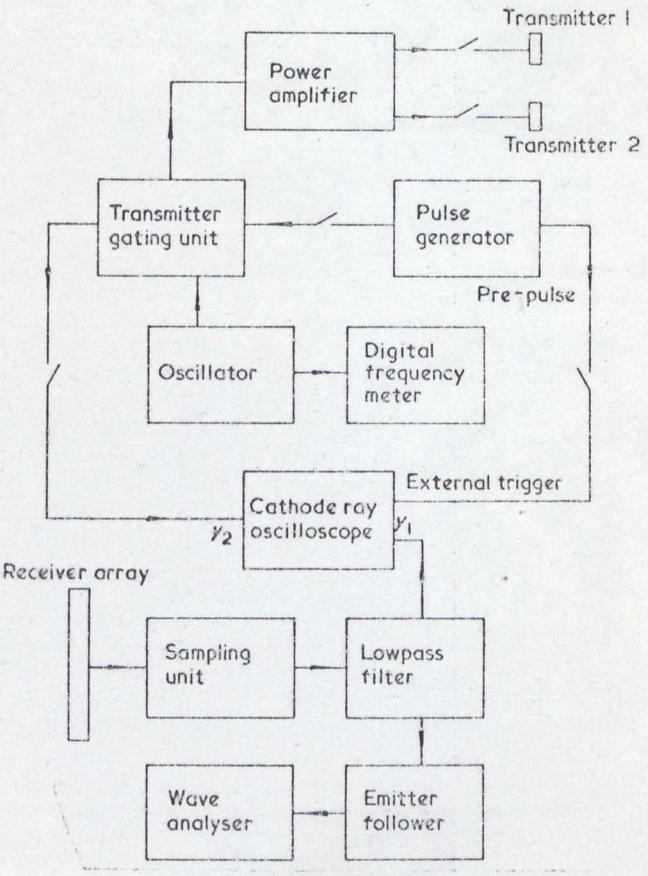

Fig.7 Block diagram of the electronic circuitry used for target simulations

spaced at a pitch of 2.4 mm (less than one wavelength in water). The whole was formed on one piece of pzt ceramic of nominal thickness resonance 500 kHz, acoustic cross coupling being reduced by grooves cut between adjacent elements.

A block diagram of the electrical system used is shown in Fig.7. The sampling unit consists of 20 FET sampling gates of the type shown in Fig.1. Each gate is connected to an array element, and driven by an astable multivibrator via a 20 stage shift register at a sampling rate of 2.26 MHz or 4.52 MHz. This produces array element sample times of around 30 ns.

Table 1 Predicted and measured characteristic frequencies obtained for various bearings of a single simulated target (f_s = 4.52 MHz)

	Experimental Results		Predicted values	
	θ [degrees]	f_{R0} [kHz]	θ [degrees]	f_{R0} [degrees]
f_T = 547 kHz	0	547	0	547
	3	322	3.3	321
	7	94.0	6.5	95.1
f_T = 528 kHz	0	528	0	528
	3	304	3.4	302
	7	76.0	6.8	76.0

Table 2 Amplitudes of various frequency components when two simulated targets are used, one at 7 degrees and the other at 10 degrees (transmitter 1 at 7 degrees; transmitter 2 at 10 degrees; f_S = 4.52 MHz; f_T = 542 kHz)

Frequency [kHz]	Corresponding angle θ [degrees]	Relative amplitudes [dB] Tx 1 on	Tx 2 on	Tx 1 and Tx 2 on
87	7	−4	−7	−4
136	10	−30	+1	0
316	3	−19	−10	−15
542	0	−16	−16	−17

Table 3 Amplitudes of various frequency components when two simulated targets are used, one at 0 degrees and the other at 10 degrees (transmitter 1 at 0 degrees; transmitter 2 at 10 degrees; f_S = 4.52 MHz; f_T = 542 kHz)

Frequency [kHz]	Corresponding angle θ [degrees]	Relative amplitudes [dB] Tx 1 on	Tx 2 on	Tx 1 and Tx 2 on
87	7	−23	−10	−12
136	10	−10	−2	0
316	3	−18	−13	−11
542	0	−1	−19	−1

Results

Table 1 shows the predicted and the measured characteristic frequencies obtained for various bearings of a single simulated target. Table 2 gives the amplitudes of the various frequency components when two simulated targets are used, one at 7 degrees and the other at 10 degrees. Table 3 shows the results when one target is at 0 degrees and the other at 10 degrees. The relatively high levels of some of the unexpected components may have been caused by reflections, since no real effort was made to reduce side or back wall echoes, although an investigation into this possibility proved inconclusive at the time. Fig.8 is a photograph of the system output displayed on an oscilloscope with one target at 0 degrees and the other at 7 degrees. The two expected frequency components are clearly visible.

Refernce to Fig.5 will show that only the right hand side or positive values of θ were used, negative values being avoided because the simple low-pass filter could not cope with demodulation near the sampling limits. These limits are indicated by the curve plotted for $f_s = 2f_{R0}$ showing the theoretical maximum angle θ for each value of p so that samples contain sufficient information to enable reconstruction or demodulation to take place. In Fig.5 it can be seen that for the results given in Tables 1, 2 and 3 a zero frequency occurs at approximately 7 degrees. This accounts for the apparent anomaly in Tables 2 and 3 where the resultant frequencies for the 10 degree targets are higher than those that would be obtained from a target at 7 degrees.

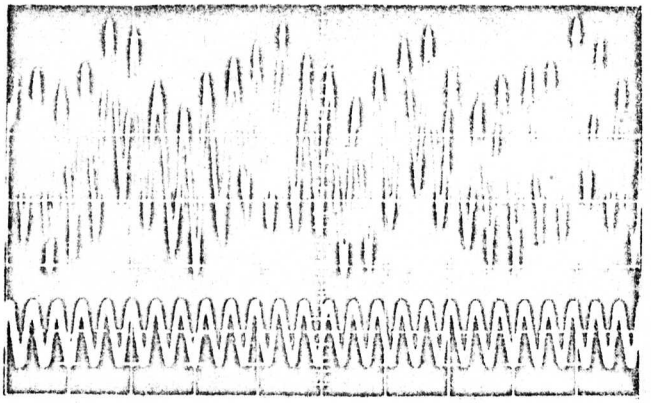

Fig.8 Oscillograph showing the characteristic frequencies for transmitter 1 at 0 degree position and transmitter 2 at 7 degree position: upper trace – output from low-pass filter; lower trace – input to transmitter power amplifier (horizontal scale – 5 μs cm^{-1}; vertical scale – 20 mV cm^{-1})

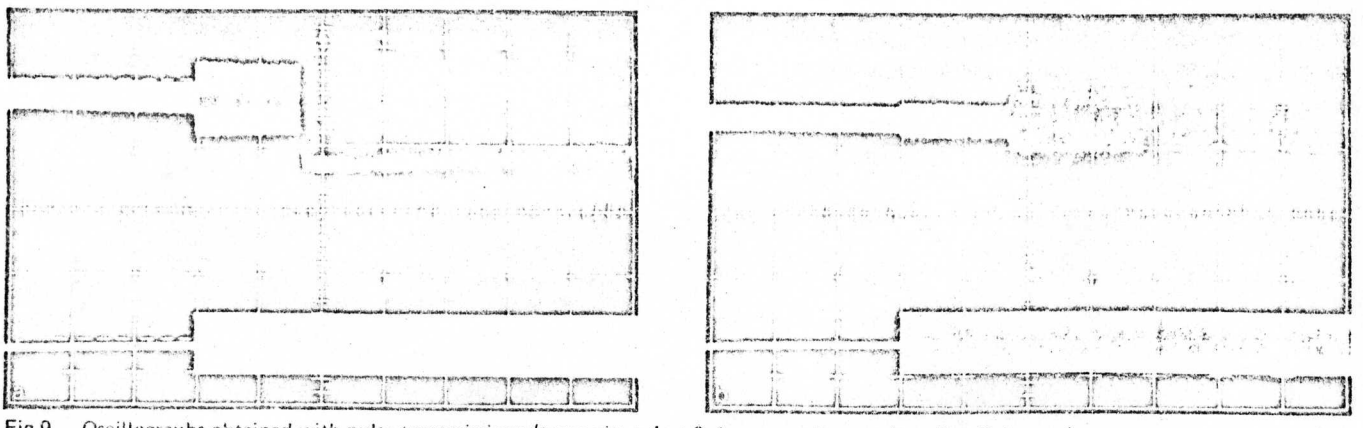

Fig.9 Oscillographs obtained with pulse transmissions (transmitter 1 at 0 degrees and transmitter 2 at 7 degrees) a: upper trace – output from bandpass filter centred on f_{R0}; lower trace – input to transmitter power amplifier; b: upper trace – output from bandpass filter centred on f_{R7}; lower trace – input to transmitter power amplifier

In order that the range of a target may be found it is necessary to use pulsed transmissions, the time delay between transmission and reception providing the required information. A bandpass filter tuned to the characteristic frequency of the required target will then enable its range to be found. In Fig.9 oscillographs show the result of this technique. The lower trace in each case is the transmitted signal from the simulated target and it will be seen that before this reaches the receiver an electrical breakthrough signal is present. Figs. 9a and b show the results of the resonant bandpass filter being tuned to the near and far target respectively. The Q of the filter was inadequate as can be clearly seen in Fig.9b where ideally only a single step in amplitude at a time of approximately 3.5 ms should have occurred.

Conclusions

The foregoing sections have demonstrated the simplicity of this method for obtaining the bearing of targets within a specified sector. It has been shown both experimentally and theoretically that the angular resolution may be considered to be approximately the array beamwidth λ_1/dn, and results have indicated that the resolution in range and bearing of more than one target is practically feasible.

Clearly much more fundamental work is required. In particular the problems of noise, resolution and useable sector in relation to sampling frequency, etc, must be more fully investigated.

The outline of a proposed system is given in Fig.10 in which it is shown how information from the sampling circuits could be processed to give a sector PPI display of targets. Again only *positive* angles of θ are considered but a complete sector is formed by scanning the array first in one direction and then the other. Use of *negative* angles requires that $f_{R\theta} > f_T$ and in consequence f_s must be high. A high value for f_s limits the range of *positive* θ, assuming that only characteristic frequencies up to the zero or *reflection* point are used (see Fig.5). The mixer included after the right to left sampling unit will frequency shift the output of the latter upwards by f_T to give the required frequencies for the *negative* angles. The angular control circuitry sets both the centre frequency of the bandpass filter, the desired beam direction, and the angular position of the display.

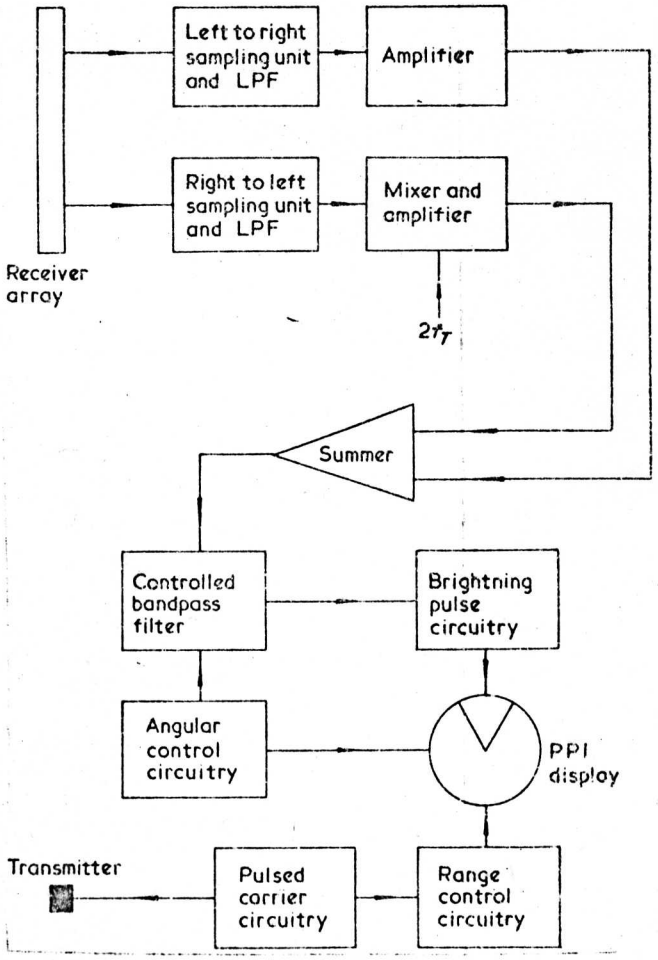

Fig.10 Possible system for PPI display of targets

Acknowledgments

All the experimental work described was carried out in the Electrical and Mechanical Engineering Departments of the Portsmouth Polytechnic, but the authors owe special thanks to the Rocket Propulsion Establishment, Westcott, who kindly lent the multi-element transducer.

References

1 **Tucker, V. G., Welsby, V. G., Kendall, R.** Electronic sector scanning, *Journal of the British Institution of Radio Engineers* (August 1958) 465

2 **Tucker, D. G., et al.** Underwater echo-ranging with electronic sector-scanning: sea trials on RRS Discovery II, *Journal of the British Institution of Radio Engineers* (November 1959) 681

3 **McCartney, B. S.** An improved electronic sector-scanning sonar receiver, *Journal of the British Institution of Radio Engineers* (December 1961) 481

4 **Welsby, V. G., Duan, J. R.** A high-resolution electronic sector-scanning sonar, *Journal of the British Institution of Radio Engineers* (September 1963) 205

5 **Voglis, G. M., Cook, J. C.,** Underwater application of advanced acoustic scanning system, *Ultrasonics* 4 (1966) 1

6 **Harrold, S. O., West, R. C.** Farfield sector scanning using a sampled multielement ultrasonic receiving array, *Electronics Letters* 7 (February 1971) 100

APPENDIX F

Editor's draft of a news article to be published in Ultrasonics, September 1974.

"FET gates for ultrasonic camera"

RESEARCH AND DEVELOPMENT

FET gates for ultrasonic camera

Ultrasonic image converters have been studied for many years but in spite of extensive development they have yet to become an accepted tool in industrial and medical applications. The important reasons for this are that an immersion technique is required and that operating a tube converter using short pulses to overcome reverberations and to give range information is difficult. However, an inherently simple and rugged transistor scanned ultrasonic transducer matrix converter, developed by S. O. Harrold at Portsmouth Polytechnic, may prove to be an acceptable tool when used in a conventional image camera system.

The development of this form of converter has relied entirely on the availability of a cheap but satisfactory electronic analogue sampling gate. The first converter constructed at Portsmouth[1] used bipolar transistors gating a 10 x 10 matrix, but the 'off' switch breakthrough and bad electrical connexions to the matrix element gave poor results. Experimental tests on a cheap vhf FET (UC734) showed it to be excellent for gating low-level signals of up to 6 MHz (measured signal to breakthrough ratio > 50 dB). A new converter was constructed using the FETs in conjunction with improvements to the electrical connectors and the transducer matrix.

A schematic of the complete camera system used is shown in Fig.1. Continuous or pulsed ultrasound at 1 MHz illuminates the object and waves diffracted by the object are focused by a concave perspex lens to form a pressure image on the surface of the converter matrix. Fig.2 is a photograph of the experimental set-up in operation.

In the pulsed mode the transmitter gate allows a 70 μs pulse of ultrasound to be transmitted at a prf between 1 -4 kHz, while the matrix element scanning rate is synchronized so that one element is sampled for each transmitted pulse, giving a frame frequency between 10 -40 Hz.

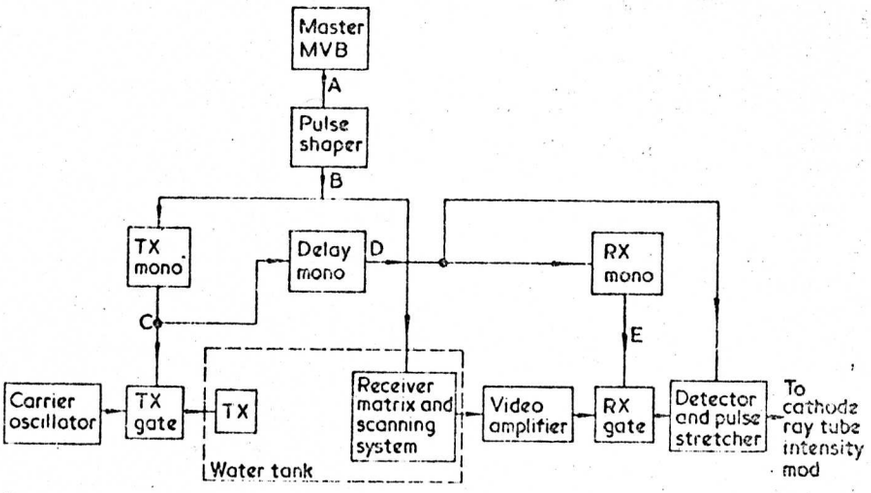

Fig.1 Schematic of the electronics for the ultrasonic camera system. 1 MHz ultrasound illuminates the object in either continuous or pulsed mode

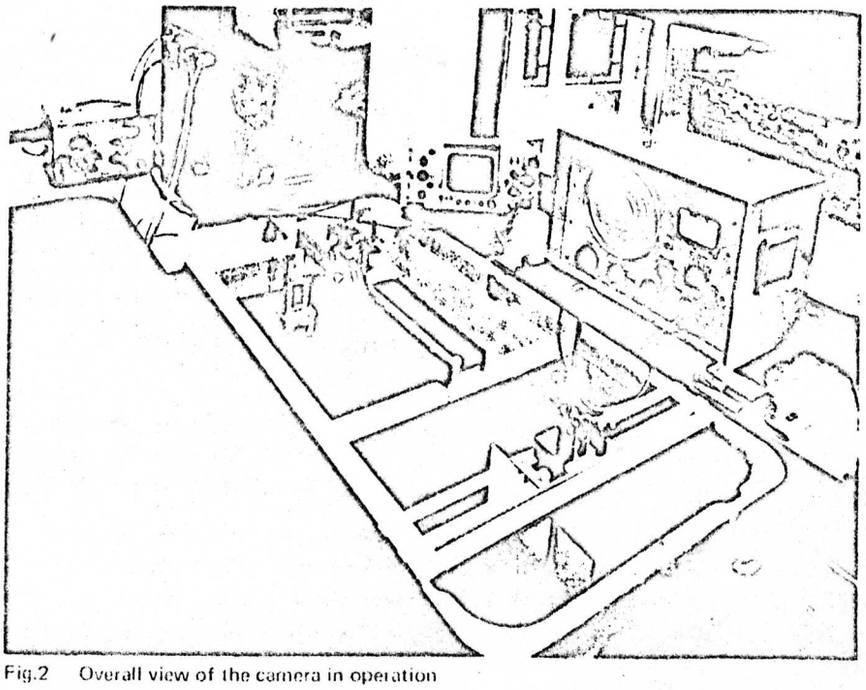

Fig.2 Overall view of the camera in operation

Results obtained with this set-up were a great improvement on those obtained using the bipolar switching matrix. Fig.3a and b shows images of a 1.5 mm crosscut through a 1 mm aluminium plate, one upright (a) and the other at 45 degrees (b). Fig.3c shows the image of two 2.5 mm diameter holes through a 1 mm aluminium plate with approximately 1.5 mm spacing between adjacent edges. Finally, Fig.3d, which demonstrates real capabilities of the system, shows images of two 3 mm spot welds between two 1 mm steel plates. These were 'good' welds and although suspected 'bad' welds were viewed no noticeable differences could be detected.

Further work is now being done to replace the lens by an on-line computer to process the matrix signals and produce a print-out picture. Early results, however, are inconclusive.

One real problem common to both the lens and lensless sytems is the resolution limitation imposed by a 10 line picture system. The use of a single silicon slice

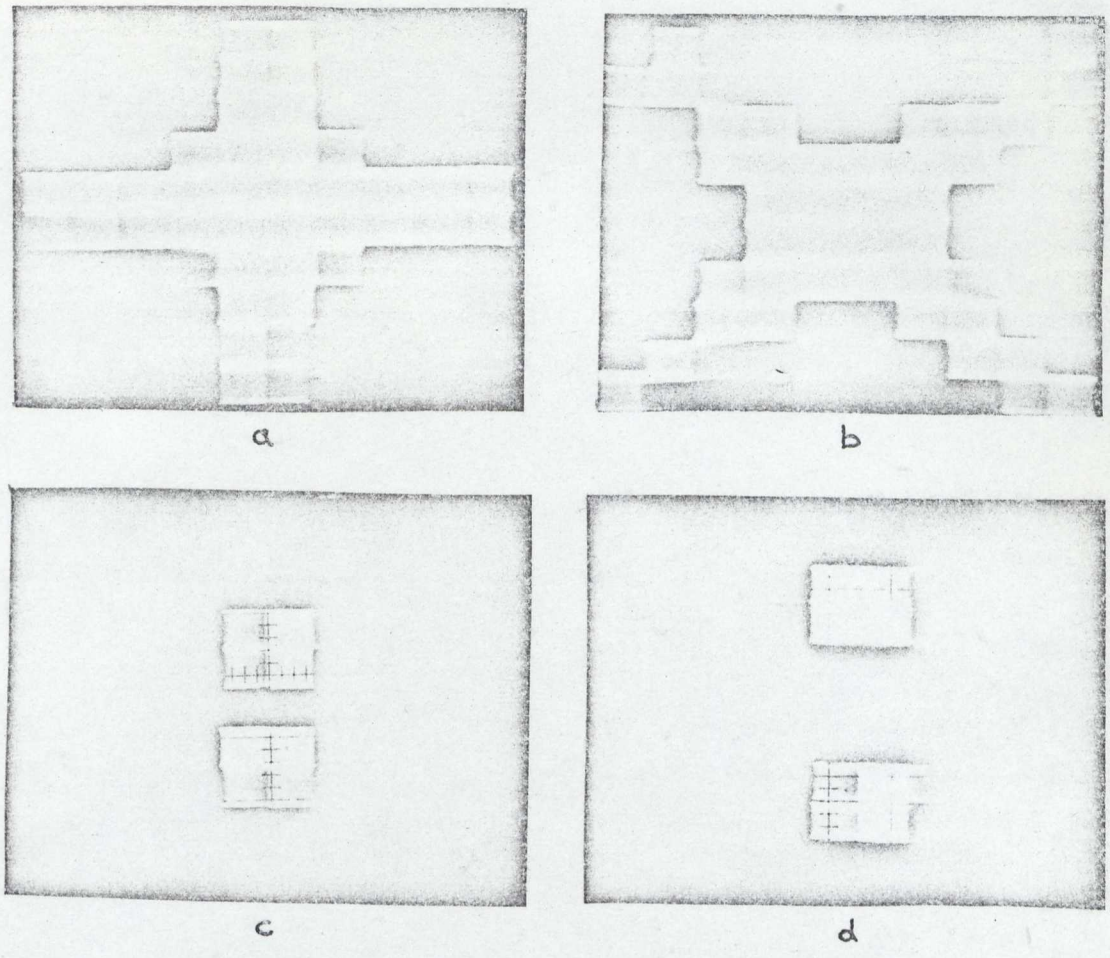

Fig.3 a – Image of an upright cross formed by 1.5 mm slots cut through 1 mm aluminium sheet; b – image of the same cross at 45 degrees; c – image of two 2.5 mm diameter holes through 1 mm aluminium sheet. Spacing between adjacent edges is about 1.5 mm; d – image of two 3 mm electric spot welds between two 1 mm steel plates

within which a complete 100 x 100 scanning matrix including shift registers is built, appears very attractive and would remove the resolution problem. Using MOS techniques it would provide a compact, reliable and comparatively cheap system but fabrication problems, such as the bonding of the connexions to the electrode matrix, have still to be overcome.

S. O. Harold, Department of Electrical and Electronic Engineering, Portsmouth Polytechnic, Portsmouth, Hampshire, UK

Reference

1 Harrold, S.O. Solid state ultrasonic camera, *Ultrasonics* 7 (1969) 95